



## Durham E-Theses

---

### *A photophysical study of substituted arylethynylenes*

Findlay, Karen Samantha

#### How to cite:

---

Findlay, Karen Samantha (2007) *A photophysical study of substituted arylethynylenes*, Durham theses, Durham University. Available at Durham E-Theses Online: <http://etheses.dur.ac.uk/2475/>

#### Use policy

---

The full-text may be used and/or reproduced, and given to third parties in any format or medium, without prior permission or charge, for personal research or study, educational, or not-for-profit purposes provided that:

- a full bibliographic reference is made to the original source
- a [link](#) is made to the metadata record in Durham E-Theses
- the full-text is not changed in any way

The full-text must not be sold in any format or medium without the formal permission of the copyright holders.

Please consult the [full Durham E-Theses policy](#) for further details.

# **A PHOTOPHYSICAL STUDY OF SUBSTITUTED ARYLETHYNYLENES**

**Karen Samantha Findlay**

Department of Chemistry,

Durham University,

Durham UK

The copyright of this thesis rests with the author or the university to which it was submitted. No quotation from it, or information derived from it may be published without the prior written consent of the author or university, and any information derived from it should be acknowledged.

Submitted in partial fulfilment of the requirements for the degree of  
Doctor of Philosophy, Durham University.

January 2007



1 1 JUN 2007

## **DECLARATION**

The work described in this thesis was carried out in the Chemistry Department in the University of Durham between October 2002 and December 2005. This thesis is the work of the author except where acknowledged by references, and has not been submitted for any other degree.

## **STATEMENT OF COPYRIGHT**

The copyright of this thesis rests with the author. No quotation from it should be published without her prior written consent and information derived from it should be acknowledged.

## ABSTRACT

Molecules based on the 1,4-bis(phenylethynyl)benzene (BPEB) architecture are an important class of compounds because of their luminescent properties. The rigid rod-like backbone and extended  $\pi$ -conjugation serves as the base upon which a wide variety of substituted species can be synthesised with a variety of photophysical properties. This thesis represents a detailed study of the photophysical properties of a series of compounds based on BPEB using a combination of steady-state and time-resolved spectroscopic methods.

A comparative study of the photophysical properties of BPEB, 1,2,4,5-tetramethyl-3,6-bis(phenylethynyl)benzene, 1,2,4,5-tetramethyl-3,6-bis-(2,4,6-trimethylphenylethynyl)benzene, 1,4-bis(2-(2-*tert*-butylphenyl)ethynyl)benzene, 1,4-bis(2-(2-*tert*-butylphenyl)ethynyl)-2,3,5,6-tetramethylbenzene, 1,4-dibromo-2,5-bis(phenylethynyl)benzene and 1,2,4,5-tetrafluoro-3,6-bis(phenylethynyl)benzene is reported. These compounds exist as a series of geometric conformers, in solution, in the ground state due to the low barrier to rotation about the carbon-carbon triple bond (C $\equiv$ C). The absorption and emission dipoles of BPEB are found to be almost linear and lie along the long axis of the molecule. The substituents red shift the absorption and emission spectra of BPEB. 1,4-Bis(2-(2-*tert*-butylphenyl)ethynyl)-2,3,5,6-tetramethylbenzene, exhibits fluorescence from both high and low energy conformations at 77 K. Only 1,4-dibromo-2,5-bis(phenylethynyl)benzene has a long lived phosphorescence emission detectable at 77 K. Time-resolved Raman spectroscopy reveals that the C $\equiv$ C stretching vibrations of BPEB, and its substituted derivatives in the excited singlet and triplet states, which shows evidence of only minor structural changes upon excitation.

The photophysical properties, and solvatochromism, of a series of compounds having donor and acceptor groups bridged by BPEB are reported. They are methyl-4-(4-(4-dimethylaminophenylethynyl)phenylethynyl)benzoate, 4-(4-(4-dimethylaminophenylethynyl)phenylethynyl)benzotrile, 4-(4-(4-dimethylamino-3,5-dimethylphenylethynyl)phenylethynyl)benzotrile, 4-(4-(4-dimethylaminophenylethynyl)phenylethynyl)-N,N-dimethylbenzenamine, 4-(4-(4-cyanophenylethynyl)phenylethynyl)benzotrile, 4-(4-(4-dimethylaminophenylethynyl)phenylethynyl)benzene, 4-(4-(4-cyanophenylethynyl)phenylethynyl)benzene and methyl-4-(4-phenylethynyl)-



phenylethynylbenzoate. The donor-acceptor systems exhibit intramolecular charge transfer (ICT) and twisted internal charge transfer in the excited state, when in polar solvents. In non-polar solvents only the locally excited state is observed. The largest change in dipole moment in the excited state occurred when the dimethylamino group was fixed perpendicular to the adjacent phenyl ring. In protic solvents, hydrogen bonds to the amino group in the ICT state to form a hydrogen-bonded ICT state.

The photophysical properties of 9,10-bis(phenylethynyl)anthracene (BPEA) and a series of nine of its donor and acceptor substituted derivatives are reported. Compounds with the strongest donor (dimethylamino) and acceptor (nitro) groups exhibit ICT. All substituted BPEA compounds had lower fluorescence quantum yields and lifetimes, and higher non-radiative decay constants than BPEA.

The molecular and photophysical properties of 2,5-bis(phenylethynyl)thiophene, 1,4-bis(2-thienylethynyl)benzene and 2,5-bis(2-thienylethynyl)thiophene were investigated with specific emphasis on the bonding character of their triplet excited states. Like the parent, BPEB, these compounds exhibit evidence of triple bond character in the excited singlet and triplet states.

## ACKNOWLEDGMENTS

First, I would like to thank Dr. Andrew Beeby for his guidance, encouragement, advice, support and enthusiasm throughout my time at Durham. It is through his assistance that this thesis was made possible.

A big thank you also goes to my colleagues with whom I have shared my time at Durham and office space. I thank Dr. Simon FitzGerald and Dr. Sylvia Bettington-Walker for showing me the ropes in the early days and making me feel welcome. To Simon Rutter, for synthesising some of the compounds on which this work is based, friendship and for 'Harry Potter Chemistry', I thank you. I am also indebted to Dr. Laurent Porrès (Dr. Woo) for valuable insight and advice on the research for this work. And I thank him for his friendship and support.

For their camaraderie, help and discussions over copious amounts of tea I would like to express my appreciation to Dave, the two Kates, Ruth, Becky, Francis, Aileen, Kathryn, Andy and Lucas.

Recognition must also go to the glassblowers (Peter and Malcolm) and the workshop technicians (Jimmy, Neil, Kelvin, and Barry) in the department who fixed and built the equipment necessary for this research.

None of this would have been made possible without the support of my parents, Monica and Earl Findlay and my sister Juliet. I will forever be indebted to them.

Thanks to the 'United Nations' for their friendship and the good times. To Grace, Harald, Maria, Manuel, Costas and Georgia, you are my Durham family.

Last but not least, warm gratitude goes to my dearest Aris for the support and encouragement, and sticking by me through the entire production of this thesis.

# CONTENTS

<b>Glossary of Abbreviations .....</b>	<b>5</b>
<b>Symbols .....</b>	<b>6</b>
<b>CHAPTER 1. ....</b>	<b>7</b>
<b>Introduction .....</b>	<b>7</b>
1.1 Poly(arylethynyls) .....	7
1.1.1 The effect of ring torsion in conjugated polymers on their photophysical properties.....	8
1.1.2 Conductivity in conjugated systems .....	11
1.2 1,4-Bis(phenylethynyl)benzene and its derivatives .....	16
1.3 Intramolecular charge transfer systems.....	20
1.4 The triplet state of poly(arylethynyls) .....	25
<b>Aims.....</b>	<b>28</b>
<b>REFERENCES.....</b>	<b>29</b>
<b>CHAPTER 2 .....</b>	<b>39</b>
<b>An introduction to fluorescence spectroscopy.....</b>	<b>39</b>
2.1 Luminescence.....	39
2.2 The effect of solvent polarity on fluorescence spectra.....	42
2.3 The Lippert equation.....	43
2.4 Specific solvent effects .....	45
2.5 The effect of temperature and solvent viscosity on fluorescence spectra.....	45
2.6 Fluorescence quantum yield.....	46
2.7 Fluorescence lifetime .....	47
2.8 Anisotropy.....	47
2.8.1 Fluorescence Anisotropy.....	48
2.8.2 Theory for fluorescence anisotropy .....	50
2.8.3 Excitation Photoselection.....	52
2.8.4 Fundamental anisotropy .....	53
2.8.5 Rotational diffusion and the Perrin Equation.....	54
2.9 An introduction to time-resolved resonance Raman spectroscopy.....	55
<b>REFERENCES.....</b>	<b>58</b>

<b>CHAPTER 3 .....</b>	<b>60</b>
<b>Experimental techniques .....</b>	<b>60</b>
3.1 UV-visible absorption spectroscopy .....	60
3.2 Fluorescence spectroscopy.....	60
3.3 Low temperature spectroscopy .....	61
3.4 Singlet oxygen quantum yields .....	61
3.4.1 Experimental details.....	62
3.5 Fluorescence lifetimes—The phase modulation technique.....	63
3.5.1 Experimental details.....	64
3.6 Fluorescence lifetimes—The time correlated single photon counting technique .....	64
3.6.1 Experimental details.....	67
3.7 Nanosecond laser flash photolysis .....	67
3.7.1 Experimental details.....	68
3.8 Anisotropy measurements.....	69
3.8.1 Experimental details.....	70
3.9 Ultra-fast absorption and fluorescence spectroscopy.....	70
3.10 Time-resolved resonance Raman spectroscopy .....	71
3.10.1 Picosecond time-resolved resonance Raman spectra .....	71
3.10.2 Nanosecond time-resolved resonance Raman spectra .....	72
3.10.3 Picosecond infrared absorption and transient excitation.....	73
3.11 General experimental details.....	74
<b>REFERENCES.....</b>	<b>75</b>
 <b>CHAPTER 4 .....</b>	 <b>77</b>
<b>Properties of 1,4-bis(phenylethynyl)benzene and its derivatives.....</b>	<b>77</b>
4.1 Introduction.....	77
<b>Results and discussion .....</b>	<b>80</b>
4.2 Steady state photophysical properties in solution .....	80
4.3 Steady state photophysical properties in a frozen matrix at 77 K.....	84
4.4 Fluorescence Anisotropy.....	89
4.5 Time-resolved spectroscopy.....	92
4.6 Time-resolved emission measurements .....	93
4.7 Transient absorption measurements .....	95
4.8 Time-resolved resonance Raman measurements .....	96

4.9	Transient absorption, ground state and time-resolved resonance Raman measurements of 1,4-bis(2-(2-tert-butylphenyl)ethynyl)-2,3,5,6-tetramethylbenzene ( <b>5</b> ).....	102
4.10	Ground state and time-resolved resonance Raman spectroscopy measurements of 1,2,4,5-tetramethyl-3,6-bis-(2,4,6-trimethylphenylethynyl)benzene ( <b>3</b> ), 1,4-bis(2-(2-tert-butylphenyl)ethynyl)benzene ( <b>4</b> ) and 1,2,4,5-tetrafluoro-3,6-bis(phenylethynyl)benzene ( <b>7</b> ) .....	104
4.11	Ground state and time-resolved resonance Raman of 1,4-dibromo-2,5-bis(phenylethynyl)benzene ( <b>6</b> ).....	110
	<b>Conclusions</b> .....	<b>112</b>
	<b>REFERENCES</b> .....	<b>115</b>
	<b>CHAPTER 5</b> .....	<b>120</b>
	<b>Properties of 1,4-bis(phenylethynyl)benzene donor–acceptor substituted compounds</b> .....	<b>120</b>
5.1	Introduction.....	120
	<b>Results and discussion</b> .....	<b>122</b>
5.2	Steady state absorbance and fluorescence measurements.....	122
5.3	Lifetime measurements .....	135
5.4	Picosecond time-resolved infrared (TRIR) spectroscopy measurements ...	138
	<b>Conclusions</b> .....	<b>144</b>
	<b>REFERENCES</b> .....	<b>146</b>
	<b>CHAPTER 6</b> .....	<b>149</b>
	<b>Properties of 9,10-bis(p-R-phenylethynyl)anthracene chromophores</b> .....	<b>149</b>
6.1	Introduction.....	149
	<b>Results and discussion</b> .....	<b>150</b>
6.2	Absorption and fluorescence.....	151
6.3	Fluorescence quantum yields and lifetime measurements .....	155
	<b>Conclusions</b> .....	<b>156</b>
	<b>REFERENCES</b> .....	<b>158</b>
	<b>CHAPTER 7</b> .....	<b>160</b>
	<b>Properties of 2,5-bis-(phenylethynyl)thiophene (<b>26</b>) and related compounds</b> .....	<b>160</b>
7.1	Introduction.....	160
	<b>Results and discussion</b> .....	<b>161</b>

7.2	Steady state photophysical measurements .....	161
7.3	Ground-state Raman scattering .....	165
7.4	Transient absorption.....	169
7.5	Time-resolved resonance Raman (TR3) scattering of the excited states ...	172
	<b>Conclusions .....</b>	<b>177</b>
	<b>REFERENCES.....</b>	<b>179</b>
	<b>SUMMARY .....</b>	<b>182</b>
	<b>FUTURE WORK .....</b>	<b>183</b>
	<b>REFERENCES.....</b>	<b>183</b>
	<b>APPENDIX A .....</b>	<b>184</b>
A.1	Additional lifetime information for Chapter 5 .....	184
	<b>APPENDIX B .....</b>	<b>185</b>
B.1	Publications .....	185
B.2	Posters presented .....	185

## GLOSSARY OF ABBREVIATIONS

A-A	Acceptor-Acceptor
AgGaS <sub>2</sub>	Silver gallium sulphide
BPEB	1,4-Bis(phenylethynyl)benzene
C <sub>6</sub> H <sub>12</sub>	Cyclohexane
CaF <sub>2</sub>	Calcium Fluoride
CHCl <sub>3</sub>	Chloroform
CT	Charge-transfer
CTS	Charge-transfer state
CW	Continuous wave
DACN-DPA	4-N,N-Dimethylamino-4'-cyanodiphenylacetylene
DCM	Dichloromethane
D-D	Donor-Donor
DPA	Diphenylacetylene
DPB	Diphenylbutadiyne
DPH	1,6-Diphenyl-1,3,5-hexatriene
EPA	Diethyl ether, pentane, alcohol
EtOH	Ethanol
HICT	Hydrogen bonded intramolecular charge transfer
ICT	Intramolecular charge transfer
ISC	Intersystem crossing
LE	Locally excited
MCH / IP	Methylcyclohexane / 2-methylbutane
MTCN-DPA	<i>p</i> -Cyano- <i>p</i> '-methylthiodiphenylacetylene
OLED	Organic light emitting diode
OPA	Optical parametric amplifier
POPOP	2,2'- <i>p</i> -Phenylene-bis(5-phenyloxazole)
PPE	Poly( <i>p</i> -phenyleneethynylene)
PPV	Poly( <i>p</i> -phenylenevinylene)
PTFE	Polytetrafluoroethylene
RET	Resonance energy transfer
TA	Transient absorption
tBPEB	1,4-Bis( <i>p</i> -tert-butylphenylethynyl)benzene
TCSPC	Time correlated singlet photon counting
TICT	Twisted intramolecular charge transfer
TRES	Time-resolved emission spectroscopy
T-T	Triplet-Triplet
VR	Vibrational relaxation

## SYMBOLS

$n$	Refractive index
$\epsilon$	Extinction coefficient, $\text{dm}^3 \text{mol}^{-1} \text{cm}^{-1}$
$\epsilon$	Dielectric constant
$r_0$	Fundamental anisotropy
$r$	Average steady-state fluorescence anisotropy
$\tau_f$	Fluorescence lifetime, ns
$\tau_c$	Rotational correlation time, ps
$\Phi_f$	Fluorescence quantum yield
$k_{\text{ISC}}$	Rate constant for intersystem crossing, $\text{s}^{-1}$
$k_{\text{IC}}$	Rate constant for internal conversion, $\text{s}^{-1}$
$k_{\text{VR}}$	Rate constant for vibrational relaxation, $\text{s}^{-1}$
$k_{\text{nr}}$	Non-radiative decay rate constant, $\text{s}^{-1}$
$\Gamma$	Emissive rate constant, $\text{s}^{-1}$



## CHAPTER 1

### Introduction

#### 1.1 Poly(arylethynylenes)

Poly(arylethynylenes) are highly conjugated, linear and rigid molecules. They consist of a backbone of aromatic groups separated by carbon–carbon triple bonds ( $C\equiv C$ ). The aryl groups are able to rotate about the  $C(sp)-C(sp^2)$  bonds in the ground state. The electrons along this rod like structure are highly delocalised, which gives rise to a linear  $\pi$ -conjugation that runs along the principle molecular axis, and is dependent on the relative orientation of the planar aromatic moieties.[1-4] The electrons in these delocalised systems are easily polarised by an external electric field, such as that found in light. The conductivity and structural rigidity of these molecules is chiefly dependent on the  $C\equiv C$ . The low barrier to rotation of the adjacent aryl rings suggests that, in solution, any dihedral angle between two aryl rings can be assumed (*vide infra*).[1, 5, 6]

Electroluminescent conjugated polymers are fluorescent polymers that emit light when excited by the flow of an electric current.[7] Electroluminescence of organic compounds was first reported for the acridine derivatives gonacrin and brilliant acridine orange E by Bernanose *et al.*[8] in 1955. In 1965 Sano *et al.* made one of the first observations of this phenomenon in anthracene.[9] Later, Tang and VanSlyke were the first to develop a thin film hetero-junction organic LED in 1987.[10] Following this, electroluminescence was reported for poly(*p*-phenylenevinylene) (PPV) as a single semiconducting layer between metallic electrodes in 1990.[11] These discoveries led to the creation of a new ‘molecular electronics’ industry and is set to challenge the domination of the commercial market in light emitting diodes (LEDs) by inorganic materials. These polymers are particularly versatile because their physical properties can be fine-tuned by the manipulation of their chemical structures.[7] Fluorescent polymers are used to make LEDs[12-14] and find applications as back lights for liquid crystal displays and, in the near future, as emissive material in alphanumeric displays.[7] Conjugated polymers, such as dialkyl-substituted poly(*p*-phenyleneethynylene)s (PPEs), are organic semiconductors and therefore, potentially, have applications in photonic and electronic devices. Examples include polymeric LEDs, ‘plastic lasers’ and polymer

based photovoltaic cells.[15] Along with their conducting properties, PPEs offer various substitution patterns around the phenyl ring system which has led to the development of a wide range of shape-persistent molecular architectures,[16, 17] and luminescent and electroluminescent materials.[18-20] In principle, conjugated polymers should be able to carry out all the functions of an inorganic semiconductor and in the future may be used as a media from which components may be made for 'molecular electronics'.[21] Also the property of electrical conduction through conjugated organic molecules makes them good candidates for 'molecular wires'.[21]

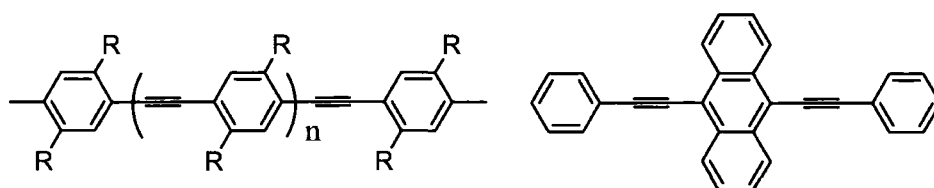
The primary interest in the use of polymers lies in the scope of low-cost manufacturing, using solution-processing of thin film polymers.[13] An increase in the understanding of the processes involved in device function and breakdown, and the systematic modification of the properties of the emissive polymers by synthetic design, have become vital components in the optimisation of light emitting devices.[7, 22] To engineer molecular devices based on conjugated frameworks, a firm understanding of the photophysics and the factors that control the geometry of the compound, and hence the  $\pi$ -conjugation pathway, in the ground and excited states is required.[1] With this in mind, the study of the model polymer compounds described herein was undertaken.

### **1.1.1 The effect of ring torsion in conjugated polymers on their photophysical properties**

It is common knowledge that the rotation of groups attached to triple bonds is nearly frictionless in the ground state.[23-25] It is expected that the barrier to rotation of phenyl rings in arylacetylene systems, in the ground state, will also be quite low. The barrier to rotation of the phenyl rings in 1,2-diphenylethyne was calculated to be 3.6 kJ mol<sup>-1</sup> in liquid crystals by Inoue *et al.*[26] Several authors, using various semi-empirical and quantum mechanical methods, have reported values for the barrier energy to rotation of aryl rings in different oligomer systems.[2, 6, 27] The threshold to rotation about the triple bond in model compound 1,4-bis(phenylethynyl)benzene (BPEB) was reported to be 8.37 kJ mol<sup>-1</sup> by Garibay *et al.*[6] using the Austin Model 1 method, and 2.31 kJ mol<sup>-1</sup> by Tretiak *et al.*[2] using a blend of quantum chemical methods including semi-empirical approaches. Majumber *et al.*[27] calculated the barrier to rotation in 4-nitro-2,5-bis-

(4-mercaptophenylethynyl)phenylamine to be  $14.2 \text{ kJ mol}^{-1}$  using the Hartree–Fock (HT), post-HT and density functional theory levels of theory. It is observed that, because the barrier is very small, theoretical calculations tend to over estimate or under estimate the true value depending on the method used. Also, there has been no actual measurement of this barrier to rotation until recently by Greaves *et al.*[5]

Greaves *et al.* measured the torsional barrier height to rotation of the model compound BPEB, using cavity ring-down spectroscopy, and found it to be  $\approx 2.7 \text{ kJ mol}^{-1}$ . [5] This is comparable with  $kT$  (energy) at room temperature ( $2.5 \text{ kJ mol}^{-1}$ ). Thus, at ambient temperature 30% of BPEB molecules in a sample will have sufficient energy to allow ‘free’ rotation of the phenyl rings about the single bonds. [5]



**Figure 1.1** General structure of poly(arylethynylene)s (left) and 9,10-bis(phenylethynyl)anthracene (right).

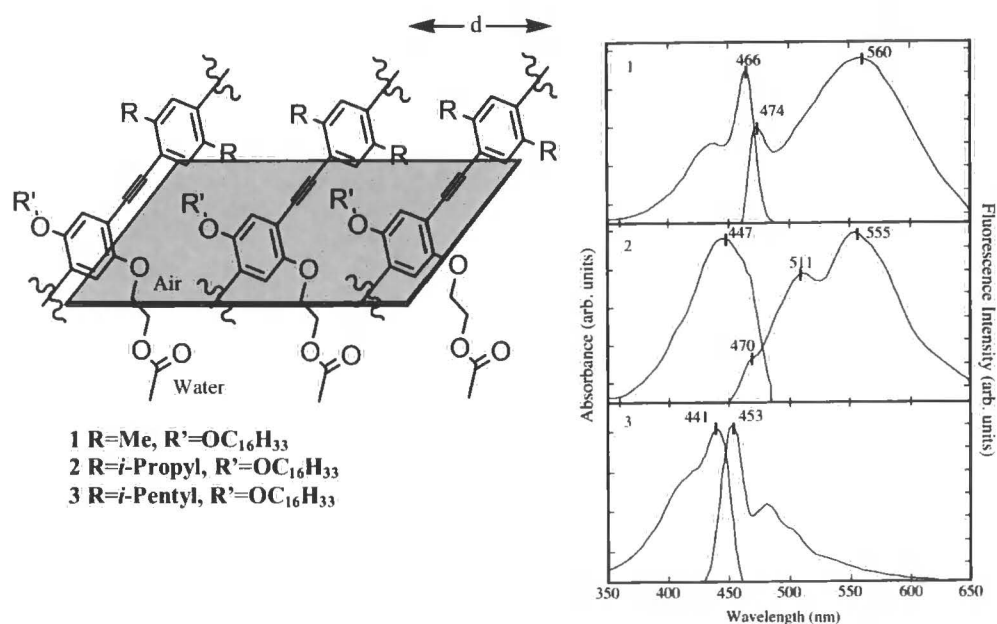
The effects of ring torsion on the photophysical and conductive properties of polyaryl and poly(arylethynylene)s (Figure 1.1) have been studied by many authors. [2, 6, 27, 28] Bunz *et al.* were the first to offer some interpretation of the spectral changes in terms of aryl groups twisting and planarisation while reporting on the thermochromicity of alkyl-substituted polymers similar to Figure 1.1 (left) (where  $R = C_{12}H_{25}$ ). [28, 29] They were able to relate observed shifts in the absorbance spectra to the planarisation of the phenyl rings in the molecular chain by using a series of semiempirical calculations on a model compound in which  $R = CH_3$  (see Figure 1.1 (left)). They noted that the twisting of the phenyl rings from planar to perpendicular orientations to each other increased the HOMO–LUMO (highest occupied molecular orbital–lowest unoccupied molecular orbital) gap. This is a result of the reduction in the delocalisation of the  $\pi$ -system over the molecule because of a decrease in the overlap between the bonding and antibonding  $p$  orbitals around the  $C(sp)-C(sp^2)$  bonds. The fluorescence excitation and emission spectra of the BPEB monomer in stretched polyethylene films, at room and low temperatures, have also been reported to be consistent with a high degree of planarisation. [6] This is evident in the higher intensity and resolution of the red edge of the absorption

bands in the films. Also, the planarisation of 9,10-bis(phenylethynyl)anthracene (Figure 1.1, right), induced at low temperatures in stretched polyethylene films, resulted in significant changes in the ultraviolet (UV) absorption spectrum.[30] Here, the authors concluded that the diminished vibrational spectrum observed in the fluid solution results from the coexistence of several conformations. In contrast, the well resolved absorbance spectrum of the polymer in the stretched film is due to the existence of purely planar conformations.

It is known that the movement of excitons (electron–hole particle pairs) along a conjugated polymer backbone is strongly dependent on the interaction and orientation of an individual polymer relative to its neighbours.[31] Inter–chain distances greatly affect the performance of electrooptical devices based on conjugated polymers. McQuade *et al.*[32] studied the relationship between cofacial interpolymer distances and solid-state photophysics. In both small molecules[33] and polymers[34] the close association of  $\pi$ –systems causes a substantial decrease in the photoluminescence (PL) quantum yield relative to the isolated chromophores. However, minimizing inter–polymer distance is necessary for optimal energy transfer of excitons between polymer chains.[34]

McQuade *et al.* synthesised polymers with varying degrees of side chain bulk as this influences the packing of the polymers at the air–water interface. Figure 1.2 (left) shows the PPEs containing a substitution where the hydrophilic and hydrophobic groups are para to each other producing an edge–on organisation at the interface. Figure 1.2 (right) illustrates the normalised UV–vis and PL spectra of the monolayer Langmuir–Schaefer (LS) films of the three polymers studied. It is observed that PPE films composed of polymers that do not strongly  $\pi$ –stack display a broad absorbance spectrum with a  $\lambda_{\text{max}}$  between 440 nm and 450 nm and a narrowed emission spectrum with a  $\lambda_{\text{max}}$  between 450 nm and 470 nm. The absorption and emission spectra of polymer **3** (with an inter–chain distance of 4.9 Å) are representative of this. In contrast, the UV–vis spectrum of polymer **1** (with an inter–chain distance of 4.0 Å) had a sharp band at 466 nm in the LS film (Figure 1.2 (right)) that is not seen in the solution spectra. This band is attributed to strong inter–chain  $\pi$ –stacking[32] and planarisation of the aryl rings.[29] The LS film of polymer **2** (with an inter-chain distance of 4.4 Å) did not contain a new band but had an emission that was red shifted by 12 nm relative to the solution data. The lack of a

new band is indicative of the isopropyl groups diminishing  $\pi$ -stacking. The solid state PL spectrum of polymer **3** shows much sharper peaks than the PL spectra of polymers **1** and **2** which indicated the inter-chain spacing of **3** is larger than the distance required for the chains to form emissive aggregates and thus **3** had the highest PL quantum yield of 16%. The PL quantum yield values of **1** and **2** were 7% and 12% respectively.



**Figure 1.2** PPEs containing substitution where the hydrophobic and hydrophilic groups are para to each other producing an edge-on organisation (left). Normalised UV-vis and PL spectra of the mono layer Langmuir - Schaefer films of polymers **1-3** cast onto hydrophobic glass slides.[32]

### 1.1.2 Conductivity in conjugated systems

The concept of a molecular wire became a reality nearly 30 years ago with the discovery of metallic conductivity in an organic polymer.[35] The simplest hydrocarbon molecular wire consists of a carbon chain in which all of the atoms are linearly  $sp$ -hybridised. This structure can be modified to include alternating single and double carbon-carbon bonds between terminating end groups. The conjugated chain can also be made up of aromatic rings linked by acetylene units. There is a complete delocalisation of the  $\pi$ -electrons across the polymer chain. The  $\pi$  (bonding) and  $\pi^*$  (antibonding) orbitals form delocalised valence and conduction wave functions, which support mobile charge carriers.[13] Alteration of the groups attached to the ring leads to changes in the properties of the wires. These include changes in solubility or use of 'linking' groups to fix the wires to a particular

substrate. This has the advantage of ‘tuning’ the physical properties of the wire to complement its environment.[36]

It has been shown theoretically that conformational changes caused by the twisting and rotational motions of oligomers, consisting only of aromatic rings, crucially affects electron/hole mobility in molecular wires.[37] The calculations of Berlin *et al.* showed that the coplanar alignment of aromatic rings allowed for the highest mobility of holes.[37] Highly twisted molecules caused a bottleneck for the transport process. The results of theoretical and experimental absorption and emission spectra of oligoarylethynyls having up to ten repeat units indicate that the conjugation length is significantly reduced by the conformational rotations about the C≡C.[2] The energy gap between excited singlet ( $S_1$ ) and triplet ( $T_1$ ) states is reported to be sensitive to ring conformation in short oligomers (<25 Å).[38] A weak confinement of electron and hole causes a dependence of the  $S_1$ – $T_1$  energy gap on different torsion angles. The smallest possible  $S_1$ – $T_1$  energy gap results from fully planar conformations.

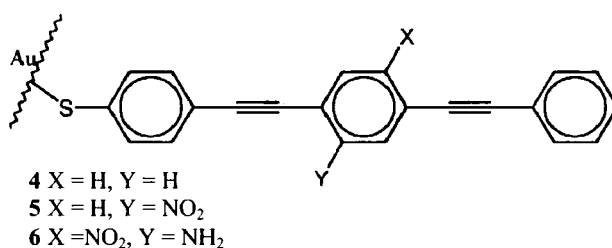
There have been many contributions made towards the understanding of conduction in polymers. Swager *et al.*[39, 40] have reported on conducting polymer-based sensors which transduce reversible, non-covalent and non-redox-dependent molecular recognition events into measurable changes in conductivity. They have also demonstrated how molecular wires can be used to interconnect receptors to produce fluorescent chemosensory systems. Bredas *et al.* have reported that conformational changes in a BPEB derivative resulted in modifications of its conductive properties in the form of a negative differential resistance (NDR) behaviour.[4] This NDR signal was the result of resonant tunnelling processes through the central ring that acted as a tunnel barrier. These properties can be applied to the development of these systems as molecular switches and by extension logic gates and memory circuits.[4] The emissive properties, and hence the electro- and photo-luminescence characteristics, of these materials are dependent on the HOMO–LUMO gap, which varies with the conjugation length.

The rates of interfacial electron-transfer through  $\pi$ -conjugated spacers have been measured by Sachs *et al.*[41, 42] It is expected that the rate of electron-transfer through insulating molecular spacers will strongly depend on the nature of the chemical bonding within the spacer. They determined the standard rate constants,  $k_0$ ,

for interfacial electron–transfer between a gold electrode and a ferrocene group covalently connected to gold by  $\pi$ -conjugated mercapto oligo(phenyleneethynylene) (OPE) spacers. The values of  $k_0$  were found to be orders of magnitude larger for an OPE spacer than for a trans alkane spacer of similar length. The slope of  $-\ln[k_0]$  vs. the spacer length,  $l$ , i.e.  $\beta$ [43, 44], was  $0.57 \pm 0.02 \text{ \AA}^{-1}$  for OPE spacers compared with  $\approx 1.0 \pm 0.02 \text{ \AA}^{-1}$  for saturated spacers.[44] These values were consistent with calculations using the generalised Mulliken–Hush theory.[45] The experimental value ( $0.57 \text{ \AA}^{-1}$ ) of  $\beta$  for the OPE was found to be intermediate between the calculated values for the perpendicular ( $0.97 \text{ \AA}^{-1}$ ) and the coplanar ( $0.39 \text{ \AA}^{-1}$ ) ring geometries and was in closest agreement with the calculated value ( $0.51 \text{ \AA}^{-1}$ ) for a uniform distribution of dihedral angles. Due to the small barrier to rotation, two possible explanations for these observations were put forward. Firstly, in order for homogeneous kinetics to be obtained in the case of the uniform distribution, interconversion among the dihedral angles would have to be rapid compared to the rate of electron–transfer.[46] Alternatively, the dihedral angles may be narrowly distributed about an intermediate value that gives a  $T_{DA}^2$  (square of the donor/acceptor (D/A) electronic coupling elements—which, for a particular process, is related to the corresponding energy gap, dipole moment and the transition moment) value similar to the average value of  $T_{DA}^2$  for the uniform distribution.[42]

More recently Seminario *et al.*[47] theoretically interpreted the conductance switching observed in experiments with oligoarylethynyls isolated in matrices of dodecanethiolate monolayers.[48] The oligomers analysed in the experiment are shown in Figure 1.3. The three oligomers showed conductance bistability, and it was reported that the substituents in molecules **5** and **6** were not a determining factor in their conductance switching.[47] The experiment suggested that restricting conformational changes through environmental arrangements reduces switching between the on and off states, since a well-ordered matrix reduces the rate at which switching occurs, while a poorly ordered matrix yields much more frequent switching. They suggested that rotations of the oligomers take place by a mechanism similar to earlier nanopore studies featuring devices with almost linear behaviour.[49, 50] The mechanism is found to be different from charge–transfer, which is the main mechanism for switching indicated in nanopore studies featuring devices with nonlinear characteristics.[49, 51] The experimental evidence

demonstrated that the switching behaviour of these molecules persists on a much longer time scale (a few hours) than that expected from the predicted rotation barrier. According to earlier calculations[50] the rotational barrier of one ring with respect to another adjacent in the oligomer is  $\approx 4.2 \text{ kJ mol}^{-1}$ . When this barrier is used in molecular dynamics simulations of these molecules assembled on gold surfaces at 300 K, they obtained rotational frequencies of 390 GHz, corresponding to a switching cycle of only 2.56 ps (picoseconds) for a molecule isolated from its neighbours. They argued that longer switching rates are expected because of steric effects when molecules are very close to each other forming a complex.



**Figure 1.3** Oligomers analysed in the scanning tunnelling microscopy experiment.[47]

Seminario *et al.* proved this quantitatively by calculating the rotational barrier of one ring with respect to the other in 1,2-diphenylethyne, when it is forming a complex with an undecane. They found that the torsional barrier increases from  $4.2 \text{ kJ mol}^{-1}$ , for the isolated tolane molecule, to  $159.6 \text{ kJ mol}^{-1}$  for the 1,2-diphenylethyne–undecane complex. From this evidence they concluded that the packing density of the self-assembled monolayer (SAM) affects the switching rates by several orders of magnitude and effectively explained the much longer time scales observed in the experiment. As the scanning tunnelling microscope (STM) was operated at constant-current mode, the height of the tip was directly related to the molecule conductance.[47] The height occurrence distributions showed bimodal behaviour in the conductance, making it possible to estimate on/off ratios. Both experimental and theoretical studies concurred in that high conductance is only possible when all the rings in the molecule are aligned.[47] However, this condition alone does not warrant high conductance. On the other hand, a change in the charge state does not necessarily yield switching and cannot be observed unambiguously above the top benzene ring.[47]



The electronic density and the molecular and electrostatic potential were calculated in order to explain the relationship between the theoretical and electrostatic results by Derosa *et al.*[52] It was determined that frontier molecular orbitals (HOMO, LUMO, and a few in their neighbourhood) fully delocalised along the whole molecule, making the molecule conductive.[52] Charge states rendering a non-conductive molecule show most of the frontier orbitals localised; nevertheless, some of them can show slight delocalisation, leading to a low but non-zero current. However, a perpendicular conformation of at least one ring with respect to another results in the impossibility of having fully delocalised molecular orbitals (MOs), yielding a very low conduction state.[51]

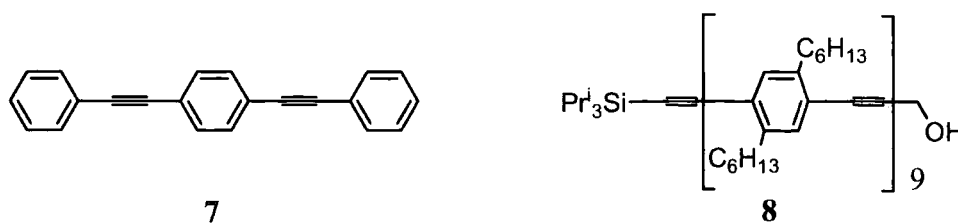
Molecules **4** and **5** in Figure 1.3 were found to conduct in their neutral charge state when theoretically analysed.[49, 51] Since the bias voltage range used in the experiment made both molecules remain uncharged during the whole experiment, only conformational changes intervene in the switching process. In this way, either molecule **4** or **5** switches to the low conductance state when the rings become perpendicular, and the conductance switches to high when the rings are parallel.[47] The experiment also revealed that **5** can be turned off when the applied voltage is increased to 3 or 4 V, and theory showed that it is non-conductive when its charge is -1; thus, when a high voltage is applied, **5** gets charged and stops conducting.[47] However, **4** did not show switching, and it was always conducting as long as its rings were parallel; therefore, according to their theoretical analysis, a higher applied voltage would not have yielded switching in **4**.

Theoretical calculations[51] and other experimental results showed that **6** is non-conductive when neutral, and conductive when charged. The observed switching for this molecule in the experiment was due to changes from the non-conductive planar conformation (when compared to its anion) to the perpendicular conformation, which is even less conductive than the planar conformation. Molecular orbital (MO) analysis showed that the HOMO for the neutral is mostly localised on the central ring but with a slight contribution from the external ring, rendering a low but non-zero conductance.[49, 51] Rotating the central ring fully localises all the frontier orbitals.[49, 51]

## 1.2 1,4-Bis(phenylethynyl)benzene and its derivatives

The interesting photophysical and electronic properties of compounds featuring the 1,4-bis(phenylethynyl)benzene (BPEB—a prototype molecular wire) motif have been studied for some time by several groups.[4, 15, 53-56] It is known that BPEB (**7** in Figure 1.4) is highly fluorescent ( $\Phi_f = 0.85$ [1]) with a lifetime typical of emissive chromophores ( $\tau_f = 0.53$  ns[1]). As mentioned before, the ground-state barrier to rotation about the alkynyl-aryl single bond ( $C(sp)-C(sp^2)$ ) is measured to be  $\approx 2.7$  kJ mol<sup>-1</sup> implying the presence of a range of conformations at room temperature.[5] The challenge has been to engineer control over the molecular conformation in materials based on the elementary framework of **7** (Figure 1.4). Progress has been made in this regard by constraining molecular and polymeric materials in Langmuir films[57], self-assembled mono-layers[58], and through the use of intramolecular tethers.[59, 60] Another goal is the elimination of collisional deactivation in solution and aggregate formation[28], in solution and solid phase, which leads to a reduction in fluorescence and loss in device function through excimer formation. To combat these problems groups have dendromized BPEB[56] or added long flexible alkyl[61] or alkoxy[62] side chains. Along with this is the need for an understanding of how conformational changes, and the addition of side groups to the phenyl ring, affect the photophysical and electronic properties of **7** in the ground and excited states.

McFarland *et al.*[59, 60] showed that the covalent conformational restriction of diphenylacetylene fluorescent chemosensors, with molecular tethers, enhances fluorescence. The enhancement is due purely to a decrease in the rate of non-radiative decay.[59] They went on to demonstrate that restricting the molecular conformation controls the excited state dynamics. This in turn can modulate the fundamental non-radiative decay pathways, intersystem crossing and internal conversion in simple fluorophores.[59]



**Figure 1.4** 1,4-bis(phenylethynyl)benzene (**7**)[1] and oligo(p-phenyleneethynylene) (**8**).[61]

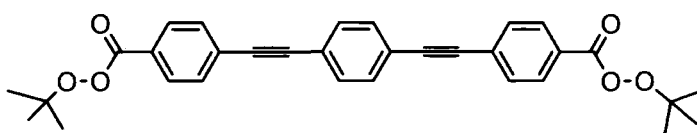
Sluch *et al.*[61] have carried out measurements to establish the dynamic processes of materials based on the framework of **7** (Figure 1.4). They measured the absorption, steady-state and picosecond time-resolved emission of oligo(*p*-phenyleneethynylene) (**8** in Figure 1.4) at ambient and low temperature. In chloroform the absorption and emission spectrum were not mirror images of each other. The underlying Frank–Condon envelope of the absorption spectrum was broadened much more than the emission spectrum. In a rigid matrix of oligostyrene at 77 K, the absorption spectrum narrows while the emission spectrum broadens and, overall, they become roughly mirror symmetric. It was suggested that the spectral features and excited state dynamics of PPEs are dominated by the collective twisting of the phenyl rings relative to the fully planar configuration.[61] As a result of the shallow ground state potential there is a broad thermal distribution of planarity in the ground state. However, in viscous solution the time required for planarisation in the excited state is similar to the fluorescence lifetime (350 ps)[61] and thus the steady-state spectra is a mixture of relaxed and un-relaxed emission.

Time-correlated single photon counting measurements, with an instrument response function of 45 ps and a 397 nm pulse excitation of the PPE in CHCl<sub>3</sub>, showed no shift of the peak in the emission spectrum and a dramatic collapse of the blue edge. The time constant for the collapse was 60 ps, thus the steady-state spectrum is relaxed in this solvent.[61] Measurements done in viscous solution showed the collapse time to be 0.5 ns, which is closer to the fluorescence lifetime, and thus the steady-state spectrum was only partially relaxed. The steady-state and the time-resolved spectra show the rate of relaxation to be dependent on solvent viscosity.

Levitus *et al.*[6] recently reported a series of photophysical measurements of the parent species **7**. They observed significant and systematic shifts in the fluorescence emission spectrum of the molecule with excitation wavelength. The two discrete spectral profiles observed by the group were attributed to planar and twisted conformational isomers of **7**. They also reported an unusually low energy shoulder at 360 nm on the UV-vis profile. These results were disputed. Such behaviour had not been observed in other systems closely related to **7**[3, 55, 63-65] and the fluorescence of **7** has been reported to be independent of wavelength by Grummt *et al.*[66] The re-examination of the spectroscopic properties of **7** indicates that it

behaves in a conventional manner, undergoing emission from the lowest vibrational level of the first excited singlet state at 283 K. In highly viscous, low-temperature glasses, inhomogeneous fluorescence behaviour and wavelength-dependent excitation and emission spectra was observed. This pointed to a slow rate of relaxation of conformers of the excited states compared to the rate of fluorescence.[1] The anomalous excited state behaviour as reported by Levitus *et al.* was later attributed to an impurity in their studied samples.[67]

In a study to characterise the excited state behaviour of compounds with an extended phenylethynyl chromophore, the photodecomposition dynamics of peroxides containing a BPEB chromophore were investigated.[68] Neckers *et al.* used various photophysical techniques in the picosecond and nanosecond time domains in their study. They reported that the peroxide oxygen-oxygen bond of 1,4-bis(2-[4-*tert*-butylperoxycarbonylphenyl]ethynyl)benzene (Figure 1.5) cleaves (with rate  $k = 3.6 \times 10^{11} \text{ s}^{-1}$ ) directly from the singlet excited state (with 60% efficiency) causing a highly reduced fluorescence yield ( $\Phi_f \approx 0.03$ ) and the production of aroyloxyl radicals.[68] This is followed by the decarboxylation of the aroyloxyl radicals. The delocalisation of the excitation energy over the BPEB chromophore induced significant structural changes. This is illustrated by an observed  $100 \text{ cm}^{-1}$  red shift of the acetylene absorption in the transient IR spectra of the excited state of the aroyloxyl radical. The presence of phenyl ester groups attached to the BPEB core accelerates intersystem crossing ( $k = 2.8 \times 10^8 \text{ s}^{-1}$ ) and reduces the quantum yield ( $\Phi_f = 0.82$ ) in comparison to 1,4-bis(4-tolyethynyl)benzene ( $\Phi_f = 0.95$ ).[68]



**Figure 1.5** 1,4-bis(2-[4-*tert*-butylperoxycarbonylphenyl]ethynyl)benzene.[68]

The electronic conduction through a molecular wire can be controlled by the functional groups attached along the backbone, as discussed at the end of the previous section. Tour *et al.*[27, 51, 69, 70] have confirmed conductance on-off switching devices based on BPEB ‘wires’ functionalised with  $\text{NH}_2$  and  $\text{NO}_2$  groups. 2’-Amino-4-ethynylphenyl-4’-ethynylphenyl-5’-nitro-1-benzenthioi (Figure 1.3 6) contains a redox centre and was used in the active self assembled monolayer in an electronic device. They reported a negative differential resistance and an on-off

peak valley ratio in excess of 1000:1.[69] Using quantum mechanical methods, they described the electrical behaviour of  $\pi$ -conjugated BPEB systems functioning as memory devices. The  $\text{NH}_2$  group localises the highest energy occupied electronic states while the  $\text{NO}_2$  group localises the lowest energy unoccupied orbitals of the oligomer systems. These effects result in two complementary molecular memories, each occupying a volume smaller than  $1 \text{ nm}^3$ .[51]

The incorporation of side groups into the BPEB polymer backbone has been reported to improve the fluorescence response to analytes. One such example is in the improvement in the efficiency of 2,4,6-trinitrotoluene (TNT) and 2,4-dinitrotoluene (DNT) detectors.[71] The inclusion of rigid three dimensional pentyptycene into the BPEB motif improved the sensitivity to the analyte by reduced  $\pi$ -stacking and increasing the porosity of their spin-cast films.[71] These improved films exhibited a very rapid fluorescence response to TNT and DNT vapours. Unlike the unsubstituted polymer, the pentyptycene groups provide cavities for analyte binding and an electron-rich polymer back bone enhances the fluorescence response.

BPEB with alkoxy substituents in the 2,5-positions on the phenyl central ring (Figure 1.9, 12) possess unique photophysical and conformational properties. Unlike BPEB, the absorption spectra of the alkoxy substituted BPEB consists of two bands. They are representative of an electronic transition from the low lying HOMO-1/HOMO-2 orbital to the LUMO (high energy band) and a HOMO-LUMO transition (low energy band). This is a result of the dialkoxy substitution which alters the central arene  $\pi$ -orbitals through the resonance interaction with oxygen lone pairs giving rise to similar orbital features for HOMO and HOMO-1/HOMO-2.[72]

The addition of different types of alkoxy side chains in an effort to produce an ordered supramolecular architecture have been reported.[62, 73] The photoluminescent properties, in solution, of these highly emissive polymers with different alkoxy substituents are quite similar to each because they are governed only by the conjugated polymer back bone.[62] While in ordered thin films, the type and length of the alkoxy side chains influences the photoluminescence properties. The variation in the quantum yields with the type of side chain results from the degree of long range order in the films. The formation of new excimer complexes which

provide non-emissive decay channels for the excited state is facilitated by the proximity of the coplanar oriented polymer chains.[62, 74]

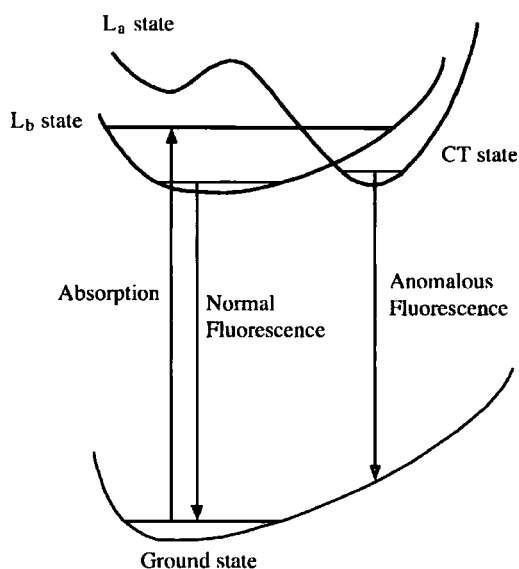
### 1.3 Intramolecular charge-transfer systems

Electrical charge separation forms the basis for numerous present and future developments in the field of molecular-scale photonics[43, 75] including organic conductors and superconductors.[76] Many fluorophores are also capable of forming internal (intramolecular) charge-transfer (ICT) states or a twisted internal charge-transfer (TICT) state upon excitation.[76] For over 50 years the theoretical framework for outer-sphere electron-transfer processes has been studied. The factors that combine to control the rates of electron-transfer are now known through the efforts of Libby[77], Marcus[78, 79], Hush[80] and others. One of the main findings described by Libby was the importance of the Frank-Condon restriction on the electron-transfer process. Libby was able to apply this principle in a qualitative way to some experimental observations.[77]

When the fluorophore contains an electron-donating (e.g. an amino group) and an electron-accepting group (e.g. a cyano group) in weak electronic communication, by way of orbitals localised on an interspersed spacer group, there is an increase in charge separation in the fluorophore following excitation. If the solvent is polar, then the species with charge separation (the ICT state) may become the lowest energy state. In non-polar solvents the species without charge separation, the locally excited (LE) state, may have the lowest energy. The solvent polarity thus governs which state has the lowest energy. Charge separation in some cases is most favourable in a twisted conformation in which the two moieties involved in charge-transfer (the donor and acceptor groups) are orbitally decoupled on the fluorophore to form a twisted intramolecular charge-transfer (TICT) state.[76] A large spectral shift to longer wavelengths is always associated with ICT and TICT states.[81, 82] It has come to light that many TICT states are non-luminescent and responsible for the rapid non-radiative decay of many important fluorescent dyes.[76]

Such charge-transfer emission can be observed in the molecule *p-N,N*-dimethylaminobenzonitrile (DMABN), which was observed to emit dual fluorescence over 40 years ago.[83] Its fluorescence consisted of two bands, one being 'normal' (referred to as the B band—an emission from the  $^1L_b$ -type state) for

closely related benzene derivatives, the other, at considerably lower energy, being an ‘anomalous’ band (Figure 1.6).[76] It was proposed that a solvent–induced reversal of excited states had occurred.[83] The anomalous band was assigned to fluorescence from the more polar  $^1L_a$ -type state (or A band) which is preferentially stabilised by solvation.[76] This assignment only holds true for DMABN. Grabowski *et al.* later suggested that the rules governing dual fluorescence involved a dynamic relaxation of DMABN with internal twisting of the dimethylamino group, coupled with electron–transfer from the amino nitrogen to the  $\pi_z^*$  orbital extending over the entire benzonitrile group.[84] There was some initial controversy over this interpretation of the data. Grabowski and others have since produced a significant amount of experimental proof to support this TICT hypothesis.[82, 84–87] Grabowski *et al.* synthesized model compounds of DMABN with the  $N(CH_3)_2$  group rigidly held in the planar or perpendicular position.[84] All the evidence indicates that the perpendicular position of the  $N(CH_3)_2$  group is associated with the low energy emission from the  $^1L_a$ -type state. The more conjugated *p*-*N,N*-dimethylamino-*p*'-cyano-diphenylacetylene also has photoinduced IC separation but no dual emission.[88] In polar solvents only the broad low energy emission from the ICT state is observed.



**Figure 1.6** Schematic energy level diagram of molecules exhibiting dual fluorescence. The reaction coordinated is the twist angle.[89]

Electron–transfer through long bridges is thought to proceed via virtual states associated with the spacer unit in what is called the superexchange mechanism.[79, 90, 91] In this mechanism the electron or hole is transferred in a single step from the

donor to the acceptor and the bridge is used as a medium of electronic coupling. Thus, electron-transfer uses the bridge LUMO whilst the hole transfer borrows electrons from the HOMO of the bridge.[79] The redox potential of the bridge does not change and the probability of transferring an electron/hole from donor to acceptor generally decreases exponentially with distance.[92] The important aspect of superexchange theory is that the coupling element ( $V_{DA}$ ) is related to the energy gap ( $\Delta E_{DB}$ ) between active orbitals on the donor and on the bridge (Equation 1.1).[79, 93]

$$V_{DA} = \frac{\alpha_{DA}\alpha_{BA}}{\Delta E_{DB}}$$

**Equation 1.1**  $V_{DA}$  – electronic matrix coupling element; atomic orbital coefficients describing the coupling between the donor and the first member of the bridge ( $\alpha_{DB}$ ) and between the last member of the bridge and the acceptor ( $\alpha_{BA}$ );  $\Delta E_{DB}$  – energy gap between the orbitals on the donor and on the bridge.[79]

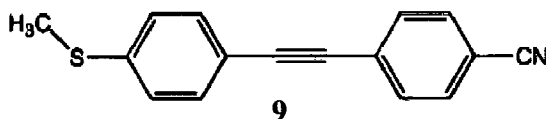
The larger the energy gap the weaker the electronic coupling and the slower the rate of electronic transfer.[79] Research into the role of the spacer unit in through-bond electron-transfer processes has determined that the dynamics of such events are heavily dependent on the structure of the bridging unit.[94] The low frequency torsional motions in long, conjugated bridging molecules significantly affect long distance electron-transfer. The rate of CT through an insulating spacer is dependent on the nature of the chemical bonding of the spacer.

Molecular-scale photonic systems are concerned with using pulsed light to drive intramolecular electron-transfer along a preferred pathway, leading to long-range charge separation or rapid signal transmission.[95] Understanding how to facilitate rapid charge separation between isolated terminals by designing the appropriate spacer unit is vital to the development and exploitation of prototypic systems.

4-Cyano-(4'-methylthio)diphenylacetylene (**9**) is a short molecular dyad with a sulphide-based donor and a cyano-based acceptor separated by an alkynyl spacer (Figure 1.7). It has been the subject of both theoretical and experimental study. It is known that UV illumination causes excitation to a polar singlet excited state that undergoes charge-recombination fluorescence and intersystem crossing to a triplet state.[96] However, the exact mechanism by which charge separation and recombination occurs are still unknown. Recently Harriman *et al.*[95] modelled the intramolecular charge-transfer in this molecule with the intension of better



representing the charge-transfer step and assigning meaningful structures for the various metastable species.



**Figure 1.7** 4-cyano-(4'-methylthio)diphenylacetylene (**9**).[95]

The photophysical properties of **9** can be described in terms of a 4-state model. Here the ground state is assumed to be non-polar. There are two singlet excited states of similar excitation energy. It is believed that one of these states has a strong charge-transfer character while the other has a polarity similar to that of the ground state. The lowest energy excited singlet state in polar solvents is the most likely to be the charge-transfer state (CTS). This species will undergo charge-recombination fluorescence with high probability. The triplet state CTS is similar in energy to the non-polar triplet state. However the chief non-radiative decay channel involves population of the non-polar triplet state. The various energy gaps can be tuned by taking advantage of the sensitivity of the singlet CTS energy to solvent polarity. Understanding effects of increasing chain length on the connector and the dynamics of the forward and reverse charge-transfer is significant for the application of similar compounds as molecular scale wires or as light harvesting, photovoltaic materials.

Theoretical studies of **9** in different solvents concluded that in polar solvents the phenyl rings were perpendicular to each other.[95] This results in the localisation of the excitation energy. It was also concluded that the charge-transfer fluorescence occurred from the twisted form of the CTS state. These findings correctly predicted the solvent effect and gave a good quantitative description of the absorption and fluorescence spectral shifts. The large Stokes shift seen in polar solvents illustrated the importance of twisting within the excited singlet state.

Harriman's quantum chemical investigation sought to explain the photophysical properties of the donor-acceptor dyad **9**. The experimental data[96] indicates that the first excited singlet state undergoes a significant change in geometry and polarity following its initial formation by UV excitation. They predicted a time-dependent Stokes shift of *ca.* 7000  $\text{cm}^{-1}$  in polar solvents. Their calculations also suggested that charge-recombination fluorescence and intersystem crossing are likely to compete with direct recombination as the path by which deactivation of the relaxed CTS

occurs. It is expected that relaxation of the planar CTS into the final twisted CTS should be rapid due to the ease of rotation around the central alkynylene bond.

The photophysics of **9** has been described in terms of the Marcus electron-transfer theory[97] and can be discussed in terms of the Englman-Jortner energy-gap law[98] for a closely-coupled system. This best describes compounds that undergo a large change in dipole moment upon excitation and have valuable properties for non-linear optical devices. The rate constant for intersystem crossing within the CTS as calculated by the Marcus theory ( $2.7 \times 10^8 \text{ s}^{-1}$ ) was found to be comparable to the experimental rate constant for radiative decay of the CTS ( $4 \times 10^8 \text{ s}^{-1}$ ). Thus the deactivation of the CTS can be accounted for in terms of triplet formation and charge-transfer fluorescence.

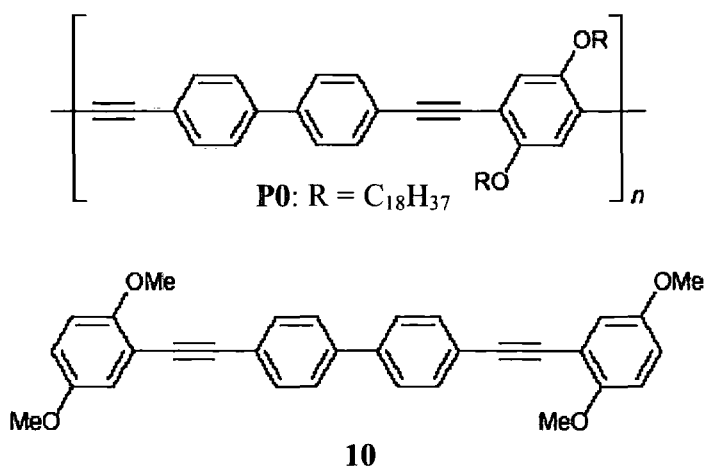
The Englman-Jortner model better represents the non-radiative processes as it takes into account the nature of the various photophysical processes undertaken by **9**. It considers the CTS as a polar excited state for which the rate constant for non-radiative decay ( $k_{nr}$ ) is expressed in terms of the electron-vibrational coupling matrix element and the single averaged vibrational frequency coupled to the non-radiative process. The energy gap between the relaxed CTS and the ground state is much larger than the energy gap between the CTS and the triplet state resulting in direct charge recombination being less significant. The averaged vibrational frequency is likely to be coupled to the intramolecular twisting process but there is not enough detailed information about the magnitude of this term to completely evaluate this system.

The optimisation of the amount of charge-transfer (CT) in  $\pi$ -conjugated push-pull systems is a critical issue in the design of non-linear optical (NLO) materials.[99] CT is important for NLO response and the delocalised  $\pi$ -system in conjugated organic compounds is considered a good bridge for CT from donor to acceptor.[79] Several such  $\pi$ -conjugated systems such as benzene, stilbene, thiophene, polyene and polyyne have been extensively studied. According to Lee *et al.*[100] the polyenic chain is a better bridge for long paths while the polyynic chain is better for short bridges because of the mobility of the  $\pi$ -electrons.

#### 1.4 The triplet state of poly(arylethylenes)

Arylacetylenes, exhibiting  $\pi$ -conjugation do not display long-lived triplet emissions (phosphorescence) at room temperature. Consequently the triplet excited states of arylacetylide groups and PPEs are difficult to analyse and thus have not been fully explained. This lack of emission is due to the excited triplet state emission to the singlet ground state being forbidden by spin selection rules. To enhance triplet state emission some authors have incorporated heavy metal atoms, such as platinum, into the polymer chain by ligation.[101-104] This introduces spin orbit coupling and enhances triplet excitation. While this modification allowed for triplet ( $\pi$ ,  $\pi^*$ ) emission at low temperature, the low energy d-d excited state of Pt(II) provides a facile means for non-radiative decay and makes observing the triplet emission in solution difficult.[105] To overcome this Au(I) has been used instead, because the  $d^{10}$  closed-shell configuration does not allow low lying d-d excited states.[105]

The triplet excited states of some organic arylacetylides were probed by Chao *et al.*[105] in order to establish a structure-function relationship and to shed light on the photophysical nature of arylacetylene oligomer and polymer materials. They were able to enhance the organic triplet emission of the arylacetylide groups at ambient conditions by ligation to a  $[\text{Au}(\text{PCy}_3)]^+$  ( $\text{PCy}_3$ -tricyclohexylphosphine) fragment. The ligation induces intersystem crossing from singlet to triplet states. They demonstrated the tunability of the triplet ( $\pi$ ,  $\pi^*$ ) emission, and hence the excited state reduction potential, by modification of the chain length. As the chain length increased the phosphorescence intensity decreased. This was explained in terms of the energy-gap law. It states that the non-radiative decay rate increases exponentially on decreasing the energy gap between the two electronic states.[106] They determined that there was a linear relationship between the singlet and triplet state energies. Delayed singlet ( $\pi$ ,  $\pi^*$ ) fluorescence seen in extended arylacetylide units was proposed to be the result of a triplet-triplet annihilation mechanism. The triplet excited state reduction potentials of arylacetylides are very negative (-1.80 to -1.17 V) and imply that they are strong photoreductants.



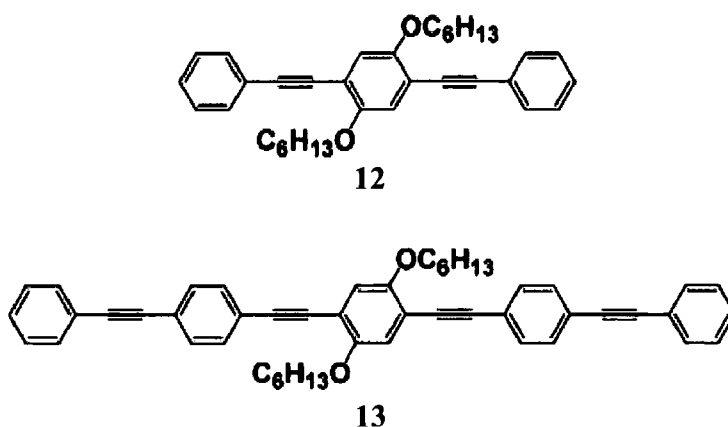
**Figure 1.8** P0 and 10.[107]

Schanze *et al.*[107] reported one of the first studies of the photophysical properties of the excited singlet and triplet states of an arylenethynylene polymer (**P0**) and model compound **10** (Figure 1.8) not bound to a metal. They observed long lived transients in solutions of **P0** and **10**, equal to 142  $\mu$ s and 169  $\mu$ s respectively, which they assigned to a triplet state. A bleaching of the ground state absorption band at  $\lambda_{\text{max}}(\mathbf{P0}) = 410$  nm and  $\lambda_{\text{max}}(\mathbf{10}) = 360$  nm in the triplet state difference absorption spectra of the two compounds is accompanied by a broad triplet–triplet (T-T) absorption band extending into the longer wavelength region (500–700 nm). The marked similarities between the difference absorption spectra of **P0** and **10** implied the triplet state electronic structures of the polymer and the model compound are quite similar. From Stern–Volmer quenching studies (using a series of triplet acceptors of varying energy) they determined the triplet energies ( $E_T$ ) of **P0** and **10** to be 17700 and 17500  $\text{cm}^{-1} \pm 5\%$  respectively.[107] The triplet state quantum yield ( $\Phi_T$ ) was determined as  $\Phi_T(\mathbf{10}) = 0.05$  and  $\Phi_T(\mathbf{P0}) = 0.12$ [107], using time-resolved thermal lensing[108, 109] and verified by photoacoustic calorimetry.[110] The lower singlet ( $E_S$ )–triplet splitting energy (defined as  $E_S - E_T$ ) in **P0** compared to **10** (5600 vs. 6500  $\text{cm}^{-1}$ ) suggested the electron exchange energy was smaller in the polymer.[111] This was presumed to be due to the delocalisation in the LUMO (and/or the HOMO) for the  $\pi^* \leftarrow \pi$  transition being greater in **P0** than in **10**.[107]

More recently other authors have characterised the triplet state of the BPEB chromophore using time–resolved spectroscopy techniques.[68, 112] Polyansky *et al.*[68] reported on the triplet excited state of the BPEB chromophore in 1,4-bis(2-[4-phenyloxycarbonylphenyl]ethynyl)benzene (**11**) from time–resolved infrared (IR)

experiments. At a laser power of 5 mJ / pulse they observed the bleaching of the ground state at  $1735\text{ cm}^{-1}$  accompanied by a new transient absorption band red shifted by *ca.*  $20\text{ cm}^{-1}$ . [68] A bleaching at  $1604\text{ cm}^{-1}$  assigned to the C-C stretch was also observed. These bands were assigned to the triplet state absorption of BPEB. The authors [68] concluded that the electron density in the triplet state is delocalised primarily through the central BPEB chromophore partially reducing the bond order of the C-C bond and driving the IR absorption to lower energies. This was implied by the shift of the phenyl C-C stretch being four times greater than that of the carbonyl vibrational shift.

Sudeep *et al.* [112] have also characterised the triplet states of model compounds **12** and **13** from nanosecond laser flash photolysis experiments (Figure 1.9). They found the triplet state absorption maximum of **12** and **13** to be 520 and 660 nm respectively. The lifetimes of the triplet states were  $140\ \mu\text{s}$  for **12** and  $218\ \mu\text{s}$  for **13**. They demonstrated the ability of **12** to sensitize the triplet state of a squaraine dye by the triplet-triplet energy transfer method. Compound **12** is shown to be able to act as a triplet energy donor to molecules having lower triplet energy. [112]



**Figure 1.9** **12** and **13**. [112]

Triplet excited states, being long-lived, can initiate degradation via singlet oxygen generation and/or electron-transfer processes resulting from self-quenching processes. [112] Thus, it is important to know the intermolecular interactions of the triplet excited state in order to determine the long-term operation of optoelectronic or luminescent devices. Sudeep *et al.* [112] investigated two self-quenching processes (i) quenching of the **12** and **13** triplet by ground-state molecules and (ii) T-T annihilation. They concluded that the decay of the triplet is not significantly affected by ground state molecules at low concentrations ( $< 10\ \mu\text{M}$ ). It was admitted that this

type of quenching could be a major contributor in films with high local concentrations of dye. Also if **12** were used as a bridging unit, unintended excitation could affect the course of electron-transfer.[112] At triplet concentrations  $\geq 5 \mu\text{M}$  the decay is observed to be dominated by a second order T-T annihilation process.

### **Aims**

The main objectives of this study are: (1) to characterise the photophysical and electronic properties, in the ground and excited state, of the model molecular wire compound BPEB and a selection of its derivatives which are divided into two groups; (i) BPEBs with branched alkane substituents and heavy atom substituents; and (ii) BPEBs with donor-acceptor, donor-donor or acceptor-acceptor groups in para positions at either end of the linker unit.

(2) to characterise some of the photophysical properties of 9,10-bis(phenylethynyl)anthracene (BPEA) and a selection of its derivatives having donor-donor or acceptor-acceptor groups in para positions at either end of the linker unit.

(3) the characterisation of some of the photophysical and electronic properties of 2,5-bis(phenylethynyl)thiophene, 1,4-bis(2-thienylethynyl)benzene and 2,5-bis(2-thienylethynyl)thiophene in the ground state and excited state. Their triplet excited states are also probed to determine if there are any changes in the bonding order in this excited state.

## REFERENCES

1. A. Beeby, K. Findlay, P. J. Low and T. B. Marder, "A re-evaluation of the photophysical properties of 1,4-bis(phenylethynyl)benzene: A model for poly(phenyleneethynylene)." *Journal Of The American Chemical Society*, 2002, **124**, 8280-8284.
2. R. J. Magyar, S. Tretiak, Y. Gao, H. L. Wang and A. P. Shreve, "A joint theoretical and experimental study of phenylene-acetylene molecular wires." *Chemical Physics Letters*, 2005, **401**, 149-156.
3. M. S. Khan, A. K. Kakkar, N. J. Long, J. Lewis, P. Raithby, P. Nguyen, T. B. Marder, F. Wittmann and R. H. Friend, "Synthesis and optical spectroscopy of linear long-chain di-terminal alkynes and their Pt-sigma-acetylide polymeric complexes." *Journal Of Materials Chemistry*, 1994, **4**, 1227-1232.
4. J. Cornil, Y. Karzazi and J. L. Bredas, "Negative differential resistance in phenylene ethynylene oligomers." *Journal Of The American Chemical Society*, 2002, **124**, 3516-3517.
5. S. J. Greaves, E. L. Flynn, E. L. Fitcher, E. Wrede, D. P. Lydon, P. J. Low, S. R. Rutter and A. Beeby, "Cavity ring-down spectroscopy of the torsional motions of 1,4-bis(phenylethynyl)benzene." *Journal Of Physical Chemistry A*, 2006, **110**, 2114-2121.
6. M. Levitus, K. Schmieder, H. Ricks, K. D. Shimizu, U. H. F. Bunz and M. A. Garcia-Garibay, "Steps to demarcate the effects of chromophore aggregation and planarization in poly(phenyleneethynylene)s. 1. Rotationally interrupted conjugation in the excited states of 1,4-bis(phenylethynyl)benzene." *Journal Of The American Chemical Society*, 2001, **123**, 4259-4265.
7. A. Kraft, A. C. Grimsdale and A. B. Holmes, "Electroluminescent conjugated polymers-seeing polymers in a new light." *Angewandte Chemie International Edition*, 1998, **37**, 402-428.
8. A. Bernanose, "Electroluminescence of organic compounds." *British Journal Of Applied Physics*, 1955, S54-S56.
9. M. Sano, M. Pope and H. Kallmann, "Electroluminescence and band gap in anthracene." *Journal Of Chemical Physics*, 1965, **43**, 2920-2921.
10. C. W. Tang and S. A. Vanslyke, "Organic electroluminescent diodes." *Applied Physics Letters*, 1987, **51**, 913-915.
11. J. H. Burroughes, D. D. C. Bradley, A. R. Brown, R. N. Marks, K. Mackay, R. H. Friend, P. L. Burns and A. B. Holmes, "Light-emitting diodes based on conjugated polymers." *Nature*, 1990, **347**, 539-541.
12. M. P. Aldred, P. Vlachos, A. E. A. Contoret, S. R. Farrar, W. Chung-Tsoi, B. Mansoor, K. L. Woon, R. Hudson, S. M. Kelly, and M. O'Neill, "Linearly polarised organic light-emitting diodes (OLEDs): synthesis and characterisation of

a novel hole-transporting photoalignment copolymer." *Journal Of Materials Chemistry*, 2005, **15**, 3208-3213.

13. R. H. Friend, R. W. Gymer, A. B. Holmes, J. H. Burroughes, R. N. Marks, C. Taliani, D. D. C. Bradley, D. A. D. Santos, J. L. Brédas, M. Lögdlund, and W. R. Salaneck, "Electroluminescence in conjugated polymers." *Nature*, 1999, **397**, 121-128.
14. S. M. Jeong, W. H. Koo, S. H. Choi, S. J. Jo, H. K. Baik, S. J. Lee and K. M. Song, "Charge injection and transport model in organic light-emitting diodes with aluminum cathodes prepared by ion beam assisted deposition." *Solid-State Electronics*, 2005, **49**, 205-212.
15. U. H. F. Bunz, "Poly(aryleneethynylene)s: Syntheses, properties, structures, and applications." *Chemical Reviews*, 2000, **100**, 1605-1644.
16. J. S. Moore, "Shape-persistent molecular architectures of nanoscale dimension." *Accounts Of Chemical Research*, 1997, **30**, 402-413.
17. S. Hoyer, "Shape-persistent macrocycles: From molecules to materials." *Chemistry-A European Journal*, 2004, **10**, 1320-1329.
18. K. Kim, S. Webster, N. Levi, D. L. Carroll, M. R. Pinto and K. S. Schanze, "Luminescent core-shell photonic crystals from poly(phenylene ethynylene) coated silica spheres." *Langmuir*, 2005, **21**, 5207-5211.
19. L. M. Ding, Z. X. Lu, D. A. M. Egbe and F. E. Karasz, "Structure-morphology-electroluminescence relationship for hybrid conjugated polymers." *Macromolecules*, 2004, **37**, 10031-10035.
20. I. A. Levitsky, J. S. Kim and T. M. Swager, "Energy migration in a poly(phenylene ethynylene): Determination of interpolymer transport in anisotropic Langmuir-Blodgett films." *Journal Of The American Chemical Society*, 1999, **121**, 1466-1472.
21. J. M. Tour, L. Jones, D. L. Pearson, J. J. S. Lamba, T. P. Burgin, G. M. Whitesides, D. L. Allara, A. N. Parikh and S. V. Atre, "Self-assembled monolayers and multilayers of conjugated thiols, alpha,omega-dithiols, and thioacetyl-containing adsorbates - understanding attachments between potential molecular wires and gold surfaces." *Journal Of The American Chemical Society*, 1995, **117**, 9529-9534.
22. E. Arias-Marin, J. C. Arnault, D. Guillon, T. Maillou, J. Le Moigne, B. Geffroy and J. M. Nunzi, "Amphiphilic phenylene-ethynylene oligomers in Langmuir-Blodgett films. Self-assembling multilayers for electroluminescent devices." *Langmuir*, 2000, **16**, 4309-4318.
23. V. A. Sipachev, L. S. Khaikin, O. E. Grikina, V. S. Nikitin and M. Traetteberg, "Structure, spectra and internal rotation of bis(trimethylsilyl) acetylene: spectral analysis by scaling quantum-chemical force fields and two methods for calculating vibrational effects." *Journal of Molecular Structure*, 2000, **523**, 1-22.



24. S. Saebø, J. Almlof, J. E. Boggs and J. G. Stark, "Two approaches to the computational determination of molecular structure: the torsional angle in tolane and the effect of fluorination on the structure of oxirane." *Journal of Molecular Structure: THEOCHEM*, 1989, **200**, 361-373.
25. A. V. Abramenkov, A. Almenningen, B. N. Cyvin, S. J. Cyvin, T. Jonvik, L. S. Khaikin, C. Romming and L. V. Vilkov, "Internal rotation in tolane-molecular structure in gas and crystal phases." *Acta Chemica Scandinavica Series A-Physical And Inorganic Chemistry*, 1988, **42**, 674-684.
26. K. Inoue, H. Takeuchi and S. Konaka, "Molecular structures of related compounds of mesogens studied by H-1 NMR using a liquid crystal solvent: Tolan and trans-azobenzene." *Journal of Physical Chemistry A*, 2001, **105**, 6711-6716.
27. C. Majumder, T. Briere, H. Mizuseki and Y. Kawazoe, "Molecular resistance in a molecular diode: A case study of the substituted phenylethynyl oligomer." *Journal Of Physical Chemistry A*, 2002, **106**, 7911-7914.
28. C. E. Halkyard, M. E. Rampey, L. Kloppenburg, S. L. Studer-Martinez and U. H. F. Bunz, "Evidence of aggregate formation for 2,5-dialkylpoly(p-phenyleneethynyls) in solution and thin films." *Macromolecules*, 1998, **31**, 8655-8659.
29. T. Miteva, L. Palmer, L. Kloppenburg, D. Neher and U. H. F. Bunz, "Interplay of thermochromicity and liquid crystalline behaviour in poly(p-phenyleneethynyl)s:  $\pi$ - $\pi$  interactions or planarization of the conjugated backbone?" *Macromolecules*, 2000, **33**, 652-654.
30. M. Levitus and M. A. Garcia-Garibay, "Polarized electronic spectroscopy and photophysical properties of 9,10-bis(phenylethynyl)anthracene." *Journal Of Physical Chemistry A*, 2000, **104**, 8632-8637.
31. M. Grell and D. D. C. Bradley, "Polarized luminescence from oriented molecular materials." *Advanced Materials*, 1999, **11**, 895-905.
32. D. T. McQuade, J. Kim and T. M. Swager, "Two-dimensional conjugated polymer assemblies: Interchain spacing for control of photophysics." *Journal Of The American Chemical Society*, 2000, **122**, 5885-5886.
33. N. J. Turro, "Modern Molecular Photochemistry", University Science Books, Mill Valley California, 1991.
34. J. A. Osaheni and S. A. Jenekhe, "Effects of molecular-structure on the electroactive and optical-properties of conjugated rigid-rod poly(benzobisazoles)." *Chemistry Of Materials*, 1995, **7**, 672-682.
35. C. K. Chiang, C. R. Fincher, Y. W. Park, A. J. Heeger, H. Shirakawa, E. J. Louis, S. C. Gau and A. G. Macdiarmid, "Electrical conductivity in doped polyacetylene." *Physical Review Letters*, 1977, **39**, 1098.

36. N. Robertson and C. A. McGowan, "A comparison of potential molecular wires as components for molecular electronics." *Chemical Society Reviews*, 2003, **32**, 96-103.
37. Y. A. Berlin, G. R. Hutchison, P. Rempala, M. A. Ratner and J. Michl, "Charge hopping in molecular wires as a sequence of electron-transfer reactions." *Journal Of Physical Chemistry A*, 2003, **107**, 3970-3980.
38. A. Köhler and D. Beljonne, "The singlet-triplet exchange energy in conjugated polymers." *Advanced Functional Materials*, 2004, **14**, 11-18.
39. Q. Zhou and T. M. Swager, "Fluorescent chemosensors based on energy migration in conjugated polymers: The molecular wire approach to increased sensitivity." *Journal Of The American Chemical Society*, 1995, 12593-12602.
40. M. J. Marsella, P. J. Carroll and T. M. Swager, "Design of chemoresistive sensory materials - Polythiophene-based pseudopolyrotaxanes." *Journal Of The American Chemical Society*, 1995, **117**, 9832-9841.
41. M. D. Newton, "Quantum chemical probes of electron-transfer kinetics - The nature of donor-acceptor interactions." *Chemical Reviews*, 1991, **91**, 767-792.
42. S. B. Sachs, S. P. Dudek, R. P. Hsung, L. R. Sita, J. F. Smalley, M. D. Newton, S. W. Feldberg and C. E. D. Chidsey, "Rates of interfacial electron transfer through  $\pi$ -conjugated spacers." *Journal Of The American Chemical Society*, 1997, **119**, 10563-10564.
43. C. X. Liang and M. D. Newton, "Ab initio studies of electron-transfer.2. Pathway analysis for homologous organic spacers." *Journal Of Physical Chemistry*, 1993, **97**, 3199-3211.
44. J. F. Smalley, S. W. Feldberg, C. E. D. Chidsey, M. R. Linford, M. D. Newton and Y. P. Liu, "The kinetics of electron-transfer through ferrocene-terminated alkanethiol monolayers on gold." *Journal Of Physical Chemistry*, 1995, **99**, 13141-13149.
45. R. J. Cave and M. D. Newton, "Generalization of the Mulliken-Hush treatment for the calculation of electron transfer matrix elements." *Chemical Physics Letters*, 1996, **249**, 15-19.
46. J. Tang, "Effects of a fluctuating electronic coupling matrix element on electron-transfer rate." *Journal Of Chemical Physics*, 1993, **98**, 6263-6266.
47. J. M. Seminario, P. A. Derosa and J. L. Bastos, "Theoretical interpretation of switching in experiments with single molecules." *Journal Of The American Chemical Society*, 2002, 10266-10267.
48. Z. J. Donhauser, B. A. Mantooth, K. F. Kelly, L. A. Bumm, J. D. Monnell, J. J. Stapleton, D. W. Price, A. M. Rawlett, D. L. Allara, J. M. Tour, and P. S. Weiss,

- "Conductance switching in single molecules through conformational changes." *Science*, 2001, **292**, 2303-2307.
49. J. M. Seminario, A. G. Zacarias and J. M. Tour, "Theoretical study of a molecular resonant tunneling diode." *Journal Of The American Chemical Society*, 2000, **122**, 3015-3020.
50. J. M. Seminario, A. G. Zacarias and J. M. Tour, "Theoretical interpretation of conductivity measurements of a thiotolane sandwich. A molecular scale electronic controller." *Journal Of The American Chemical Society*, 1998, **120**, 3970-3974.
51. J. M. Seminario, A. G. Zacarias and P. A. Derosa, "Theoretical analysis of complementary molecular memory devices." *Journal Of Physical Chemistry A*, 2001, **105**, 791-795.
52. P. A. Derosa and J. M. Seminario, "Electron transport through single molecules: Scattering treatment using density functional and green function theories." *Journal Of Physical Chemistry B*, 2001, **105**, 471-481.
53. C. Y. Dai, P. Nguyen, T. B. Marder, A. J. Scott, W. Clegg and C. Viney, "Control of single crystal structure and liquid crystal phase behaviour via arene-perfluoroarene interactions." *Chemical Communications*, 1999, 2493-2494.
54. C. Zhou, M. R. Deshpande, M. A. Reed, L. Jones and J. M. Tour, "Nanoscale metal self-assembled monolayer metal heterostructures." *Applied Physics Letters*, 1997, **71**, 611-613.
55. M. Biswas, P. Nguyen, T. B. Marder and L. R. Khundkar, "Unusual size dependence of nonradiative charge recombination rates in acetylene-bridged compounds." *Journal of Physical Chemistry A*, 1997, 1689-1695.
56. B. C. Englert, M. D. Smith, K. I. Hardcastle and U. H. F. Bunz, "Jacketed poly(p-phenyleneethynylene): Nonaggregating conjugated polymers as blue-emitting rods." *Macromolecules*, 2004, **37**, 8212-8221.
57. J. Kim and T. M. Swager, "Control of conformational and interpolymer effects in conjugated polymers." *Nature*, 2001, **411**, 1030-1034.
58. W. A. Reinert, L. Jones, T. P. Burgin, C. W. Zhou, C. J. Muller, M. R. Deshpande, M. A. Reed and J. M. Tour, "Molecular scale electronics: syntheses and testing." *Nanotechnology*, 1998, **9**, 246-250.
59. S. A. Mcfarland and N. S. Finney, "Fluorescent signaling based on control of excited state dynamics. Biarylacetylene fluorescent chemosensors." *Journal Of The American Chemical Society*, 2002, **124**, 1178-1179.
60. G. T. Crisp and T. P. Bubner, "Preparation of sterically constrained arylalkynes." *Tetrahedron*, 1997, **53**, 11881-11898.

61. M. I. Sluch, A. Godt, U. H. F. Bunz and M. A. Berg, "Excited-state dynamics of oligo(*p*-phenyleneethynylene): Quadratic coupling and torsional motions." *Journal Of The American Chemical Society*, 2001, **123**, 6447-6448.
62. C. Weder and M. S. Wrighton, "Efficient solid-state photoluminescence in new poly(2,5-dialkoxy-*p*-phenyleneethynylene)s." *Macromolecules*, 1996, **29**, 5157-5165.
63. P. Nguyen, Y. A. Zheng, L. Agocs, G. Lesley and T. B. Marder, "Synthesis of symmetrical and unsymmetric 1,4-bis(*p*-R-phenylethynyl)benzenes via palladium copper-catalyzed cross-coupling and comments on the coupling of aryl halides with terminal alkynes." *Inorganica Chimica Acta*, 1994, **220**, 289-296.
64. P. Nguyen, S. Todd, D. Vandenbiggelaar, N. J. Taylor, T. B. Marder, F. Wittmann and R. H. Friend, "Facile route to highly fluorescent 9,10-bis(*p*-R-phenylethynyl)anthracene chromophores via Palladium-Copper catalyzed cross-coupling." *Synlett*, 1994, 299-301.
65. P. Nguyen, G. Lesley, T. B. Marder, I. Ledoux and J. Zyss, "Second-order nonlinear optical properties of push-pull bis(phenylethynyl)benzenes and unsymmetric platinum bis(phenylacetylide) complexes." *Chemistry Of Materials*, 1997, **9**, 406-408.
66. E. Birckner, U.-W. Grummt, A. H. Göller, T. Pautzsch, D. A. M. Egbe, M. Al-Higari and E. Klemm, "Photophysics of arylene and heteroaryleneethynylenes." *Journal Of Physical Chemistry A*, 2001, 10307-10315.
67. M. Levitus, K. Schmieder, H. Ricks, K. D. Shimizu, U. H. F. Bunz and M. A. Garcia-Garibay, "Steps to demarcate the effects of chromophore aggregation and planarization in poly(phenyleneethynylene)s. 1. Rotationally interrupted conjugation in the excited states of 1,4-bis(phenylethynyl)benzene (vol 123, pg 4259, 2001)." *Journal Of The American Chemical Society*, 2002, **124**, 8181-8181.
68. D. E. Polyansky, E. O. Danilov, S. V. Voskresensky, M. A. J. Rodgers and D. C. Neckers, "Photodecomposition of peroxides containing a 1,4-bis(phenylethynyl)benzene chromophore." *Journal of Physical Chemistry A*, 2006, **110**, 4969-4978.
69. J. Chen, M. A. Reed, A. M. Rawlett and J. M. Tour, "Large on-off ratios and negative differential resistance in a molecular electronic device." *Science*, 1999, **286**, 1550-1552.
70. J. M. Tour, A. M. Rawlett, M. Kozaki, Y. X. Yao, R. C. Jagessar, S. M. Dirk, D. W. Price, M. A. Reed, C. W. Zhou, J. Chen, W. Y. Wang, and I. Campbell, "Synthesis and preliminary testing of molecular wires and devices." *Chemistry-A European Journal*, 2001, **7**, 5118-5134.
71. J. S. Yang and T. M. Swager, "Fluorescent porous polymer films as TNT chemosensors: Electronic and structural effects." *Journal Of The American Chemical Society*, 1998, **120**, 11864-11873.

72. P. V. James, P. K. Sudeep, C. H. Suresh and K. G. Thomas, "Photophysical and theoretical investigations of oligo(*p*-phenyleneethynylene)s: Effect of alkoxy substitution and alkyne-aryl bond rotations." *The Journal of Physical Chemistry A*, 2006, **110**, 4329-4337.
73. J. M. Rodriguezparada, R. Duran and G. Wegner, "A comparative-study of mesophase formation in rigid chain polyesters with flexible side-chains." *Macromolecules*, 1989, **22**, 2507-2516.
74. B. Xu and S. Holdcroft, "Molecular control of luminescence from poly(3-hexylthiophenes)." *Macromolecules*, 1993, **26**, 4457-4460.
75. C. X. Liang and M. D. Newton, "Ab initio studies of electron-transfer - pathway analysis of effective transfer integrals." *Journal Of Physical Chemistry*, 1992, **96**, 2855-2866.
76. W. Rettig, "Charge separation in excited-states of decoupled systems - TICT compounds and implications regarding the development of new laser-dyes and the primary processes of vision and photosynthesis." *Angewandte Chemie-International Edition In English*, 1986, **25**, 971-988.
77. W. F. Libby, "Theory of electron exchange reactions in aqueous solution." *Journal Of Physical Chemistry*, 1952, **56**, 863-868.
78. R. A. Marcus, "Theory of oxidation-reduction reactions involving electron transfer.1." *Journal Of Chemical Physics*, 1956, **24**, 966-978.
79. A. C. Benniston and A. Harriman, "Charge on the move: How electron-transfer dynamics depend on molecular conformation." *Chemical Society Reviews*, 2006, **35**, 169-179.
80. N. S. Hush, "Adiabatic theory of outer sphere electron-transfer reactions in solution." *Transactions Of The Faraday Society*, 1961, **57**, 557-580.
81. J. R. Lakowicz, "Principles of fluorescence spectroscopy", 2nd ed, Kluwer Academic / Plenum Publishers, New York, 1999.
82. Z. R. Grabowski, K. Rotkiewicz and W. Rettig, "Structural changes accompanying intramolecular electron transfer: Focus on twisted intramolecular charge-transfer states and structures." *Chemical Reviews*, 2003, **103**, 3899-4031.
83. E. Lippert, W. Lüder and H. Boos. in *Adv. Mol. Spectrosc. Proc. Intl. Meet. 4th*. 1962.
84. Z. R. Grabowski, K. Rotkiewicz and A. Siemiarczuk, "Dual fluorescence of donor-acceptor molecules and the twisted intra-molecular charge-transfer (TICT) states." *Journal Of Luminescence*, 1979, **18-19**, 420-424.
85. K. Rotkiewicz, W. X. Rubaszewska and Lawa, "Intramolecular electron-transfer excited state in 6-cyanobenzquinuclidine." *Chemical Physics Letters*, 1980, **70**, 444-448.

86. M. Hashimoto and H.-O. Hamaguchi, "Structure of the twisted-intramolecular-charge-transfer excited singlet and triplet states of 4-(dimethylamino)benzointrile as studied by nanosecond time-resolved infrared spectroscopy." *Journal of Physical Chemistry*, 1995, 7875-7877.
87. W. M. Kwok, C. Ma, P. Matousek, A. W. Parker, D. Phillips, W. T. Toner, M. Towrie and S. Umaphy, "A determination of the structure of the intramolecular charge transfer state of 4-dimethylaminobenzointrile (DMABN) by time-resolved resonance Raman spectroscopy." *Journal Of Physical Chemistry A*, 2001, **105**, 984-990.
88. Y. Hirata, T. Okada and T. Nomoto, "Photoinduced intramolecular charge separation of p-N,N-dimethylamino-p'-cyano-diphenylacetylene in polar solvents." *Chemical Physics Letters*, 1997, **278**, 133-138.
89. S. Zilberg and Y. Haas, "The nature of the intramolecular charge transfer excited state in p-pyrrolocyanobenzene (PBN) and other derivatives of benzene substituted by electron donor and acceptor groups." *Journal Of Physical Chemistry A*, 2002, **106**, 1-11.
90. H. McConnell, "Intramolecular charge transfer in aromatic free radicals." *Journal Of Chemical Physics*, 1961, **35**, 508-515.
91. C. Joachim and M. A. Ratner, "Molecular wires: guiding the super-exchange interactions electrodes between two electrodes." *Nanotechnology*, 2004, **15**, 1065-1075.
92. E. A. Weiss, M. J. Tauber, R. F. Kelley, M. J. Ahrens, M. A. Ratner and M. R. Wasielewski, "Conformationally gated switching between superexchange and hopping within oligo-*p*-phenylene-based molecular wires." *Journal Of The American Chemical Society*, 2005, **127**, 11842-11850.
93. N. P. Redmore, I. V. Rubtsov and M. J. Therien, "Synthesis, electronic structure, and electron transfer dynamics of (aryl)ethynyl-bridged donor-acceptor systems." *Journal Of The American Chemical Society*, 2003, **125**, 8769-8778.
94. I. Daizadeh, E. S. Medvedev and A. A. Stuchebrukhov, "Effect of protein dynamics on biological electron transfer." *Proceedings Of The National Academy Of Sciences Of The United States Of America*, 1997, **94**, 3703-3708.
95. A. Amini and A. Harriman, "Intramolecular charge transfer in 4-cyano-(4'-methylthio)diphenylacetylene." *Physical Chemistry Chemical Physics*, 2003, **5**, 1344-1351.
96. L. R. Khundkar, A. E. Stiegman and J. W. Perry, "Solvent-tuned intermolecular charge-recombination rates in a conjugated donor- acceptor molecule." *Journal Of Physical Chemistry*, 1990, **94**, 1224-1226.
97. W. Nadler and R. A. Marcus, "Dynamic effects in electron-transfer reactions.2. Numerical-solution." *Journal Of Chemical Physics*, 1987, **86**, 3906-3924.

98. R. Englman and J. Jortner, "Energy gap law for radiationless transitions in large molecules." *Molecular Physics*, 1970, **18**, 145-164.
99. J. Zyss, I. Ledoux, S. Volkov, V. Chernyak, S. Mukamel, G. P. Bartholomew and G. C. Bazan, "Through-space charge transfer and nonlinear optical properties of substituted paracyclophane." *Journal Of The American Chemical Society*, 2000, **122**, 11956-11962.
100. J. Y. Lee, S. B. Suh and K. S. Kim, "Polyenes vs polyynes: Efficient  $\pi$ -frame for nonlinear optical pathways." *Journal Of Chemical Physics*, 2000, **112**, 344-348.
101. D. Beljonne, Z. Shuai, G. Pourtois and J. L. Bredas, "Spin-orbit coupling and intersystem crossing in conjugated polymers: A configuration interaction description." *Journal Of Physical Chemistry A*, 2001, **105**, 3899-3907.
102. D. Beljonne, H. F. Wittmann, A. Kohler, S. Graham, M. Younus, J. Lewis, P. R. Raithby, M. S. Khan, R. H. Friend, and J. L. Bredas, "Spatial extent of the singlet and triplet excitons in transition metal-containing poly-ynes." *Journal Of Chemical Physics*, 1996, **105**, 3868-3877.
103. N. Chawdhury, A. Kohler, R. H. Friend, W. Y. Wong, J. Lewis, M. Younus, P. R. Raithby, T. C. Corcoran, M. R. A. Al-Mandhary, and M. S. Khan, "Evolution of lowest singlet and triplet excited states with number of thienyl rings in platinum poly-ynes." *Journal Of Chemical Physics*, 1999, **110**, 4963-4970.
104. J. S. Wilson, N. Chawdhury, M. R. A. Al-Mandhary, M. Younus, M. S. Khan, P. R. Raithby, A. Kohler and R. H. Friend, "The energy gap law for triplet states in Pt-containing conjugated polymers and monomers." *Journal Of The American Chemical Society*, 2001, **123**, 9412-9417.
105. H. Y. Chao, W. Lu, Y. Q. Li, M. C. W. Chan, C. M. Che, K. K. Cheung and N. Y. Zhu, "Organic triplet emissions of arylacetylide moieties harnessed through coordination to [Au(PCy3)](+). Effect of molecular structure upon photoluminescent properties." *Journal Of The American Chemical Society*, 2002, **124**, 14696-14706.
106. H. F. Wittmann, R. H. Friend, M. S. Khan and J. Lewis, "Optical spectroscopy of platinum and palladium-containing poly-ynes." *Journal Of Chemical Physics*, 1994, **101**, 2693-2698.
107. K. A. Walters, K. D. Ley and K. S. Schanze, "Triplet state photophysics in an aryleneethynylene  $\pi$ -conjugated polymer." *Chemical Communications*, 1998, 1115-1116.
108. R. T. Cambron and J. M. Harris, "Time-resolved photothermal lens calorimetry for investigating mixed-order photoinitiated reaction-kinetics in liquids." *Journal Of Physical Chemistry*, 1993, **97**, 13598-13607.

109. S. E. Braslavsky and G. E. Heibel, "Time-resolved photothermal and photoacoustic methods applied to photoinduced processes in solution." *Chemical Reviews*, 1992, **92**, 1381-1410.
110. D. Cahen, H. Garty and R. S. Becker, "Photoacoustic calorimetry of concentrated fluorescent solutions." *Journal Of Physical Chemistry*, 1980, **84**, 3384-3389.
111. S. P. McGlynn, F. J. Smith and G. Cilento, "Some aspects of the triplet state." *Photochemistry And Photobiology*, 1964, **3**, 269-294.
112. P. K. Sudeep, P. V. James, K. G. Thomas and P. V. Kamat, "Singlet and triplet excited-state interactions and photochemical reactivity of phenyleneethynylene oligomers." *Journal Of Physical Chemistry A*, 2006, **110**, 5642-5649.



## CHAPTER 2

### An introduction to fluorescence spectroscopy

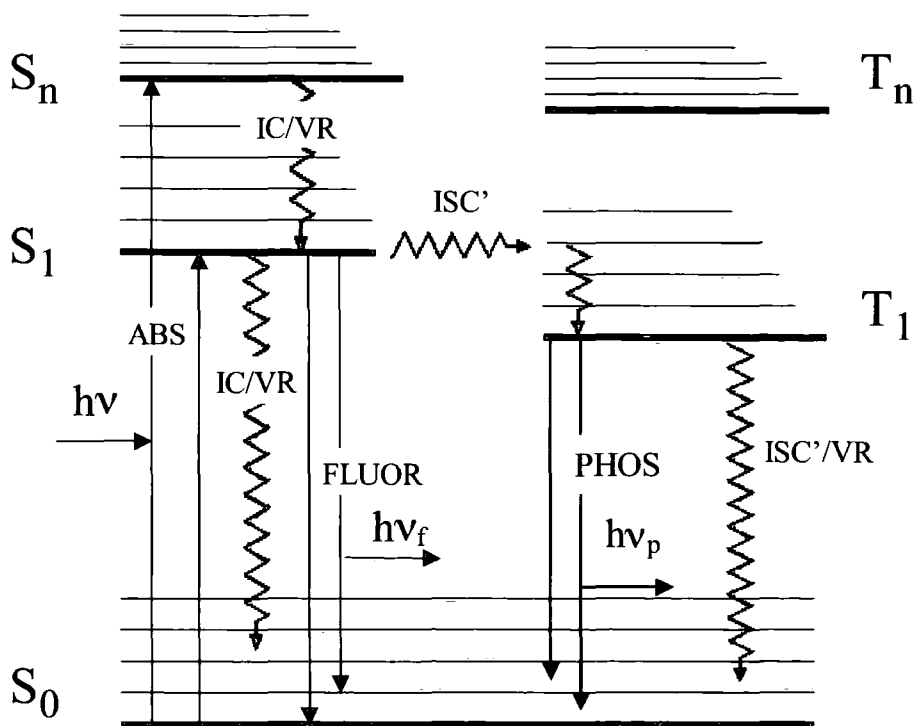
#### 2.1 Luminescence

Luminescence is the emission of light from the electronically excited states of any material, which usually does not result in a rise in temperature. Materials exhibiting this property are called phosphors or fluorophores. Examples of types of luminescence include photoluminescence[1] which is produced by excitation using light, bioluminescence[2] from organic or biological chemical reactions, chemiluminescence[3] from inorganic chemical reactions, sonoluminescence[3] produced by sound waves, electroluminescence[3] generated by the passing of an electric current through the specimen and triboluminescence[3] which is a result of a suitable phosphor being subjected to pressure or friction. In all the work described here, ultraviolet and visible electromagnetic radiation was used to excite the organic fluorophores to higher energy levels, in order to observe their photoluminescence.

Luminescence is divided into fluorescence and phosphorescence depending on the nature of the excited states involved in the transitions and the electron spin orientation.[1] These types of emission are usually associated with molecules having  $\pi$ -electron systems. Fluorescence describes the process in which  $\Delta S = 0$ , where  $\Delta S$  is the change in spin quantum number. Light is emitted from the excited singlet states in which the electron in the excited orbital is spin paired with an electron in the lowest occupied molecular orbital. As the return to the ground state is spin-allowed, it occurs rapidly with the emission of a photon. The rate constant for fluorescence is typically  $10^8 \text{ s}^{-1}$ . [1]

Phosphorescence is the emission of light from triplet excited states in which the electron in the excited orbital has the same spin orientation as the electron in the lowest occupied molecular orbital, i.e.  $\Delta S \neq 0$ . Phosphorescence tends to be lower in energy than fluorescence. The transitions are spin forbidden with low emission rates from  $10^{-3}$  to  $10^0 \text{ s}^{-1}$ . Phosphorescence is not usually observed at room temperature in solutions due to non-radiative decay, quenching and other processes.[1] Molecules containing heavy atoms such as bromine or iodine are frequently phosphorescent. The heavy atoms facilitate intersystem crossing which enhances phosphorescent quantum yields.[1]

The simplified Jabłoński diagram in Figure 2.1 illustrates the transitions occurring after the absorption of light by a typical organic molecule.  $S_0$ ,  $S_1$  and  $S_n$  represent the ground electronic state and the first two excited electronic states respectively. Each of these electronic energy levels has a number of vibrational energy levels ( $S_n^*$ ) associated with them. The vibrational levels are due to the motion of the nuclei. The instantaneous absorption of light of the appropriate wavelength populates the upper vibrational levels of the excited states, at the expense of the ground state, via the transitions  $S_n^* \leftarrow S_0$ . The transitions between states occur in about  $10^{-15}$  s and thus there is no time for any significant displacement of the nuclei. This is the Frank–Condon principle.[1] The intensity of the absorption transition depends on the extent of the overlap of the wavefunctions of the upper and lower vibrational energy levels (the Frank–Condon factor). Prior to any emission the molecule relaxes to the lowest vibrational excited state via non–radiative processes e.g.  $S_n^* \rightarrow S_n \rightarrow S_1^* \rightarrow S_1$ . The first of these processes is vibrational relaxation (VR). Here the molecule loses its vibrational energy by collisions with solvent molecules.



**Figure 2.1** The Jabłoński diagram for a typical organic molecule.  $S_0$  represents the ground state.  $S_1$ – $S_n$  and  $T_1$ – $T_n$  represent the singlet and triplet excited states respectively. ABS  $h\nu$ –the light energy absorbed, IC/VR–internal conversion and vibrational relaxation, ISC'–intersystem crossing and FLUOR  $h\nu_f$  and PHOS  $h\nu_p$ –fluorescence and phosphorescence emissions.

If the sample is in a solid matrix, VR occurs by exchange with the vibrational motions or phonons of this matrix. This is followed by internal conversion (IC)

whereby the molecule undergoes a transition to the lowest energy level in a highly excited vibrational level[4] e.g.  $S_1^* \rightarrow S_1$ . The process results in very little energy change. The electrons then return to the higher excited vibrational ground state levels. The lowest vibrational energy level of the ground state is reached by VR. Transitions can also occur between isoenergetic levels of different multiplicities, e.g.  $S_1 \rightarrow T_1$ , when it is termed intersystem crossing (ISC). VR and IC are usually very rapid processes and are complete within  $10^{-8}$  s. IC is faster for the upper excited states but VR is always faster. Fluorescence lifetimes are typically  $10^{-1}$  s to  $10^{-12}$  s so fluorescence emission generally occurs from the lowest-energy vibrational state of  $S_1$ . [1] The slower process of ISC ( $k_{ISC} \approx 10^8 \text{ s}^{-1}$ ) populates the first excited triplet state ( $T_1$ ) from which phosphorescence occurs.

Emission energy is always less than that of absorption. This is because of the non-radiative decay processes (IC and VR) that relax the molecules to lower energy levels prior to emission. Thus, fluorescence always occurs at longer wavelengths. This was first observed by Sir G.G. Stokes and is referred to as Stokes shift.[1] Emission from fluorescent molecules, under normal conditions, always takes place from the lowest excited electronic state. In addition to this, it is always the lowest vibrational level of the lowest excited state that is involved. This is known as Kasha's rule.[1]

Fluorescence typically occurs from aromatic molecules.[1] Examples of fluorophores include quinine, Fluorescein, Rhodamine B and *p*-bis[2-(5-phenyl-oxazolyl)]benzene (POPOP).[1] In this study we are primarily investigating the highly conjugated substituted 1,4-bis(phenylethynyl)benzene and 9,10-bis(phenylethynyl)anthracene molecules, which are highly fluorescent in solution and low temperature glasses.

Fluorescent emission spectra vary widely and depend on the chemical structure of the fluorophores and the solvent polarity. As a rule, the emission is generally the mirror image of the  $S_1 \leftarrow S_0$  absorption transition only and not the total absorption spectra. This similarity occurs because electronic excitation does not greatly alter the nuclear geometry.[1] Thus the spacing of the vibrational energy levels of the excited state is similar to that of the ground state.[1]

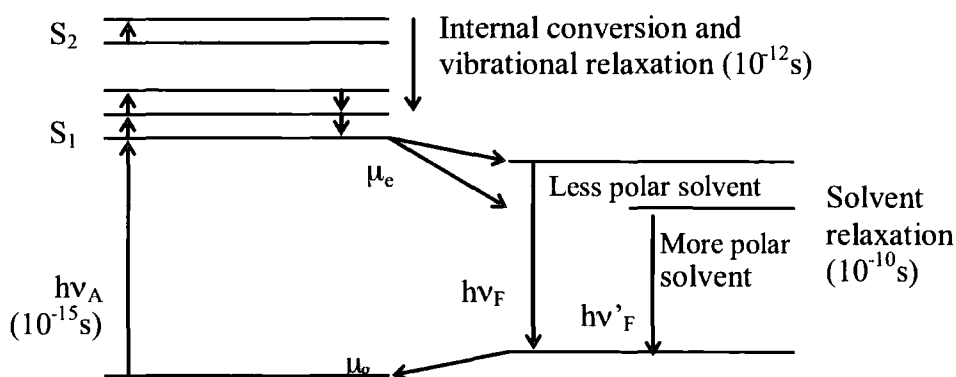
There are occasions when the mirror image rule is not obeyed. This is sometimes due to the molecule being excited to the second excited state ( $S_2$ ) which relaxes rapidly to  $S_1$ .<sup>[1]</sup> The emission spectra may also indicate the change in molecular geometry due to excitation. The spectra of *p*-terphenyl is such an example.<sup>[1]</sup> The lack of fine structure in the absorbance spectrum of a molecule and the presence of fine structure in its emission spectrum seems to indicate coplanarity of phenyl rings in the excited state.<sup>[1]</sup> Generally the opposite is observed. This is due to emission predominantly occurring from the lowest singlet state of  $S_1$ .

## 2.2 The effect of solvent polarity on fluorescence spectra

Solvent polarity and the local environment significantly affect the emission spectra of polar fluorophores. These effects, together with the previously mentioned processes of IC and VR, contribute to Stokes shift.<sup>[1]</sup> The high sensitivity of some polar fluorophores to changes in the polarity of their solvent environment makes them good probes for studying solute–solvent interactions.<sup>[5]</sup> The effects of solvent polarity on emission spectra are complex and are not completely explained by one theory. Generally, the energy of the excited state decreases with increasing solvent polarity. This effect can be accounted for by the Lippert equation (*vide infra*).<sup>[1]</sup> This describes the Stokes shift in terms of changes in dipole moment, which occur upon excitation, and the energy of a dipole in solvents at various dielectric constants ( $\epsilon$ ) or refractive indices ( $n$ ).<sup>[6]</sup> However, spectral shifts are also due to specific fluorophore–solvent interactions and charge separation in the excited state.

Fluorophores emit at longer wavelengths than those at which absorption occurs due to the loss of energy via the dynamic processes previously mentioned. Polar solvents have a stabilizing effect on the excited state of the fluorophore. The result is a shift in the emission to even lower energies. The process is outlined in the Jabłoński diagram in Figure 2.2.<sup>[1]</sup>

Fluorophores typically have a larger dipole moment in the excited state ( $\mu_e$ ) than in the ground state ( $\mu_g$ ).<sup>[1]</sup> After excitation, the solvent dipoles reorient around  $\mu_e$ , which lowers the energy of the excited state.<sup>[1]</sup> A possible mechanism for the high sensitivity to solvent polarity is the following. Consider a molecule with a strong electron donor substituent (e.g. dimethylamino group) on one end and a strong electron acceptor (e.g. cyano group) on the other end.



**Figure 2.2** Jablonski diagram for fluorescence with solvent relaxation.  $S_1$  and  $S_2$  represent the first and second excited states.  $h\nu_A$  and  $h\nu_F$  represent the light energy absorbed and fluorescence respectively.  $\mu_e$  and  $\mu_g$  represent the excited state and ground state dipoles respectively.[1]

This results in a large dipole moment in the ground state. Charge separation is likely to increase in the excited state. The result is a larger dipole moment than in the ground state. The important parameter for solvent effects is the dipole moment. This depends on charge separation in the fluorophore. Non-polar molecules, such as unsubstituted aromatic hydrocarbons, are much less sensitive to solvent polarity.[1]

Typically fluorescent lifetimes are 1–10 ns which are much longer than the time required for solvent reorientation. Absorption of light occurs in about  $10^{-15}$  s while solvent relaxation occurs in 10–100 ps in solutions at room temperature.[1] Thus, emission spectra of fluorophores are representative of the solvent relaxed state.

Solvent–fluorophore interactions are diverse and the solvent–dependent emission spectra cannot be described quantitatively by a single theory. Trends observed with solvent polarity follow the theory of general solvent effects but there are often additional shifts due to specific interactions (*vide infra*) and to the formation of internal charge–transfer states.[1]

### 2.3 The Lippert equation

The description of general solvent effects considers the fluorophore to be a dipole in a continuous medium of uniform dielectric constant.[1] Thus, deviations from the theory by way of solvent–fluorophore interactions, or formation of ICT states can be identified. This model lacks chemical interactions and so the theory cannot explain the effects of specific solvent–fluorophore interactions.

The Lippert equation [2.1] describes the difference in energy (in  $\text{cm}^{-1}$ ) between the ground and excited state of a fluorophore in terms of the refractive index ( $n$ ) and the dielectric constant ( $\epsilon$ ) of the solvent.

$$\overline{\nu}_A - \overline{\nu}_F = \frac{2}{hc} \left( \frac{\epsilon - 1}{2\epsilon + 1} - \frac{n^2 - 1}{2n^2 + 1} \right) \frac{(\mu_e - \mu_g)^2}{a^3} + \text{constant} \quad [2.1][1]$$

Here  $\overline{\nu}_A$  and  $\overline{\nu}_F$  are the wavenumbers (in  $\text{cm}^{-1}$ ) of the absorption and emission respectively.  $h$  is Planck's constant ( $6.6256 \times 10^{-27}$  erg s),  $c$  is the speed of light in  $\text{cm s}^{-1}$ , and  $a$  is the radius of the cavity in which the fluorophore resides in Å. Despite this equation only being an approximation, there is reasonable correlation between the observed and calculated energy losses in aprotic solvents. In the approximation the higher-order terms have been neglected. These terms would account for second-order effects, such as dipole moments induced in the solvent molecules by the excited fluorophore and vice versa.[1]

It is observed that an increase in refractive index ( $n$ ) decreases the Stokes shift. Furthermore, an increase in the dielectric constant ( $\epsilon$ ) increases the Stokes shift. This is a result of the refractive index being dependent on the near instantaneous motion of the electrons in the solvent molecule. When  $n$  is increased the ground and excited states are instantaneously stabilised by the redistribution of the electrons within the molecule. Consequently there is a decrease in the energy difference between the ground and excited states. This accounts for the red shift in the absorption spectrum of most fluorophores in solvents relative to the vapour phase.[7-9] On the other hand,  $\epsilon$  is a static property that is dependent on the electronic and molecular motions or solvent reorganisation around the excited state. The ground and excited states are also stabilised by an increase in  $\epsilon$ , but the energy decrease of the excited state due to the dielectric constant occurs only after reorientation of the solvent dipoles. This requires the movement of the entire solvent molecule. Thus stabilisation of the ground and excited states of a fluorophore is time-dependent and depends on  $\epsilon$ . Temperature and solvent viscosity determines the rate of solvent relaxation. The excited state shifts to lower energy on a time scale comparable to the solvent reorientation time.[1]

The term within the large parentheses in the equation [2.1] is referred to as the orientation polarisability ( $\Delta f$ ) and accounts for spectral shifts due to reorientation of solvent molecules. It is the difference between the spectral shifts due to reorientation of the solvent dipoles, and redistribution of the electrons in the solvent molecules (first term), and the redistribution of the electrons (second term). Solvent

reorientation, and thus the dielectric constant, is expected to have the greater effect on Stokes shift.

## **2.4 Specific solvent effects**

Specific solvent effects are the result of the interactions between one or a few neighbouring solvent molecules and the fluorophore. They are determined by the specific chemical properties of both the fluorophore and the solvent.[1] Possible origins of specific effects include hydrogen bonding, acid–base chemistry and charge–transfer interactions. These interactions can lead to substantial spectral shifts and their recognition is important for the detailed interpretation of emission spectra.

By examining the emission spectra of fluorophores in a variety of solvents specific solvent–fluorophore interactions can be identified. The addition of a low concentration of polar solvent to a non–polar solvent–fluorophore solution, which results in a decrease in the initial intensity of the emission spectrum and the appearance of a red shifted spectrum, is an indication of specific solvent effects. Such is the case for 2-anilinonaphthalene in cyclohexane and 3% ethanol (EtOH).[1] Here it is proposed that the effect is due to hydrogen bonding of EtOH to the amino groups as opposed to the stabilisation of an ICT state by a more polar solvent.

Specific solvent–fluorophore interactions can take place in the ground state or the excited state. The polar additive will not affect the absorption spectrum if the interaction only occurs in the excited state. The absorption spectrum is expected to change if the interaction occurs in the ground state. The time scale of these interactions is determined by their presence in the ground state or in the excited state. An immediate spectral shift is expected if the solvent and the fluorophore are associated in the ground state. On the other hand, if the interaction with the polar solvent only occurs in the excited state then the rates of diffusion of the polar solvent and the fluorophore determines the appearance of the specific solvent effect.

## **2.5 The effect of temperature and solvent viscosity on fluorescence spectra**

Solvent viscosity increases at low temperature and thus the time needed for solvent reorientation increases. If the solvent relaxation rate is slower than the emission decay rate then the emission spectra of the un-relaxed Frank–Condon (F) state is expected. This will be at a higher energy than the relaxed (R) state emission observed in fluid solvents. At intermediate temperatures, where the rates of solvent

relaxation and decay are approximately equal, the emission spectrum occurs in between the F and R states.[1] This intermediate spectrum is usually broader than the F state and R state spectra because of contributions from both states.

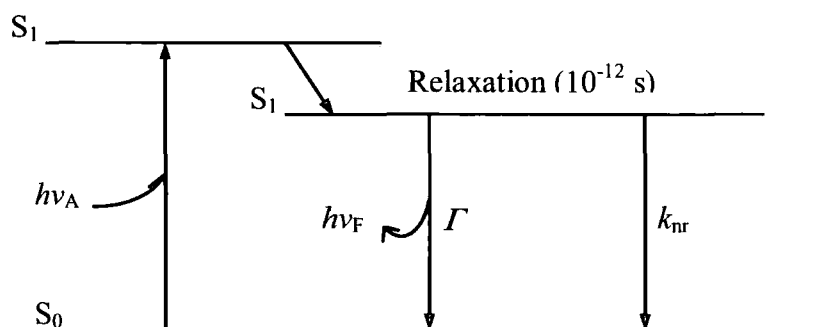
Solvents such as glycerol or methylcyclohexane/isopropanol (4:1), which increases in viscosity as the temperature decreases, can be used to immobilise the fluorophore. In the case of polyphenylethylenes it is thought that the rotation of the benzene rings relative to each other is also slowed down or stopped altogether. This is inferred from the increased vibrational structure observed as temperature decreases.[10] Insight into the conformation of these molecules upon excitation is gained from studying the photoluminescent properties of these low temperature systems.

## 2.6 Fluorescence quantum yield

The fluorescence quantum yield ( $\Phi_f$ ) of a fluorophore is the ratio of photons emitted to photons absorbed. The processes governed by the emissive rate of the fluorophore ( $\Gamma$ ) and the rate of non-radiative decay ( $k_{nr}$ ) to  $S_0$ , both depopulate the excited state (Figure 2.3). Here,  $k_{nr}$  is equal to all the deactivating rate constants ( $k_{IC} + k_{VR} + k_{ISC}$ ). The proportion of fluorophores which decay through emission, i.e. the quantum yield, is given by equation[1]:

$$\Phi_f = \frac{\Gamma}{\Gamma + k_{nr}}$$

If  $k_{nr} \ll \Gamma$ ,  $\Phi_f$  can be close to unity. However,  $\Phi_f$  is always less than unity because of Stokes losses.



**Figure 2.3** A simplified Jablonski diagram illustrating the relaxation processes leading to the relaxed  $S_1$  state.  $h\nu_A$  and  $h\nu_F$  represent absorbance and fluorescence energies respectively.  $\Gamma$  and  $k_{nr}$  represent the emissive rate of the fluorophore and the rate of non-radiative decay to  $S_0$  respectively.



## 2.7 Fluorescence lifetime

The lifetime ( $\tau$ ) of a fluorophore determines the time it has to interact with, or diffuse in, its environment. The lifetime of the excited state is defined by the average time the molecules spend in the excited state prior to returning to the ground state.[1] The observed fluorescence lifetime ( $\tau_f$ ) of fluorophores is usually about 10 ns, but individual systems have characteristic lifetimes and these are given by the equation[1]:

$$\tau_f = \frac{1}{\Gamma + k_{nr}}$$

Here,  $\Gamma$  and  $k_{nr}$  are as previously mentioned (section 2.6). For a single exponential decay, 63% of the molecules would have decayed before  $t = \tau$  and 37% at  $t > \tau$ . The intrinsic or natural lifetime of a fluorophore occurs in the absence of non-radiative decay and is given by  $\tau_n = 1/\Gamma$ . It is easily derived if the  $\Phi_f$  and  $\tau_f$  are known.

## 2.8 Anisotropy

The excitation of an isotropic sample with plane polarised light usually leads to the emission being partially polarised and the degree of polarisation is given by the fluorescence anisotropy ( $r$ ). A non-zero anisotropy indicates polarised emission. The origin of this phenomena is the fact that the transition dipole moments for absorption and emission lie along specific directions within the fluorophore structure.[1] In an isotropic solution, fluorophores are randomly orientated in the ground state. When exposed to polarised light, those fluorophores which have their absorption transition moments oriented parallel to the electric vector of the incident light are preferentially excited.[1] This leads to the generation of a population of molecules in the excited state having their transition moments orientated along the electric vector of the polarised exciting light.

A number of phenomena can result in the depolarisation of the emission, including factors such as scatter and re-absorption of emission. In dilute solution, the most important cause of depolarisation is rotational diffusion of the molecule in the time between absorption and emission. Anisotropy measurements allow the determination the average angular displacement of the fluorophore between the absorption and emission processes. This angular displacement depends on the rate and extent of rotational diffusion during the lifetime of the excited state, which is

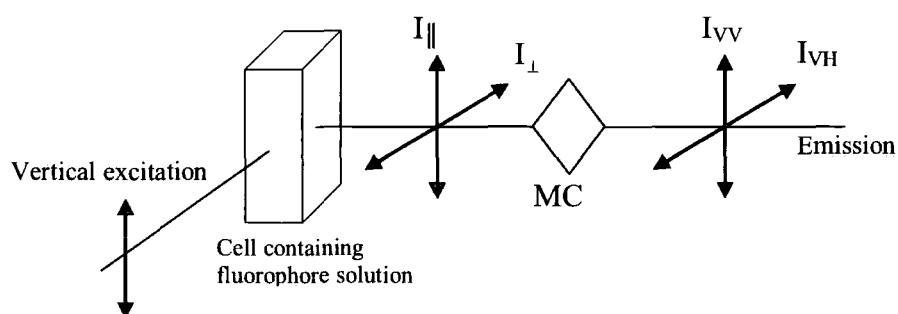
characterised by a rotational correlation time,  $\tau_c$ . [1] Rotational diffusion is dependent on the solvent viscosity, temperature and the size and shape of the rotating molecule. The simplest model is to consider that, in solution, the rate of fluorophore rotation depends on the viscous drag imposed by the solvent. Changing the solvent viscosity therefore results in a change in fluorescence anisotropy. For small fluorophores, in solutions of low viscosity, the rate of rotational diffusion is typically much faster than the rate of emission ( $\tau_c \ll \tau_f$ ). [1] Under these conditions, the anisotropy is close to zero and the emission is depolarised.

### 2.8.1 Fluorescence Anisotropy

The fluorescence anisotropy ( $r$ ) is defined by:

$$r = \frac{I_{\parallel} - I_{\perp}}{I_{\parallel} + 2I_{\perp}} \quad [2.2][1]$$

Here,  $I_{\parallel}$  and  $I_{\perp}$  are the fluorescence intensities of the vertically ( $\parallel$ ) and horizontally ( $\perp$ ) polarised emission. The fluorescence anisotropy is determined by exciting the sample with vertically polarised light and then detecting of the fluorescence  $90^\circ$  to the sample with parallel and perpendicular polarisers,  $I_{\parallel}$  and  $I_{\perp}$  (Figure 2.4).



**Figure 2.4** Schematic diagram for measurements of fluorescence anisotropy. MC–Monochromater.  $I_{\parallel}$  and  $I_{\perp}$  are the actual parallel and perpendicular emission intensities;  $I_{VV}$  and  $I_{VH}$  are the measured parallel and perpendicular intensities uncorrected for the MC transmission efficiency. [1]

In order to measure the actual horizontal and vertical intensities of the emission a correction has to be made for the detection system. This is known as the G-factor and is the ratio of the sensitivity of the detection system to polarised light. [1] The G-factor is measured using horizontally polarised light and is determined from the equation:

$$G = \frac{I_{HV}}{I_{HH}} \quad [2.3][1]$$

Here, the subscripts indicate the orientation of the excitation and emission polarisers respectively. Thus,  $I_{HV}$  corresponds to horizontally polarised excitation and vertically polarised emission. Once the G-factor is known, the ratio  $I_{\parallel}/I_{\perp}$  can be calculated from

$$\frac{I_{VV}}{I_{VH}G} = \frac{I_{\parallel}}{I_{\perp}} \quad [2.4][1]$$

The anisotropy is given by

$$r = \frac{(I_{\parallel}/I_{\perp}) - 1}{I_{\parallel}/I_{\perp} + 2} \quad [2.5][1]$$

Substituting equation [2.4] into [2.5] gives the following formula

$$r = \frac{I_{VV} - GI_{VH}}{I_{VV} + 2GI_{VH}} \quad [2.6][1]$$

The total luminescence intensity is given by  $I_{\parallel} + 2I_{\perp}$  as a result of the dependence of the intensity on  $\cos^2\alpha$ . Here,  $\alpha$  is the angle between the transition moment and the transmitting direction of the polariser. If one considers a collection of fluorophores where each one emits with intensity  $I_i$ , then the total intensity is given by

$$I_T = \sum_{i=1}^n I_i \quad [2.7][1]$$

If the intensity is observed through a polariser oriented along some axis  $p$ , the intensity is given by

$$I_p = \sum_{i=1}^n I_i \cos^2 \alpha_{pi} \quad [2.8][1]$$

Here  $\alpha_{pi}$  is the angle between the direction of the  $i$ th emission dipole and the axis of the polariser. Now measuring the intensity along the three Cartesian axes where  $\alpha_{pi}$  are the angles between the  $i$ th dipole and the representative axis gives a total intensity,  $I_T$ , of

$$I_x + I_y + I_z = \sum_{i=1}^n I_i (\cos^2 \alpha_{xi} + \cos^2 \alpha_{yi} + \cos^2 \alpha_{zi}) \quad [2.9][1]$$

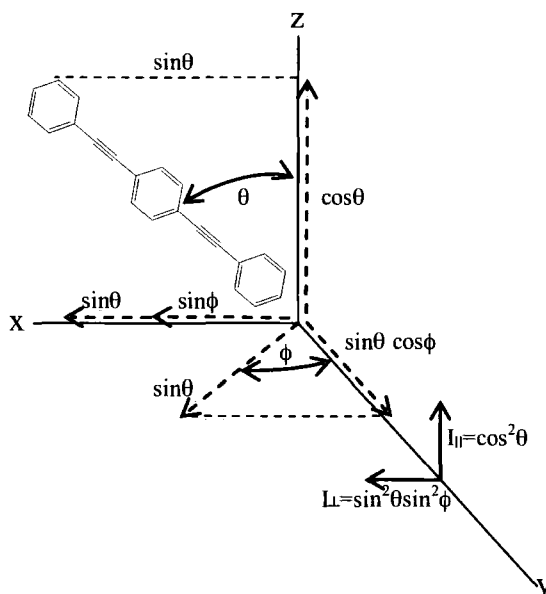
Since  $\cos^2 \alpha_{xi} + \cos^2 \alpha_{yi} + \cos^2 \alpha_{zi} = 1$  is always true, equation [2.9] becomes

$$I_x + I_y + I_z = \sum_{i=1}^n I_i = I_T \quad [2.10][1]$$

For vertically polarised excitation  $I_x=I_y$ , thus  $I_T = I_{||} + 2I_{\perp}$ . [1]

### 2.8.2 Theory for fluorescence anisotropy

Weber[11] derived the theory for fluorescence anisotropy using a single molecule. Assuming that absorption and emission moments of the molecule are parallel, there is no rotational diffusion and the molecule is oriented with angles  $\theta$  relative to the z-axis and  $\phi$  relative to the y-axis (Figure 2.5). This is only the case when the state that is being directly excited is the same as the one that is emitting.



**Figure 2.5** The emission intensities for a single fluorophore in a coordinate system.[1]

Fluorescing molecules behave like radiating dipoles[12] and the intensity of the light from a dipole is proportional to the square of the vector projected onto the axis of observation. It can also be reasoned that the emission is polarised along the transition moment. The intensity observed through a polariser is proportional to the square of the projection of the electric field of the radiating dipole onto the transmission axis of the polariser.[1] These projections (see Figure 2.5) are given by

$$I_{||}(\theta, \phi) = \cos^2 \theta \quad [2.11][1]$$

$$I_{\perp}(\theta, \phi) = \sin^2 \theta \sin^2 \phi \quad [2.12][1]$$

The anisotropy is calculated by performing the appropriate average based on excitation photoselection (*vide infra*) and how the selected molecules contribute to the measured intensity.[1] Consider the excitation polarised along the z-axis (Figure 2.5). This excitation will excite all molecules having an angle  $\phi$  with respect to the y-axis with equal probability. Any experimentally accessible population of molecules will be oriented with values of  $\phi$  from 0 to  $2\pi$  with equal probability. The dependence of equation [2.12] on  $\phi$  is therefore eliminated. Since the average value of  $\sin^2\phi$  is  $1/2$ [1] we can simplify equations [2.11] and [2.12] to give

$$I_{\parallel}(\theta) = \cos^2 \theta \quad [2.13][1]$$

$$I_{\perp}(\theta) = \frac{1}{2} \sin^2 \theta \quad [2.14][1]$$

If we consider a collection of fluorophores oriented relative to the z-axis with a probability of  $f(\theta)$ , the measured fluorescence intensities for these molecules are

$$I_{\parallel} = \int_0^{\pi/2} f(\theta) \cos^2 \theta \, d\theta = k \langle \cos^2 \theta \rangle \quad [2.15][1]$$

$$I_{\perp} = \frac{1}{2} \int_0^{\pi/2} f(\theta) \sin^2 \theta \, d\theta = \frac{k}{2} \langle \sin^2 \theta \rangle \quad [2.16][1]$$

Here, the probability that a fluorophore is oriented between  $\theta$  and  $\theta+d\theta$  is  $f(\theta) \, d\theta$  and  $k$  is an instrumental constant. Using equation [2.2] and the identity  $\sin^2\theta = 1 - \cos^2\theta$  it is found that

$$r = \frac{3\langle \cos^2 \theta \rangle - 1}{2} \quad [2.17][1]$$

The anisotropy is determined by the average value of  $\cos^2\theta$  where  $\theta$  is the angle of the emission dipole relative to the z-axis.

For a single fluorophore oriented along the z-axis with collinear absorption and emission transitions,  $\theta = 0^\circ$  and  $r = 1.0$ . However, it is not possible to obtain a perfectly oriented excited-state population in a homogenous solution. Anisotropies are therefore always less than 1.0. When  $\theta = 54.7^\circ$ ,  $r = 0$  which is the result of the average value of  $\cos^2\theta$  being equal to  $1/3$ , where  $\theta$  is the angular displacement between the excitation and emission moments. A more complex expression than

equation [2.17] is needed to describe most fluorophores because the transition moments are rarely collinear and the effects of excitation photoselection on the  $r$  values have to be also considered.[1]

### 2.8.3 Excitation Photoselection

When a sample is illuminated with polarised light, the electric dipole of the fluorophore need not be precisely aligned with the  $z$ -axis to absorb light polarised along this axis. The probability of absorption is proportional to  $\cos^2\theta$ . Here,  $\theta$  is the angle the absorption dipole makes with the  $z$ -axis.[11] The result is a population of excited fluorophores that are symmetrically distributed around the  $z$ -axis. This phenomenon is called photoselection.[1] In a disordered solution in the ground state the number of molecules at an angle between  $\theta$  and  $\theta+d\theta$  is proportional to  $\sin\theta d\theta$ . This quantity is proportional to the surface area of a sphere within the angles  $\theta$  and  $\theta+d\theta$ . [1] The distribution of molecules excited by vertically polarised light is given by

$$f(\theta)d\theta = \cos^2 \theta \sin \theta d\theta \quad [2.18][1]$$

The maximum photoselection that can be obtained using one-photon excitation of a homogeneous solution is given by equation [2.18].

If the absorption and emission dipoles are collinear the maximum value of  $\langle \cos^2\theta \rangle$  is given by

$$\langle \cos^2\theta \rangle = \frac{\int_0^{\pi/2} \cos^2 \theta f(\theta) d\theta}{\int_0^{\pi/2} f(\theta) d\theta} \quad [2.19][1]$$

Substituting equation [2.18] into [2.19] yields  $\langle \cos^2\theta \rangle = 3/5$ . On substituting this value into equation [2.17], one finds a maximum anisotropy of 0.4. This value corresponds to collinear absorption and emission dipoles and the absence of depolarisation processes. Under these conditions the excited-state population is preferentially oriented along the  $z$ -axis and the value of  $I_{\perp}$  is a third of the value of  $I_{\parallel}$ .

#### 2.8.4 Fundamental anisotropy

Generally,  $r$  is less than 0.4 and dependent on the excitation wavelength. This is a result of the fluorophore transition moments being displaced by an angle  $\beta$  relative to each other. Equation [2.17] demonstrated how the displacement of the emission dipole from the  $z$ -axis by an angle  $\theta$  resulted in a decrease in the anisotropy by a factor of  $(3 \cos^2\theta-1)/2$ . The displacement of the absorption and emission dipoles by an angle  $\beta$  leads to a further loss of anisotropy. The observed anisotropy in a low temperature glass matrix of a dilute solution is a product of the loss of anisotropy due to photoselection (which is 0.4) and that due to the angular displacement of the dipoles. Therefore the fundamental anisotropy ( $r_0$ ) of a fluorophore—which is the observed anisotropy in the absence of other depolarising processes—is given by

$$r_0 = \frac{2}{5} \left( \frac{3 \cos^2 \beta - 1}{2} \right) \quad [2.20][1]$$

$r_0$  values of about 0.39 (for 1,6-Diphenyl-1,3,5-hexatriene (DPH), where  $\beta \approx 7.4^\circ$ )[13], or slightly lower[14] have been reported. For an isotropic solution which has undergone single-photon excitation,  $r_0$  can only have values in the range -0.2 to 0.4.

In order to measure  $r_0$ , rotational diffusion must be eliminated. This is achieved by using solvents which form a clear glass at low temperature. Additionally depolarisation due to radiative re-absorption and emission or as a result of resonance energy transfer (RET) must be avoided. To achieve this, solutions must also be optically dilute. Under these conditions, the fluorophores undergo no interchromophore interactions during the lifetime of the excited state.[1] Therefore  $\beta$  can be calculated from equation [2.20] using the measured anisotropy values ( $r_0$ ). The orientation of the absorption dipoles vary for each absorption band so  $\beta$  is dependent on the excitation wavelength.

Emission is generally from the lowest singlet state so  $r$  is independent of emission wavelength. The changes in  $r_0$  with the excitation wavelength can be explained in terms of the changing contributions of two or more electronic transitions, each with a different value of  $\beta$ . The largest  $r_0$  values are typically observed for the longest absorbance wavelengths. This is because emission normally arises from the

transition between the lowest singlet state and the ground state—which is the same as that responsible for the longest-wavelength absorption band (Kasha's rule).[1] Thus the absorption and emission have nearly collinear moments. When the higher electronic states are excited, angle  $\beta$  can be large and these states do not usually emit directly, but decay to lower states by internal conversion to the lowest excited singlet state,  $S_1$ .

It is thought that the absorption and emission dipoles of nearly all fluorophores lie in the plane of the rings.[1] This is because the ground and excited state vibrational wave functions have the greatest overlap in the plane of the rings. For most fluorophores  $r_0$ , as illustrated in anisotropy vs. excitation wavelength spectra, is expected to be relatively constant across the  $S_1 \leftarrow S_0$  transition band and then gradually increase at longer wavelengths. A decrease in the excitation wavelength results in the anisotropy becoming more strongly wavelength dependent.[1]

### 2.8.5 Rotational diffusion and the Perrin Equation

The dominant cause of fluorescence depolarisation of fluorophores is rotational diffusion. The Perrin equation describes rotational diffusion for spherical rotors

$$\frac{1}{r} = \frac{1}{r_0} + \frac{\tau_f}{r_0 \tau_c} \quad [2.21][1]$$

Here,  $\tau_f$  is the fluorescence lifetime,  $\tau_c$  is the rotational correlation time and  $r$  is the measured steady-state fluorescence anisotropy. Assuming the fluorophore is spherical we can calculate  $\tau_c$  after substituting experimentally determined values of  $r$ ,  $r_0$  and  $\tau$  into equation [2.21]. The rotational correlation time is related to the viscosity by the equation

$$\tau_c = \frac{\eta V}{RT} \quad [2.22]$$

for a spherical fluorophore. Here,  $\eta$  is the viscosity,  $T$  is the temperature in Kelvin,  $R$  is the gas constant and  $V$  is the volume of the rotation unit.[1] The rotational diffusion coefficient ( $D$ ) is also related to  $\tau_c$  by  $\tau_c = (6D)^{-1}$ . [1] It is expected that for small molecules in cyclohexane,  $\tau_c$  will be much shorter than the  $\tau_f$  and  $r$  will be near zero. For example, perylene has a lifetime of 6 ns and  $r_0 = 0.36$ . In EtOH, the rotational diffusion is expected to decrease  $r$  to 0.005.[1]

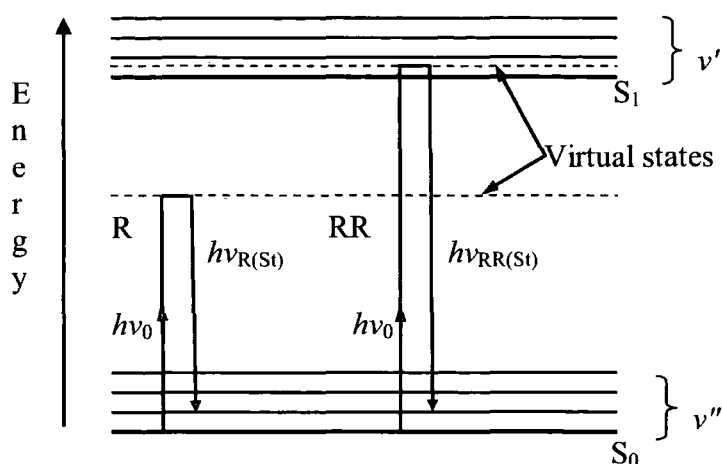


Herein, the fundamental and fluorescence anisotropies of BPEB were measured to determine the rotational correlation time and the angle of displacement between the absorption and emission dipoles.

## 2.9 An introduction to time-resolved resonance Raman spectroscopy

Raman scattering is one of the phenomenon that occur when electromagnetic radiation interacts with a molecule.[15] It was first experimentally observed in liquid benzene by C. V. Raman in 1928.[16, 17] Radiation scattering is a two photon process which can be thought of as the incident photon being momentarily absorbed to create a virtual state (non-stationary energy level) (Figure 2.6). A new photon is created and scattered from this virtual level.[18] When scattering proceeds without any change in the energy of the incident photon it is referred to as *Rayleigh scattering*. If there is a change in the energy of the incident photon then it is referred to as *Raman scattering*[15] or inelastic scattering.[19] The term “inelastic” refers to the transfer of energy between the photon and the material, so that the scattered light may have a longer or shorter wavelength than the incident light.

The interaction of a molecule and a photon of visible light, with energy lower than the energy difference between the ground state and first excited electronic levels of the molecule, give rise to the normal Raman scattering effect. When the photon energy does not correspond to the difference between any two stationary energy levels, the scattering of radiation takes place almost immediately after the interaction of the photon with a molecule (within  $\approx 10^{-14}$  s).[15] The interaction of a photon of initial energy  $h\nu_0$  excites the molecule to a virtual level (Figure 2.6). These virtual states correspond to possible normal vibrations of the molecule. The photon may then leave the molecule with either decreased energy  $h\nu_{R(S)}$  (Raman Stokes scattering), with increased energy  $h\nu_{R(aS)}$  (Raman anti-Stokes scattering) or no change in energy (Rayleigh scattering). The intensity of the Rayleigh scatter is  $10^3$ – $10^4$  times greater than the corresponding Raman scatter.[15] The anti-Stokes scattering occurs at higher energies as it stems from transitions between the first excited vibrational state and a virtual electronic state.



**Figure 2.6** Diagram of transitions of Raman Stokes scattering (R)  $h\nu_{R(S_0)}$  and resonance Raman Stokes scattering (RR)  $h\nu_{RR(S_0)}$ .  $S_0$ –ground electronic state,  $S_1$ –first excited electronic state.  $\nu''$  and  $\nu'$ –ground and excited state vibrational energy levels respectively.

The absolute differences between the frequencies of the incident photon and both Raman Stokes and anti-Stokes scattered photons are the same and equal to the molecular vibration frequency ( $\nu_v$ )[15]:

$$\nu_0 - \nu_{R(St)} = \nu_v$$

$$\nu_{R(aSt)} - \nu_0 = \nu_v$$

These differences in frequencies are measured by subtracting the frequency of the mono-energetic incident laser light from the frequency of the scattered photons. As it is only the energy of the different vibrational levels that are important, the Raman spectrum is symmetric relative to the Rayleigh band. The differences in frequency between the exciting radiation and the scattered radiation is thus characteristic of a molecule and independent of the frequency of the exciting radiation.[15] The spontaneous Raman effect occurs off resonance from the electronic transitions of the molecule and are very weak.[18] While the intensities of the Raman Stokes bands are very weak, the Raman anti-Stokes bands are even weaker still because of the difference in population of the ground and excited states of molecules at room temperature. According to Boltzmann's law, only a small percentage of molecules will occupy the first excited vibrational state at room temperature.[15]

Different *selection rules* determine if a molecular vibration appears in the infrared and/or in the Raman spectrum. A vibration is Raman active if the polarisability of the molecule changes with the vibrational motion[15], while a vibration that causes a change in the dipole moment is active in the infrared (IR) spectrum. The fulfilment

of one or both of these conditions depends on the symmetry of the molecule. In molecules possessing high symmetry, notably a centre of symmetry, this leads to the *mutual exclusion rule*, which states that a vibration that is infrared allowed is Raman forbidden and vice versa.[15] Molecules without a centre of symmetry will have a number of vibrations appearing in both spectra. However, the relative intensity of the bands will differ, for example the double and triple bonds and the carbon skeleton vibrations are readily observed in Raman spectra, while vibrations of highly polar functional groups are more easily observed in IR spectra.[15] Totally symmetric vibrations are best visible in the Raman spectrum.

The application of high powered laser excitation sources has led to the discovery of a number of new effects. One such effect is the resonance Raman (RR) effect. This is observed when the exciting radiation frequency is very close to, or lies within the range of an electronic absorption band of the molecule (Figure 2.6).[15] The result is a significant increase in the intensity of the Raman scattering by several orders of magnitude. Tuneable dye lasers may be used to achieve the RR spectroscopy for structural analysis because they can be tuned to emit the appropriate absorption frequency for the molecule under investigation.

Pulsed laser sources allow the study of the time-resolved resonance Raman ( $TR^3$ ). Normal Raman is too weak and the transient concentration is low, thus no signal for the transient can be detected. However, the high intensity of RR allows for easy monitoring of its transients over time. In this process, the molecule is excited with a short burst of light from a high powered laser (pump pulse) into an excited electronic state. After the required time delay, a second laser pulse (probe pulse) excites the Raman spectrum of the transient species that was created by the first pulse.[18]  $TR^3$  enables us to track changes in structural features in the picosecond and nanosecond time frame.

From the  $TR^3$  vibrational spectrum of a molecule, we gain information about its chemical composition because different chemical groups in organic compounds have characteristic vibrational frequencies. It is thus possible to deduce the bonding in a molecule. The electronic triplet and singlet states of molecules can also be identified via  $TR^3$ .

## REFERENCES

1. J. R. Lakowicz, "Principles of fluorescence spectroscopy", 2nd ed, Kluwer Academic / Plenum Publishers, New York, 1999.
2. S. H. D. Haddock, C. M. McDougall and J. F. Case. *The bioluminescence web page*. [web page] 1997 2006 [cited 01/12/2006]; Available from: <http://lifesci.ucsb.edu/~biolum>.
3. M. Hoyland and D. Ormsby. *Delights of chemistry*. [web page] 02/07/2003 [cited 01/12/2006]; Available from: <http://www.chem.leeds.ac.uk/delights/texts/Appendix.htm>.
4. J.-C. Bunzli, "Luminescence probes", in *Lanthanide Probes in Chemical and Earth Sciences*, J.-C. Bunzli and G. R. Chopin, Editors, Elsevier, Amsterdam, 1989, p. 219 - 293.
5. M. C. Rezende, "Solvatochromism", in *Encyclopedia of supramolecular chemistry*, A. J. L. and S. J. W., Editors, Marcel Dekker, New York, 2004, p. 1330-1336.
6. N. Mataga, Y. Kaifu and M. Koizumi, "Solvent effects upon fluorescence spectra and the dipole moments of excited molecules." *Bulletin Of The Chemical Society Of Japan*, 1956, **29**, 465-470.
7. E. G. Mearns, "Theory of solvent effects on molecular electronic spectra - frequency shifts." *Journal Of Physical Chemistry*, 1957, **61**, 562-572.
8. N. S. Bayliss and E. G. Mearns, "Solvent effects in organic spectra - Dipole forces and the Franck-Condon principle." *Journal Of Physical Chemistry*, 1954, **58**, 1002-1006.
9. N. S. Bayliss, "The effect of the electrostatic polarization of the solvent on electronic absorption spectra in solution." *Journal Of Chemical Physics*, 1950, **18**, 292-296.
10. A. Beeby, K. Findlay, P. J. Low and T. B. Marder, "A re-evaluation of the photophysical properties of 1,4-bis(phenylethynyl)benzene: A model for poly(phenyleneethynylene)." *Journal Of The American Chemical Society*, 2002, **124**, 8280-8284.
11. G. Weber, "Polarization of the fluorescence of solutions", *Fluorescence and Phosphorescence Analysis*, ed. D. M. Hercules, John Wiley & Sons, New York, 1966.
12. P. Selényi, "Wide-angle interferences and the nature of the elementary light sources." *Physics Review*, 1939, 477-479.
13. G. Weber, "Uses of fluorescence in biophysics - some recent developments." *Annual Review Of Biophysics And Bioengineering*, 1972, **1**, 553-570.

14. M. Shinitzky and Y. Barenholz, "Dynamics of hydrocarbon layer in liposomes of lecithin and sphingomyelin containing dicetylphosphate." *Journal Of Biological Chemistry*, 1974, **249**, 2652-2657.
15. H. Baranska, A. Labudzinska and J. Terpinski, "Laser Raman spectrometry: analytical applications", Ellis Horwood Series in Analytical Chemistry, ed. D. R. A. Chalmers and D. M. Masson, Ellis Horwood Limited England and PWN-- Polish Scientific Publishers Poland, Chichester, 1987.
16. C. V. Raman, "A change of wave-length in light scattering." *Nature*, 1928, **121**, 619.
17. C. V. Raman and K. S. Krishnan, "A new type of secondary radiation." *Nature*, 1928, **121**, 501-502.
18. M. Diem, "Introduction to modern vibrational spectroscopy", John Wiley & Sons, New York, 1993.
19. D. Wolverson, "Raman spectroscopy", in *An Introduction to Laser Spectroscopy*, D. L. Andrews and A. A. Demidov, Editors, Plenum Press, New York, 1995, p. 231.

## CHAPTER 3

### Experimental techniques

A number of standard and specialised spectroscopic techniques were used in the work discussed in this thesis. The general theory behind these techniques and the required experimental conditions are discussed below.

#### 3.1 UV–visible absorption spectroscopy

All UV–visible absorption spectra were obtained on an ATI Unicam UV / VIS UV2 spectrometer and were background corrected. Quartz cells with a path length of 10 mm were used to acquire spectra over the desired wavelength range.

The molar extinction coefficient ( $\epsilon$ ) is a measure of the how well a particular substance absorbs light. The molar extinction coefficients of the fluorophores studied, at a specified wavelength, were determined from Beer–Lambert plots (absorption vs. molar concentration) using 7 dilutions over the concentration range  $10^{-4}$  to  $10^{-6}$  mol dm<sup>-3</sup>. From the Beer–Lambert law:

$$\epsilon = A / c l \quad [3.1]$$

where A is absorbance at a specified wavelength, c is the concentration of the absorbing species in mol dm<sup>-3</sup> and l is the optical path length of the cuvette in cm. The units of  $\epsilon$  are dm<sup>3</sup> mol<sup>-1</sup> cm<sup>-1</sup>.

#### 3.2 Fluorescence spectroscopy

Emission and excitation spectra were recorded on a Jobin–Yvon Horiba Fluorolog 3-22 Tau-3 spectrofluorimeter[1] with a 0.5–2 nm band pass. The spectra of dilute solutions with absorbance of less than 0.1 (in a 10 mm quartz cuvette) in the 200 nm to 400 nm range were recorded using conventional 90 degree geometry.[2] All spectra were fully corrected using the manufacturer's correction curves for the spectral response of the excitation and emission optical components.

The fluorescence quantum yields reported herein were estimated by the comparative method of Williams *et al.*[3] using quinine sulphate in 0.1 M H<sub>2</sub>SO<sub>4</sub> ( $\Phi_f = 0.55$ ), POPOP in cyclohexane ( $\Phi_f = 0.97$ ),  $\beta$ -carboline in 0.5 M H<sub>2</sub>SO<sub>4</sub> ( $\Phi_f = 0.6$ ) and fluorescein in 0.1 M NaOH ( $\Phi_f = 0.9$ ) as standards. The quantum yields of the standards used are largely independent of excitation wavelength, which enables them

to be used wherever they display a useful absorption. The determination of the quantum yield is accomplished by comparison of the wavelength-integrated intensity of the unknown to that of the standard. Quantum yields were calculated from the expression

$$\Phi_{unk} = \Phi_{std} \left( \frac{grad_{unk}}{grad_{std}} \right) \left( \frac{\eta_{unk}}{\eta_{std}} \right)^2 \quad [3.2]$$

where  $\Phi_{unk}$  and  $\Phi_{std}$  are the quantum yields of the unknown fluorophore (*unk*) and the known standard (*std*) respectively, *grad* are the gradients of the unknown fluorophore and the standards determined from plots of their wavelength-integrated emission intensities against absorbance.  $\eta$  is the refractive index of the solvent in which the unknown and the standard fluorophores are dissolved. At least five increasing concentrations of the fluorophore and each of the standards were used to avoid concentration effects. All solutions were prepared with absorbances below 0.15 in a 10 mm path length cuvette to avoid re-absorption.

### 3.3 Low temperature spectroscopy

All the spectrometers used were adapted to hold a cryostat. Low temperature excitation and emission spectra measurements were recorded in a liquid nitrogen cooled Oxford Instruments DN 1704 cryostat.[4] A model ITC 6 temperature controller (also from Oxford instruments) was used to regulate the sample temperature from 298 K to 77 K. Samples were dissolved in a solution of either EPA (5:5:2 v/v/v diethylether / 2-ethylbutane / ethanol) or MCH / IP (4:1 v/v methylcyclohexane / 2-methylbutane). The solutions were held in the cryostat in a 10 mm path length quartz cell specially designed for low temperature conditions. Samples were allowed to equilibrate for at least 15 minutes at each temperature prior to recording their spectra.

Corrected low temperature phosphorescence emission and excitation spectra were recorded on a Perkin Elmer LS-50B luminescence spectrometer.

### 3.4 Singlet oxygen quantum yields

Singlet oxygen ( $^1O_2$ ) is generated after the quenching of a triplet state molecule by ground state molecular oxygen ( $^3\Sigma_g^-O_2$ ) and precedes via a collision complex.[5] Singlet oxygen has two states,  $^1\Sigma_g^+$  and  $^1\Delta_g$ . However, the  $^1\Delta_g$  state, which has a

lifetime of several minutes in gaseous media, is far more stable than the  $^1\Sigma_g^+$  state and is assumed to be more reactive. This is attributed to the spin forbidden nature of the  $^1\Delta_g \rightarrow ^3\Sigma_g^-$  transition.[6]

The quantum yield of singlet oxygen formation,  $\Phi_\Delta$ , for the compounds studied, were determined relative to perinaphthanone in cyclohexane ( $\Phi_\Delta \approx 1.0$ ) using a method described by Nonell.[7] This method makes use of the relationship between  $\Phi_\Delta$  and the ‘zero-time’ phosphorescence intensity,  $S(0)$ , according to the equation

$$S(0) = \frac{\kappa}{\eta_r^2} k_R \Phi_\Delta \frac{E_1(1 - 10^{-A})}{N_A h\nu V} \quad [3.3]$$

Here,  $\kappa$  is the proportionality constant, including electronic and geometrical factors,  $\eta_r$  is the solvent refractive index,  $k_R$  is the radiative rate constant,  $\Phi_\Delta$  is the quantum yield of singlet oxygen production,  $E_1$  is the energy of the laser flash,  $A$  is the sensitizer absorbance at the excitation wavelength,  $\nu$  is the laser frequency and  $V$  is the irradiated volume.

The absorbance of the sample and the reference were recorded at 355 nm. The singlet oxygen emission decay was recorded for each sample, and the reference compound, using five laser powers of 355 nm wavelength. The data from each measurement was fitted to an exponential decay of the form  $S(t) = S(0)\text{exp}(-t/\tau)$  using a fitting function optimised for  $S(0)$ . A plot of  $S(0)$  versus laser power (in mV) was drawn for each sample and the reference from which the gradient,  $S(0)_{EA}$ , was determined. This was repeated for five different absorbances (ranging from 0.06 to 0.19, uncorrected, at wavelength 355 nm) of each sample and the reference, and a plot of the slopes obtained versus  $1-10^{-A}$  was drawn. The gradient of these plots are proportional to the quantum yield which was calculated using

$$\Phi_{\Delta, \text{sample}} = \Phi_{\Delta, \text{reference}} \frac{S(0)_{EA, \text{sample}}}{S(0)_{EA, \text{reference}}} \quad [3.4]$$

### 3.4.1 Experimental details

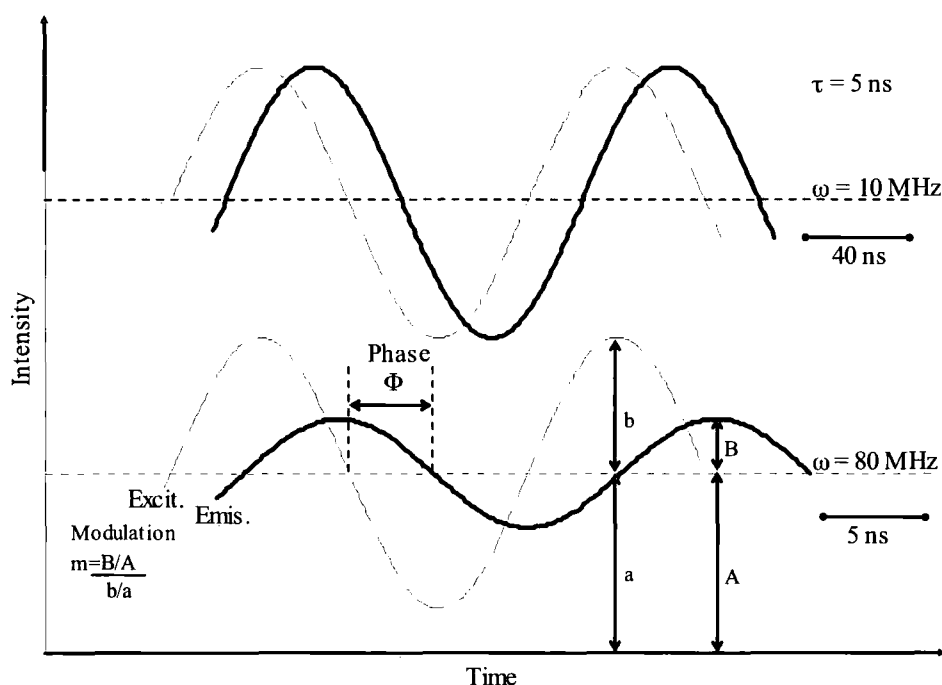
The samples and the reference compounds were analysed in the same solvent because of the heavy dependence of the radiative and non-radiative rate constants for deactivation of the triplet states on the solvent. The singlet oxygen emission was



detected at 1269 nm from solutions in a 10 mm path length quartz cuvette after being excited with 355 nm laser wavelength from a Q-switched Nd:YAG laser (Spectra Physics, Quanta Ray GCR-150-10) with a 10 Hz repetition rate. The phosphorescence was collected at 90° by a liquid nitrogen cooled germanium photodiode (North Coast E0-817P) after passing through an interference filter centred at 1270 nm. The photodiode output is amplified and AC coupled to a digital oscilloscope which digitized and averaged the transients. The averaged data were then transferred to a PC where they were analysed using the Microsoft Excel package.

### 3.5 Fluorescence lifetimes—The phase modulation technique

The phase-modulation technique[8] is one of the two methods used to determine fluorescence lifetimes in this work. In this method an intensity-modulated light source is used to excite the sample being studied. The time lag between absorption and emission results in the emission being delayed in time relative to the modulated excitation as illustrated in Figure 3.1. At each modulation frequency this delay is described as the phase shift ( $\phi_\omega$ ).



**Figure 3.1** Schematic diagram of phase modulation. The heavy line represents the phase and modulation fluorescence in response to intensity-modulated excitation represented by the thin line. The lifetime is 5 ns and the modulation frequency is 10 MHz (top) and 80 MHz (bottom).[8]

This phase shift increases from 0° to 90° with increasing modulation frequency ( $\omega$ ). The phase angle displayed by any sample is usually a fraction of 90°. The demodulation of the emission, by a factor  $m_\omega$ , is also a result of the finite time response of the sample.  $m_\omega$  decreases from 1.0 to 0 with increasing modulation frequency and increasing lifetime. The emission closely follows excitation at low frequency. However at higher modulation frequencies the finite lifetime of the excited state prevents the emission from following the excitation intensity. The result is a phase delay in the emission, and a decrease in the peak-to-peak amplitude of the modulated emission measured relative to the modulated excitation. The phase modulation graph constitutes the frequency response of the emission from the fluorophore. The decay of the fluorophore emission is a single exponential. The lifetime can be calculated by using the phase angle or modulation at any frequency. The phase and modulation are related to the decay time ( $\tau$ ) by

$$\tan \phi_\omega = \omega\tau \quad [3.5] \quad \text{and}$$

$$m_\omega = (1 + \omega^2\tau^2)^{-1/2} \quad [3.6] \quad [2]$$

The measured lifetimes of the compounds studied were deemed satisfactory based on their chi-squared values and the fit of the residuals.

### 3.5.1 Experimental details

Fluorescence lifetimes were recorded using the Jobin-Yvon Horiba Fluorolog 3-22 Tau-3 spectrofluorimeter operating in the phase-modulation mode. Sample solutions were prepared with absorbances  $\leq 0.08$  at the excitation wavelength, to avoid over loading the detector. The instrument response function was measured using a dilute suspension of Ludox® silica in water as the scattering medium. The phase shift and modulation were recorded over the frequency range 50–300 MHz and the data fitted using the Jobin-Yvon software package.

### 3.6 Fluorescence lifetimes—The time correlated single photon counting technique

The technique of time correlated single photon counting[2, 9, 10] was used to record the fluorescence lifetimes of the group of donor and acceptor substituted 1,4-bis(phenylethynyl)benzene chromophores discussed in this work. What follows is a

brief description of the technique with further details to be found in Lakowicz[2], and O'Connor and Phillips *et al.*[9, 10]

A sub-nanosecond pulsed excitation source is used to repeatedly excite the sample in order to record its decay. In this system, only a single randomly selected photon is detected following each excitation pulse and the time taken between pulse and photon arrival is recorded for each event. The voltage ramp of a time to amplitude converter (TAC) is used to measure the time interval. A histogram of the number of photons arriving versus the time interval is built up by a pulse height analyser (PHA)—the histogram represents the probability of detecting a photon at a given time after the excitation pulse.[9] The probability of photon emission is greater for a short time interval after excitation than after a long interval when the fluorescence has decayed. Hence, the resulting histogram is a direct representation of the variation of fluorescence intensity with time.

In the time between start and stop pulses the TAC charges the capacitor. The TAC is the rate-limiting component in the experiment. This is due to the several microseconds it takes the capacitor to discharge and the TAC to reset. This limitation leads to the TAC being over loaded if a high repetition laser source (such as a 1 MHz source) is used. This problem is overcome by operation the TAC in the 'reverse mode', in which the first photon selected provides the start pulse, and the signal from the subsequent excitation pulse is the stop signal.[9] In this way, the TAC is only activated if an emitted photon is detected. The resulting histogram is reversed but easily corrected by software.

The measured intensity decay obtained from a photon counting experiment is a convolution of the exponential decay with the excitation and instrument response functions.[2, 10] The excitation pulse can be considered as a series of  $\delta$ -functions with varying amplitudes, such that each  $\delta$ -function will yield one decay from the sample.[9] The measured intensity decay is thus the sum of these individual exponential decays.

Non-linear least-square analysis[11] provides the most reliable method for the analysis of the convolved data. This involves the iterative reconvolution of the instrument response function,  $X(t)$ , with a chosen function and non-linear least squares-fitting. First, the excitation pulse profile is recorded, the instrument

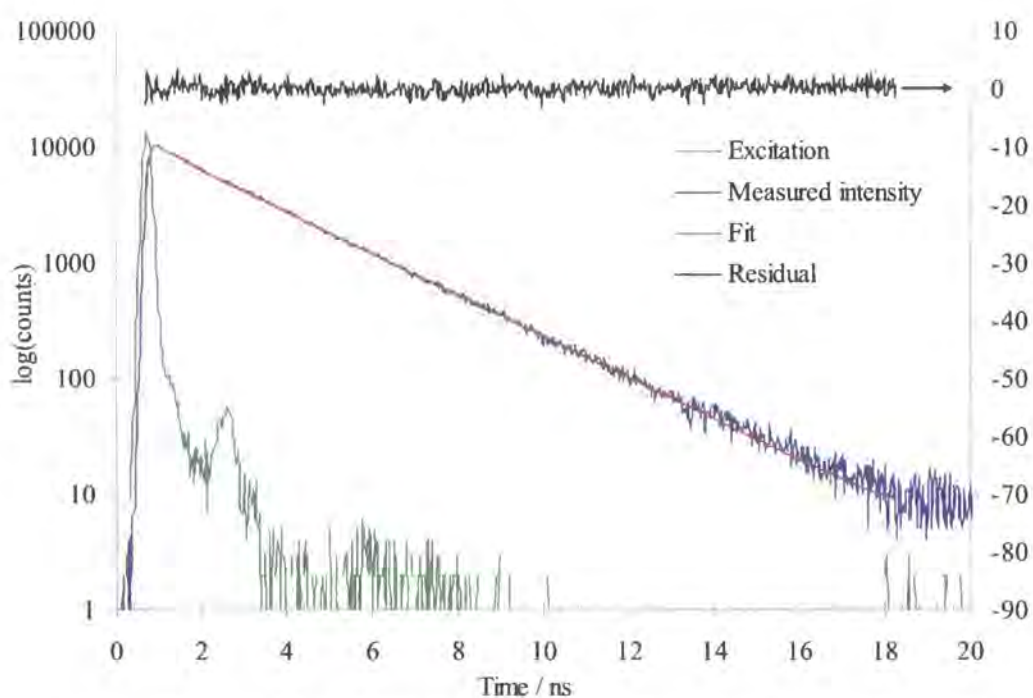
response function is then convolved with a theoretical exponential decay and finally the theoretical decay is matched to the measured intensity decay by optimising its parameters. The Solver function on Microsoft Excel is used to carry out the fitting procedure and gives values for amplitude ( $A$ ) and lifetime ( $\tau$ ).

The decay of the first excited singlet state, via fluorescence, is usually a first order process represented by a single exponential decay. When there is a multiple of emitting species, the decay is better described by a sum of exponential terms

$$I(t) = A_1 \exp(-t/\tau_1) + A_2 \exp(-t/\tau_2) + \dots \quad [3.7][9]$$

where  $I(t)$  is the total intensity of the fluorescence at time  $t$ ,  $A_n$  represents the fluorescence intensity at time  $t = 0$  for the  $n^{\text{th}}$  component and  $\tau_n$  is the lifetime for the  $n^{\text{th}}$  component. The yield gives the contribution of each component to the overall fluorescence intensity and is calculated thus:

$$\text{Yield of the } n^{\text{th}} \text{ component} = \frac{A_n \tau_n}{\sum_i A_i \tau_i} \times 100 \quad [3.8][9]$$



**Figure 3.2** Data and fit obtained by time correlated single photon counting for 4-(4-(4-dimethylaminophenylethynyl)phenylethynyl)benzoate in THF,  $\lambda_{\text{ex}} = 366 \text{ nm}$ ,  $\tau_f = 2.4 \text{ ns}$ .

The relevant lifetimes of the compounds studied were considered satisfactory as judged by reduced chi-squared[2], weighted residuals[2], autocorrelation

residuals[12] and the Durbin Watson parameter.[13, 14] An example of a good quality fit is shown in Figure 3.2.

### 3.6.1 Experimental details

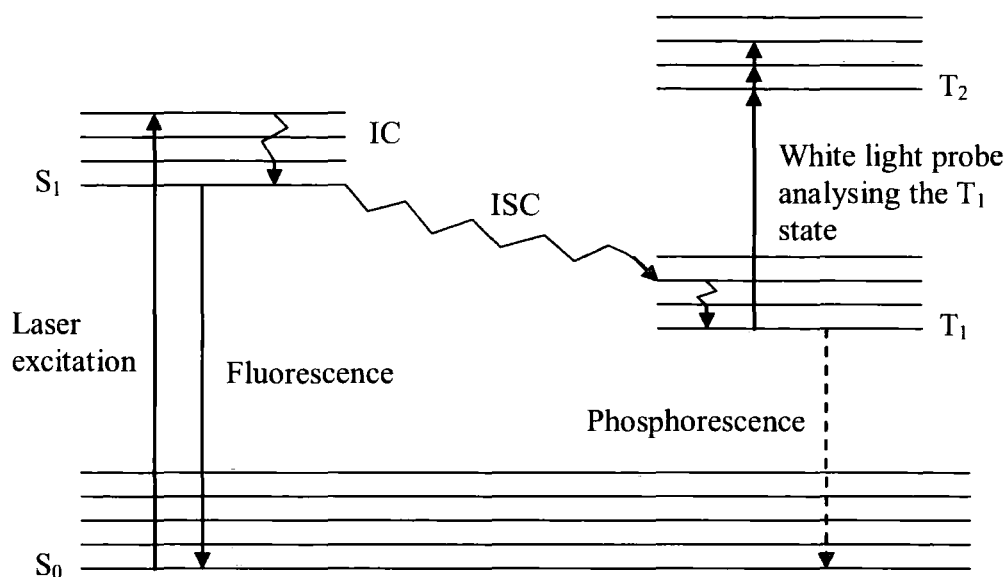
The absorption of all the solutions studied were  $\leq 0.1$  (solvent corrected) at the laser excitation wavelength and no greater than 0.5 at the absorption maximum. The excitation sources consisted of a Coherent Verdi-pumped MIRA-D Titanium-Sapphire laser, with a cavity dumper, used for 296 nm wavelength generation and a 366 nm diode laser (IBH NanoLED Model-11) with  $< 200$  ps pulse duration and a repetition rate of 1 MHz. The fluorescence was collected at  $90^\circ$  to the excitation source and the emission wavelength selected using a Jobin-Yvon Triax 190 monochromator. The instrument response function was measured using a dilute suspension of Ludox® silica in water as the scattering medium. The averaged time per channel value was 24 ps giving a full range of 49 ns over the 2048 point data set. A good signal is 800 Hz and above and the slit widths were increased from their 2 nm minimum position to achieve this when necessary. Lifetime data was acquired for a minimum of 10,000 counts in the peak channel of the pulse height analyser.

### 3.7 Nanosecond laser flash photolysis

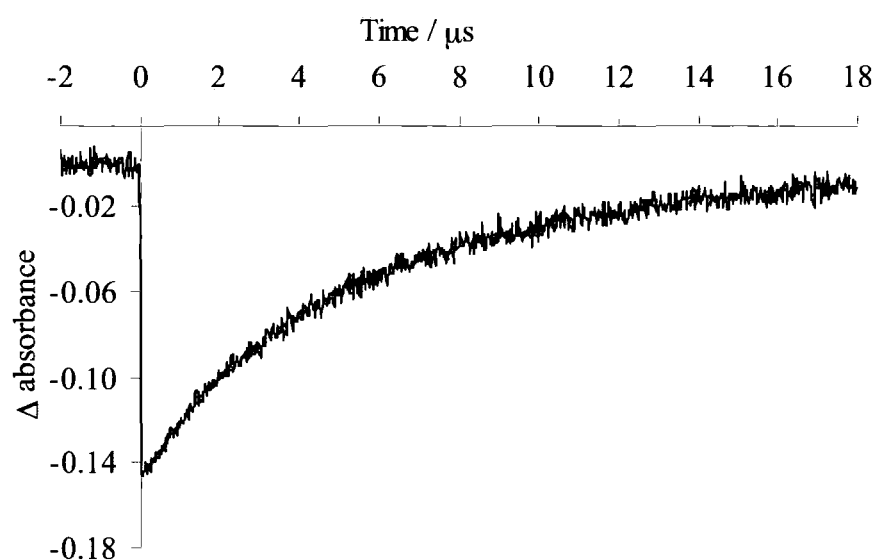
Nanosecond laser flash photolysis allows us to probe transient species with millisecond to sub-nanosecond lifetimes. The sample is excited by a short pulse of light which generates the first excited singlet state ( $S_1$ ). This state will decay by a number of processes including ISC to the triplet state. The excited sample is then probed with a white light beam to gain information about the triplet ( $T_1$ ) state (Figure 3.3). Changes in the probe light's intensity corresponds to its absorption by the  $T_1$  state. This is monitored to give information about the concentration of  $T_1$  as a function of time. Figure 3.4 is a typical transient decay from which the lifetime of  $T_1$  can be calculated using iterative least squares fitting. The intensity has been converted to delta absorbance ( $\Delta A$ ) using the equation

$$\Delta A = \log_{10} \left( \frac{I_0}{I_0 - I(a)} \right) \quad [3.9]$$

Here,  $I_0$  represents the intensity of the incident probe beam and  $I(a)$  represents the intensity of the absorbed probe light.



**Figure 3.3** Jablonski diagram illustrating the flash photolysis process.



**Figure 3.4** A typical transient decay.

Transient absorption spectra is built up by repeating the acquisition of  $\Delta A$  decays at different probe wavelengths and plotting  $\Delta A$  at time zero against the monitored wavelength.

### 3.7.1 Experimental details

The excitation source was a Q-switched Nd:YAG laser (Spectra Physics, Quanta Ray GCR-150-10) with a 10 Hz repetition rate. It was tuned to lase at 355 nm (the 3<sup>rd</sup> harmonic) with a typical output energy of about 2 mJ per pulse with a pulse duration of  $\approx 5$  ns. The transient was probed with a CW xenon lamp fitted with a

Cu<sub>2</sub>SO<sub>4</sub> solution filter to block IR light from the lamp. This probe beam gives the base line absorbance. After passing through the sample the probe beam reaches the computer controlled monochromator (Jobin–Yvon Triax 320). A Hamamatsu R928 silicon avalanche diode measured the intensity of the light at given wavelengths. To avoid damaging the detector, it is set at 90° to the excitation beam. A Tektronix TDS-340 digital storage oscilloscope was used to capture and average the transient decays. The data was transferred to a computer, converted to absorbance units and the triplet state absorption spectra plotted, as previously mentioned, using the Microsoft Excel package.

All samples were dissolved in cyclohexane and degassed by the freeze–pump–thaw method three times to remove oxygen which acts as a triplet state quencher.

### 3.8 Anisotropy measurements

The emission and excitation anisotropy of 1,4-bis(phenylethynyl)benzene was measured in cyclohexane, glycerol and at 77 K in EPA. It is a measure of the degree of polarisation of the emission. By measuring the anisotropy ( $r$ ) we can determine the fundamental anisotropy ( $r_0$ ), the rotational correlation time ( $\tau_c$ ) and the angle of displacement between absorption and emission dipoles ( $\beta$ ).

The emission and excitation anisotropy are determined from the equation

$$r = \frac{I_{VV} - GI_{VH}}{I_{VV} + 2GI_{VH}} \quad [3.10][2]$$

where  $I$  is the measured intensity and  $G$  is the ratio of the sensitivities of the detection system for vertically and horizontally polarised light. The subscripts indicate the orientation of the excitation and emission polarizers respectively, i.e.  $I_{HV}$  corresponds to horizontally (90°) polarised excitation and vertically (0°) polarised emission.  $G$  is determined from the equation

$$G = \frac{I_{HV}}{I_{HH}} \quad [3.11][2]$$

The emission intensities of the compound in the different media are measured with the excitation and emission polarisers in the orientations, VV, VH, HH and HV.  $G$  is determined by dividing the  $I_{HV}$  spectra by the  $I_{HH}$  spectra (equation [3.11]).  $r$  is determined by applying equation [3.10] to the other polarised intensity values.

This was repeated for excitation intensities and the resulting anisotropy versus excitation wavelength graphs were plotted.

### **3.8.1 Experimental details**

All the polarised emission and excitation spectra were recorded with a Jobin–Yvon Horiba Fluorolog 3-22 Tau-3 spectrofluorimeter[1] with a 2–5 nm band pass. Samples were measured in a quartz cuvette with a 10 mm path length. The cryostat was used for measurements at 77 K. The solutions all had absorptions of less than 0.1 at room temperature over the 200 to 400 nm range. The glycerol solution was made up by dissolving a minute quantity of the compound in 0.5 ml of EtOH in a large vial, then adding  $\approx$  6 ml of glycerol and stirring the mixture over night in a 55 C° water bath while the vial is loosely capped to allow the EtOH to escape. The data was captured on a computer and processed using the Microsoft Excel package.

### **3.9 Ultra–fast absorption and fluorescence spectroscopy**

Transient absorption (TA) and time–resolved emission measurements described in this work were carried out at the Central Laser Facility, Rutherford Appleton Laboratory at room temperature. From these measurements we gain important information about fast molecular dynamic events by probing the electronic transitions on the picosecond time scale.

In TA spectroscopy, the pump–probe technique is employed. Here, high concentrations of electronically excited transient species are generated with a femtosecond laser pump pulse. The changes in the transient absorption are measured using a second, time delayed, probe pulse in the form of a white light continuum, focused on the same region as the pump pulse. The probe intensity is monitored before and after the sample. The resulting beams are dispersed on two identical silicon 128 element arrays coupled to a XDAS readout system. Each camera’s signal is downloaded to a personal computer (PC) where they are normalised shot by shot across each pixel and stored as an average in an array. The transient absorption spectra at given time delays are recorded as well as the kinetic information which can be viewed by plotting the absorbance signal versus delay time at a given wavelength.

Samples were excited with at 267 nm wavelength with a pulse energy of  $\approx$  1 mJ generated from the 800 nm fundamental output of a Ti:Sapphire laser by a visible



light optical parametric amplifier (OPA) fitted with a sum frequency mixing unit. The transient absorption spectrum of the samples was recorded over the 400–750 nm range in cyclohexane. The samples are prepared with an absorbance of about 0.2 at the maximum absorbance wavelength of the sample in a 1 mm quartz cuvette. A 20 ml sample solution is allowed to flow through a 1 mm thick fused silica flow cell, using a chemically inert PTFE peristaltic pump.

The time-resolved emission spectroscopy (TRES) technique was used to measure the time-resolved spectra of BPEB in cyclohexane with a time resolution of 4 ps. The sample was excited with the same 267 nm laser pulse used for TA. The resulting emission is recorded at delay times ranging from 6–600 ps by a spectrometer with a low density (100 gr/mm) grating which provides a wide spectral coverage for fluorescence detection. The emission intensity over the 325 to 475 nm wavelength range was captured by an ISA CCD / 2000 x 800 pixels back illuminated UV enhanced detector. The resulting data is captured and processed on a PC using Microsoft Excel. The kinetics of the  $S_1$  state is also elucidated from this data by plotting the intensity of a given wavelength against time.

A 15 ml solution of BPEB was made up with an absorbance of about 0.1 at 267 nm. The sample solution was flowed through an open jet  $\approx$  0.5 mm in diameter using a PTFE peristaltic pump. This reduces the risk of sample decomposition due to strong absorption of the excitation radiation.

### **3.10 Time-resolved resonance Raman spectroscopy**

Picosecond and nanosecond time-resolved resonance Raman ( $TR^3$ ) spectroscopy measurements were carried out on a series of compounds studied in this work at the Central Laser Facility, Rutherford Appleton Laboratory at room temperature. From these measurements we gain information about the bond order of the excited state short lived transients using the pump and probe method.

#### **3.10.1 Picosecond time-resolved resonance Raman spectra**

Picosecond  $TR^3$  spectroscopy involves pumping the sample solution with at 267 nm wavelength derived from the 800 nm fundamental output of a Ti:Sapphire laser and an OPA system. The generated  $S_1$  excited state is then probed with 588 or 583 nm wavelength laser light from the same Ti:Sapphire / OPA system. An ISA Triplemate Raman spectrometer and a CCD / 2000 x 800 pixels back illuminated UV

enhanced detector linked to a PC were used to capture and store the measured Raman spectra at different time delays. The data was analysed using purpose written software and the Raman spectra, for time delays ranging from 3 to 1000 ps, were plotted using the Microsoft Excel package. The kinetics of the  $S_1$  state is also elucidated from this data by plotting the intensity of a given wavelength against time.

About 15 ml of sample solutions were made up with an absorbance of about 0.1 in 1 mm path length quartz cell at 267 nm allowed to flow through an open jet, about 0.5 mm in diameter, using a PTFE peristaltic pump.

The fluorescence background is excluded by employing a Kerr gate between the sample and the detection system. A short pulsed Raman signal is generated by the pulsed laser and transmitted through Kerr gate, while the longer lived fluorescence is rejected in the time domain.[15] The Kerr gate consists of two crossed polarisers and a Kerr medium. Fluorescence is blocked by the crossed polarisers in the closed state. At the time of Raman scattered emission from the sample, a short gating pulse of 800 nm that bypasses the polarisers creates a transient anisotropy within the Kerr medium by the optical Kerr effect.[15] The  $45^\circ$  polarised gating beam has its intensity adjusted to create an effective  $\lambda/2$  waveplate and rotate the polarisation of the light from the sample by  $90^\circ$ . This allows the light from the sample to be transmitted through the cross polariser for the duration of the gating pulse.[15]

### **3.10.2 Nanosecond time-resolved resonance Raman spectra**

Nonosecond- $TR^3$  spectroscopy uses the pump-probe technique to investigate the triplet excited state of a molecule. From this we gain insight into the type of bonding present in the triplet excited state.

The sample solutions were pumped by a Nd-YAG laser operating at a 355 nm wavelength with a repetition rate of 10 Hz and a 7 ns pulse length. The resulting excited state transient was probed using a 550 nm wavelength from a Lambda Physik FL003 Dye laser operating at 10 Hz with a pulse length of  $\approx 15$  ns, using Coumarin 153 laser dye. The excited singlet and triplet states resonance Raman spectra were recorded when the pump and probe beams were overlapped and for delays of 50 ns and 1  $\mu$ s.

The sample solutions, in cyclohexane, were purged with argon, for 10 minutes, to eliminate quenching of the triplet state by oxygen. One set of measurements was

taken for each compound after being purged with oxygen at a probe delay of 1  $\mu\text{s}$  for comparison. The purged solutions are pumped through a quartz tube  $\approx 10$  cm in length with a 2 mm inner diameter, and a 3 mm outer diameter, in an air tight circulating system, using a PTFE peristaltic pump. This tube is set at right angles to the path of the laser beams. The Raman scatter was collected at right angles to the pump and probe beams by a Spex Triplemate 1877 Series spectrograph with two 600 gr/mm gratings in the filter stage and a 1200 gr/mm grating in the spectrograph stage. A Princeton Instruments CCD camera (1024 x 256 pixels) was used to capture the intensities of the Raman shifts over the 600 to 2260  $\text{cm}^{-1}$  range. A photodiode and oscilloscope were used to monitor the pump and probe separation. All data were stored and analysed on a PC using purpose written software and the Raman spectra were plotted using the Microsoft Excel package.

### 3.10.3 Picosecond infrared absorption and transient excitation

The picosecond infrared absorption and transient excitation (PIRATE) system was used to measure fast solution phase processes by IR absorption and excitation spectroscopy. In the work presented in this thesis, the PIRATE system was used to measure the time-resolved infrared (TRIR) spectra of a group of donor-bridge-acceptor compounds, in protic and aprotic solvents, in an attempt to gain insight into the bonding order in their excited states. All measurements were carried out at the Central Laser Facility, Rutherford Appleton Laboratory at room temperature.

In this technique, the sample solutions were excited by a 266 nm pump beam with diameter of 150  $\mu\text{m}$ , a 1 kHz repetition rate and pulse energy of  $\approx 4$   $\mu\text{J}$ . The beam was generated by frequency-tripling a fraction of the 800 nm wavelength from a solid state Spectra Physics / Positive Light SuperSpitfire regenerative amplifier output. A broadband IR beam was generated by mixing the femtosecond signal and idler outputs of an OPA (pumped by the rest of the 800 nm beam) in  $\text{AgGaS}_2$ . By using a 50% germanium beam splitter, the sub-picosecond IR beam was split into probe and reference beams. The probe beam was focused on the sample cell and the transmitted light captured by a spectrometer. The reference beam was similarly treated, minus being passed through the sample. The resulting transmitted and reference spectra are recorded on two 64-element Mid IR array detectors with 5  $\text{cm}^{-1}$  resolution readout on each shot, and normalised point-by-point. The data was

stored and processed in a PC using purpose written software and the Microsoft Excel package.

The samples were made in 15 ml volumes of spectroscopic grade solvents with absorptions of  $\approx 1.5$  in a 2 mm quartz cell. Solutions were circulated through a flow cell with  $\text{CaF}_2$  windows with a path length of 2 mm using a PTFE peristaltic pump. This ensured fresh material was exposed on every shot.

### 3.11 General experimental details

All solvents used in this work were of spectrophotometric grade quality. The compounds analysed in the last four chapters of this work were synthesised in Durham University Chemistry department by three groups. Compounds discussed in Chapter 4 are mainly courtesy of Dr. P. J. Low's group; those in Chapter 5 and 6 were primarily made by Prof. T. B. Marder's group; and those in Chapter 7 were made by Dr. A. Beeby's group. The following compounds were also made by Dr. A. Beeby's group: 1,4-bis(2-(2-*tert*-butylphenyl)ethynyl)benzene and 1,4-bis(2-(2-*tert*-butylphenyl)ethynyl)-2,3,5,6-tetramethylbenzene, Chapter 4; 4-(4-(4-dimethylaminophenylethynyl)phenylethynyl)benzonitrile and 4-(4-(4-dimethylamino-3,5-dimethylphenylethynyl)phenylethynyl)benzonitrile, Chapter 5; and 9,10-bis(2-(2,4,6-triisopropylphenyl)ethynyl)anthracene, Chapter 6.

## REFERENCES

1. J. Y. Horiba, "Fluorolog-3 operation and maintenance manual", 1996.
2. J. R. Lakowicz, "Principles of fluorescence spectroscopy", 2nd ed, Kluwer Academic / Plenum Publishers, New York, 1999.
3. A. T. R. Williams, S. A. Winfield and J. N. Miller, "Relative fluorescence quantum yields using a computer-controlled luminescence spectrometer." *Analyst*, 1983, **108**, 1067-1071.
4. "Oxford research instruments variable temperature liquid nitrogen Cryostat operator's handbook", 1993.
5. O. L. Gijzeman, F. Kaufman and G. Porter, "Oxygen quenching of aromatic triplet-states in solution.1." *Journal Of The Chemical Society-Faraday Transactions II*, 1973, **69**, 708-720.
6. R. M. Badger, A. C. Wright and R. F. Whitlock, "Absolute intensities of discrete and continuous absorption bands of oxygen gas at 1.26 and 1.065  $\mu\text{m}$  and radiative lifetime of 11amdag state of oxygen." *Journal Of Chemical Physics*, 1965, **43**, 4345-4350.
7. S. Nonell and S. L. Braslavsky, "Time resolved singlet oxygen detection", in *Singlet Oxygen, UV-A and Ozone, Methods in Enzymology*, P. L. and S. H., Editors, Academic Press, 2000.
8. J. R. Lakowicz, ed. "Frequency-domain fluorescence spectroscopy", Topics in Fluorescence Spectroscopy, ed. J. R. Lakowicz. Plenum Press, New York, 1991 Vol. 1.
9. S. Fitzgerald, Ph.D. Thesis, A photophysical study of novel silicon and zinc phthalocyanines, Durham University, 2002.
10. D. V. O'connor and D. Phillips, "Time correlated single photon counting", Academic Press, London, 1984.
11. D. V. Oconnor, W. R. Ware and J. C. Andre, "Deconvolution Of Fluorescence Decay Curves - Critical Comparison Of Techniques." *Journal Of Physical Chemistry*, 1979, **83**, 1333-1343.
12. A. Grinvald and I. Steinbe, "Analysis of fluorescence decay kinetics by method of least-squares." *Analytical Biochemistry*, 1974, **59**, 583-598.
13. J. Durbin and G. S. Watson, "Testing for serial correlation in least squares regression.1." *Biometrika*, 1950, **37**, 409-428.
14. J. Durbin and G. S. Watson, "Testing for serial correlation in least squares regression.2." *Biometrika*, 1951, **38**, 159-178.

15. P. Matousek, M. Towrie, A. W. Parker, C. Ma, W. M. Kwok, D. Phillips and W. T. Toner, "Fluorescence suppression in Raman spectroscopy using a high performance picosecond Kerr Gate." *Central Laser Facility Annual Report*, 2000/2001, 168-169.

## CHAPTER 4

### Properties of 1,4-bis(phenylethynyl)benzene and its derivatives

#### 4.1 Introduction

The photophysical properties of 1,4-bis(phenylethynyl)benzene (**1**), and substituted poly(*p*-phenyleneethynylene) (PPE) derivatives have been investigated by several workers.[1-11] Some of these studies were performed in conjunction with studies of the potential of this class of molecules as fluorescent chemosensors[12], light emitting diodes[3] and photoluminescent polarisers[13] which exploit the highly conjugated skeleton of this type of material.

One of the earliest studies of PPE compounds was the effect of the triple bonds and phenyl groups on the conjugation, molecular conformation and the photophysical properties of 1,4-bis(*p*-tert-butylphenylethynyl)benzene (tBPEB) and other molecules containing phenyl groups and triple bonds, by Razumov *et al.*[1] From their comparative study, they concluded that the relative contribution of the triple bond to conjugation in tBPEB is comparable with the contribution from a double bond or phenyl ring; its structure is rigid and planar in all states; and the introduction of a phenyl ring into compounds with triple bonds increases their fluorescence. The assumption about molecular structure has since been contested by Magyer *et al.* who calculated the barrier to free rotation about the triple bond in phenyl-acetylene molecules to be as little as 0.05 eV (4.82 kJ mol<sup>-1</sup>).[14] Theoretical and experimental results have shown that in the ground state there are a range of conformations in which the phenyl rings are orientated between 45° and 90° to each other because of this low barrier to rotation.[14] It is the excited state structure that is planar or close to planar in these types of molecules.[14] Magyar *et al.* also demonstrated that conjugational length is significantly reduced by conformational rotation about the triple bond.

Sluch *et al.*[15] investigated the dynamics of the fluorescence of poly(*p*-phenyleneethynylene)s and suggested that the unusual spectral features result from twisting of the phenyl rings about the polymer axis and could be interpreted in terms of a quadratic coupling model. Their model suggests that the potential well is very shallow in the ground electronic state. This results in a broad thermal distribution of conformers in the ground state. They assumed that the excited state is


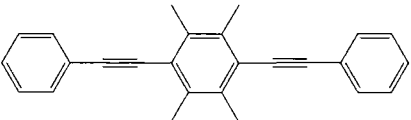
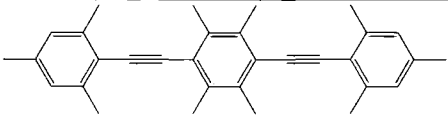
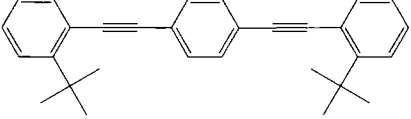
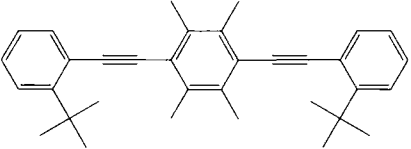
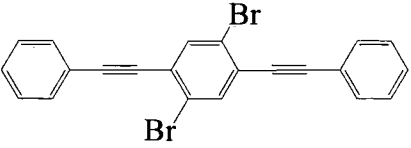
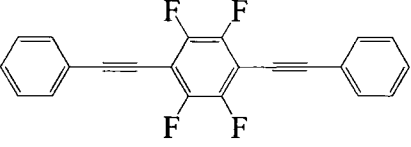
strongly influenced by quinoidal/cumulenic conformations and the narrowing of the emission spectrum is a result of the twisting of the phenyl rings into a few nearly planar configurations. Using fast time-resolved emission spectroscopy they demonstrated that the blue edge of the spectrum collapsed rapidly with a time constant of 60 ps, evidence of the rapid planarisation of the excited state. These interpretations are largely supported by works reported by Garcia-Garibay *et al.*[16, 17] and Beeby *et al.*[18]. Time-resolved resonance Raman spectroscopy measurements of **1** have shown that the assumption of quinoidal/cumulenic conformations dominating the excited state is not valid.[19] It was shown that the bonding in the first excited state was of weakened C=C character.

Other insights in to the photophysical properties of **1** and molecules like it include the observation of a linear relationship between Hammett's constants for substituents in the *para*-position ( $\sigma_p$ ) and the absorption wavenumber. This has been reported by Nakatsuji *et al.*[2] for **1** and its derivatives containing OCH<sub>3</sub>, CH<sub>3</sub> and Br substituents in the *para*-positions. Li *et al.*[20] reported that the fluorescence of **1**, in solution and in thin films, had a strong dependency on concentration. Increased intermolecular interaction leads to excimer formation, evident from the red shifted fluorescence spectra. Further increases in concentration produces aggregates which may interact with the excited molecules, resulting in a more complicated excited-state structure which increases the red shift of the fluorescence spectra. Introducing cyano (CN) groups in the *ortho* and *para* positions on **1** has been shown to significantly increase its fluorescence efficiency and emission wavelength maximum.[21] This was attributed to the easier formation of dipolar units (excitons) by CN groups which explained the increase in the radiative rate and decrease in the radiationless rate constants of the CN substituted molecules.

In this chapter, the results of the study of **1** with different substituents are presented. The aims of this study are: to confirm some of the reported photophysical properties of **1**; to determine the nature of the bonding in the ground and excited states of **1** and a selection of its derivatives by using time-resolved Raman spectroscopy techniques; to measure the anisotropy of **1** and record the effect of solvent viscosity on its value; and to assess the effect bulky groups and electron rich substituents have on the photophysical properties of **1**.



**Table 4.1** Compounds investigated.

Compound	Structure	Code
1,4-Bis(phenylethynyl)benzene		<b>1</b>
1,2,4,5-Tetramethyl-3,6-bis(phenylethynyl)benzene		<b>2</b>
1,2,4,5-Tetramethyl-3,6-bis-(2,4,6-trimethyl-phenylethynyl)benzene		<b>3</b>
1,4-Bis(2-(2- <i>tert</i> -butylphenyl)ethynyl)benzene		<b>4</b>
1,4-Bis(2-(2- <i>tert</i> -butylphenyl)ethynyl)-2,3,5,6-tetramethylbenzene		<b>5</b>
1,4-Dibromo-2,5-bis(phenylethynyl)benzene		<b>6</b>
1,2,4,5-Tetrafluoro-3,6-bis(phenylethynyl)benzene		<b>7</b>

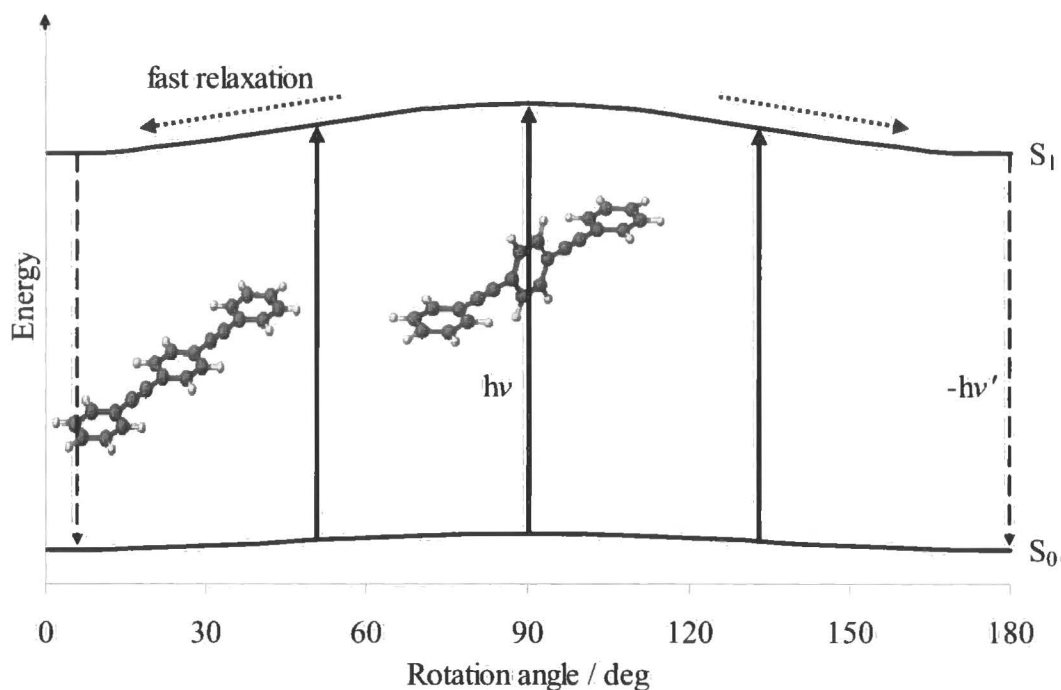
A list of the compounds studied, their structure and the numbering scheme that will be used throughout is given in Table 4.1. The absorption spectra, extinction coefficients ( $\epsilon$ ), fluorescence spectra, fluorescence lifetimes ( $\tau_f$ ) and fluorescence quantum yields ( $\Phi_f$ ) of all the molecules in this study were measured and compared. The first anisotropy data for **1** in solvents of different viscosities are reported herein. The first pico and nanosecond time-resolved resonance Raman spectroscopy data for **1**, **3**, **4**, **6**, and **7** are also presented and discussed.

## Results and discussion

### 4.2 Steady state photophysical properties in solution

The normalised absorption and fluorescence spectra of molecules **1** to **7**, in cyclohexane at room temperature, are presented in Figure 4.2. In all cases the observed excitation and emission spectra of each molecule are independent of the emission and excitation wavelengths. A summary of the characteristic absorption and emission peaks, lifetimes, extinction coefficients and quantum yields of the molecules investigated is given in Table 4.2.

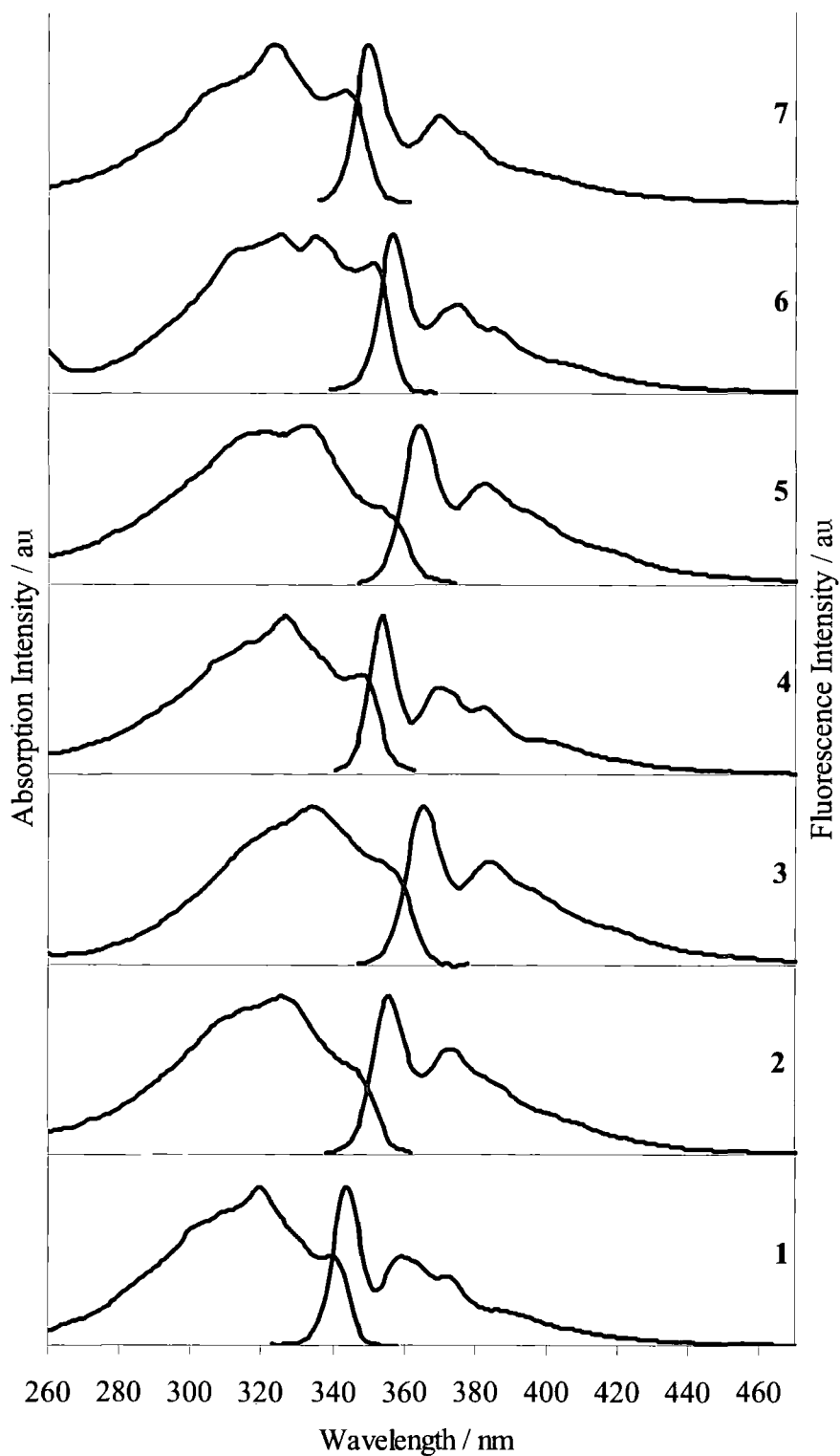
At ambient temperature, in cyclohexane, the absorption spectra of **1** to **7** show a characteristic intense band below 380 nm. There is some evidence of vibrational fine structure with a shoulder on the red edge of each spectrum. The absorption profile of **1** agrees with the spectra reported by Biswas *et al.*, in hexane and methanol[22], and by Birckner *et al.*, in dioxane.[23] Compounds **3** and **5** carry the most electron donating groups and exhibit the largest bathochromic shift of the absorption maxima (14 nm) when compared to **1**. The spectral profile of **6** indicates the molecular conformation is affected by the bromine heavy atoms. This is a possible indication of a restricted rotation of the central phenyl ring. Compound **7** has four fluorine atoms, which are known to be  $\pi$ -electron donating and  $\sigma$ -electron withdrawing[24], but this seems to have little effect on its absorption when compared to the unsubstituted **1** and the emission spectra shows only a slight bathochromic shift. The generally broad unresolved absorption spectra of the investigated molecules, over the 260–340 nm spectral range is the result of two factors. Firstly, at room temperature the barrier to rotation of the phenyl rings of **1** was found experimentally to be about 2.7 kJ mol<sup>-1</sup> in the ground state.[25] As this is comparable to  $kT$  at ambient temperature (2.5 kJ mol<sup>-1</sup>), 30% of the molecules will have enough energy to allow free rotation of the phenyl rings.[25] Thus all possible conformations will exist in the ground state (Figure 4.1).[8, 26] Secondly, calculations on **1** have demonstrated that the S<sub>1</sub>←S<sub>0</sub> transition represents a HOMO to LUMO transition.[8, 26] Based on the similarities of the absorption spectra of these seven molecules, it is proposed that they are all due to a similar HOMO to LUMO transition.



**Figure 4.1** Conformational energies of the ground state and first excited state of **1** in solution. The lower line represents the ground state rotational energy potential surface with a maximum of  $\approx 2.7 \text{ kJ mol}^{-1}$ . An equilibrium mixture of conformers results in a broad absorption spectrum (upward arrows). In the excited state, rapid relaxation to more planar conformations within its lifetime results in a homogeneous emission from the coplanar conformer (downward arrows).

In contrast to the absorbance spectra, all the emission spectra possess well-defined vibrational fine structure in cyclohexane. After excitation, the range of conformations undergo relaxation, in the  $S_1$  state potential surface, to the more stable planar conformation (Figure 4.1).[15, 18, 26] In the case of **1**, its emission profile is similar to that observed by Levitus *et al.*[8] and is reported to be from the planar conformation.[8, 26] It has been reported that the planar geometry in unsubstituted and substituted cases is the most stable with the lowest energy.[26] As all the fluorescence profiles are very similar, it can be deduced that the presence of the alkyl and halo substituents are not bulky enough to cause any significant steric hindrance, and hence distortion of the excited state in solution. The substituted molecules are still able to attain a planar, or near planar, geometry before emitting.

All the molecules were determined to have relatively large extinction coefficients and high fluorescence quantum yields (Table 4.2). All seven had similar fluorescence profiles, over the 330–460 nm spectral range, with the major (0,0) transition occurring between 343 and 365 nm.



**Figure 4.2** The normalised absorption (left) and fluorescence (right) spectra of molecules 1–7 in cyclohexane.

The fluorescence lifetimes of compounds **1** to **7** ranged from 0.53 to 0.72 ns, with the exception of **6** which had a lifetime of < 0.1 ns. The  $\tau_f$ ,  $\Phi_f$  and  $\epsilon$  values of **1** are very similar to the values reported previously.[8, 23]

**Table 4.2** The major absorption and emission peaks, lifetimes ( $\tau_f$ ), extinction coefficients ( $\epsilon$ ) and quantum yields ( $\Phi_f$ ) of **1** to **7** in cyclohexane.

Cpd.	Major peaks / nm		$\tau_f$ / ns $\pm 0.05$ ( $\chi^2$ )	$\epsilon$ / mol <sup>-1</sup> dm <sup>3</sup> cm <sup>-1</sup> $\pm 1,000$ (absorption / nm)	$\Phi_f$ $\pm 0.05^b$
	Absorption	Emission			
<b>1</b>	320, 340 (sh)	344, 359, 372	0.53 (0.80)	58,400 (320)	0.85 <sup>c</sup>
<b>2</b>	325, 345 (sh)	356, 373	0.62 (1.17)	47,800 (326)	0.89
<b>3</b>	334, 356 (sh)	365, 384	0.63 (0.20)	49,100 (335)	0.92
<b>4</b>	327, 348 (sh)	354, 370, 383	0.60 (1.51)	56,900 (326)	0.89
<b>5</b>	334, 355 (sh)	364, 382	0.72 (1.49)	53,200 (334)	0.89
<b>6</b>	325, 335, 351 (sh)	357, 374, 385 358, 580 (sh) <sup>a</sup>	< 0.1 (1.01), 4.0 ms <sup>a</sup>	46,700 (325)	0.05
<b>7</b>	324, 344 (sh)	350, 370	0.57 (1.75)	67,100 (324)	0.97

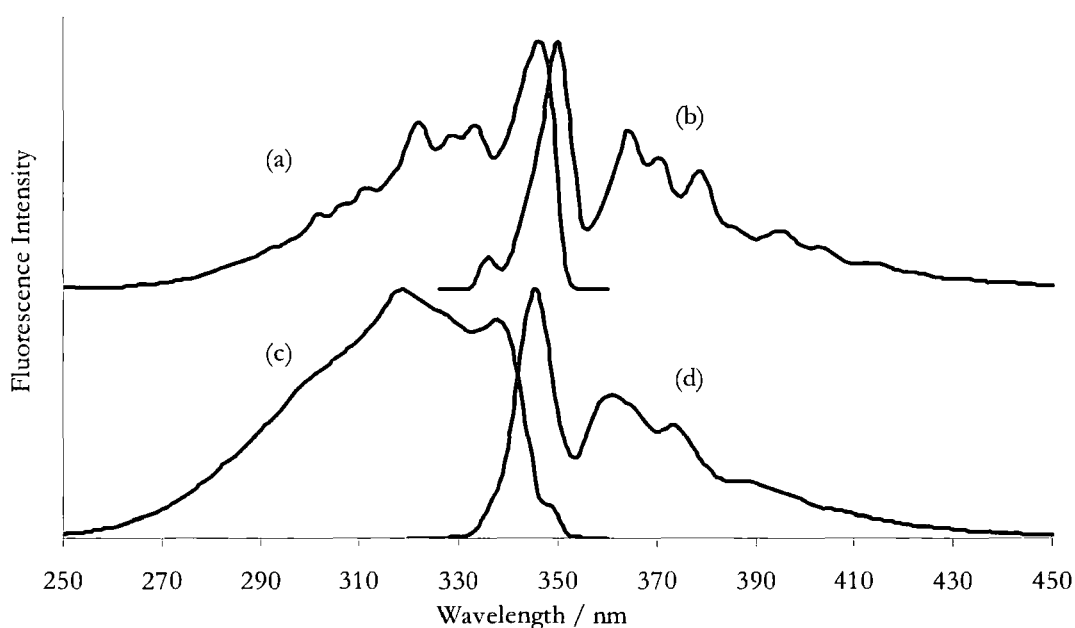
Key: sh- shoulder. <sup>a</sup> Phosphorescence emission peaks and lifetime in a transparent glass matrix of EPA at 77 K  $\lambda_{ex}$  = 335 nm. <sup>b</sup> Relative to the standards quinine sulphate in 0.1 M H<sub>2</sub>SO<sub>4</sub> ( $\Phi_f$  = 0.55) and POPOP in cyclohexane ( $\Phi_f$  = 0.97). <sup>c</sup> Relative to the standards quinine sulphate in 0.1 M H<sub>2</sub>SO<sub>4</sub> and  $\beta$ -carboline in 0.5 M H<sub>2</sub>SO<sub>4</sub> ( $\Phi_f$  = 0.6).

The dibromo derivative, **6**, had the smallest extinction coefficient ( $\epsilon$  = 46,700 mol<sup>-1</sup> dm<sup>3</sup> cm<sup>-1</sup>) and the lowest fluorescence quantum yield ( $\Phi_f$  = 0.05). It was also the only one to exhibit phosphorescence in low temperature glasses and had a phosphorescence lifetime of 4.0 ms in EPA (diethylether:2-ethylbutane:ethanol, 5:5:2) at 77 K. The deviation in photophysical properties of **6** from the rest, is due to the presence of the heavy bromine atoms which have a large spin-orbit coupling and hence promote intersystem crossing and phosphorescence.[27] On the other hand, the presence of the fluorine atoms on the central phenyl ring has made derivative **7** the most fluorescent of this group ( $\Phi_f$  = 0.97) with the largest extinction coefficient (67,100 mol<sup>-1</sup> dm<sup>3</sup> cm<sup>-1</sup>). The highly electronegative fluorine substituents lower the energy of the HOMO which makes the energy gap between the ground and the excited state wider.[28] According to the energy gap law, this results in a decrease of the nonradiative decay rate and thus enhances the fluorescence. The absorbance

and emission spectra for all the molecules exhibited very small Stokes shifts (from 6 to 11 nm or 342 to 896  $\text{cm}^{-1}$ ) and strong spectral overlapping.

### 4.3 Steady state photophysical properties in a frozen matrix at 77 K

The emission and excitation spectra, of **1** to **7**, were recorded in MCH/IP (methylcyclohexane:2-methylbutane, 4:1) and EPA at 298 K and as glassy matrices at 77 K. The comparative spectra are illustrated in Figure 4.3 to Figure 4.9. Table 4.3 lists the characteristic fluorescence and excitation peaks at 298 K and 77 K along with the average vibrational energy gaps calculated from the difference between the 0,0 and 0,1 bands of the excited singlet ( $S_1$ ) and ground singlet ( $S_0$ ) state transitions.

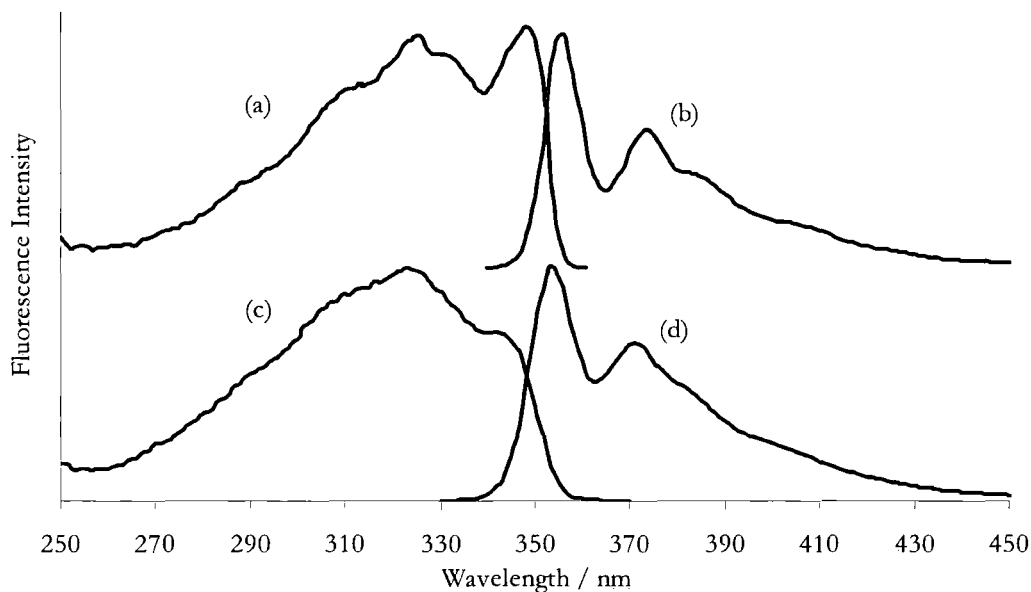


**Figure 4.3** Normalised excitation and emission spectra of **1** in MCH/IP at 77 K, (a) and (b), and 300 K, (c) and (d), determined using emission at 350 nm and excitation at 335 nm.

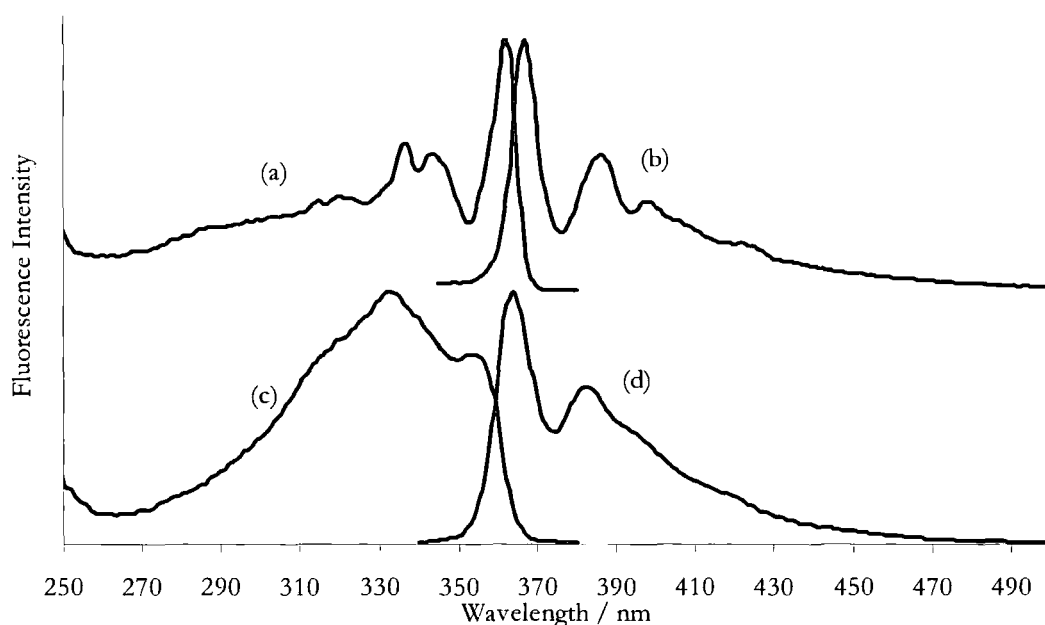
The excitation profiles of **2** to **5** and **7**, at room temperature in EPA, are quite similar to that of **1**. In all cases the absorption maxima are more red-shifted than in **1**. The absorption spectrum of **6** has slightly more vibrational fine structure than the rest. The room temperature fluorescence spectra are all comparable to that of **1**. At low temperature, 77 K, the excitation and emission spectra of all the molecules, except **5**, follow Kasha's rule.[29] They are mirror images of each other with significantly more vibrational fine structure than the room temperature profiles and have a larger bathochromic shift. This 'mirror image' relationship is indicative of the molecule having very similar molecular conformations and bonding in the ground state and excited states, and suggests that in the ground state at low

temperature the molecule has adopted a more planar conformation.[18] The investigated molecules all exhibit very strong spectral overlap of the (0,0) transitions and minor Stokes shifts (from 2 to 7 nm or 160 to 566  $\text{cm}^{-1}$ ) at 77 K.

At 77 K the dominant transition in both the excitation and emission spectra is the (0,0) transition between the  $S_0$  and  $S_1$  states. The emission spectrum of **5** exhibits a new peak at 339 nm at 77 K (Figure 4.7).

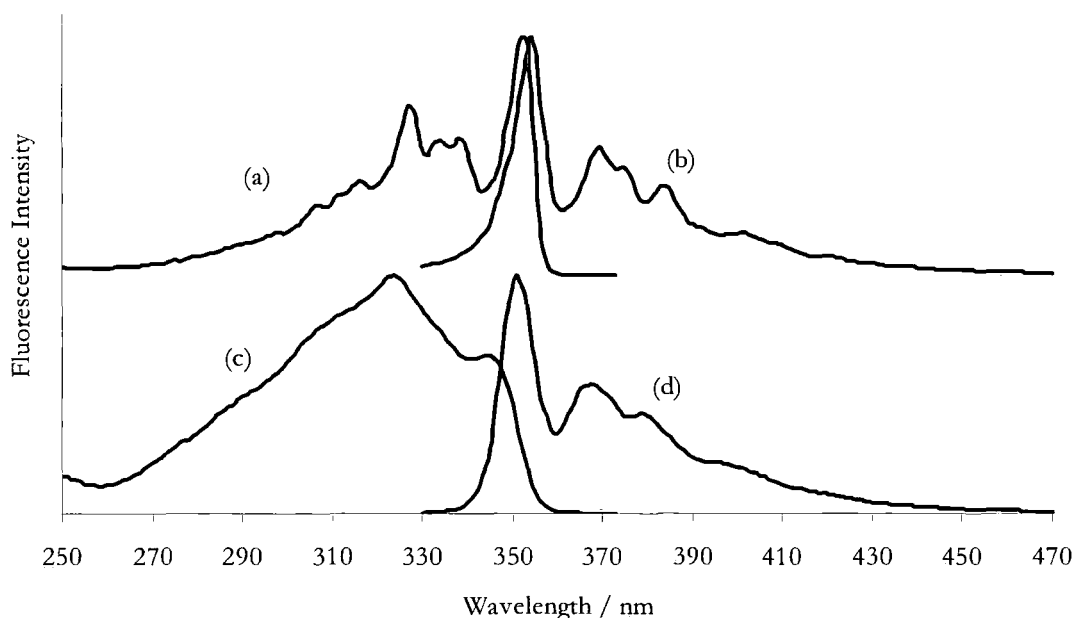


**Figure 4.4** Normalised excitation and emission spectra of **2** in EPA at 77 K, (a) and (b), and 298 K, (c) and (d), determined using emission at 380 nm and excitation at 325 nm.

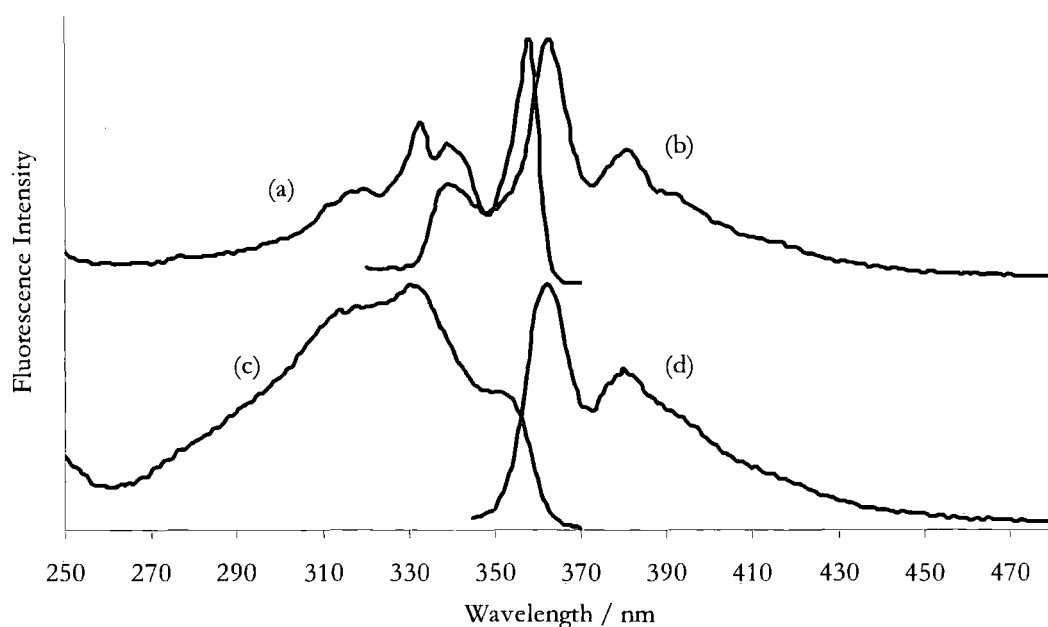


**Figure 4.5** Normalised excitation and emission spectra of **3** in EPA at 77 K, (a) and (b), and 298 K, (c) and (d), determined using emission at 380 nm and excitation at 300 nm.

This compound is the most sterically hindered of the group and this new peak is evidence of the presence of a high energy molecular conformation at the time of emission. The inability of all the molecules to attain the lowest energy conformation before emission is due to the reduced rotation about the  $C\equiv C$  bond. This is a result of steric hindrance caused by the bulky *t*-butyl groups and the further constraint of the high viscosity of the low temperature glass matrix.[18]



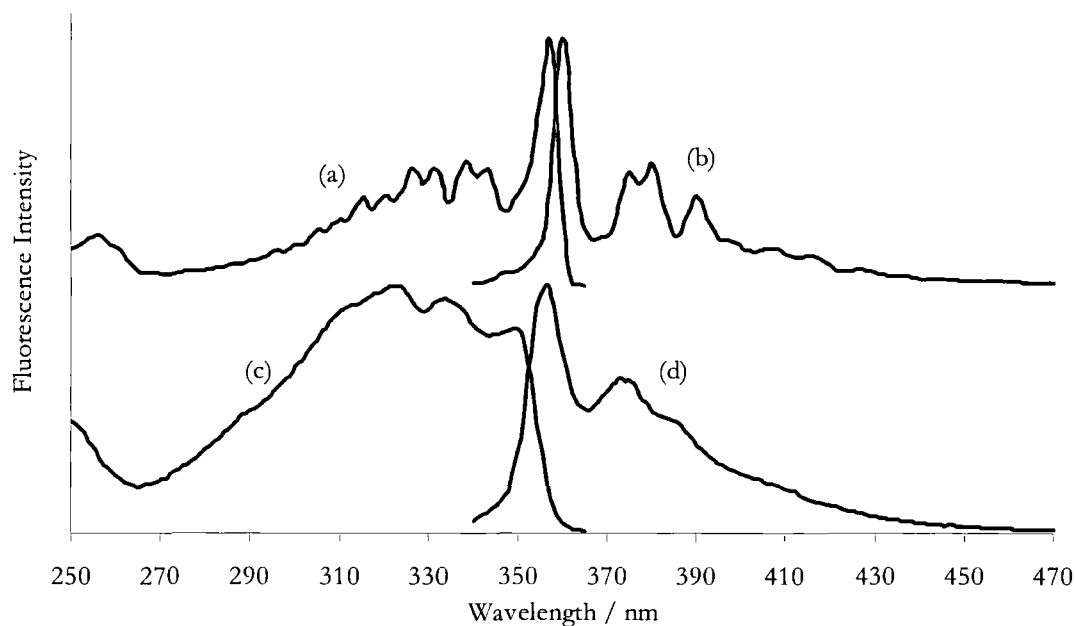
**Figure 4.6** Normalised excitation and emission spectra of **4** in EPA at 77 K, (a) and (b), and 298 K, (c) and (d), determined using emission at 383 nm and excitation at 320 nm.



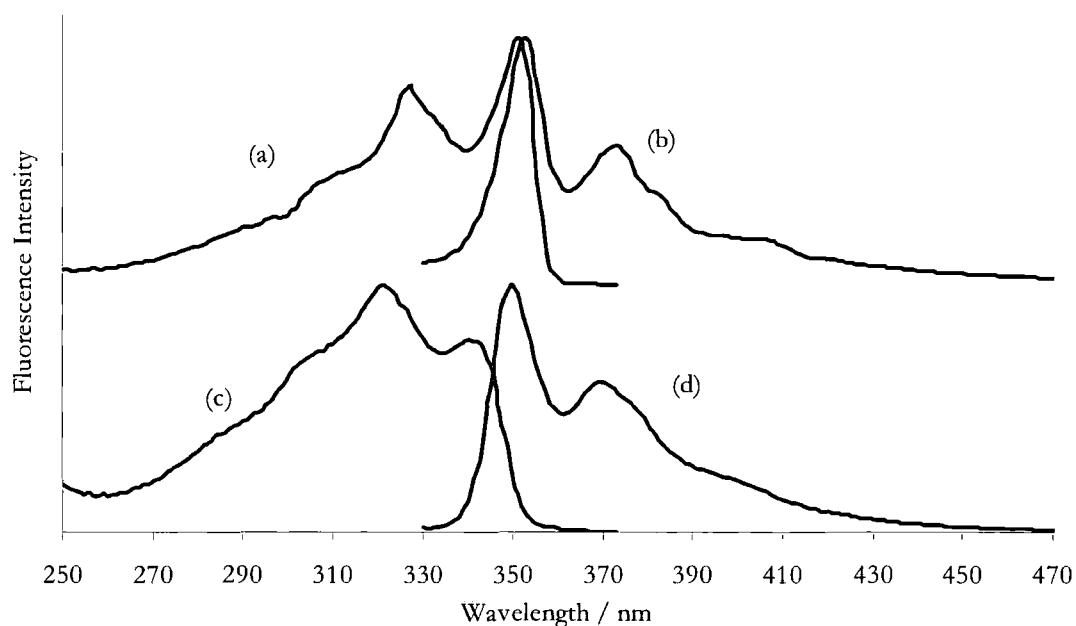
**Figure 4.7** Normalised excitation and emission spectra of **5** in EPA at 77 K, (a) and (b), and 298 K, (c) and (d), determined using emission at 400 nm and excitation at 313 nm.



Calculations of the vibrational level spacings in the ground and excited states from the low temperature fluorescence spectra were made. This allowed for the tentative assignment of the vibrational modes based on theoretical and experimental Raman vibration calculations (Table 4.3). It is observed that all the main vibrational spacings are in the typical region of the aromatic C-C ring stretching modes of 1300–1500  $\text{cm}^{-1}$ .



**Figure 4.8** Normalised excitation and emission spectra of **6** in EPA at 77 K, (a) and (b), and 298 K, (c) and (d) determined using emission at 375 nm and excitation at 330 nm.



**Figure 4.9** Normalised excitation and emission spectra of **7** in EPA at 77 K, (a) and (b), and 298 K, (c) and (d), determined using emission at 400 nm and excitation at 300 nm.

**Table 4.3** The major excitation and emission peaks of **1** to **7** in MCH/IP<sup>a</sup> and EPA in the liquid and glass matrix phase are listed in columns 2 and 4. Columns 3 and 5 lists the approximate vibrational energy spacings, in wavenumber, based on the difference between the 0-0 and 0-1 transitions in the excited ( $\nu_{S1}$ ) and ground ( $\nu_{S0}$ ) states.

Cpd.	$\lambda_{\text{exci}} / \text{nm}$		$\Delta\nu_{S1} / \text{cm}^{-1}$		$\lambda_{\text{emi}} / \text{nm}$		$\Delta\nu_{S0} / \text{cm}^{-1}$	
	298 K	77 K	298 K	77 K	298 K	77 K	298 K	77 K
<b>1<sup>a</sup></b>	319, 338 (sh)	312, 322, 328, 333, 346	1760	1130	345, 361, 373, 388	350, 364, 370, 379, 395	1280	1100
<b>2</b>	323, 344 (sh)	311, 325, 331, 348	1890	1480	354, 371	355, 373, 384	1290	1360
<b>3</b>	332, 355 (sh)	315, 320, 337, 343, 362	1950	1550	364, 382	367, 386, 399, 421	1290	1340
<b>4</b>	324, 344 (sh)	316, 327, 334, 338, 352	1790	1180	351, 368, 379	354, 369, 375, 384, 402	1320	1150
<b>5</b>	330, 351 (sh)	320, 333, 339, 358	1810	1560	362, 380	339, 363, 381, 391	1310	1300
<b>6</b>	323, 334, 349 (sh)	315, 320, 327, 331, 338, 343, 357	1290	1140	356, 373, 386	360, 375, 380, 390, 408, <sup>b</sup> 538, 580(sh)	1280	1110
<b>7</b>	302, 321, 340 (sh)	308, 327, 351	1740	2090	350, 370	353, 373, 382	1540	1520

Key: sh - shoulder. <sup>b</sup> Phosphorescence for 335 nm wavelength excitation.

There are no vibrational bands attributable to C≡C stretching modes[23] which usually occur between 2000–2300  $\text{cm}^{-1}$ . Reported theoretical fluorescence spectra of **1** predict the high energy C≡C vibration to occur at 2490  $\text{cm}^{-1}$ . [14]

The energies of the lowest  $S_1$  state of **1** is 3.59 eV (346.4 kJ mol<sup>-1</sup>)—calculated from the emission spectra (0,0) transition at 298 K. The energy of the  $S_1$  state of **1** in benzene has been determined to be 3.44 eV (331.9 kJ mol<sup>-1</sup>).<sup>[30]</sup> The addition of the substituents lowers this  $S_1$  state energy by various degrees. The lowest  $S_1$  state energies of **2**, **4** and **7** range from 3.53 to 3.50 eV (340.6 to 337.7 kJ mol<sup>-1</sup>). While the more heavily substituted molecules **3**, **5** and **6** have  $S_1$  state energies from 3.48 to 3.41 eV (335.8 to 329.0 kJ mol<sup>-1</sup>).

#### 4.4 Fluorescence Anisotropy

The fluorescence anisotropy (see Chapter 2) was measured to determine the fundamental anisotropy ( $r_0$ ), the rotational correlation time ( $\tau_c$ ) and the angle of displacement between the absorption and emission dipoles ( $\beta$ ) of **1**.

The fundamental anisotropy, of **1** was determined from excitation anisotropy measurements made in an optically dilute solution of the fluorophore in EPA at 77 K (Figure 4.10). In this vitrified solution the dominant conformation is that with all the three rings coplanar, and molecular rotation is prevented by the viscous glass host. Theoretical calculations have predicted that all the lowest energy transitions lie along the long axis of **1**.<sup>[8]</sup> This was proven experimentally from dichroic measurements<sup>[8]</sup> using the stretched polyethylene film method.<sup>[31]</sup> In the region of the  $S_1 \leftarrow S_0$  absorption band the  $r_0$ , at its highest, was calculated to be 0.37 at an excitation wavelength of 342 nm. Such a value is expected for fluorophores with parallel absorption and emission dipoles. The value also represents an absence of depolarising processes such as rotational diffusion or RET with near linear electronic transitions. It is slightly higher than the  $r_0$  value, of 0.26, calculated for **1** by Birckner *et al.*<sup>[23]</sup> They used time correlated single photon counting to measure the emission decay curves, of **1** in dioxane, with a parallel and perpendicular orientated analyzer. With this equipment they were able to determine the rotational correlation time directly from the kinetic measurements. Details on how the  $r_0$  was determined from the time-resolved polarisation measurements were not given.

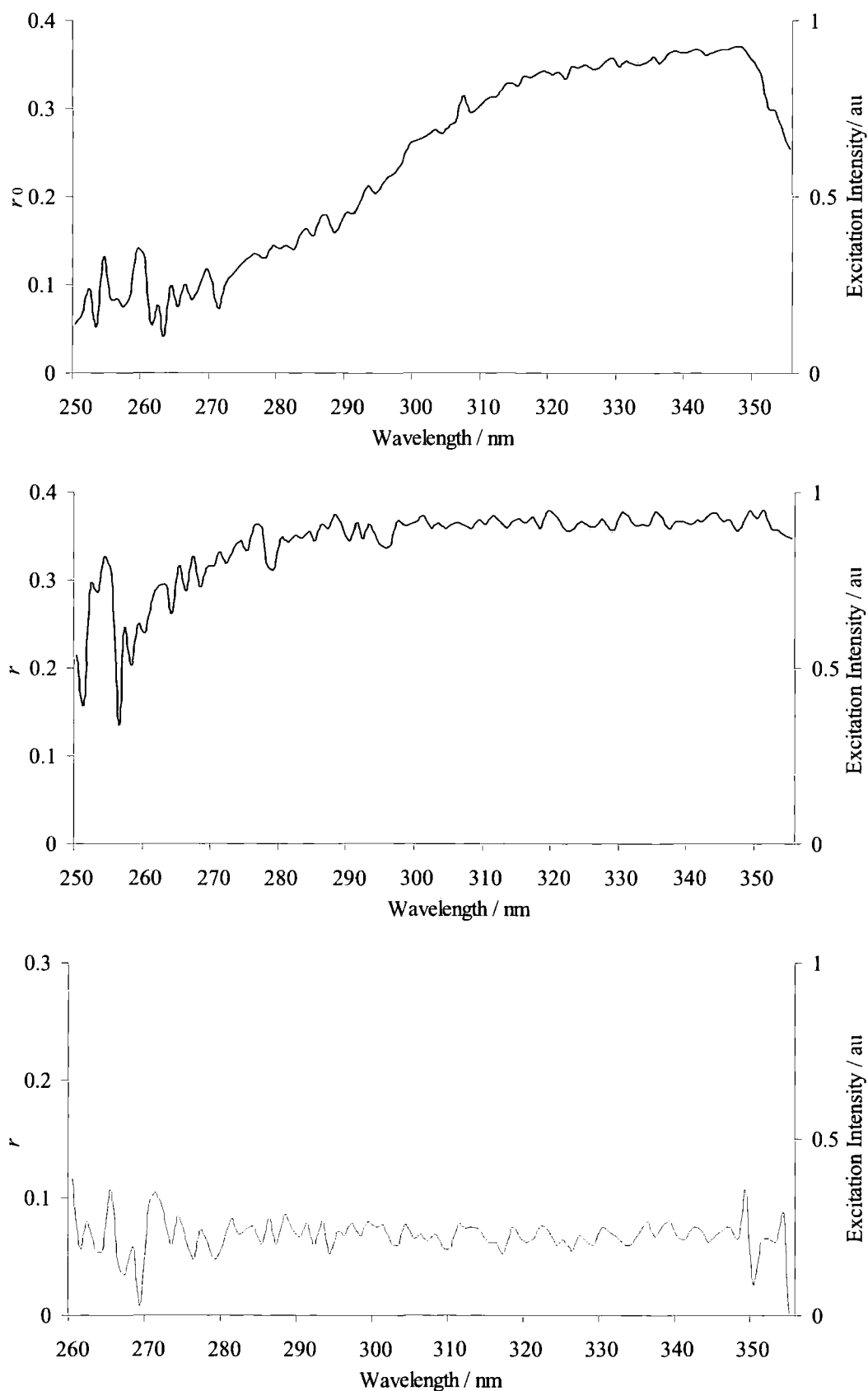
$\beta$  was calculated from equation [2.20] in Chapter 2. Here, the  $r_0$  value at wavelength 342 nm in the excitation spectrum of **1** measured at 77 K was used. From this,  $\beta$  was determined to be 13.8° (Table 4.4).  $r_0$  is more excitation wavelength dependent at higher energies because of the changing contributions from

electronic transitions to higher electronic states, each of which have different  $\beta$  values.

The excitation anisotropy in glycerol was almost equivalent to  $r_0$  and is indicative of the slowing of rotational diffusion of the fluorophore in this highly viscous solvent. Interestingly,  $r$  is also observed to be less wavelength dependent at higher transition energies. In glycerol, **1** exists as a continuum of conformers. Exciting the sample with, for example, vertically polarised light results in the excitation of all the vertically polarised molecular conformers with different absorption energies—assuming all the lowest energy electronic transitions of each conformation lie along the molecules longest axis. The resulting anisotropy spectrum is actually a summation of the excitation anisotropy of these various conformers. This is reflected in the dissimilarities between the excitation spectra of **1** in EPA at 77 K and in glycerol. At 77 K the low energy planar conformation is most dominant and the resulting excitation spectrum is red shifted and has better resolved vibrational peaks. On the contrary, the excitation spectrum in glycerol is generally broad (similar to the spectrum in cyclohexane) and only partially resolved due to the presence of the many conformers. All the excited conformers contribute equally to the resulting polarised emission as the majority will become planar and relax to the lowest excited state prior to emitting. This is evident from the relative similarities between the highly resolved emission spectra of **1** in EPA at 77 K and in glycerol.

At ambient temperature in cyclohexane, the emission of **1** is almost completely depolarised. The excitation and emission anisotropy is 0.07 and totally independent of excitation wavelength. Birckner *et al.*[23] calculated a value of 0.08 from steady state measurements in dioxane at room temperature. Under these conditions  $r$  is near zero due to the rotational correlation time being much shorter than the emission lifetime in this non-viscous solvent. It is also expected that free rotation of the aryl rings about the C=C will result in the presence of a range of conformers.[8, 18]

The fluorescence anisotropy of **1** in cyclohexane and glycerol, at 298 K, and in EPA at 77 K were also measured and were all independent of the emission wavelength. The average fluorescence anisotropy was almost equal to the excitation anisotropy at 342 nm at low temperature and in glycerol (Table 4.4).



**Figure 4.10** From top to bottom: (—) the fundamental anisotropy ( $r_0$ ) of **1** dissolved in EPA at 77 K, anisotropy ( $r$ ) of **1** in glycerol and in cyclohexane, at 298 K; (...) the normalised vertically polarised excitation spectra of **1** for 380 nm emission.

**Table 4.4** The changes in the excitation and fluorescence anisotropy ( $r$ ) value, the angular displacement of transition moments value ( $\beta$ ) and the rotational correlation time value ( $\tau_c$ ) of **1** at 342 nm with increasing solvent viscosity.

Solvent	Excitation $r$ at 342 nm / $\pm 0.02$	$\beta$ / degrees $\pm$ 0.3	Average fluorescence $r \pm 0.02$	$\tau_c$ / ns $\pm 0.05$
EPA at 77 K	0.37 <sup>a</sup>	13.8 <sup>b</sup>	0.35	
Glycerol at 298 K	0.37	13.5	0.36	19
Cyclohexane	0.07	47.4	0.07	0.12

<sup>a</sup> fundamental anisotropy ( $r_0$ ). <sup>b</sup> the angular displacement of transition moments in the absence of depolarisation processes.

The fluorescence lifetime and  $r$  are related by the Perrin equation (Chapter 2):

$$\frac{1}{r} = \frac{1}{r_0} + \frac{\tau_f}{r_0 \tau_c}$$

where  $r$  is the observed anisotropy,  $r_0$  is the fundamental anisotropy,  $\tau_f$  is the fluorescence lifetime and  $\tau_c$  is the rotational correlation time. The extent to which the fluorescence anisotropy is decreased strongly depends on the rotational correlation time. For **1** in cyclohexane, assuming  $r_0 = 0.37$  and  $\tau_f = 0.53$  ns,  $\tau_c$  was determined to be  $\approx 120$  ps. In glycerol  $\tau_c$  is extremely long with a calculated value of  $\approx 19$  ns. Table 4.4 lists the measured  $r$  and  $r_0$  values for **1** together with calculated values of  $\beta$  and  $\tau_c$ . It is expected that  $r$  will approach  $r_0$  when  $\tau_c$  is very large—as observed in viscous solvents—and  $r$  will be near zero when  $\tau_c$  is quite small.

The time-resolved polarisation measurements of **1** in dioxane determined  $\tau_c$  to be 0.22 ns[23] which is in keeping with our results. The measured  $\tau_c$  characterises the depolarisation movement as the torsion perpendicular to the long molecular axis containing the transition moment.[23]

#### 4.5 Time-resolved spectroscopy

A time-resolved spectroscopy technique is broadly defined as anything that allows the measurement of the temporal dynamics and kinetics of photophysical processes.[32] More specifically, changes in properties such as excited state population and excited state structure over time can be measured. In this study time-resolved emission spectroscopy (TRES), transient absorption (TA) spectroscopy and time-resolved resonance Raman (TR<sup>3</sup>) spectroscopy were the three techniques used

to investigate the excited state population, molecular structure and bond order of **1** to 7. All three techniques utilise pump laser pulses that are shorter in width than the decay of the excited state of the sample.

Time-resolved emission measurements involve exciting the dissolved sample with a laser pulse, of specific wavelength, and recording its total emission intensity after different time delays. In our study, the emission for time delays from 6 to 600 ps was measured to investigate the molecular conformation in the early stages after excitation.

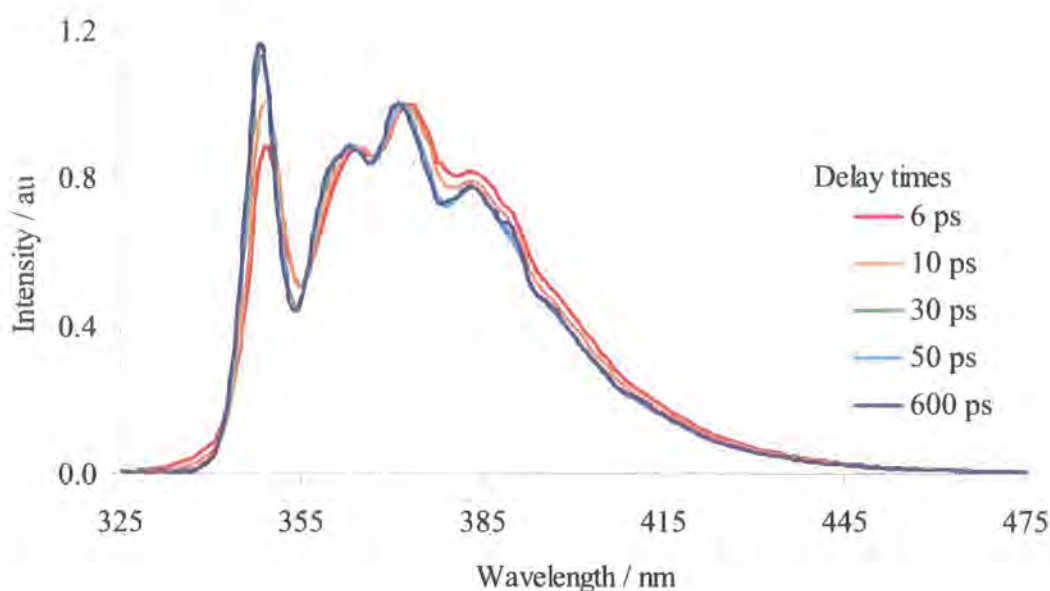
Transient absorption studies utilises ultra-fast pump probe spectroscopy to measure the  $S_n \leftarrow S_1$  and  $T_n \leftarrow T_1$  transitions. The equipment used for these studies (at the Central Laser Facility, Rutherford Appleton Laboratory) limited the time window over which these bands were observed to the first 2 ns after excitation. A solution of the sample is pumped with a laser pulse of a specific wavelength to its  $S_1$  state. After a suitable time delay a weaker probe pulse, of white light, is passed through the excited sample. The resulting transient spectrum is recorded as the difference in absorption before and after the pump pulse as a function of wavelength.

Time-resolved resonance Raman spectroscopy is used, in combination with TA spectroscopy, to probe the molecular structure and the bond order of molecules in the first tens of picoseconds after excitation. The TA spectra are required to identify the excitation wavelengths needed for resonance enhancement of the Raman scattering of the transient state. In TR<sup>3</sup>, the sample solution is exposed to a laser pulse (pump) which excites the molecules into an excited electronic state. A short interval later, a second pulse (probe) excites the resonance Raman spectrum of the transient species created by the first pulse.[33] The resonance Raman spectrum is then recorded with a highly sensitive detection system (see Chapter 3). The  $C \equiv C$  and skeletal C-C stretching frequencies are easily discernable from the Raman spectra. By recording the resonance Raman of transient species on the ps delay time scale, changes, if any, in the characteristic molecular vibrations and structure, *vide infra*, can be monitored.

#### **4.6 Time-resolved emission measurements**

An investigation into the molecular structure and the type of bonding in the ground state, and  $S_1$  excited state of **1** was carried out. The TRES of **1** in cyclohexane were recorded, with the Kerr gate system at the Central Laser Facility, Rutherford

Appleton Laboratory (see Chapter 3), following excitation at 267 nm (Figure 4.11). The TRES of **1** differs in appearance from its steady state profile because the spectrum has not been corrected for spectral response from the spectrometer. Interestingly there are subtle changes in the emission profiles within the first 30 ps after excitation. The changes are most pronounced on the blue edge of the spectra (around 338 and 347 nm). At longer delay times the spectra remains constant and decays with a fluorescence lifetime of 530 ps. These subtle changes on the early time scale indicates the molecule is still in the processes of relaxing to the lowest energy conformation of the singlet excited state, with some of the blue edge emission coming from the non-relaxed conformers.



**Figure 4.11** Time-resolved, spectrally uncorrected, emission spectra of **1** in cyclohexane after excitation at 267 nm. Spectra normalised at 372 nm to emphasize changes on the blue edge during early delay times.

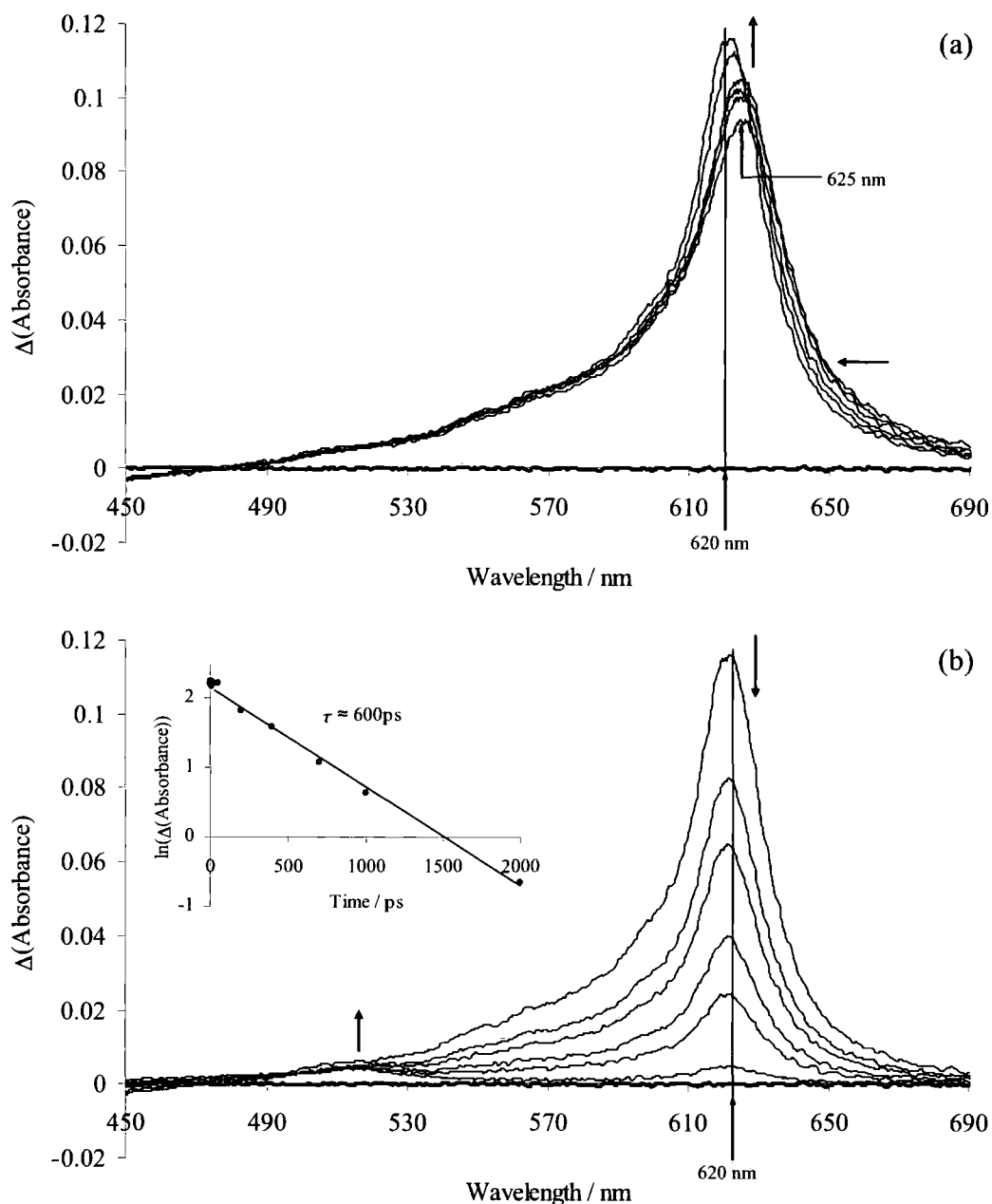
The differences in the fluorescence kinetics on the blue edge of the emission spectrum of **1** can also be argued to be attributed to non-relaxed, or hot, fluorescence. This emission arises from a vibrationally excited state after one or more quanta of vibrational energy have been lost through anharmonic decay.[34-36] It has been measured for various compounds in different environments in femtosecond[37] and picosecond[35, 38-40] kinetics studies of vibrational relaxation in molecules. It is possible that the initial fluorescence, from **1**, at 338 nm originates from non-relaxed vibronic states while the fluorescence component at 347 nm could be the relaxed fluorescence from the lowest electronic excited state. It is observed



that as the 338 nm edge decays the 347 nm band increases in intensity over the some 6–30 ps time scale. This increase in intensity is attributed to the increasing population of the lowest electronic excited state from the upper vibrationally excited states via non-radiative decay mechanisms. Barbara *et al.* have made similar observations for salicylidenaniline in ether[36] and tetraphenylethylene in 3-methylpentane[41], both at 4 K. In the case of salicylidenaniline, they observed a fast component on the blue edge of the fluorescence with a rise time ( $\tau_r$ ) of  $< 5$  ps and lifetime of 10 ps and a long wavelength component with a 10 ps  $\tau_r$  and a  $\tau_f \approx 3$  ns. Mataga *et al.*[34] have observed the dynamics of hot fluorescence for Zn-tetraphenylporphyrin and Zn-diphenylporphyrin derivatives in the femtosecond–picosecond time regimes. They concluded the hot fluorescence emission probably originated from the non-relaxed vibronic states immediately after  $S_2 \rightarrow S_1$  IC, and higher vibronic states in addition to the almost relaxed state near the bottom of  $S_1$  formed by ultra fast vibronic redistribution, all over the wavelength region between  $S_2$  and  $S_1$ .

#### 4.7 Transient absorption measurements

The  $S_n \leftarrow S_1$  transient absorption (TA) spectra of **1** in cyclohexane (Figure 4.12) were recorded by ultra-fast pump probe spectroscopy to determine the optimum wavelength for TR<sup>3</sup> spectroscopy. The transient absorption spectra show a strong band at 625 nm immediately following excitation. The band intensity increases by *ca.* 20% and shifts to 620 nm over the first 50 ps following excitation after which the absorption band decayed with a lifetime of *ca.* 600 ps. These shifts are attributed to the changing conformations of the molecule. The rate of radiative decay of the excited singlet state of **1** is reported to be  $1.75 \times 10^9 \text{ s}^{-1}$ . [42] The absorption decay of the 620 nm band is accompanied by the development of a weak band at 509 nm, after about 700 ps, which persists for  $> 2$  ns. This weak band is assigned to a  $T_n \leftarrow T_1$  absorption. Nanosecond–flash photolysis experiments with 1,4-bis(phenylethynyl)-2,5-bis(hexyloxy)benzene supports this assignment.[43] Our results are also in keeping with triplet state measurements made using the pulse radiolysis energy transfer method [44-46] by Burrows.[30] In this method, the triplet state of **1** is selectively produced in an argon saturated benzene solution using biphenyl as a sensitizer. A triplet state absorbance band at 530 nm with a lifetime of 150  $\mu\text{s}$  was recorded.



**Figure 4.12** Transient absorption spectra of the  $S_n \leftarrow S_1$  band of **1** in cyclohexane excited at 267 nm and probed between 450 and 700 nm. (a) shows the - 50 to 50 ps delay period and (b) the 50 to 2000 ps delay period. (b) inset shows the liner relationship between  $\ln(\Delta(\text{Absorbance}))$  of the total spectra and time. Unlabeled arrows show the increases, decreases and shifts in intensity over time.

#### 4.8 Time-resolved resonance Raman measurements

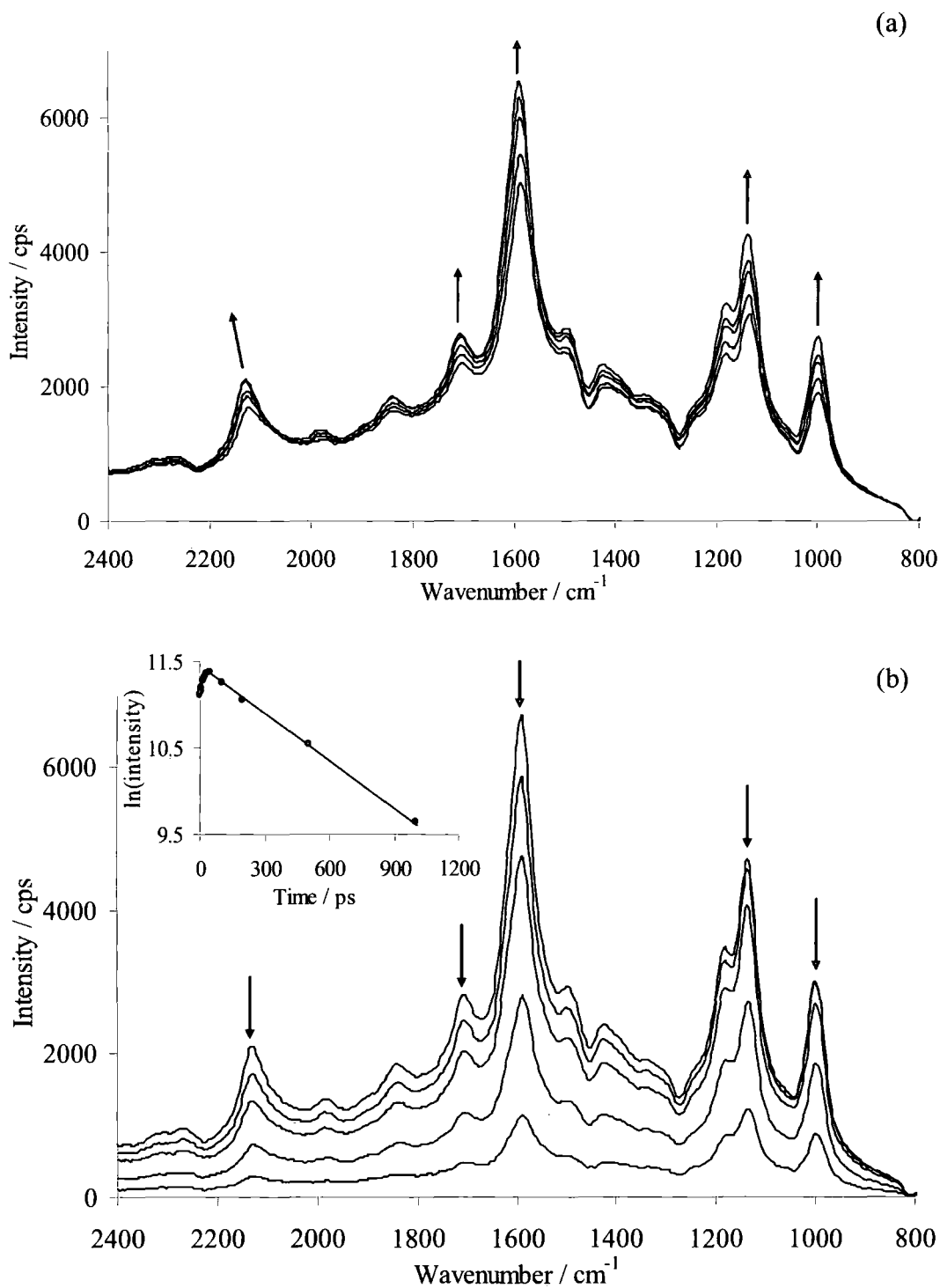
The picosecond time-resolved resonance Raman (ps-TR<sup>3</sup>) spectra of the  $S_1$  state of **1** in a cyclohexane solution, after excitation at 267 nm, for delays ranging from 3 to 1000 ps, are depicted in Figure 4.13 (a) and (b). The spectra were recorded when probing at 588 nm, to the blue of the transient absorption band. This wavelength, whilst not optimal for the absorption band, was used as longer wavelength excitation

gave weaker detected Raman signals due to the reduced sensitivity of the spectrometer at longer wavelengths.

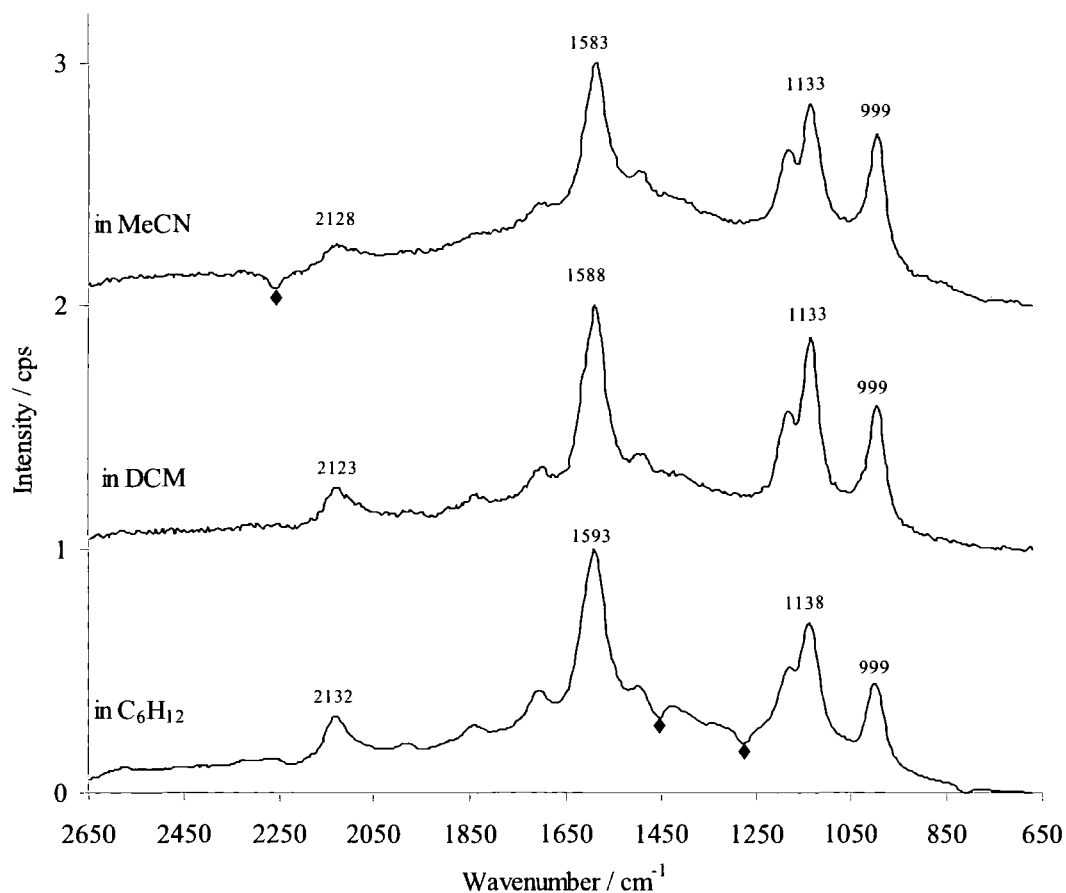
The ps-TR<sup>3</sup> spectra show subtle shifts and changes in intensity in the first 50 ps after excitation. Most notable is the C≡C stretching band around 2123 cm<sup>-1</sup> which shifts by 9 cm<sup>-1</sup> to 2132 cm<sup>-1</sup>. This shift starts after 15 ps and stops at 50 ps. After 50 ps the peak remains at 2128 cm<sup>-1</sup>. The spectrum of the S<sub>1</sub> state of **1** also shows prominent bands at 1593, 1138, and 999 cm<sup>-1</sup>. These have been assigned as carbon-phenyl stretching, carbon-hydrogen parallel bending and ring breathing modes respectively based on ground state theoretical calculations by Chernia *et al.*[47] and Beeby.[48] During the first 50 ps, the intensity of all the bands increased by *ca.* 24–36%. After the initial rapid changes, the TR<sup>3</sup> signal decayed mono-exponentially (Figure 4.13 (b) inset) with a lifetime matching that of the excited singlet state. These subtle changes in the first 50 ps are attributed to the free rotations of the aryl rings in **1** and changes in the Raman excitation profiles. The transient absorption and emission spectra data mentioned earlier also supports this conclusion.

The ps-TR<sup>3</sup> of **1** in dichloromethane (DCM) and acetonitrile (MeCN) were recorded to determine the effect of solvent polarity on the Raman vibrations in the S<sub>1</sub> state on the ultra-fast time scale. There are no distinct changes in the Raman spectra of **1** in DCM and MeCN over the 10 to 1500 ps delay period. Between 2050 and 1650 cm<sup>-1</sup> **1** shows less vibrational structure in DCM and MeCN than in cyclohexane (Figure 4.14). The excited state lifetimes follow a mono-exponential decay in the polar solvents and are similar to that in cyclohexane. Generally, the vibrational modes are unaffected by solvent polarity.

To investigate structure and bonding of **1** in the excited triplet state, the ns-TR<sup>3</sup> spectra were recorded after a 320 nm excitation for delays of 0, 50 and 1000 ns under argon and probing at 540 nm. There are no variations in the vibrational fine structure of the transient Raman spectra over the selected delay periods. The vibration bands are better resolved in the ns-TR<sup>3</sup> profile than in the ps-TR<sup>3</sup> spectra. The shorter time scale has broader bands due to the limitation on the band width because of the uncertainty principle. The C≡C is a significantly weaker band than the other signature vibrational bands of **1**. The C≡C stretch is also observed to be up shifted from its frequency in the S<sub>1</sub> state by 14 cm<sup>-1</sup> to 2146 cm<sup>-1</sup> in the T<sub>1</sub> state (Figure 4.15).

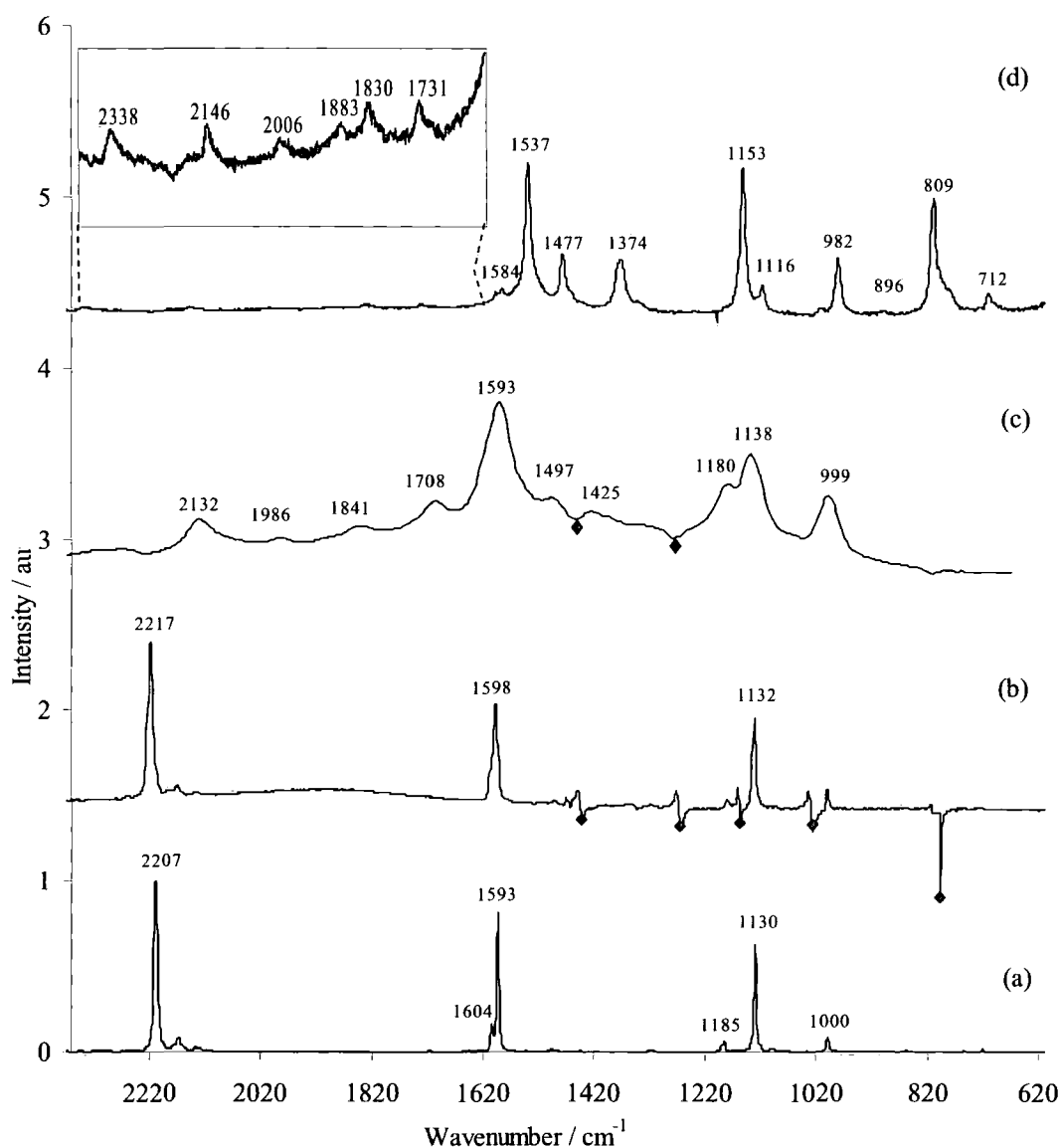


**Figure 4.13** The time-resolved resonance Raman spectra of the  $S_1$  1 in cyclohexane after 267 nm excitation and probing at 588 nm. (a) shows the 3 to 30 ps delay period and (b) the 50 to 1000 ps delay period. (b) inset shows the linear relationship between  $\ln(\text{intensity})$  of the Raman spectra and time. The arrows show the increases, decreases, and shifts in the intensity over time.



**Figure 4.14** Time-resolved Raman spectra of **1** in cyclohexane, DCM and MeCN after 50 ps, exciting at 267 nm and probing at 588 nm. ♦ denotes miss-cancelled solvent peaks.

The Raman spectra of **1** in the ground state and the  $S_1$  and  $T_1$  excited states after 50 ps and 50 ns time delays are compared in Figure 4.15. The ground state spectra show the presence of the four major bands mentioned earlier. A comparison of the solid ground state Raman spectra of **1**, with that of **1** with four deuterium substituents bonded to the central ring[48] shows them to be identical except for one peak. The  $1593\text{ cm}^{-1}$  vibration in **1** is down shifted to  $1566\text{ cm}^{-1}$  in deuterated **1**, thus confirming that this vibration corresponds to the symmetric stretching of the phenyl rings. In Figure 4.15 (b), the  $1,000\text{ cm}^{-1}$  band observed in the ground state Raman spectra of **1** in the solid state (Figure 4.15 (a)) is masked by the cyclohexane solvent peak. Table 4.5 lists all the Raman vibrations shown in Figure 4.15 and the mode assignments based on  $A_g$  symmetry of the ground state[47] for the major peaks and ground state calculations using the *Gaussian 03* package[49] with the B3LYP density functional and the 6-31G\* basis set.



**Figure 4.15** Ground state Raman of **1** in (a) the solid state probing at 633 nm, (b) in cyclohexane probing at 532 nm. Time-resolved resonance Raman of **1** after (c) 50 ps, pumping at 267 nm and probing at 588 nm and (d) 50 ns, pumping at 320 nm probe 540 nm under argon. ◆ indicate missed solvent peaks remain following spectral subtraction.

When compared to the solution  $S_0$  state, the acetylene bond stretch decreases in wavenumber by  $71\text{ cm}^{-1}$  in the  $T_1$  excited state and by  $85\text{ cm}^{-1}$  in the  $S_1$  excited state, making it the most shifted band of the four. The Raman bands at 1598 and  $1000\text{ cm}^{-1}$  are all down shifted while the  $1132\text{ cm}^{-1}$  band is up-shifted by  $+6$  and  $+21\text{ cm}^{-1}$  in the  $S_1$  and  $T_1$  states respectively. The  $\text{C}\equiv\text{C}$  bond, though considerably weakened, still persists in the triplet excited state.

**Table 4.5** The non-resonance<sup>a</sup> and time-resolved resonance Raman<sup>b</sup> bands of **1** with vibrational mode assignments.

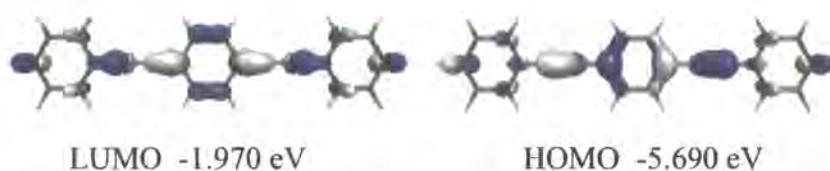
Ground state / $\text{cm}^{-1 a}$		Excited states in $\text{C}_6\text{H}_{12}$ / $\text{cm}^{-1 b}$				Mode description <sup>c</sup>
Solid state	In $\text{C}_6\text{H}_{12}$	$S_1$ after 50 ps	Shift <sup>e</sup>	$T_1$ after 50 ns	Shift <sup>e</sup>	
				2338 vw		
2207 s <sup>d</sup>	2217 s	2132 m	-85	2146 vw	-71	
		1986 vw		2006 vw		
		1841 vw		1883 vw		
		1708 w		1731 vw		
1604 sh				1584 w		
1593 s	1598 s	1593 s	-5	1537 s	-61	
		1497 m		1477 m		
		1425 vw		1374 m		
1185 vw		1180 sh				
1130 s	1132 s	1138 s	+6	1153 s	+21	
				1116 w		
1000 vw	1000 vw	999 m	-1	982 m	-18	
				896 vw		
				809 s		
				712 w		

<sup>c</sup> Vibrational mode assignments are made on the basis of work done by Chernia *et al.*[47] and calculations done by Beeby[48] using the *Gaussian 03* package[49] with the B3LYP density functional and the 6-31G\* basis set. <sup>d</sup> Qualitative Raman: 's', 'm', 'sh', 'w' and 'vw' refers to the peak intensities respectively as 'strong', 'medium', 'shoulder', 'weak' and 'very weak'. <sup>e</sup> Vibrational shifts in the excited state spectra from the ground state spectrum in cyclohexane.

Significantly, these time-resolved experiments give no indication of a completely cumulenic/quinoidal structure existing in the  $S_1$  state as suggested elsewhere. The observed significant acetylenic character in the  $S_1$  state is not inconsistent with the



molecular orbital structure of **1**.<sup>[50]</sup> Theoretical calculations determined that in the planar geometry of **1**, the frontier orbitals are fully delocalised. The HOMO is calculated to have bonding character between the carbon atoms of the acetylenes, and antibonding character with respect to the C(sp)–C(sp<sup>2</sup>) bonds, whilst the reverse is true of the LUMO (Figure 4.16). There are also other lower lying, highly delocalised, orbitals which contribute to the acetylene bonding character of **1**.<sup>[48, 51]</sup> These allow for first excited state LUMO←HOMO transitions to occur with little change in the bond order.



**Figure 4.16** Orbital contour plots of the LUMO and HOMO in **1** depicting the delocalisation of the frontier orbitals.<sup>[51]</sup>

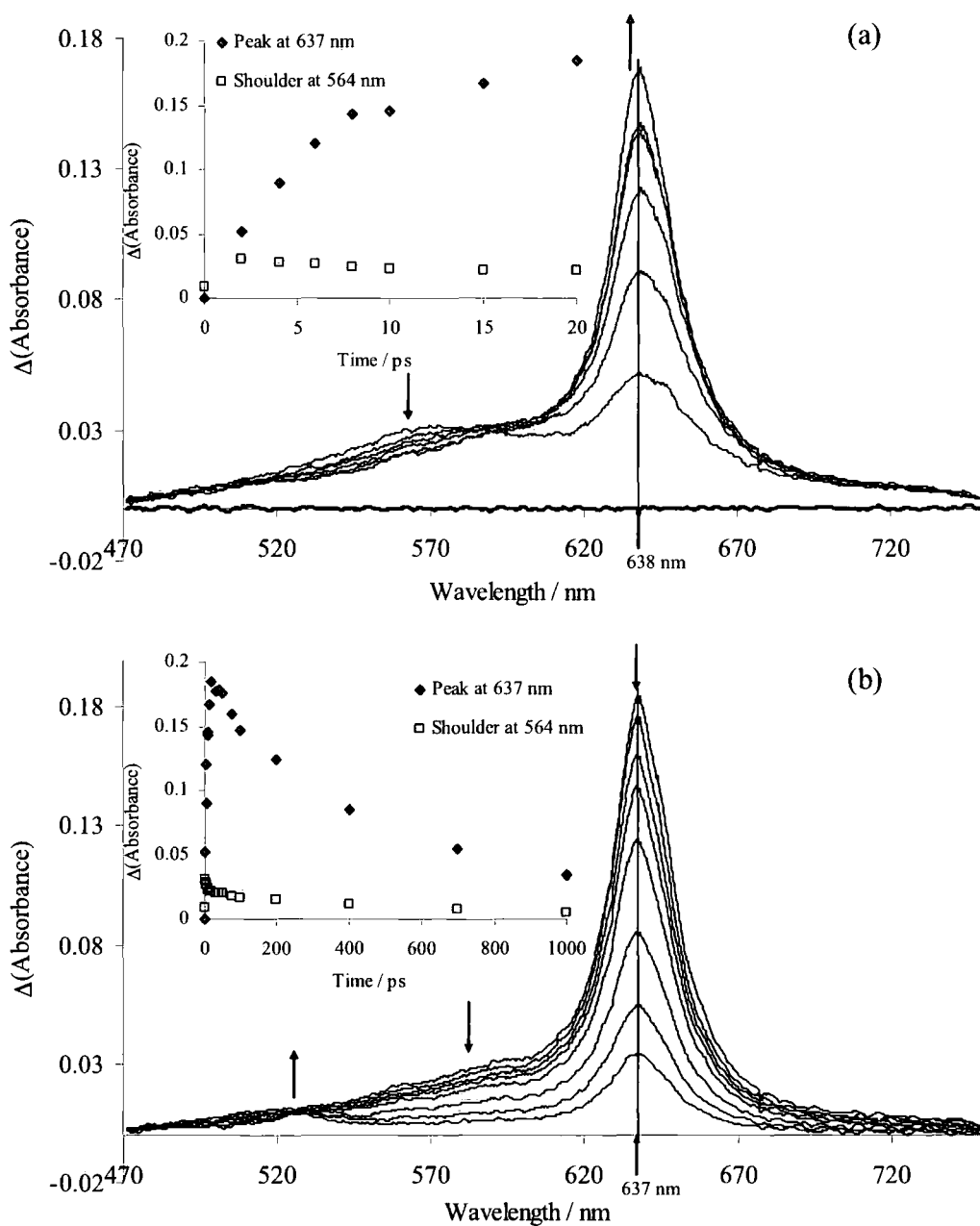
#### 4.9 Transient absorption, ground state and time-resolved resonance Raman measurements of 1,4-Bis(2-(2-*tert*-butylphenyl)ethynyl)-2,3,5,6-tetramethylbenzene (**5**).

The TA of **5** (Figure 4.17) is similar to **1** in the 620 to 700 nm region. The main transient is red shifted in **5** and is centred at 637 nm. However, over the 470 to 620 nm region a broad shoulder at  $\approx 564$  nm is observed. The absorbance intensity increases with a rate of  $\approx 1.06 \times 10^{10} \text{ s}^{-1}$  (in 2 ps) after which the 564 nm shoulder decays rapidly in the first 15 ps with a lifetime of  $\approx 37$  ps (and a rate of  $\approx 8.96 \times 10^8 \text{ s}^{-1}$ ) (Figure 4.17 (a)). The 637 nm peak increases in intensity in the 15 ps interval with an initial rate of  $\approx 2.5 \times 10^{10} \text{ s}^{-1}$ . This could be evidence of the different conformers of **5** becoming planar—the slowing down of this process being due to the presence of the substituents causing steric hindrance or drag through the solvent. After this time, a weak peak starts growing in at 528 nm and persists for  $> 1$  ns, this is assigned to a  $T_0 \leftarrow T_1$  absorption.

The ground state and excited state Raman spectra of **5** are compared in Figure 4.18. The C≡C stretching vibration is readily identified in the ground state (2190 cm<sup>-1</sup>) and first excited state (2099 cm<sup>-1</sup>). However, the C=C stretches and in-plane ring deformations (1585 cm<sup>-1</sup>) are more predominant in the resonance Raman of the excited state. These vibrations appear in the ground state at 1596 and 1575 cm<sup>-1</sup>. Compound **5** has more vibrational fine structure than **1** in the 1510 to

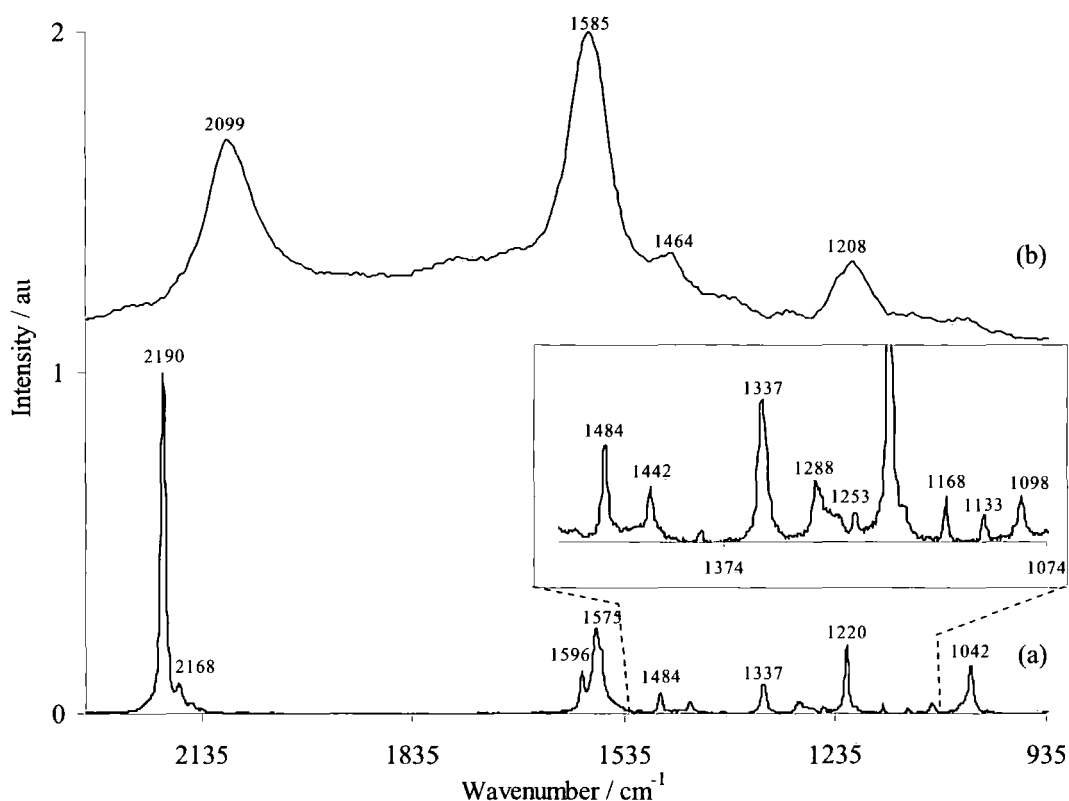


1170  $\text{cm}^{-1}$  region. This is attributed to the various methyl group vibrational modes expected in this region.



**Figure 4.17** Transient absorption spectra of the  $S_n \leftarrow S_1$  band of **5** in cyclohexane excited at 267 nm and probed between 470 and 750 nm. (a) shows the -50 to 15 ps delay period and (b) the 20 to 1000 ps delay period. The insets depict the rates of change in intensity over time at wavelengths 564 and 637 nm. Unlabelled arrows show the increase and decrease in the band intensities over time.

The peak at  $1220 \text{ cm}^{-1}$  in the ground state and  $1208 \text{ cm}^{-1}$  in the  $S_1$  state is tentatively assigned to the *t*-butyl vibrations. The  $1042 \text{ cm}^{-1}$  peak is most likely to represent outer ring breathing vibrations.[52]



**Figure 4.18** (a) The ground state Raman spectrum of solid **5**, probing at 633 nm. (b) The ps-TR<sup>3</sup> of **5** in cyclohexane pumping at 267 nm, probing at 583 nm with 60 ps delay.

#### 4.10 Ground state and time-resolved resonance Raman spectroscopy measurements of 1,2,4,5-tetramethyl-3,6-bis-(2,4,6-trimethyl-phenylethynyl)-benzene (**3**), 1,4-bis(2-(2-*tert*-butylphenyl)ethynyl)benzene (**4**) and 1,2,4,5-tetrafluoro-3,6-bis(phenylethynyl)benzene (**7**)

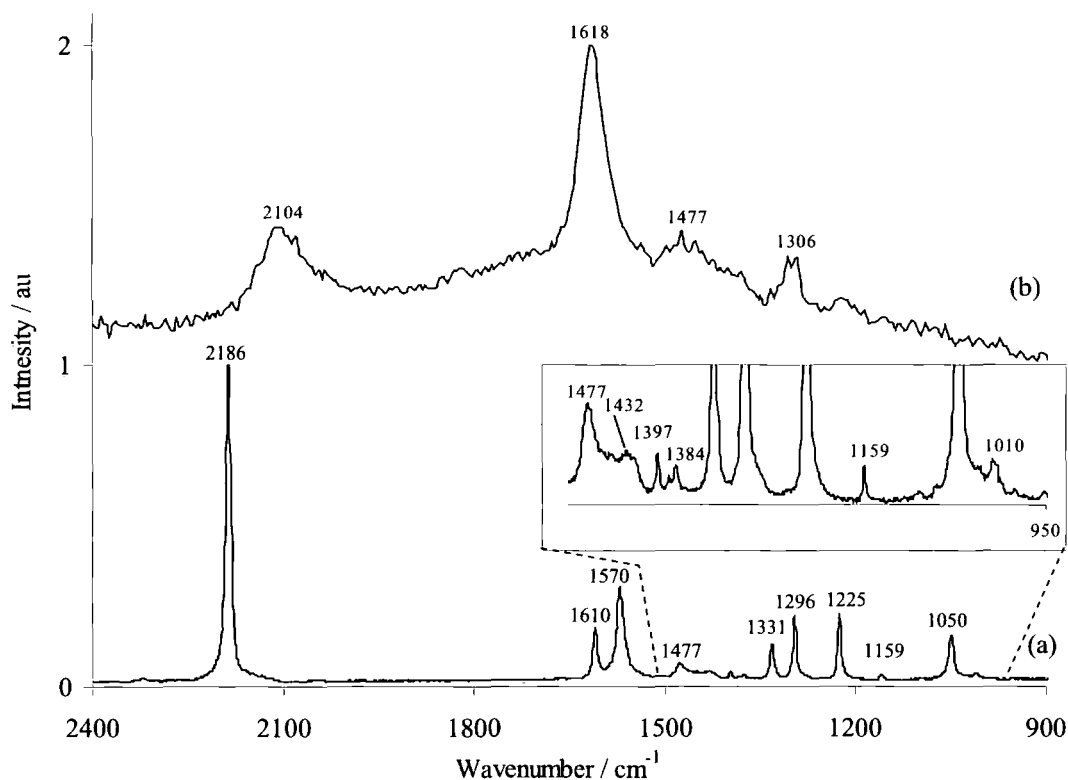
The Raman solid state spectra and ps-TR<sup>3</sup> excited singlet state spectra in cyclohexane of **3**, **4** and **7**, are compared in Figure 4.19–Figure 4.21. The Raman solid state spectra were measured by probing at 633 nm. The excited singlet state spectra were recorded after a 50 ps time delay, pumping at 267 nm and probing at 588 nm.

The C≡C stretching frequency (between 2215 and 2186 cm<sup>-1</sup>) in the three molecules in the ground state, is the dominant peak in the Raman profiles. This is expected as carbon triple bond vibrations are very intense in the Raman spectrum.[52] In the S<sub>1</sub> state the C≡C signature bands move down to the 2132 to 2103 cm<sup>-1</sup> region and are of weaker intensity than the ring stretching vibrations which are at around 1600 cm<sup>-1</sup>. The changes in the excited state are indicative of a

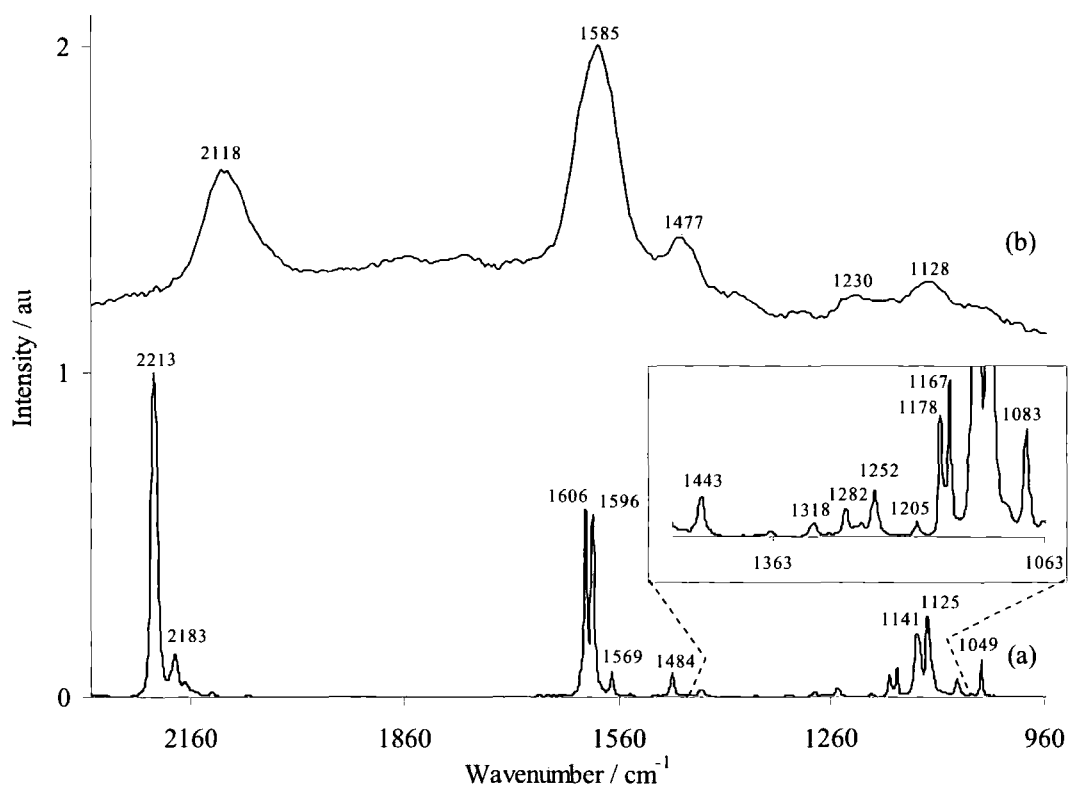
slight weakening of the  $C\equiv C$  character as seen in **1**. The carbon triple bond vibration is most diminished in the  $S_1$  excited state of **7** (Figure 4.21).

The ground state of all three shows a lot of vibrational fine structure in the 1720 to 900  $cm^{-1}$  region. An attempt was made to assign the main vibrational modes based on Raman ground state calculations, the known band positions of the functional groups and comparisons to the Raman spectrum of **1**.

The 1610 and 1570  $cm^{-1}$  bands of **3** (Figure 4.19) are thought to be similar to the phenyl anti-symmetric and symmetric stretches observed in **1** in the same region. The bands between 1506 and 1208  $cm^{-1}$  are likely to be methyl group deformation vibrations with some ring deformation.[52] The 1050  $cm^{-1}$  peak is a possible outer ring breathing mode.[52]



**Figure 4.19** (a) The ground state Raman spectrum of solid **3**, probing at 633 nm. (b) The ps-TR<sup>3</sup> of **3** in cyclohexane pumping at 276 nm, probing at 588 nm with 50 ps delay.

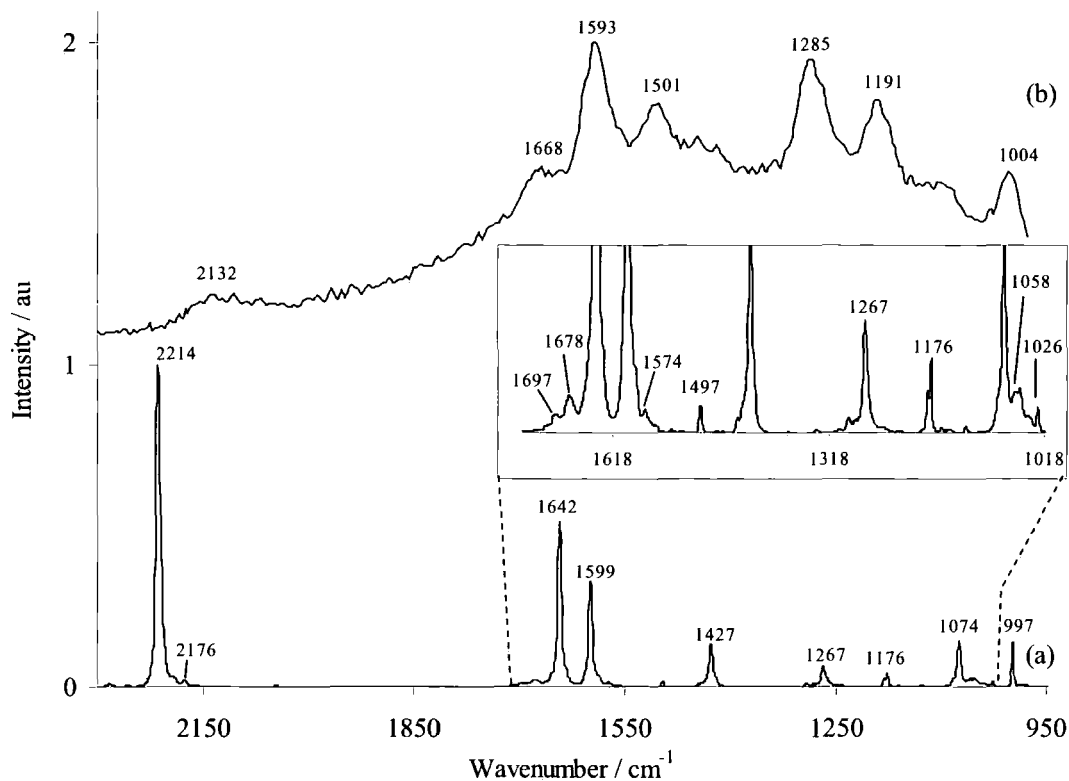


**Figure 4.20** (a) The ground state Raman spectrum of solid **4**, probing at 633 nm. (b) The ps-TR<sup>3</sup> of **4** in cyclohexane pumping at 267 nm, probing at 583 nm with 60 ps delay.

In **4**, the phenyl anti-symmetric and symmetric stretching modes are characterised by two strong bands at 1606 and 1596 cm<sup>-1</sup> of almost equal intensity. The bands at 1484 and 1443 cm<sup>-1</sup> are identified as the methyl group deformation vibrations while the *t*-butyl vibrational modes are expected to occur between 1215 and 1065 cm<sup>-1</sup>.<sup>[52]</sup> Compared to **1**, the central ring C-H in-plane deformation in **4** is likely to be the 1205 cm<sup>-1</sup> band and the central ring breathing mode is either the 1141 or the 1125 cm<sup>-1</sup> band. The 1049 cm<sup>-1</sup> band is identified as the outer ring breathing mode.

For compound **7**, the ground state vibrational peak assignments are based on theoretical calculations.<sup>[49]</sup> The weak to strong vibrational mode assignments of **7** are listed in Table 4.6. The excited state resonance Raman spectrum of **7** shows more vibrational fine structure than the alkyl substituted compounds (Figure 4.21). The strongest bands are associated with ring symmetric stretching (1593 and 1285 cm<sup>-1</sup>) and ring breathing (1004 cm<sup>-1</sup>) modes. The carbon-fluorine symmetric stretch is seen as a medium peak at 1427 cm<sup>-1</sup> in the ground state but is not discernable in the excited state. Of all the vibration bands of **7**, the acetylene stretching vibration has the largest shift, of -82 cm<sup>-1</sup>, to lower energy (see Table 4.6).

The medium bands at 1642 and 1599  $\text{cm}^{-1}$  in the ground state are identified as the inner ring and the outer rings symmetric stretching modes respectively.



**Figure 4.21** (a) The ground state Raman spectrum of solid **7**, probing at 633 nm. (b) The ps-TR<sup>3</sup> of the S<sub>1</sub> excited state of **7** in cyclohexane pumping at 267 nm, probing at 588 nm after 50 ps delay.

**Table 4.6** The non-resonance<sup>a</sup> and time-resolved resonance<sup>b</sup> Raman bands of **7**, shown in Figure 4.21, with ground state vibrational mode assignments<sup>c</sup>.

Ground state / $\text{cm}^{-1a}$	S <sub>1</sub> excited state / $\text{cm}^{-1b}$ (shift)	Mode description <sup>c</sup>
2214 s	2132 vw (-82)	
2176 vw		
1697 vw		
1678 vw	1668 vw (-10)	
1642 s		
1599 s	1593 s (-6)	

Table 4.6 (Continued).

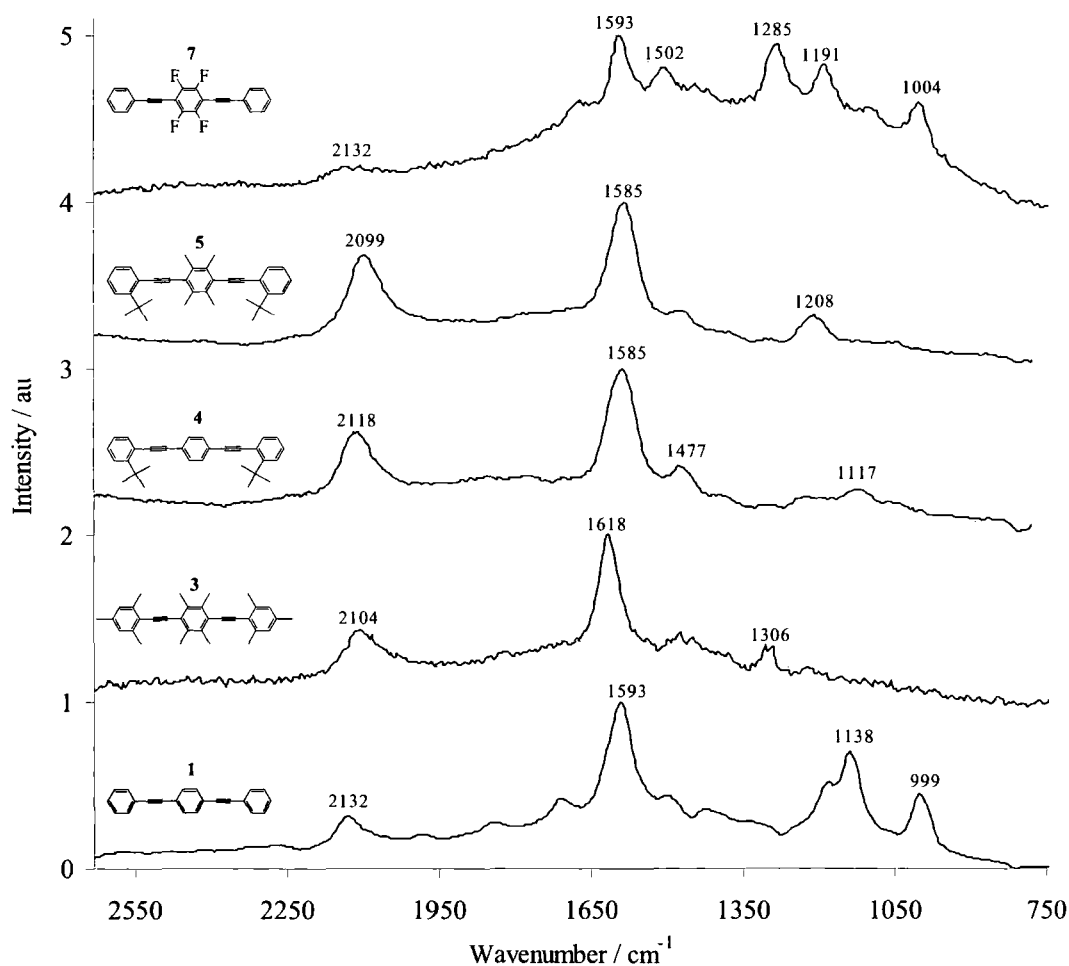
Ground state / $\text{cm}^{-1a}$	$S_1$ excited state / $\text{cm}^{-1b}$ (shift)	Mode description <sup>c</sup>
1574 vw		
1497 vw	1501 m (+4)	
1427 m		
1267 w	1285 s (+18)	
1176 w	1191 m (+15)	
1074 m		
1058 vw		
1026 vw		
997 m	1004 m (+7)	

Qualitative Raman: 's', 'm', 'w' and 'vw' refers to the peak intensities respectively as 'strong', 'medium', 'weak' and 'very weak'. <sup>c</sup> Mode descriptions are based on ground state Raman vibration calculations using the *Gaussian 03* package[49] with the B3LYP density functional and the 6-31G\* basis set. <sup>d</sup> Vibrational shifts in the excited state spectra from the ground state spectrum.

Inner ring symmetric stretching and outer ring out of plane deformation modes are associated with the  $1074\text{ cm}^{-1}$  band while the  $997\text{ cm}^{-1}$  band is assigned to outer ring breathing. All the vibrations between  $1500$  and  $980\text{ cm}^{-1}$  increase in energy in the first excited state while ring symmetric stretches and acetylene stretches all decrease in energy. In Table 4.6 we also observe an enhancement of the vibrations in the excited state in the  $1500$  to  $1000\text{ cm}^{-1}$  region.

A comparison of the ps-TR<sup>3</sup> spectra of **1** with those of **3**, **4**, **5** and **7** (Figure 4.22) show quite a few similarities. The acetylene bond component of the spectra is prominent in all the substituted forms of **1** except in **7** where it is weakest but in exactly the same position as in **1**. The strongest vibration in all five compounds is

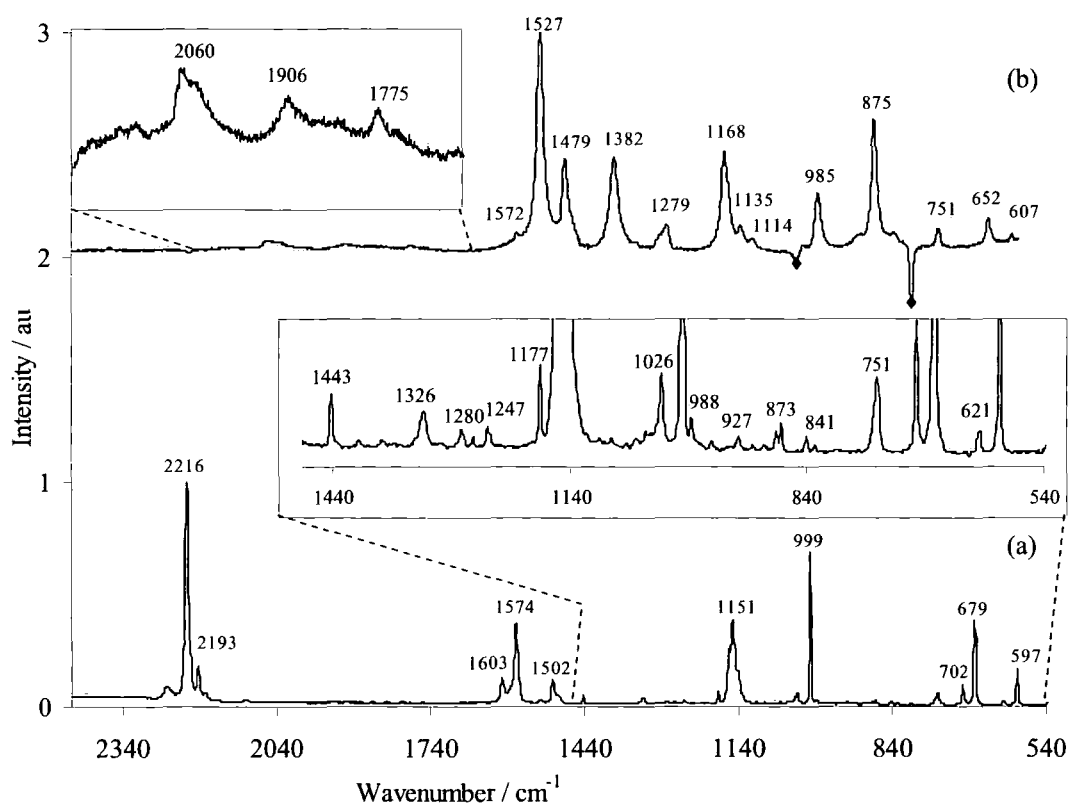
centred around  $1593\text{ cm}^{-1}$  and represents the symmetric stretching of the ring carbons and some ring in-plane deformations. Over the range  $1470\text{--}1000\text{ cm}^{-1}$  most of the ring breathing and ring stretching frequencies are found in all the ground state spectra. However, in the excited state **3**, **4** and **5** exhibit very weak vibrations in this area. The methyl and *t*-butyl groups appear to reduce the intensity of the Raman bands for these ring vibrations in the excited state. This could be the result of these electron donating substituents reducing the polarisability of the phenyl ring which in turn reduces the intensity of the Raman vibrations.



**Figure 4.22** The ps-TR<sup>3</sup> spectra of (from bottom to top) **1**, **3**, **4**, **5** and **7**. Delay = 50 ps pump = 267 nm, probe = 588 nm for all except **4** and **5** which were probed at 583 nm after 60 ps delay.

#### 4.11 Ground state and time-resolved resonance Raman of 1,4-dibromo-2,5-bis(phenylethynyl)benzene (6)

Time-resolved resonance Raman scatter of **6**, in cyclohexane under argon, on the nanosecond time scale gives insight into the bond order of the molecule in the triplet state. The presence of the heavy atoms in this compound means that its triplet yield



**Figure 4.23** (a) The ground state Raman spectrum of solid **6** probing at 633 nm. (b) The ns-TR<sup>3</sup> spectrum of the triplet excited state of **6** in cyclohexane, under argon, with a 0 ns delay, pumping at 320 nm and probing at 540 nm. ♦ indicates miss-cancelled peaks.

**Table 4.7** The non-resonance<sup>a</sup> and time-resolved resonance Raman<sup>b</sup> bands of **6**, shown in Figure 4.23, with ground state vibrational mode assignments.

Ground state of solid / cm <sup>-1 a</sup>	T <sub>1</sub> excited state / cm <sup>-1 b</sup>	Mode description <sup>c</sup> (shift)	Ground state of solid / cm <sup>-1 a</sup>	T <sub>1</sub> excited state / cm <sup>-1 b</sup>	Mode description <sup>c</sup> (shift)
2216 s	2060 vw	C≡C stretch (-156)	1026 vw	1114 vw	
2193 w			999 s	985 m	Outer ring z-deformation. Inner ring breathing (-14)
	1906 vw		988 vw		



Table 4.7 (Continued)

Ground state of solid / $\text{cm}^{-1 a}$	$T_1$ excited state / $\text{cm}^{-1 b}$	Mode description <sup>c</sup> (shift)	Ground state of solid / $\text{cm}^{-1 a}$	$T_1$ excited state / $\text{cm}^{-1 b}$	Mode description <sup>c</sup> (shift)
	1775 vw		927 vw		Outer and inner ring z-deformation
1603 w	1572 vw	Outer rings in-plane deformation. C-H wagging (-31)	873 vw	875 s	
1574 m	1527 s	Outer and inner rings anti symmetric stretch. C-H wagging (-47)	841 vw		
1502 w	1479 m	Outer rings anti symmetric stretch. C-H in-plane wagging (-23)	751 w	751 w	Outer and inner ring z-deformation
1443 vw	1382 m		702 w		Inner ring symmetric stretch. Outer ring breathing.
1326 vw		Inner ring C-H in-plane wagging	679 m	652 w	
1280 vw	1279 w		621 vw		
1247 vw			597 w	607 w	C≡C and ring z-deformation (+10)
1177 vw		Outer ring C-H scissoring			
1151 m	1168 m	Inner ring breathing (+17)			
	1135 w				

Qualitative Raman: 's', 'm', 'w' and 'vw' refers to the peak intensities respectively as 'strong', 'medium', 'weak' and 'very weak'. z-deformation refers to out of plane distortions. <sup>c</sup> Mode descriptions are based on ground state Raman vibrational calculations using the *Gaussian 03* package [49] with the B3LYP density functional and the 6-31G\* basis set.

is much greater than its parent (1). Figure 4.23 of the resonance Raman spectra of **6** shows a very weak acetylene bond at  $2060 \text{ cm}^{-1}$  in the triplet state. This band is  $156 \text{ cm}^{-1}$  lower in frequency than in the ground state. The ns-TR<sup>3</sup> of **6** was recorded after 0, 50 and 1000 ns delays. All three delay times gave the same vibrational profile with no changes in peak ratios. The Raman ground state and ns-TR<sup>3</sup> state vibrations are listed in Table 4.7. Mode assignments of the peaks are based on

theoretical calculations.[49] Not all the peaks observed were predicted by the calculations.

The acetylene bond vibration in **1** in the triplet state is also very weak but higher in energy (+86 cm<sup>-1</sup>, Figure 4.15 (d)) than the corresponding band in **6**. The addition of the Br atoms to the chromophore has reduced the energy of the acetylene bond but has not increased its vibrational intensity in the triplet state as expected. This weak band in **6** does not appear to be a vibrational overtone as it is not twice, or near twice, the wavenumber of any other band in the spectra. A low intensity C≡C stretching band at 1920 cm<sup>-1</sup> was also observed in the transient resonance coherent anti-Stokes Raman spectra of bis(4-biphenyl)acetylene (pumping at 355 nm and probing at 549 nm) in the triplet excited state by Kamisuki *et al.*[53] Their explanation of this observation can be extended to the ns-TR<sup>3</sup> spectra of **1** and **6** in which cases the low intensity of the C≡C bands, compared to other bands, indicate that the electronic transitions of the T<sub>n</sub>←T<sub>1</sub> bands in the electronic resonance effect are mainly responsible for structural changes of the phenyl rings.

Comparing the ground state and excited state spectra allows for a tentative assignment of some of the triplet excited state vibrations. We observe that the 1574 cm<sup>-1</sup> ring anti-symmetric stretching band in the ground state is yet again the most resonance enhanced band, this time in the triplet state. Some of the vibration mode intensities between 1580 and 540 cm<sup>-1</sup> are also enhanced in the triplet state and tend to be of lower energy than the ground state bands.

## Conclusions

The photophysical and spectroscopic properties of compounds **1** to **7** were measured in the ground and excited state, to determine the nature of their molecular structure and bonding. With the exception of **5**, all the molecules behave according to Kasha's rule, undergoing excitation to a vibrationally excited Frank-Condon state, before rapid relaxation to the lowest vibrational level of the S<sub>1</sub> state and subsequent emission and/or non-radiative decay. The photophysical properties of **1** are found to be affected by solvent viscosity, steric hindrance and the presence of heavy atoms and π-electron donor groups. The lowest singlet state energy of **1** is also affected by the presence of substituents.

Compound **1** exists in a range of conformers in the ground state due to the small barrier to the rotation of its phenyl rings (2.7 kJ mol<sup>-1</sup>). The subtle changes on the blue edge of the TRES of **1**, in the first 30 ps, is indicative of molecules still in the process of relaxing prior to emission from the most stable planar state. The steady state absorbance and fluorescence emission data show that the addition of alkyl and halo substituents to **1** does not significantly affect its free rotation in the ground state. Nor do these substituents affect **1**'s ability to become planar before fluorescence emission, from its lowest excited state, in solution. In a low temperature glassy matrix we see that the presence of bulky substituents, as in compound **5**, results in fluorescence emission from both high and low energy conformations. The presence of a rapidly decaying shoulder at 564 nm in the ps-TA spectra of **5** is further evidence of the *t*-butyl substituents causing drag through the solvent which slows down the molecules ability to become planar prior to emission.

The alkyl and halo substituents on **1** generally increased its conjugation and red shifted the absorption and emission spectra. The bulky alkyl substituents and fluorine substituents all increase the fluorescence lifetime of **1**. **5** causes the largest increase in the fluorescence lifetime ( $\tau_f$  of **1** = 0.53 ns while  $\tau_f$  of **5** = 0.72 ns) while bromine substituted **6** reduces it. The bromine atoms in **6** enhance intersystem crossing to the triplet state to such a degree that long lived phosphorescence could be detected at low temperature ( $\tau_{ph}$  = 4.0 ms). Fluorine substituents (**7**) cause the biggest enhancement of the fluorescence quantum yield ( $\Phi_f$  of **1** = 0.85 while  $\Phi_f$  of **7** = 0.97) and the largest increase in the extinction coefficient ( $\epsilon$  of **1** = 58,400 mol<sup>-1</sup> dm<sup>3</sup> cm<sup>-1</sup> while  $\epsilon$  of **7** = 67,100 mol<sup>-1</sup> dm<sup>3</sup> cm<sup>-1</sup>).

The main vibrational spacings in the low temperature excitation and emission spectra of the seven compounds are tentatively assigned to aromatic ring stretching modes as they are calculated to be in the 1300–1500 cm<sup>-1</sup> region. The presence of substituents decreased the lowest singlet excited state energy of **1** (3.59 eV or 346.4 kJ mol<sup>-1</sup>) by a maximum of 0.18 eV (17.4 kJ mol<sup>-1</sup>).

It was observed, for the first time, that the effect of viscous drag slows down the rotation of the aryl rings in relation to each other to such a degree that the excitation anisotropy in glycerol is in fact a summation of the anisotropies of various conformers of **1** with different absorption dipoles. Its fundamental anisotropy, in

EPA at 77 K, is 0.37, and the angle of displacement between the absorption and emission dipoles is 13.8°. This is in keeping with molecules which have near linear absorption and emission dipoles. The rotational correlation time of **1** is shown to be *ca.* 120 ps in cyclohexane and 19 ns in glycerol.

The characteristic S<sub>1</sub> Raman bands of **1** are 2132, 1593 1138 and 999 cm<sup>-1</sup>, which are assigned to the C≡C stretching, carbon–phenyl stretching, C-H parallel bending and ring breathing modes. The TR<sup>3</sup> spectra of all compounds studied illustrates that they all have C≡C bonding character in the excited singlet state. The fluorine substituents reduces the resonance enhancement of the C≡C band in the excited state the most, as seen in the TR<sup>3</sup> spectrum of **7**. Ring symmetric and anti symmetric stretching, and alkyl group deformation vibrations are more dominant and more resonance enhanced in the S<sub>1</sub> state. The C≡C bond in **1**, though significantly weaker, is found to persist in the triplet excited state which was measured using ns-TR<sup>3</sup>. The presence of heavy atoms does not enhance or reduce the Raman acetylene bonding character of **1** in the triplet state. Noteworthy from the time–resolved experiments is the lack of evidence of any cumulenic/quinoidal structure existing in the S<sub>1</sub> state or, indeed, the T<sub>1</sub> state. The highly delocalised, lower lying, bonding orbitals—which have been shown to be present from theoretical calculations—are thought to contribute to the acetylene bonding character of **1**.

## REFERENCES

1. V. F. Razumov, V. A. Sazhnikov, M. V. Alfimov, I. L. Kotlyarevskii, M. I. Bardamova and S. F. Vasilevskii, "The photophysical properties of molecules with triple bonds." *Izvestiya Akademii Nauk SSSR, Seriya Khimicheskaya*, 1979, 358-362.
2. S. Nakatsuji, K. Matsuda, Y. Uesugi, K. Nakashima, S. Akiyama and W. Fabian, "Synthesis and absorption/emission spectroscopic properties of bis(phenylethynyl)benzenes and 9,10-bis(phenylethynyl)anthracenes." *Journal Of The Chemical Society-Perkin Transactions 1*, 1992, 755-758.
3. L. S. Swanson and J. Shinar, "Photoluminescence, electroluminescence, and optically detected magnetic-resonance study of 2,5-dialkoxy derivatives of poly(p-phenyleneacetylene) (Ppa) and Ppa-based light-emitting-diodes." *Synthetic Metals*, 1993, **55**, 1-6.
4. T. M. Swager, C. J. Gil and M. S. Wrighton, "Fluorescence studies of poly(p-phenyleneethynylene)s - The effect of anthracene substitution." *Journal Of Physical Chemistry*, 1995, **99**, 4886-4893.
5. R. Fiesel, C. E. Halkyard, M. E. Rampey, L. Kloppenburg, S. L. Studer-Martinez, U. Scherf and U. H. F. Bunz, "Aggregation and chiroptical behavior of a high molecular weight chirally substituted dialkylpoly(p-phenyleneethynylene)." *Macromolecular Rapid Communications*, 1999, **20**, 107-111.
6. T. Miteva, L. Palmer, L. Kloppenburg, D. Neher and U. H. F. Bunz, "Interplay of thermochromicity and liquid crystalline behaviour in poly(p-phenyleneethynylene)s:  $\pi$ - $\pi$  interactions or planarization of the conjugated backbone?" *Macromolecules*, 2000, **33**, 652-654.
7. C. Schmitz, P. Posch, M. Thelakkat, H. W. Schmidt, A. Montali, K. Feldman, P. Smith and C. Weder, "Polymeric light-emitting diodes based on poly(p-phenylene ethynylene), poly(triphenyldiamine), and spiroquinoxaline." *Advanced Functional Materials*, 2001, **11**, 41-46.
8. M. Levitus, K. Schmieder, H. Ricks, K. D. Shimizu, U. H. F. Bunz and M. A. Garcia-Garibay, "Steps to demarcate the effects of chromophore aggregation and planarization in poly(phenyleneethynylene)s. 1. Rotationally interrupted conjugation in the excited states of 1,4-bis(phenylethynyl)benzene." *Journal Of The American Chemical Society*, 2001, **123**, 4259-4265.
9. C. Y. Tan, M. R. Pinto and K. S. Schanze, "Photophysics, aggregation and amplified quenching of a water-soluble poly(phenylene ethynylene)." *Chemical Communications*, 2002, 446-447.
10. J. N. Wilson, M. Josowicz, Y. Q. Wang and U. H. F. Bunz, "Cruciform pi-systems: hybrid phenylene-ethynylene/phenylene-vinylene oligomers." *Chemical Communications*, 2003, 2962-2963.

11. H. Kukula, S. Veit and A. Godt, "Synthesis of monodisperse oligo(para-phenyleneethynylene)s using orthogonal protecting groups with different polarity for terminal acetylene units." *European Journal Of Organic Chemistry*, 1999, 277-286.
12. Q. Zhou and T. M. Swager, "Fluorescent chemosensors based on energy migration in conjugated polymers: The molecular wire approach to increased sensitivity." *Journal Of The American Chemical Society*, 1995, 12593-12602.
13. A. R. A. Palmans, M. Eglin, A. Montali, C. Weder and P. Smith, "Tensile orientation behavior of alkoxy-substituted bis(phenylethynyl)benzene derivatives in polyolefin blend films." *Chemistry Of Materials*, 2000, **12**, 472-480.
14. R. J. Magyar, S. Tretiak, Y. Gao, H. L. Wang and A. P. Shreve, "A joint theoretical and experimental study of phenylene-acetylene molecular wires." *Chemical Physics Letters*, 2005, **401**, 149-156.
15. M. I. Sluch, A. Godt, U. H. F. Bunz and M. A. Berg, "Excited-state dynamics of oligo(p-phenyleneethynylene): Quadratic coupling and torsional motions." *Journal Of The American Chemical Society*, 2001, **123**, 6447-6448.
16. M. Levitus and M. A. Garcia-Garibay, "Polarized electronic spectroscopy and photophysical properties of 9,10-bis(phenylethynyl)anthracene." *Journal Of Physical Chemistry A*, 2000, **104**, 8632-8637.
17. K. Schmieder, M. Levitus, H. Dang and M. A. Garcia-Garibay, "Photophysical properties of coplanar and twisted 1,4-bis(9-ethynylanthracenyl)benzene. Rotational equilibration in the excited states of diaryalkynes." *Journal Of Physical Chemistry A*, 2002, **106**, 1551-1556.
18. A. Beeby, K. Findlay, P. J. Low and T. B. Marder, "A re-evaluation of the photophysical properties of 1,4-bis(phenylethynyl)benzene: A model for poly(phenyleneethynylene)." *Journal Of The American Chemical Society*, 2002, **124**, 8280-8284.
19. A. Beeby, K. S. Findlay, P. J. Low, T. B. Marder and P. Matousek, "Studies of the S<sub>1</sub> state in a prototypical molecular wire using picosecond time-resolved spectroscopies." *Chemical Communications*, 2003, 2406-2407.
20. H. Li, D. R. Powell, T. K. Firman and R. West, "Structures and photophysical properties of model compounds for arylethylene disilylene polymers." *Macromolecules*, 1998, **31**, 1093-1098.
21. Y. Yamaguchi, T. Ochi, T. Wakamiya, Y. Matsubara and Z. Yoshida, "New fluorophores with rod-shaped polycyano  $\pi$ -conjugated structures: Synthesis and photophysical properties." *Organic Letters*, 2006, **8**, 717-720.
22. M. Biswas, P. Nguyen, T. B. Marder and L. R. Khundkar, "Unusual size dependence of nonradiative charge recombination rates in acetylene-bridged compounds." *Journal of Physical Chemistry A*, 1997, 1689-1695.

23. E. Birckner, U.-W. Grummt, A. H. Göller, T. Pautzsch, D. A. M. Egbe, M. Al-Higari and E. Klemm, "Photophysics of arylene and heteroaryleneethynyls." *Journal Of Physical Chemistry A*, 2001, 10307-10315.
24. T. X. Carroll, T. D. Thomas, H. Bergersen, K. J. Børve and L. J. Sæthre, "Fluorine as a  $\pi$  Donor. Carbon 1s Photoelectron Spectroscopy and Proton Affinities of Fluorobenzenes." *Journal Of Organic Chemistry*, 2006, **71**, 1961-1968.
25. S. J. Greaves, E. L. Flynn, E. L. Futcher, E. Wrede, D. P. Lydon, P. J. Low, S. R. Rutter and A. Beeby, "Cavity ring-down spectroscopy of the torsional motions of 1,4-bis(phenylethynyl)benzene." *Journal Of Physical Chemistry A*, 2006, **110**, 2114-2121.
26. P. V. James, P. K. Sudeep, C. H. Suresh and K. G. Thomas, "Photophysical and theoretical investigations of oligo(*p*-phenyleneethynylene)s: Effect of alkoxy substitution and alkyne-aryl bond rotations." *The Journal of Physical Chemistry A*, 2006, **110**, 4329-4337.
27. D. S. McClure, "Triplet-singlet transitions in organic molecules. Lifetime measurements of the triplet state." *Journal Of Chemical Physics*, 1949, **17**, 905-913.
28. S. Okada, K. Okinaka, H. Iwawaki, M. Furugori, M. Hashimoto, T. Mukaide, J. Kamatani, S. Igawa, A. Tsuboyama, T. Takiguchi, and K. Ueno, "Substituent effects of iridium complexes for highly efficient red OLEDs." *Dalton Transactions*, 2005, 1583-1590.
29. M. Kasha, "Characterization of electronic transitions in complex molecules." *Complex Molecules*, 1950.
30. H. Burrows, *Personal communication*, 25<sup>th</sup> September 2006., University of Coimbra.
31. E. W. Thulstrup and J. Michl, "Orientation and linear dichroism of symmetrical aromatic-molecules imbedded in stretched polyethylene." *Journal Of The American Chemical Society*, 1982, **104**, 5594-5604.
32. J. Ouellette, "Time-resolved spectroscopy comes of age." *The Industrial Physicist*, 2004, **10**, 16-19.
33. M. Diem, "Introduction to modern vibrational spectroscopy", John Wiley & Sons, New York, 1993.
34. N. Mataga, Y. Shibata, H. Chosrowjan, N. Yoshida and A. Osuka, "Internal conversion and vibronic relaxation from higher excited electronic state of porphyrins: Femtosecond fluorescence dynamics studies." *Journal Of Physical Chemistry B*, 2000, **104**, 4001-4004.

35. W. S. Li, X. W. Fan, B. J. Yang, D. Z. Shen, Y. M. Lu, J. Y. Zhang, L. C. Chen, Y. B. Chi and Y. M. Li, "Multiphonon Raman scattering in ZnSe/Zn<sub>0.80</sub>Cd<sub>0.20</sub>Se superlattices." *Thin Solid Films*, 1995, **271**, 147-150.
36. P. F. Barbara, P. M. Rentzepis and L. E. Brus, "Photochemical kinetics of salicylidenaniline." *Journal Of The American Chemical Society*, 1980, **102**, 2786-2791.
37. R. Nakamura, P. Wang, R. Fujii, Y. Koyama, H. Hashimoto and Y. Kanematsu, "Vibrational relaxation pathways in the electronic excited state of carotenoid." *Journal Of Luminescence*, 2006, **119**, 442-447.
38. A. Freiberg, J. Aaviksoo and K. Timpmann, "Picosecond spectrochronography - A new method for the studying of ultrafast dynamics of excitations in molecules and solids." *Journal Of Molecular Structure*, 1986, **142**, 563-566.
39. P. F. Barbara, P. M. Rentzepis and L. E. Brus, "Direct picosecond observation of unrelaxed fluorescence from tetracene in condensed media." *Journal Of Chemical Physics*, 1980, **72**, 6802-6803.
40. T. Tamm and P. Saari, "Hot luminescence study of the intra-molecular thermal bath of aromatics." *Chemical Physics*, 1979, **40**, 311-319.
41. P. F. Barbara, S. D. Rand and P. M. Rentzepis, "Direct measurements of tetraphenylethylene torsional motion by picosecond spectroscopy." *Journal Of The American Chemical Society*, 1981, **103**, 2156-2162.
42. D. E. Polyansky, E. O. Danilov, S. V. Voskresensky, M. A. J. Rodgers and D. C. Neckers, "Photodecomposition of peroxides containing a 1,4-bis(phenylethynyl)benzene chromophore." *Journal of Physical Chemistry A*, 2006, **110**, 4969-4978.
43. P. K. Sudeep, P. V. James, K. G. Thomas and P. V. Kamat, "Singlet and triplet excited-state interactions and photochemical reactivity of phenyleneethynylene oligomers." *Journal Of Physical Chemistry A*, 2006, **110**, 5642-5649.
44. A. P. Monkman, H. D. Burrows, L. J. Hartwell, L. E. Horsburgh, I. Hamblett and S. Navaratnam, "Triplet energies of  $\pi$ -conjugated polymers." *Physical Review Letters*, 2001, **86**, 1358-1361.
45. A. P. Monkman, H. D. Burrows, M. D. Miguel, I. Hamblett and S. Navaratnam, "Triplet state spectroscopy of conjugated polymers studied by pulse radiolysis." *Synthetic Metals*, 2001, **116**, 75-79.
46. R. Bensasso and E. J. Land, "Triplet-triplet extinction coefficients via energy transfer." *Transactions Of The Faraday Society*, 1971, **67**, 1904-1971.
47. Z. Chernia, T. Livneh, I. Pri-Bar and J. E. Koresh, "Mode assignment for linear phenyl acetylene sequence: phenylacetylene, di-phenylacetylene and 1,4-di(phenylethynyl)benzene." *Vibrational Spectroscopy*, 2001, **25**, 119-131.



48. A. Beeby, *Unpublished data*, Durham University.
49. M. J. Frisch, G. W. Trucks, H. B. Schlegel, G. E. Scuseria, M. A. Robb, J. R. Cheeseman, J. J. A. Montgomery, T. Vreven, K. N. Kudin, J. C. Burant, J. M. Millam, S. S. Iyengar, J. Tomasi, V. Barone, B. Mennucci, M. Cossi, G. Scalmani, N. Rega, G. A. Petersson, H. Nakatsuji, M. Hada, M. Ehara, K. Toyota, R. Fukuda, J. Hasegawa, M. Ishida, T. Nakajima, Y. Honda, O. Kitao, H. Nakai, M. Klene, X. Li, J. E. Knox, H. P. Hratchian, J. B. Cross, C. Adamo, J. Jaramillo, R. Gomperts, R. E. Stratmann, O. Yazyev, A. J. Austin, R. Cammi, C. Pomelli, J. W. Ochterski, P. Y. Ayala, K. Morokuma, G. A. Voth, P. Salvador, J. J. Dannenberg, V. G. Zakrzewski, S. Dapprich, A. D. Daniels, M. C. Strain, O. Farkas, D. K. Malick, A. D. Rabuck, K. Raghavachari, J. B. Foresman, J. V. Ortiz, Q. Cui, A. G. Baboul, S. Clifford, J. Cioslowski, B. B. Stefanov, G. Liu, A. Liashenko, P. Piskorz, I. Komaromi, R. L. Martin, D. J. Fox, T. Keith, M. A. Al-Laham, C. Y. Peng, A. Nanayakkara, M. Challacombe, P. M. W. Gill, B. Johnson, W. Chen, M. W. Wong, C. Gonzalez, and J. A. Pople, *Gaussian 03, Revision C.02*. 2004, Gaussian Inc.: Wallingford CT.
50. J. M. Seminario, A. G. Zacarias and P. A. Derosa, "Theoretical analysis of complementary molecular memory devices." *Journal Of Physical Chemistry A*, 2001, **105**, 791-795.
51. L. Zhao, I. F. Perepichka, F. Turksay, A. S. Batsanov, A. Beeby, K. S. Findlay and M. R. Bryce, "2,5-Di(aryleneethynyl)pyrazine derivatives: synthesis, structural and optoelectronic properties, and light-emitting device." *New Journal Of Chemistry*, 2004, **28**, 912-918.
52. H. Baranska, A. Labudzinska and J. Terpiniski, "Laser Raman spectrometry: analytical applications", Ellis Horwood Series in Analytical Chemistry, ed. D. R. A. Chalmers and D. M. Masson, Ellis Horwood Limited England and PWN-- Polish Scientific Publishers Poland, Chichester, 1987.
53. T. Kamisuki, M. Akita, Y. Morooka and C. Hirose, "Raman spectroscopic study of bis(4-biphenyl)acetylene in the  $S_0$ ,  $S_2$  and  $T_1$  states." *Journal Of Raman Spectroscopy*, 1997, **28**, 791-796.

## CHAPTER 5

### Properties of 1,4-bis(phenylethynyl)benzene donor–acceptor substituted compounds

#### 5.1 Introduction

Molecules composed of an electron donating group and an electron accepting group, separated by a spacer unit, can undergo intramolecular electron–transfer (ET) reactions upon photoexcitation. During ET, an electron is moved from the donor to the acceptor site. The reaction product is called an intramolecular charge–transfer (ICT) state.[1] True ICT states are usually different from the parent ground states in their electronic structure and molecular geometry, provided the molecular skeleton is not too rigid.[1]

Thirty three years ago Grabowski *et al.* put forward a structural hypothesis[2] which later became known as the twisted intramolecular charge–transfer (TICT) model.[3, 4] This model explained the geometry and charge separation in the excited state which was responsible for the dual fluorescence observed in 4-(N,N-dimethylamino)benzonitrile (DMABN) in highly polar solvents. According to the TICT model the higher energy emission band of DMABN is due to a moderately polar ICT isomer with a planar geometry while the lower energy band is from a fully charge separated isomer with methyl groups orthogonal to the phenyl ring. Since then, many more donor–acceptor (D–A) systems have been reported to exhibit dual fluorescence.[5]

Fluorescence from the ICT and TICT states of  $\pi$ -conjugated D–A molecules, in polar solvents, has also been reported.[6-9] The D–A systems undergo a large change between the ground and excited state dipole moments ( $\Delta\mu_{eg}$ ) due to a shift in the electron density from the D to the A group.[9] Theoretical calculations by Broo[10] indicate that the excited state of 4-cyano-4'-methylthiodiphenylacetylene (MTCN-DPA) is a TICT state in which the two phenyl rings are perpendicular to each other with a dipole moment ( $\mu_e$ ) of 24.18 D. The intramolecular charge separation process in 4-N,N-dimethylamino-4'-cyanodiphenylacetylene (DACN-DPA) was investigated by Hirata *et al.* who concluded that the dipole moment of the ICT state is about 36 D based on the Stokes shift in aprotic solvents.[7] This is quite

large and indicates that the electronic structure of the ICT state is close to that of the ion pair.[7]

Lengthening the  $\pi$ -conjugated system connecting the D and A moieties is expected to increase charge separation and the  $\Delta\mu_{eg}$  term.[9] This has been shown to be false in the case of some diphenylpolyenes[11] where the  $\mu_e$ , for derivatives of 4-(N,N-dimethylamino)-4'-nitro-*trans*-stilbene with one to three *trans* ethane units, ranged from 22.0 to 27.0 D. The lower than expected values were put down to internal mesomeric stabilization in larger solutes.[11] The  $\mu_e$  was estimated from experimental data and ranges from 21.7 to 27.3 D[9] for 4-N,N-dibutylamino-4'-cyanoterphenyl (DCT) and its conformationally more planar and more twisted analogues, but theoretical computations predicted values from 51.7 to 50.4 D. The authors interpreted this discrepancy to be the result of an over estimation of the solvent stabilization, due to the uncertainty in the Onsager radius, in calculating  $\mu_e$  from experimental values.

By using steady state fluorescence and time-resolved infrared measurement techniques, we investigated the ICT process and the excited state structure and bonding in a group of D-A compounds with the longer and less sterically hindered 1,4-bis(phenylethynyl)benzene spacer group in solvents of increasing polarity. This was done with the aim of finding out what effect this type of spacer unit has on the photophysical properties of these D-A pairs; determining the effect of solvent polarity; looking for evidence of TICT states upon excitation in polar solvents; and estimating their excited state dipole moments.

The compounds studied are listed in Table 5.1. They consist of the following:

- (a) Three types of D-A pairs: methyl-4-(4-(4-dimethylaminophenylethynyl)-phenylethynyl)benzoate (**8**)—a strong donor-weak acceptor pair; 4-(4-(4-dimethylaminophenylethynyl)phenylethynyl)benzotrile (**9**)—a strong donor-strong acceptor pair; and 4-(4-(4-dimethylamino-3,5-dimethylphenylethynyl)phenylethynyl)benzotrile (**10**)—a strong donor-strong acceptor pair with the donor group permanently orthogonal to the phenyl ring.

- (b) The D–D and A–A pairs of 4-(4-(4-dimethylaminophenylethynyl)phenylethynyl)-N,N-dimethylbenzenamine (**11**) and 4-(4-(4-cyanophenylethynyl)phenylethynyl)benzonitrile (**12**) respectively.
- (c) The mono-substituted donor system 4-(4-(4-dimethylaminophenylethynyl)phenylethynyl)benzene (**13**); and two mono-substituted acceptor systems of 4-(4-(4-cyanophenylethynyl)phenylethynyl)benzene (**14**) and methyl 4-(4-phenylethynyl)phenylethynylbenzoate (**15**).

**Table 5.1** Compounds investigated.

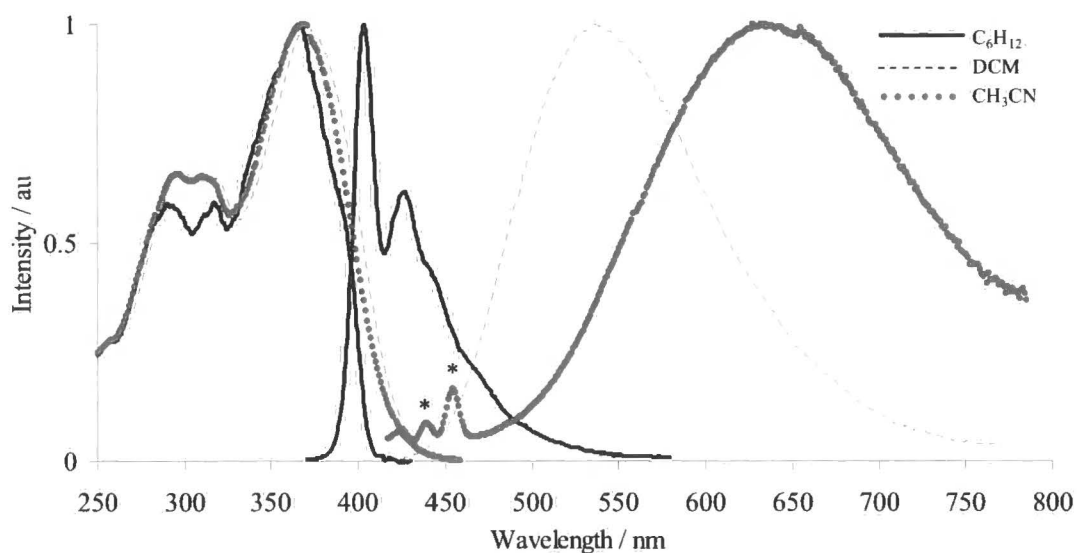
Compound	Structure	Code
Methyl-4-(4-(4-dimethylamino phenylethynyl)phenylethynyl)benzoate		<b>8</b>
4-(4-(4-Dimethylamino phenylethynyl)phenylethynyl)benzonitrile		<b>9</b>
4-(4-(4-Dimethylamino-3,5-dimethylphenylethynyl)phenylethynyl)benzonitrile		<b>10</b>
4-(4-(4-Dimethylamino phenylethynyl)phenylethynyl)-N,N-dimethylbenzenamine		<b>11</b>
4-(4-(4-Cyano phenylethynyl)phenylethynyl)benzonitrile		<b>12</b>
4-(4-(4-Dimethylamino phenylethynyl)phenylethynyl)benzene		<b>13</b>
4-(4-(4-Cyano phenylethynyl)phenylethynyl)benzene		<b>14</b>
Methyl-4-(4-phenylethynyl)phenylethynylbenzoate		<b>15</b>

## Results and discussion

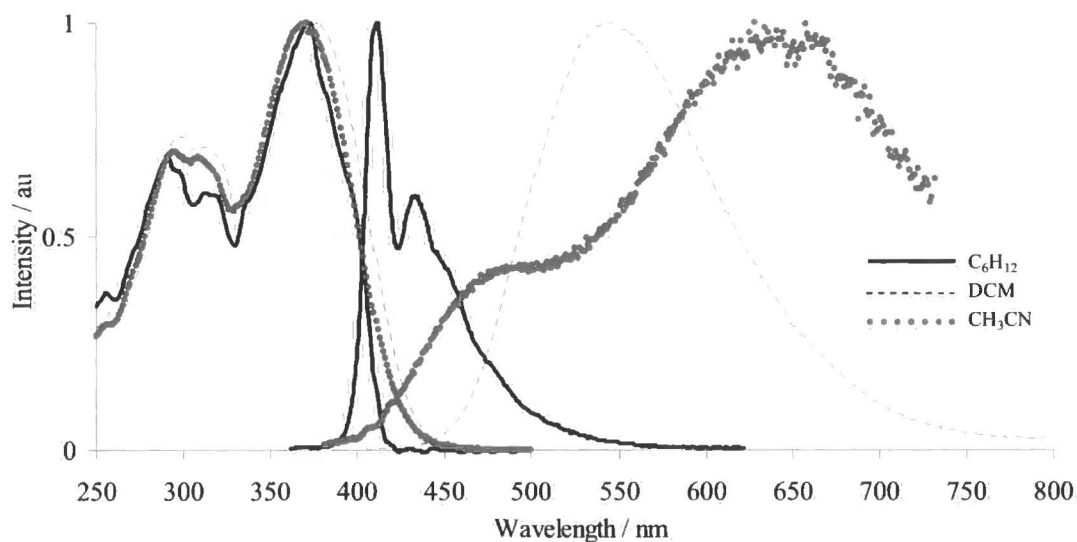
### 5.2 Steady state absorbance and fluorescence measurements

The absorbance and fluorescence spectra of the compounds in Table 5.1 were recorded in a range of solvents with varying polarity. These solvents were

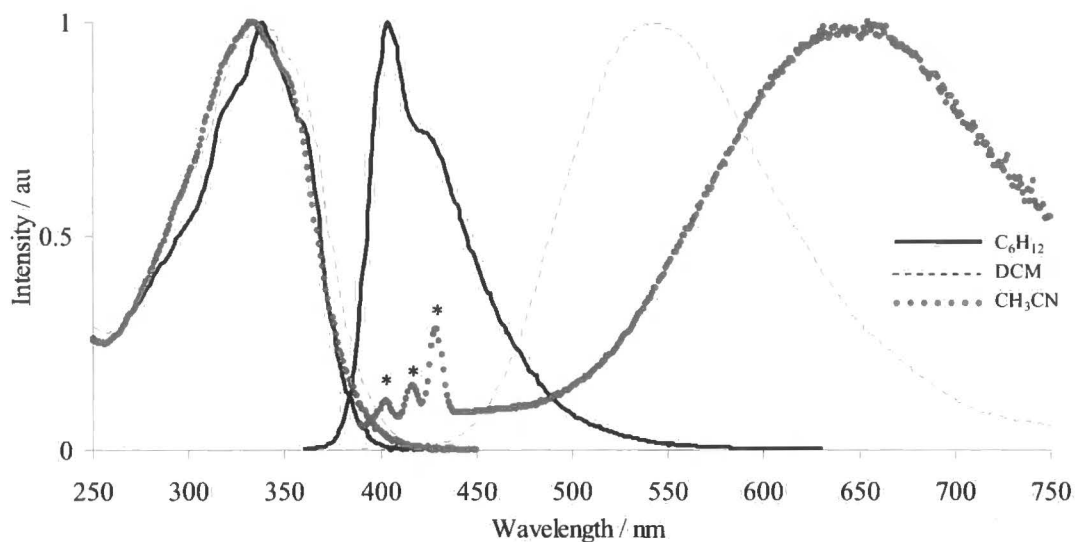
cyclohexane ( $C_6H_{12}$ ), chloroform ( $CHCl_3$ ), ethyl acetate ( $CH_3CO_2C_2H_5$ ), tetrahydrofuran (THF), dichloromethane (DCM), ethanol (EtOH) and acetonitrile (MeCN). The spectra of these compounds in cyclohexane, dichloromethane and acetonitrile are presented in Figure 5.1 to Figure 5.8. Table 5.2 collates all the major absorption and emission peaks. Table 5.4 lists the measured lifetimes in all seven solvents.



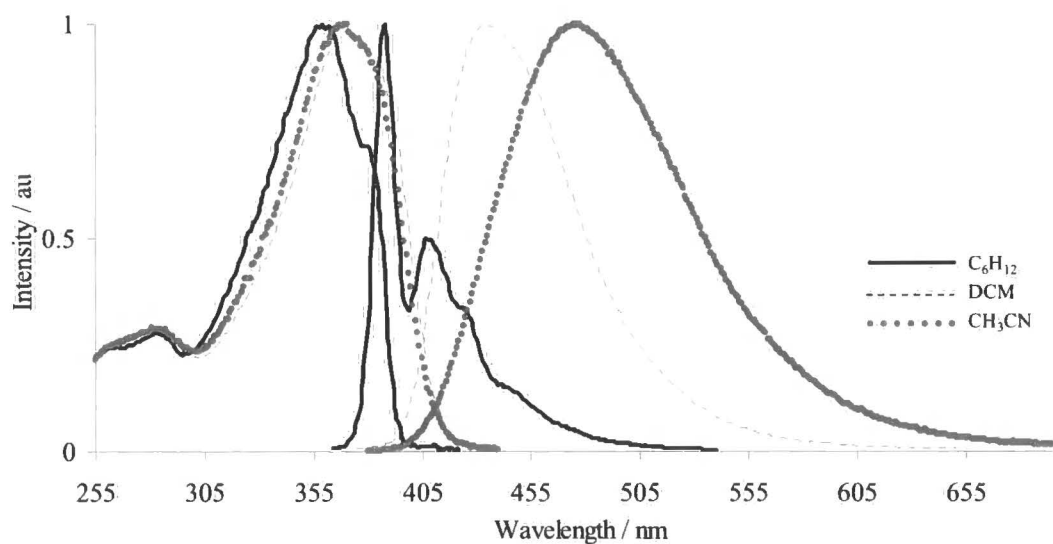
**Figure 5.1** Absorption and emission spectra of **8**. In  $C_6H_{12}$ ,  $\lambda_{ex} = 318$  nm; DCM,  $\lambda_{ex} = 390$  nm; and  $CH_3CN$ ,  $\lambda_{ex} = 400$  nm. \* denotes the weak  $CH_3CN$  Raman bands.



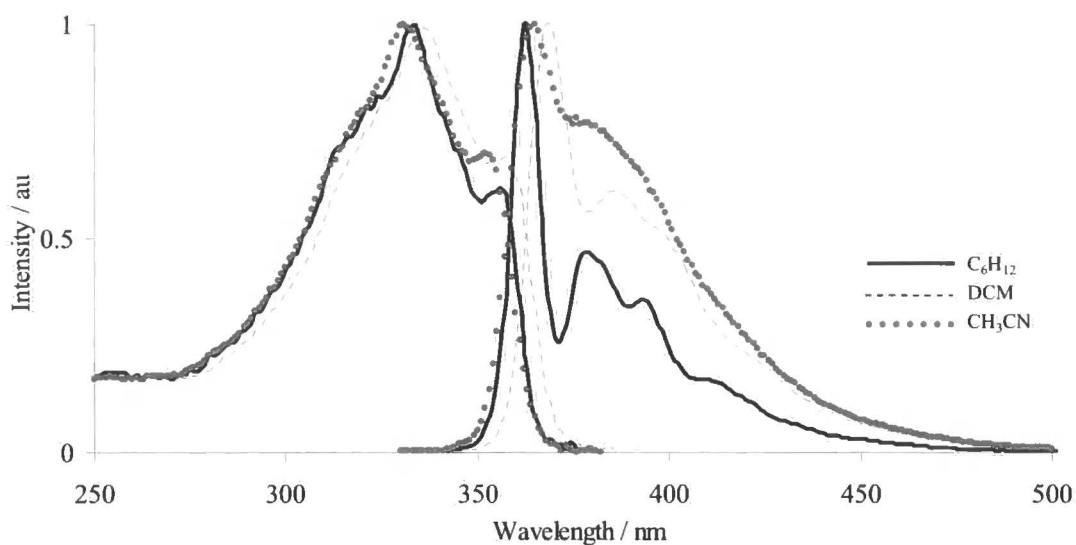
**Figure 5.2** Absorption and emission spectra of **9**. In  $C_6H_{12}$ ,  $\lambda_{ex} = 316$  nm; DCM,  $\lambda_{ex} = 400$  nm;  $CH_3CN$ ,  $\lambda_{ex} = 371$  nm.



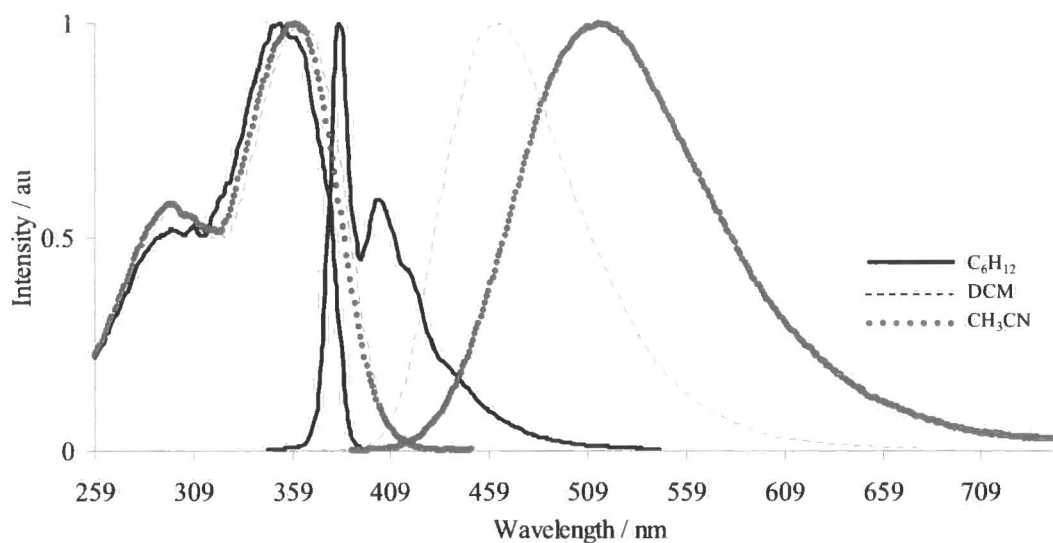
**Figure 5.3** Absorption and emission spectra of **10**. In  $C_6H_{12}$ ,  $\lambda_{ex} = 320$  nm; DCM,  $\lambda_{ex} = 380$  nm;  $CH_3CN$ ,  $\lambda_{ex} = 380$  nm. \* denotes the weak  $CH_3CN$  Raman bands.



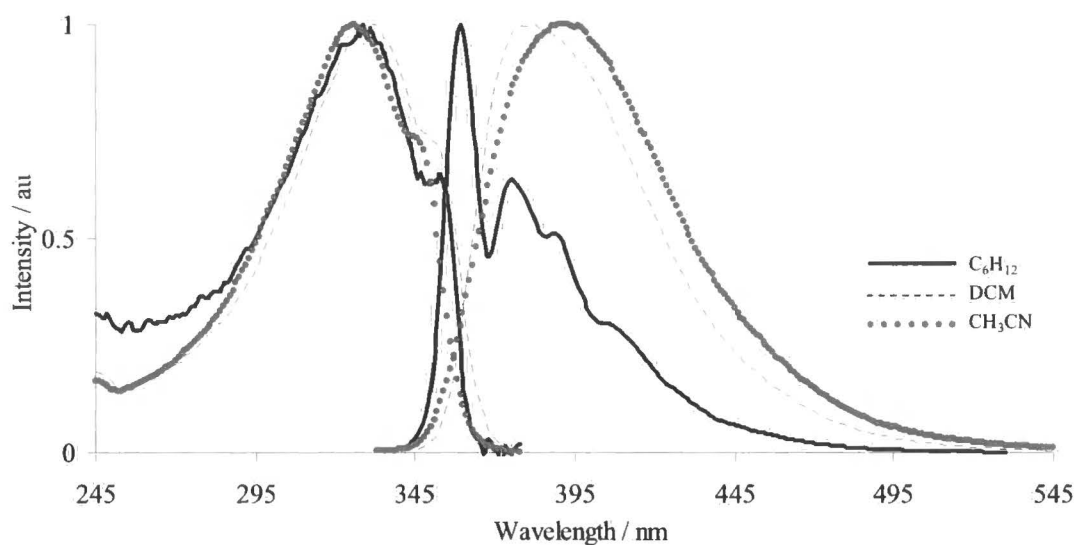
**Figure 5.4** Absorption and emission spectra of **11**. In  $C_6H_{12}$ ,  $\lambda_{ex} = 320$  nm; DCM,  $\lambda_{ex} = 330$  nm;  $CH_3CN$ ,  $\lambda_{ex} = 370$  nm.



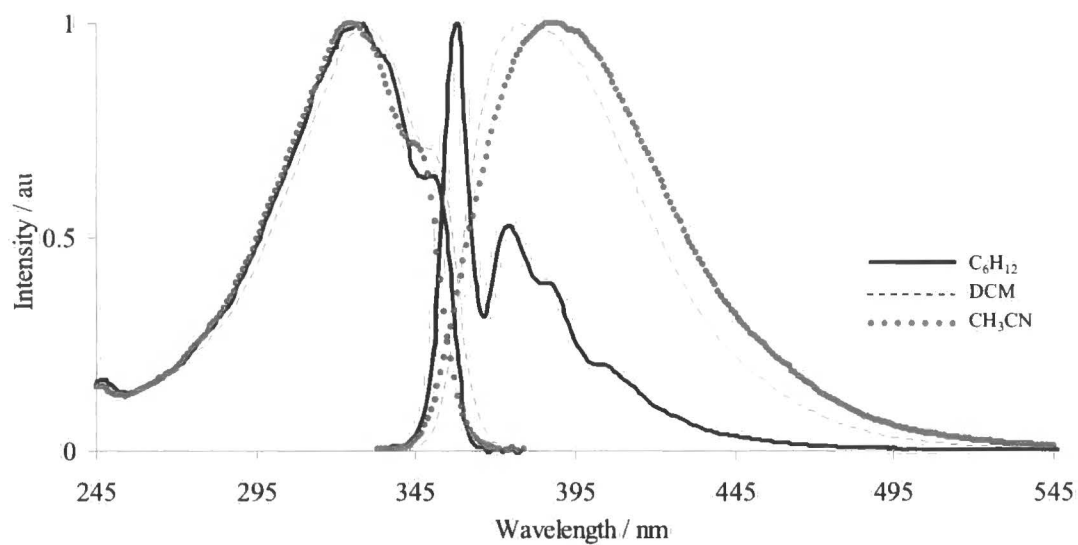
**Figure 5.5** Absorption and emission spectra of **12**. In  $C_6H_{12}$ ,  $\lambda_{ex} = 320$  nm; DCM,  $\lambda_{ex} = 336$  nm;  $CH_3CN$ ,  $\lambda_{ex} = 320$  nm.



**Figure 5.6** Absorption and emission spectra of **13**. In  $C_6H_{12}$ ,  $\lambda_{ex} = 300$  nm; DCM,  $\lambda_{ex} = 364$  nm;  $CH_3CN$ ,  $\lambda_{ex} = 380$  nm.



**Figure 5.7** Absorption and emission spectra of **14**. In  $C_6H_{12}$ ,  $\lambda_{ex} = 331$  nm; DCM,  $\lambda_{ex} = 300$  nm;  $CH_3CN$ ,  $\lambda_{ex} = 300$  nm.



**Figure 5.8** Absorption and emission spectra of **15**. In  $C_6H_{12}$ ,  $\lambda_{ex} = 280$  nm; DCM,  $\lambda_{ex} = 300$  nm;  $CH_3CN$ ,  $\lambda_{ex} = 300$  nm.



**Table 5.2** The absorption and emission peaks of 8–15 in solvents of increasing polarity.

Cpd.	Solvents	Absorption Peaks (Range) / nm	Emission Peaks (Range) / nm
<b>8</b>	C <sub>6</sub> H <sub>12</sub>	290, 317, 365 (260-405)	404, 427 (383-560)
	CHCl <sub>3</sub>	299, 321, 370 (270-430)	490(b) (420-690)
	CH <sub>3</sub> CO <sub>2</sub> C <sub>2</sub> H <sub>5</sub>	290, 366 (270-430)	525(b) (430-730)
	THF	306(b), 371 (280-430)	534(b) (440-760)
	DCM	306(b), 371(b) (280-430)	536(b) (440-760)
	C <sub>2</sub> H <sub>5</sub> OH*	297, 317, 367 (260-430)	543(b) (420-750). * 405
	CH <sub>3</sub> CN	296, 315, 368 (260-430)	637(b) (460-780). * 425, 440, 454, + 426(b) for $\lambda_{ex} = 330$ [ca. 216%]
<b>9</b>	C <sub>6</sub> H <sub>12</sub>	291, 313, 372 (260-410)	412, 435 (390-530)
	CHCl <sub>3</sub>	299, 317, 371 (266-445)	500 (420-700). + 362 & 383 for $\lambda_{ex} = 300$ [ca. 9%]
	CH <sub>3</sub> CO <sub>2</sub> C <sub>2</sub> H <sub>5</sub>	294, 310, 370 (260-430)	536 (440-750). + 406(b) for $\lambda_{ex} = 340$ [ca. 3%]
	THF	296, 314, 372, (260-430)	555(b) (430-780)
	DCM	297, 312, 371 (260-445)	546(b) (440-780)
	C <sub>2</sub> H <sub>5</sub> OH	295, 316, 369 (260-440)	583(b) (430-790). + 431(b) for $\lambda_{ex} = 335$ [ca. 71%]
	CH <sub>3</sub> CN	296, 309, 371 (260-450)	629(b) (400-730). + 486(b) for $\lambda_{ex} = 371$ [ca. 43%]

KEY: \* solvent Raman bands; + - the additional band arising from the formation of decomposition products in polar solvents; [%] - intensity of the decomposition product band compared to the major emission band; b - broad; sh - shoulder.

Table 5.2 (Continued)

Cpd.	Solvents	Absorption Peaks (Range) / nm	Emission Peaks (Range) / nm
10	C <sub>6</sub> H <sub>12</sub>	338 (250-400)	404, 426(sh) (375-550)
	CHCl <sub>3</sub>	339(b) (250-410)	494(b) (410-700)
	CH <sub>3</sub> CO <sub>2</sub> C <sub>2</sub> H <sub>5</sub>	334(b) (254-400)	553(b) (430-740)
	THF	336(b) (260-405)	547(b) (430-750)
	DCM	338(b) (260-410)	542(b) (435-750). <sup>+</sup> 360 for $\lambda_{ex} = 300$ [ca. 5%]
	C <sub>2</sub> H <sub>5</sub> OH	334(b) (255-405)	581(b) (380-740). <sup>+</sup> 397(b) for $\lambda_{ex} = 310$ [ca. 24%]
	CH <sub>3</sub> CN	334(b) (255-405)	655(b) (470-740). *403, 417 & 429, <sup>+</sup> 400(b) for $\lambda_{ex} = 332$ [ca. 33%]
11	C <sub>6</sub> H <sub>12</sub>	286, 359, 380(sh) (280-394)	388, 407, 425 (370-510)
	CHCl <sub>3</sub>	286, 368 (280-415)	420(b) (380-610)
	CH <sub>3</sub> CO <sub>2</sub> C <sub>2</sub> H <sub>5</sub>	298, 359 (280-410)	431(b) (388-610)
	THF	280, 370(b) (270-418)	432(b) (391-600)
	DCM	286, 370(b) (280-415)	433(b) (390-610)
	EtOH	280, 365(b) (280-415)	446(b) (385-650)
	CH <sub>3</sub> CN	280, 370(b) (280-420)	475(b) (400-680)

KEY: \* solvent Raman bands; <sup>+</sup> - the additional band arising from the formation of decomposition products in polar solvents; [%] - intensity of the decomposition product band compared to the major emission band; b - broad; sh - shoulder.

Table 5.2 (Continued)

Cpd.	Solvents	Absorption Peaks (Range) / nm	Emission Peaks (Range) / nm
12	C <sub>6</sub> H <sub>12</sub>	314, 334, 356(sh) (260-367)	363, 378, 393 (348-470)
	CHCl <sub>3</sub>	336, 359(sh) (270-375)	368, 386 (350-490)
	CH <sub>3</sub> CO <sub>2</sub> C <sub>2</sub> H <sub>5</sub>	332, 353(sh) (260-367)	362, 379 (346-490)
	THF	334, 357(sh) (280-379)	366, 383 (350-490)
	DCM	335, 359(sh) (280-370)	368, 385 (353-490)
	C <sub>2</sub> H <sub>5</sub> OH	332, 354(sh) (280-368)	366, 382 (345-390)
	CH <sub>3</sub> CN	331, 352(sh) (260-367)	365, 382 (347-490)
13	C <sub>6</sub> H <sub>12</sub>	300, 353(b) (255-390)	383, 403 (366-520)
	CHCl <sub>3</sub> *	302, 359(b) (260-410)	438(b) (388-600). + 357 for $\lambda_{ex} = 330$ [ca. 10%]
	CH <sub>3</sub> CO <sub>2</sub> C <sub>2</sub> H <sub>5</sub>	298, 358(b) (260-412)	460(b) (393-650)
	THF	299, 362(b) (260-419)	464(b) (393-650)
	DCM	299, 362(b) (260-419)	465(b) (400-650)
	C <sub>2</sub> H <sub>5</sub> OH*	298, 358(b) (257-418)	478(b) (400-710). + 377(b) for $\lambda_{ex} = 300$ [ca. 8%]
	CH <sub>3</sub> CN	297, 361(b) (257-419)	515(b) (417-750)

KEY: + - the additional band arising from the formation of decomposition products in polar solvents; [%] - intensity of the decomposition product band compared to the major emission band; b - broad; sh - shoulder.

Table 5.2 (Continued)

Cpd.	Solvents	Absorption Peaks (Range) / nm	Emission Peaks (Range) / nm
<b>14</b>	C <sub>6</sub> H <sub>12</sub>	329, 350(sh) (250-365)	359, 375, 388 (346-485)
	CHCl <sub>3</sub>	331, 354(sh) (260-370)	373 (350-510)
	CH <sub>3</sub> CO <sub>2</sub> C <sub>2</sub> H <sub>5</sub>	326, 350(sh) (260-364)	372(b) (350-510)
	THF	328, 350(sh) (260-360)	373(b) (350-510)
	DCM	333, 350(sh) (260-370)	382(b) (350-520)
	C <sub>2</sub> H <sub>5</sub> OH	327, 346(sh) (260-370)	384(b) (345-540)
	CH <sub>3</sub> CN	326, 345(sh) (260-370)	390(b) (345-550)
<b>15</b>	C <sub>6</sub> H <sub>12</sub>	325, 350(sh) (250-360)	358, 374, 387, 404 (343-470)
	CHCl <sub>3</sub>	328, 350(sh) (250-360)	370(b) (350-520)
	CH <sub>3</sub> CO <sub>2</sub> C <sub>2</sub> H <sub>5</sub>	325, 345(sh) (250-360)	363, 375(sh) (345-500)
	THF	326, 350(sh) (250-360)	367(b) (345-500)
	DCM	327, 350(sh) (250-360)	378(b) (350-520)
	C <sub>2</sub> H <sub>5</sub> OH	324(b), 346(sh) (260-360)	389(b) (345-550)
	CH <sub>3</sub> CN	324, 346(sh) (250-360)	387(b) (345-550)

As expected, the spectra of all the compounds are red shifted from that of 1,4-bis(phenylethynyl)benzene (BPB), revealing a smaller HOMO–LUMO gap due to substituent effects. In cyclohexane, the size of the shifts in the absorption spectra of **10**, **12**, **14** and **15** (being between 480 and 167 cm<sup>-1</sup>) are consistent with a substituent effect.[12] While the shifts observed for **8**, **9**, **11** and **13** (being between 2900 and 4400 cm<sup>-1</sup>) suggests a greater electronic interaction between the substituents and the bis(phenylethynyl)benzene bridging moiety.

Very little solvatochromism is observed in any of the compounds' absorption spectra. The absorption spectra of D-A compounds **8** and **9** are quite similar (Figure 5.1 and Figure 5.2). Their absorbance spectra are characterised by broad bands

centred around 296 nm and 369 nm. In cyclohexane, the higher energy band of **8** consists of two peaks at 290 nm and 317 nm. While the same band for **9** consists of two peaks at 291 nm and 313 nm. In polar solvents the separations between the bands around 296 nm becomes less discernable, however, the only change in the intense lower energy band is a slight broadening and an increase of absorbance in the red tail region. A similar profile was observed in the UV spectra of the model D-A systems, 4-cyano-(4-methylthio)diphenylacetylene [8, 12, 13] and 4-N,N-dimethylamino-4-cyanodiphenylacetylene.[7] The intense lower energy bands observed in this case were reported to be an intramolecular charge-transfer (ICT) transition resulting from the excitation from the donor to the acceptor group. The low energy bands observed in the UV spectra of **8** and **9** can also be considered to be ICT absorption bands. The high energy bands are attributed to  $\pi^* \leftarrow \pi$  transitions.[6] It is expected that this transition will also have some charge transfer character and is better described as the promotion of an electron from a  $\pi$  bonding level to an orbital localised more on the acceptor group.[13] These two main energy bands may not represent pure transitions but may be composed of several weaker transitions to other excited states.[13] The absorption spectra of **10**, in contrast, has only one blue shifted broad band centred at about 336 nm in all the solvents (Figure 5.3) compared to **8** and **9**. It also has the smallest spectral shift ( $1664 \text{ cm}^{-1}$  in cyclohexane) of the three D-A pairings. The perpendicular orientation decouples the dimethylamino donor group from the rest of the molecule and the cyano group.[9] Compound **10** is thus expected to have complete charge separation in the excited state. This sole absorption band is hence attributed to a predominantly ICT transition. The blue shift of the band is due to the reduced electron delocalisation because of the orthogonal geometry. Based on the energy of the ICT transitions the magnitude of the charge separation in the D-A pairs can be ordered  $\text{N}(\text{Me})_2$  (coplanar) - CN >  $\text{N}(\text{Me})_2$  (coplanar) -  $\text{CO}_2\text{Me}$ .

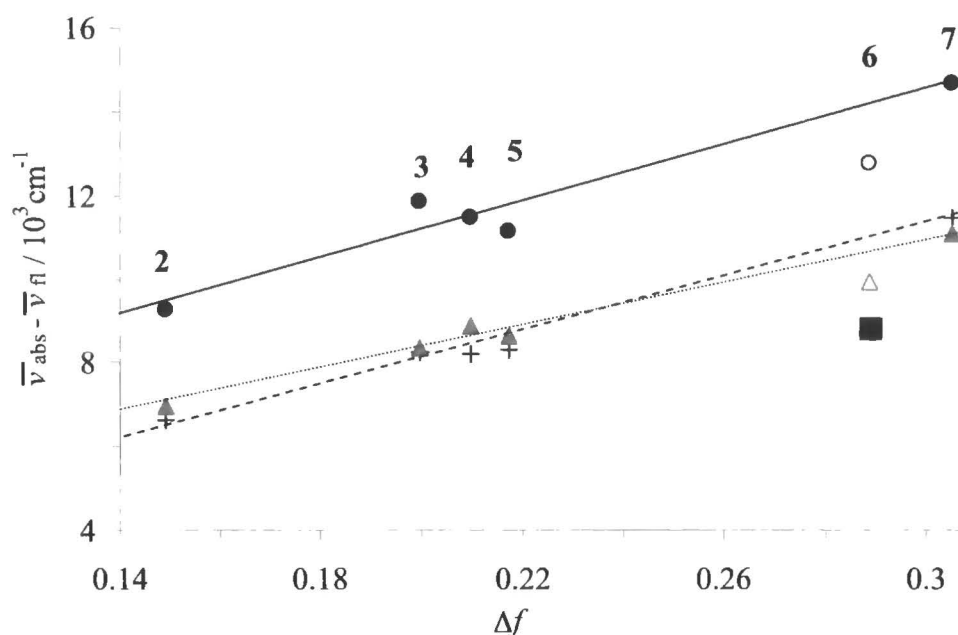
The emission spectra, in cyclohexane, of **8** and **9** are characterised by two well defined peaks at 404 nm and 427 nm, and at 412 nm and 435 nm respectively. Both have a Stokes shift of about  $2600 \text{ cm}^{-1}$ . The emission spectrum of **10** has one main peak at 404 nm with a shoulder at 426 nm and a considerably large Stokes shift of  $4800 \text{ cm}^{-1}$ . As the solvent polarity increases, all the emission spectra become broader and structureless with large solvatochromic shifts (Table 5.2). The Stokes

shifts increase dramatically and in acetonitrile **8**, **9** and **10** have shifts of  $\approx 11500$ , 11000 and 14700  $\text{cm}^{-1}$  respectively. Similar observations were made by Hirata *et al.*[7], when studying 4-N,N-dimethylamino-4-cyanodiphenylacetylene and Delmond *et al.*[9] in a report on 4-N,N-dibutylamino-4-cyanoterphenyl and its sterically hindered derivatives. Our results also indicate that in non-polar solvents the fluorescence state of **8**, **9** and **10** is the locally excited (LE) singlet state and in polar solvents intramolecular charge separation occurs in the excited state. The more pronounced red shift in **10** suggests a larger excited state dipole moment associated with this perpendicular geometry. The three peaks observed at 425, 440, and 454 nm for **8** and at 403, 417 and 429 nm for **10**, in acetonitrile, are solvent Raman bands. The fact that the Raman scatter for MeCN is evident is testimony of the weakness of these emissions in highly polar solvents. Also, photo degradation products are observed in all three compounds in the more polar solvents (see Table 5.2).

In Figure 5.9, the Stokes shifts of the fluorescence of **8**, **9** and **10** are observed to follow the Lippert equation[14] (see Chapter 2)

$$\bar{\nu}_{abs} - \bar{\nu}_{fl} = \frac{2(\Delta\mu)^2}{hca^3} \Delta f + c, \text{ where } \Delta f = \frac{\epsilon - 1}{2\epsilon + 1} - \frac{n^2 - 1}{2n^2 + 1}.$$

Here,  $\bar{\nu}_{abs} - \bar{\nu}_{fl}$  is the frequency shift between absorption and emission;  $\Delta\mu$  is the difference in dipole moments between the ground and excited states;  $h$  is Plank's constant;  $c$  is the speed of light;  $a$  is the approximate radius of the spherical cavity containing the dipole;  $\Delta f$  is the orientation polarisability; and  $c$  is the intercept. The straight lines show the best fits for the Stokes shift in aprotic solvents for the three D-A systems. The observed liner relationship suggests that  $\Delta\mu$  is almost a constant for these aprotic solvents.



**Figure 5.9** Lippert plot of **10** (●, —), **9** (▲, .....), and **8** (+, ----). The straight lines show the best fits to the Stokes shift in aprotic polar solvents. The Stokes shifts in ethanol are labelled **10** (○), **9** (△) and **8** (■). Solvents are (2) chloroform, (3) ethyl acetate, (4) tetrahydrofuran, (5) dichloromethane, (6) ethanol and (7) acetonitrile.

**Table 5.3** The calculated change in dipole moments ( $\Delta\mu$ ) and the excited state dipole moments ( $\mu_e$ ) from the gradients (Grad.) and y-intercepts (c) of the Lippert plots of molecules **8**, **9** and **10** in **Figure 5.9**. The approximate radius of the spherical cavity ( $a$ ) and the ground state dipole moments where estimated from theoretical calculations using the *Gaussian 03* package[15] with the B3LYP density functional and the 6-31G\* basis set.

Cpd.	Grad. / $\text{cm}^{-1}$	c / $\text{cm}^{-1}$	a / Å	$\mu_g / \text{D}$	$\mu_e / \text{D}$	$\Delta\mu / \text{D}$
<b>8</b>	31,088	1,858	9.67	4.92	56.16	51.24
<b>9</b>	25,967	3,163	10.42	6.92	57.52	50.60
<b>10</b>	33,477	4,443	10.24	6.71	62.32	55.61

The calculated excited state dipole moments ( $\mu_e$ ) of the three D-A molecules are collected in Table 5.3 along with the gradients calculated from the Lippert plots in Figure 5.9. From the similarities between the gradients, it is expected that all three molecules would have similar changes in dipole moments. The larger frequency shift values of **9** and **10** are due to them being more polar than **8** and thus more susceptible to the orientation polarizability of the solvents. As predicted from the steady state fluorescence, orthogonal geometry in **10** results in it having the largest  $\mu_e$ . The effects of TICT and ICT states are not accounted for in the theory of general solvent effects described by the Lippert equation.[14] Hence, while the linearity of these plots are evidence of the domination of general solvent effects, the greater

frequency shifts in **10** when compared to **8** and **9** indicates that the effect of the formation of the TICT state is different to that of the ICT state.

The  $\mu_e$  for three molecules were calculated by taking  $a$  as half the approximate length of each molecule. Compound **10** has the largest  $\mu_e$  of the three (62.32 D) while **8** and **9** have  $\mu_e$  of 56.16 D and 57.52 D respectively. These values are similar to that of DACN-DPA (58.0 D for  $a = 9.2 \text{ \AA}$ ).<sup>[7]</sup> The longer bridging unit is thus shown to not significantly increase the already large dipole moment in the charge separated state. These values indicate that the electronic structure of the ICT state is close to that of the ion pair.<sup>[7]</sup>

In ethanol, the three molecules show deviations from the Lippert equation because of specific solvent effects. This is characteristic for the interaction of fluorophores with hydrogen-bonding solvents.

The absorption spectrum of donor-donor (D-D) system **11** (Figure 5.4), in cyclohexane, is similar to that of **8** and **9**. The main difference being the peak around 286 nm is about half the intensity of the corresponding peak in **8** and **9**. There is a minor red shift in the absorbance spectra of **11**, of about 11 nm, as solvent polarity increases. The emission spectrum of **11**, in cyclohexane, is characterised by two well defined peaks at 388 and 407 nm and is similar in profile to **8** and **9** in cyclohexane. As the solvent polarity is increased the emission spectra becomes broad and featureless. The maximum Stokes shift of **11** is in acetonitrile and is  $5974 \text{ cm}^{-1}$ , about half of what is observed in the D-A systems. The strong electron donating effect of the dimethylamino groups is causing the large difference between the dipole moments of the ground and excited states. There exists a large delocalised negative charge on the spacer unit and a positive charge on the terminal groups. This explains the sensitivity of the emission spectrum of **11** to solvent polarity.

The absorbance and emission spectra of the strong donor only substituted **13** (Figure 5.6) are quite similar to that of D-D substituted **11**, but the emission spectra of **13** are more red sifted. The Stokes shift of **13** in acetonitrile is  $8283 \text{ cm}^{-1}$ , some  $2309 \text{ cm}^{-1}$  more than that of **11**. This indicates there is a larger charge separation along the molecular long axis in the excited state of **13** than in **11**.

Compound **14** has a cyano acceptor (A) group and **15** has a methyl ester A group and are both weakly polar. Solvent polarity has little effect on their absorption



spectra (Figure 5.7 and Figure 5.8). The emission of **14** and **15** show spectral broadening in polar solvents and a maximum Stokes shift in acetonitrile of only  $3344\text{ cm}^{-1}$  and  $3062\text{ cm}^{-1}$  respectively. These observations are primarily due to general solvent effects and not to ICT.

The absorption and emission profiles of the acceptor-acceptor (A-A) substituted compound, **12** (Figure 5.5), are almost identical to BPEB (Chapter 4, Figure 4.2) in cyclohexane. The absorbance and emission spectra of **12** are red shifted by only 14 and 19 nm respectively in comparison to those of BPEB and there is strong spectral overlapping. As the solvent polarity increases the absorption profile of **12** is unaffected and is only slightly red shifted. Meanwhile, the emission spectra retain most of their vibrational fine structure and also show very minor red shifts. The Stokes shift in acetonitrile of **12** is only  $1012\text{ cm}^{-1}$ . This observed general lack of sensitivity to solvent polarity is the result of very little charge separation in **12**.

### 5.3 Lifetime measurements

The lifetimes ( $\tau_f$ ), in solvents of increasing polarity, of the D-A family of compounds studied are collated in Table 5.4. They were measured by TCSPC (see Chapter 3). All the lifetimes, except **10** in ethyl acetate, had to be analysed as double exponential functions. This is interpreted as being the result of the dynamic Stokes shift of the fluorescence.[7] There is a sharp, near-linear increase in the fluorescence lifetime of the three D-A compounds as the solvent polarity increases from cyclohexane (0.00) to DCM (0.217). The lifetimes of **8**, **9** and **10** increases from 0.65 to 2.50 ns, 0.97 to 2.64 ns and 1.00 to 2.86 ns respectively. Khundkar[8] made a similar observation for 4-cyano-4'-methylthiodiphenylacetylene (MTCN-DPA). It was proposed by Broo[10] that this increase in lifetimes indicated that a conformational change of the excited state occurs and the change is larger for more polar solvents.

However, in ethanol and acetonitrile the lifetimes are close to the lower lifetime limit ( $\approx 0.1\text{ ns}$ ) of the detection system for all three except **9** in ethanol were  $\tau_f = 0.18\text{ ns}$ .

**Table 5.4** Fluorescence lifetimes of **8** to **15** in solvents of increasing polarity<sup>b</sup>.

	$\tau_f \pm 0.05 / \text{ns}^a$													
	C <sub>6</sub> H <sub>12</sub>		CHCl <sub>3</sub>		CH <sub>3</sub> CO <sub>2</sub> C <sub>2</sub> H <sub>5</sub>		THF		DCM		C <sub>2</sub> H <sub>5</sub> OH		CH <sub>3</sub> CN	
	0.0 <sup>b</sup>		0.149 <sup>b</sup>		0.200 <sup>b</sup>		0.210 <sup>b</sup>		0.217 <sup>b</sup>		0.289 <sup>b</sup>		0.305 <sup>b</sup>	
	$\tau_1$ (yield)	$\tau_2$ (yield)	$\tau_1$ (yield)	$\tau_2$ (yield)	$\tau_1$ (yield)	$\tau_2$ (yield)	$\tau_1$ (yield)	$\tau_2$ (yield)	$\tau_1$ (yield)	$\tau_2$ (yield)	$\tau_1$ (yield)	$\tau_2$ (yield)	$\tau_1$ (yield)	$\tau_2$ (yield)
<b>8</b>	0.65 (80.83%)	0.21 (19.17%)	1.90 (83.16%)	0.53 (16.84%)	2.24 (86.55%)	0.69 (13.45%)	2.39 (88.89%)	0.56 (11.11%)	2.50 (89.52%)	0.71 (10.48%)	0.13 <sup>c</sup> (70.19%)	1.78 (29.81%)	0.1 <sup>c</sup> (88.85%)	0.10 (11.15%)
<b>9</b>	0.97 (81.35%)	0.22 (18.65%)	1.92 (84.79%)	0.19 (15.21%)	2.34 (80.38%)	0.10 (19.62%)	2.49 (91.74%)	0.18 (8.26%)	2.64 (93.5%)	0.18 (6.5%)	0.18 (98.89%)	0.92 (1.11%)	0.12 <sup>c</sup> (97.27%)	1.00 (2.73%)
<b>10</b>	1.00 (75.24%)	0.23 (24.76%)	2.05 (93.36%)	0.41 (6.64%)	2.49 (100%)	-	2.68 (88.3%)	0.14 (11.7%)	2.86 (90.37%)	0.10 (9.63%)	0.13 <sup>c</sup> (99.3%)	0.10 (0.7%)	1.68 (0.77%)	0.10 <sup>c</sup> (99.23%)
<b>11</b>	0.41 (50.63%)	0.77 (49.37%)	0.55 (57.08%)	1.06 (42.92%)	1.02 (69%)	0.43 (31%)	1.02 (81.3%)	0.20 (18.7%)	1.10 (68.92%)	0.41 (31.08%)	0.34 (57%)	0.11 (43%)	1.77 (82.98%)	0.11 (17.02%)

<sup>a</sup>  $\lambda_{\text{ex}}$  and  $\lambda_{\text{em}}$  are listed in Appendix A.1. <sup>b</sup> Solvent polarity based on the Lippert-Mataga equation. <sup>c</sup> Lifetimes were  $\leq 0.1$  ns and at the detection limits of the TCSPC equipment.

Table 5.4 (Continued)

	$\tau_f \pm 0.05 / \text{ns}^a$													
	<chem>C6H12</chem>		<chem>CHCl3</chem>		<chem>CH3CO2C2H5</chem>		THF		DCM		<chem>C2H5OH</chem>		<chem>CH3CN</chem>	
	0.0 <sup>b</sup>		0.1492 <sup>b</sup>		0.1996 <sup>b</sup>		0.2096 <sup>b</sup>		0.2171 <sup>b</sup>		0.2887 <sup>b</sup>		0.3054 <sup>b</sup>	
	$\tau_1$ (yield)	$\tau_2$ (yield)	$\tau_1$ (yield)	$\tau_2$ (yield)	$\tau_1$ (yield)	$\tau_2$ (yield)	$\tau_1$ (yield)	$\tau_2$ (yield)	$\tau_1$ (yield)	$\tau_2$ (yield)	$\tau_1$ (yield)	$\tau_2$ (yield)	$\tau_1$ (yield)	$\tau_2$ (yield)
<b>12</b>	0.56 (75.04%)	0.20 (24.96%)	0.61 (94.15%)	0.19 (5.85%)	0.59 (81.33%)	0.16 (18.67%)	0.62 (77.18%)	0.12 (22.82%)	0.62 (82.56%)	0.14 (17.44%)	0.66 (76.91%)	0.25 (23.09%)	0.65 (79.51%)	0.12 (20.49%)
<b>13</b>	0.80 (73.35%)	0.28 (26.65%)	1.19 (80.55%)	0.33 (19.45%)	1.53 (84.19%)	0.39 (15.81%)	1.58 (93.41%)	0.46 (6.59%)	1.66 (90.18%)	0.51 (9.82%)	0.61 (73.82%)	0.22 (26.18%)	2.47 (90.79%)	0.57 (9.21%)
<b>14</b>	0.64 (70.91%)	0.16 (29.09%)	0.74 (82.35%)	0.18 (17.65%)	0.75 (88.84%)	0.17 (11.16%)	0.76 (84.26%)	0.16 (15.74%)	0.80 (80.63%)	0.13 (19.37%)	0.85 (80.28%)	0.21 (19.72%)	0.91 (91.14%)	0.30 (8.86%)
<b>15</b>	0.63 (74.51%)	0.19 (25.49%)	0.73 (78.24%)	0.20 (21.76%)	0.72 (80.39%)	0.13 (19.61%)	0.73 (78.74%)	0.16 (21.26%)	0.78 (85.26%)	0.10 (14.74%)	0.89 (78.41%)	0.30 (21.59%)	0.89 (82.96%)	0.13 (17.04%)

<sup>a</sup>  $\lambda_{\text{ex}}$  and  $\lambda_{\text{em}}$  are listed in Appendix A.1. <sup>b</sup> Solvent polarity based on the Lippert-Mataga equation. <sup>c</sup> Lifetimes were  $\leq 0.1$  ns and at the detection limits of the TCSPC equipment.

The very short lifetimes in ethanol are believed to be due to hydrogen bonding to the amino group of the ICT state.[14] The sterically hindered 2,6-dimethyl-4-N,N-dimethylamino-4'-cyanoterphenyl is reported to also show a dramatic decrease in lifetime in MeCN.[9] This observation in these similar types of D-A systems have been attributed to the faster kinetic population of the TICT state from the ICT state and the population of a TICT state with more forbidden character in which one or two rings are perpendicular to each other and the molecular plane.[9] This explanation is supported by quantum chemical calculations in which it was found that the TICT state is of low enough energy in polar solvents to become photophysically relevant.[9]

The lifetimes of the D-D compound **11**, and single donor compound **13**, in cyclohexane, are 0.41 ns and 0.80 ns respectively. Their lifetimes both increase more gradually with aprotic solvent polarity. Compounds **13** and **11** have the longest and second longest lifetimes in acetonitrile at 2.47 ns and 1.77 ns respectively. However, in ethanol both exhibit the much shorter lifetimes of 0.61 ns (**13**) and 0.34 ns (**11**). This is a clear indication of hydrogen bonding to the amino group in the excited state.[14] The resulting product, being not very stable in the excited state, decays rapidly.

The lifetimes of **12**, **14** and **15** all show very little sensitivity to solvent polarity. This is expected of non-polar or weakly polar molecules. The lifetime of **12** ranged from only 0.56 to 0.65 ns while **14** and **15** had lifetimes ranging from 0.63 to 0.91 ns.

#### **5.4 Picosecond time-resolved infrared (TRIR) spectroscopy measurements**

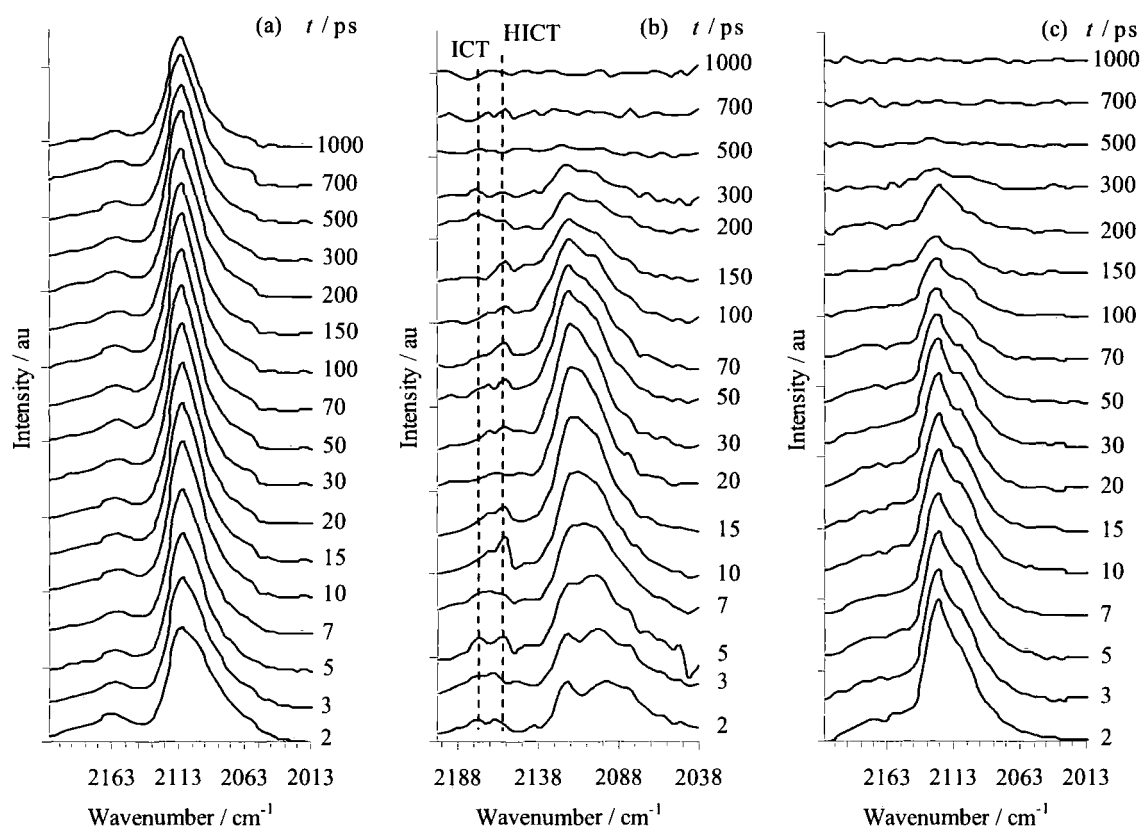
The time-resolved infrared (TRIR) absorption spectra of **8**, **9**, and **10** in DCM, EtOH and MeCN were recorded using the Picosecond Infrared Absorption and Transient Excitation (PIRATE) system at the Central Laser Facility, Rutherford Appleton Laboratory, exciting at 267 nm (see Chapter 3). The spectral region between 2000 and 2220  $\text{cm}^{-1}$  is investigated as this covers the  $\text{C}\equiv\text{N}$  band of the ground, LE and ICT states.[16-19] The ground state  $\text{C}\equiv\text{C}$  band is also present in this region.[13] This technique was used in an attempt to shed some light on the type of bonding taking place in the ICT state of the three D-A molecules. The TRIR spectra of **13**, **14** and **15** were also recorded to monitor the effect of the individual donor

and acceptor groups on the vibrational spectra of the C≡C of the bridging unit and the effect the bridging unit had on the charge separation.

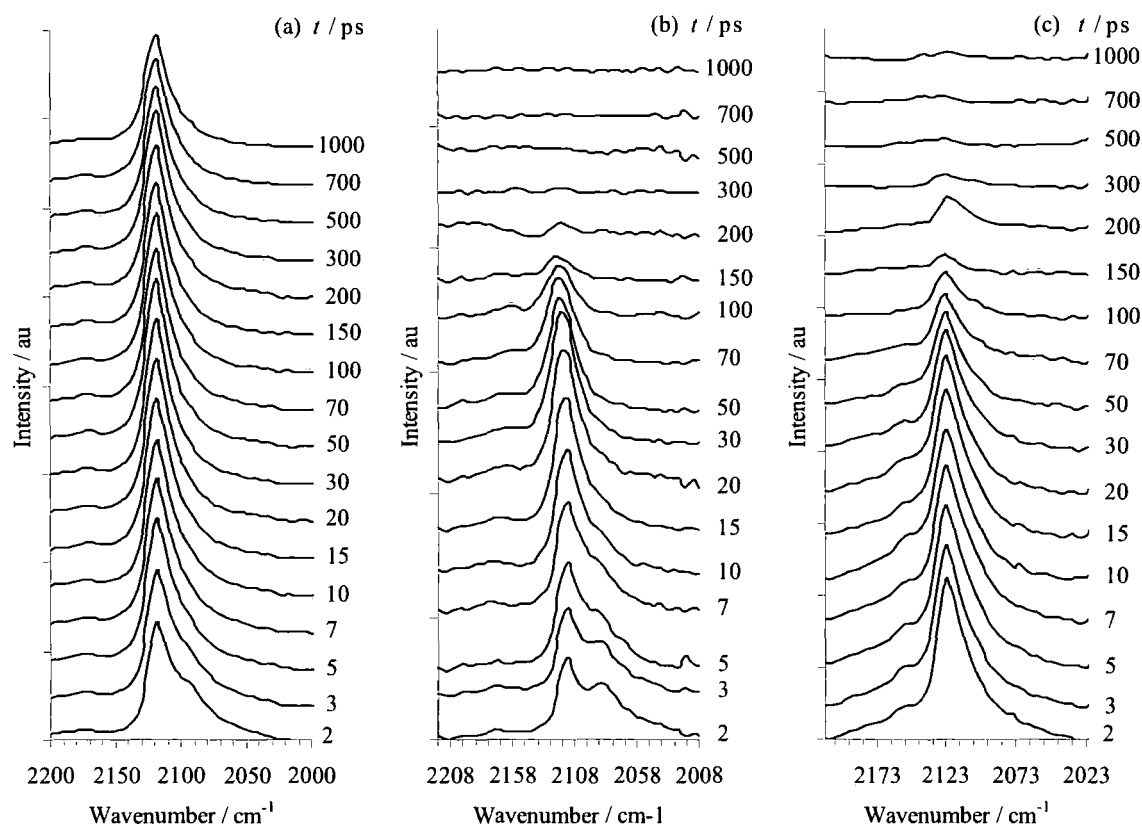
The TRIR absorption spectra of 4-dimethylaminobenzonitrile (DMABN) in a protic solvent was reported to show a hydrogen-bonded intramolecular charge transfer state (HICT) at 2091 cm<sup>-1</sup> as well as an ICT state at 2109 cm<sup>-1</sup>.<sup>[20]</sup> The following study addresses the question of what effect a longer bridging unit has on the ICT and HICT states in a protic solvent and the ICT state in an aprotic solvent.

It is found that the TRIR absorption spectra of all six molecules are generally dominated by the excited state C≡C stretching vibrations, in both protic and aprotic solvents, between 2040 and 2165 cm<sup>-1</sup> (Figure 5.10 to Figure 5.12 and Table 5.5). The solid ground state IR C≡C stretching bands are at higher energies, around 2206 cm<sup>-1</sup>, for **8**, **9** and **10**.<sup>[21]</sup> The identification of the excited state C≡C region is based on comparisons between TRIR spectra of molecules with and without C≡N bonding. The C≡N band tended to be very weak and broad in the excited state. In the solid ground state IR spectra of **9** and **10** the C≡N band is around 2358 cm<sup>-1</sup> and is weaker than the C≡C band.<sup>[21]</sup>

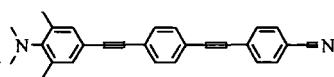
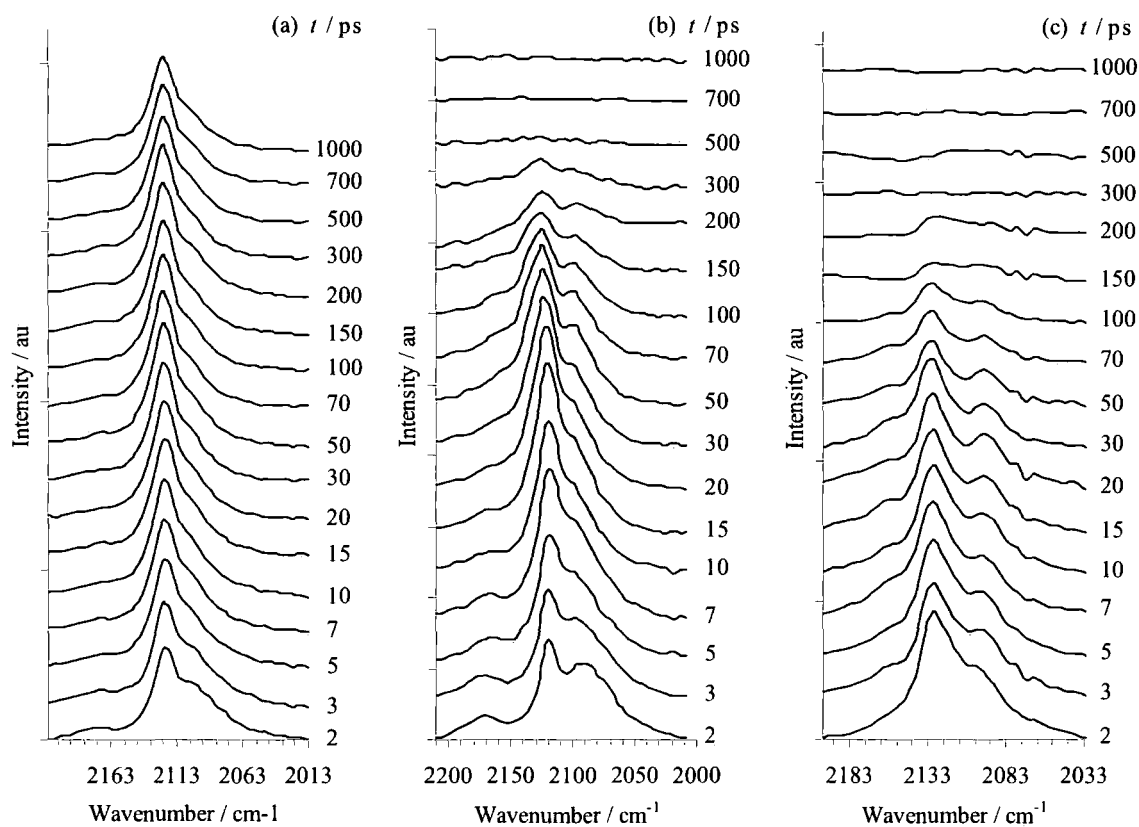
First, we evaluate the C≡N band and the effect of solvent environment and molecular geometry on the ICT state. The C≡N IR band in **9** appears as a weak single peak in aprotic solvents and as two weak peaks in a protic solvent (Figure 5.10). The evidence suggests that in EtOH, the C≡N band at 2175 cm<sup>-1</sup> decays—but not completely—while the band at 2158 cm<sup>-1</sup> intensifies over 300 ps. The distinction between these bands is not as clear as that reported for DMABN in methanol.<sup>[20]</sup> However, the presence of these two C≡N bands can be attributed to an interaction occurring in the protic solvent, after charge separation, which does not occur in the aprotic solvents. Based on similar observations in DMABN<sup>[20]</sup>, the 2158 cm<sup>-1</sup> band is attributed to hydrogen bonding between EtOH and the ICT state of **9** and is designated the HICT state. As the 2175 cm<sup>-1</sup> band differs by only 6 cm<sup>-1</sup> from that observed for the ICT in MeCN, we can attribute this band to a state similar to the free ICT state in aprotic solvents.



**Figure 5.10** The TRIR spectra of N#CC1=CC=C(C=C1)/C=C/C2=CC=C(C=C2)/C=C/C3=CC=C(C=C3)N#C (**9**) in DCM (a), EtOH (b) and MeCN (c) obtained at different pump-probe time delays with excitation at 266 nm, showing the  $\bar{\nu}$  (C≡N) and  $\bar{\nu}$  (C≡C) bands.



**Figure 5.11** The TRIR spectra of N#CC1=CC=C(C=C1)/C=C/C2=CC=C(C=C2)/C=C/C3=CC=C(C=C3)C(=O)O (**8**) in DCM (a), EtOH (b) and MeCN (c) obtained at different pump-probe time delays with excitation at 266 nm, showing the  $\bar{\nu}$  (C≡C) band.



**Figure 5.12** The TRIR spectra of **(10)** in DCM (a), EtOH (b) and MeCN (c) obtained at different pump–probe time delays with excitation at 266 nm, showing the  $\bar{\nu}$  (C≡N) and  $\bar{\nu}$  (C≡C) bands.

**Table 5.5** Collection of all the TRIR absorption stretching frequencies of **9**, **8**, **10**, **13**, **14** and **15** in the ICT state in DCM, EtOH and MeCN after a delay of 20 ps.

Cpd.		Stretching frequencies in different solvents / $\text{cm}^{-1}$		
		DCM	EtOH	MeCN
<b>9</b>	C≡N	2160	2158 (HICT), 2175 (ICT)	2169
	C≡C	2110	2118, 2101(sh)	2124, 2107(sh)
<b>8</b>	C≡C	2113	2113, 2085(sh)	2124
<b>10</b>	C≡N	2164	2164	2152
	C≡C	2119, 2102(sh)	2124, 2096(sh)	2130, 2096(sh)
<b>13</b>	C≡C	2097w, 2049s	2097w, 2049s	2097w, 2054s
<b>14</b>	C≡N	2147s	2147s	2147s
	C≡C	2114m, 2018m (b)	2108m, 2033m (b)	2114m, 2044m (b)
<b>15</b>	C≡C	2160m, 2064m (b)	2113vw ?, 2034w (b)	2114w, 2039w(b)

Key: sh – shoulder band; b – broad band. Band intensities: vw – very weak; w – weak; m – medium; s – strong band. ? – band with uncertain assignment.

The ICT band in DCM differs from that in EtOH by  $15\text{ cm}^{-1}$  (Table 5.5) because of the greater differences in solvent polarity (see Table 5.4). The poor signal to noise ratio makes a kinetics study impossible. This loss in resolution of the  $\text{C}\equiv\text{N}$  bands, in both protic and aprotic solvents, and the shorter decay times (the HICT and ICT states of DMABN persist for at least 3 ns) is a clear result of the effect of the longer bridging unit on the system. The separation between the ICT and HICT bands in **9** is comparable to that of DMABN. However the ICT and HICT bands in **9** are up-shifted by  $66\text{ cm}^{-1}$  and  $67\text{ cm}^{-1}$  respectively.

The  $\text{C}\equiv\text{N}$  TRIR absorption band of **10** shows up as a very weak single band in aprotic solvents and as one weak, slightly broader and more pronounced band in EtOH (Figure 5.12). In DCM the  $\text{C}\equiv\text{N}$  band persists for  $> 1\text{ ns}$ , while in MeCN and EtOH it completely decays after 300 ps. These lifetimes are in-keeping with the fluorescence decay lifetimes of the  $\text{S}_1$  state in these solvents (Table 5.4). There is no evidence to suggest that more than one type of ICT state is present for **10** in EtOH. The single band at  $2164\text{ cm}^{-1}$  could represent the hydrogen-bonded ICT state based on the fact that it is only  $6\text{ cm}^{-1}$  up-shifted from the HICT band identified in **9** (Table 5.5). Although the cyano group band in DCM and EtOH are the same, the shorter lifetime in EtOH is indicative of some interaction occurring in EtOH that does not happen in DCM. The twisted geometry of **10** is evidently responsible for the occurrence of the single  $\text{C}\equiv\text{N}$  band in the ICT state in EtOH. If the single  $\text{C}\equiv\text{N}$  band in **10** is indicative of a HICT state then it suggests that the decaying ICT band and rising HICT bands in **9** are indicative of a planar to perpendicular twisting of the dimethylamino group out of the plane of the neighbouring phenyl ring over the 2–300 ps. This would indicate that the hydrogen bonding in the excited state is occurring in the TICT state.

Secondly, we evaluate the  $\text{C}\equiv\text{C}$  bands and the influence of the D and A groups, solvent environment and molecular geometry on the ICT state. In the three D-A systems the  $\text{C}\equiv\text{C}$  band is the dominant peak found from  $2110$  to  $2130\text{ cm}^{-1}$  (see Figure 5.10 to Figure 5.12 and Table 5.5). This band also moves to progressively higher energies as the solvent polarity increases. The  $\text{C}\equiv\text{C}$  vibration is not normally strong in infrared spectra, so this enhancement is attributed to the charge separation in the ICT state of the D-A systems. The more polar the solvent, the shorter the decay time of the  $\text{C}\equiv\text{C}$  band, with compound **10** having the shortest decay time in



MeCN. The TRIR spectrum of **8** monitors changes in the C≡C stretching frequency over time. We observe a main band at 2113 cm<sup>-1</sup> in DCM and EtOH which moves up 11 cm<sup>-1</sup> to 2124 cm<sup>-1</sup> in MeCN. Also, a shoulder appears in the beginning at 2085 cm<sup>-1</sup> in EtOH which completely decays after 7 ps. A shoulder is present on the main band in **9** in EtOH and MeCN and in **10** in all three solvents. Here the shoulder has the same lifetime as the main band. This suggests that the greater charge separation and the twisted geometry of the phenyl rings in the excited state affects the stretching frequencies of the C≡C. The persistence of the shoulder band may be evidence of the two C≡C having different stretching frequencies in highly polar solvents.

TRIR spectra of all three mono-substituted compounds (**13–15**) have two C≡C bands. In **13** these bands persist for over 1 ns in DCM and MeCN, and for less than 1 ns in EtOH. In **14** and **15** these C≡C vibration bands persist for less than 1 ns. This is in keeping with the lifetimes of their S<sub>1</sub> excited states. The higher energy C≡C bands in mono-substituted compounds **13** and **14** do not increase in energy in direct proportion to solvent polarity but generally remain stationary. While the same high energy band in compound **15** decreases with solvent polarity and is hardly discernable in EtOH (see Table 5.5).

Compound **13** has a strong band at 2049 cm<sup>-1</sup> in DCM and EtOH and at 2054 cm<sup>-1</sup> in MeCN also assigned to a C≡C stretching mode. The peaks move by about 16 cm<sup>-1</sup> over 2 ns to higher energy in all three solvents. In MeCN, after a 5 ps delay a shoulder grows into the 2049 cm<sup>-1</sup> peak at 2018 cm<sup>-1</sup> and decays at the same rate as the other two peaks. The lower energy broad band in **14** at around 2018 cm<sup>-1</sup>, moves progressively to higher energies as the solvent polarity increases. Judging from the intensities of these two C≡C vibrational bands in **13** and **14**, it can be concluded that the strong donor substituent enhances the lower energy vibration while the strong acceptor substituent enhances the higher energy vibration in all the solvents. Although **15** has an acceptor substituent it is not strong enough to influence the intensity of the C≡C vibration, particularly in polar solvents. Both C≡C energy bands are quite weak, particularly in EtOH.

## Conclusions

The photophysical properties of eight donor and acceptor substituted compounds, **8** to **15**, were measured using steady state fluorescence and time-resolved infrared techniques and the results discussed.

On the whole, all the D-A compounds (**8** to **10**) exhibit ICT and TICT in the excited state in solvents of increasing polarity. In non-polar solvents the excited state observed is the LE state. Compound **10** exhibits the largest charge separation, which is associated with its perpendicular geometry, with a 55.61 D change in dipole moment in the excited state. The extended conjugation of the spacer was found to not significantly increase the dipole moment of the charge separated state.

Strong donor only substituted compounds, **11** and **13**, also show charge separation in polar solvents. However, the acceptor substituted compounds, **12**, **14** and **15** are only weakly polar and show very little sensitivity to solvent polarity.

The lifetimes of the three D-A systems increased sharply as solvent polarity increased, from cyclohexane to DCM, and this is proposed to be the result of conformational changes in the excited state which become larger in more polar solvents. However, in MeCN the striking decrease in the lifetime is thought to be the result of the faster kinetic population of a TICT state with a more forbidden character in which one or two rings are perpendicular to each other. In protic solvents the dramatic shortening of the lifetimes of **8** to **11** and **13** is explained in terms of hydrogen bonding to the amino group in the ICT state.

From the TRIR spectroscopy measurements, we are able to identify the  $2158\text{ cm}^{-1}$  band as representing the hydrogen-bonded ICT state (HICT) of compound **9** in EtOH and the  $2175\text{ cm}^{-1}$  band as the ICT state. The presence of only one  $\text{C}\equiv\text{N}$  vibrational band for **10**, in EtOH, at  $2164\text{ cm}^{-1}$  is purported to be the HICT state. The low resolution of the  $\text{C}\equiv\text{N}$  bands is a direct result of the extended conformation of the spacer unit.

The  $\text{C}\equiv\text{C}$  vibration is the dominant band in all the TRIR spectra of the compounds in this study. This band moves to higher energies as the solvent polarity increases for the three D-A systems and is found from  $2110$  to  $2130\text{ cm}^{-1}$ . In compounds **13** to **15**, two bands represent the  $\text{C}\equiv\text{C}$  vibrations—one a sharp peak the other a broad band. It is suggested that the  $\text{NMe}_2$  (strong donor) group and the  $\text{C}\equiv\text{N}$  (strong

acceptor) group influence the vibrations of the  $C\equiv C$  closest to them by changing the polarisability of the bond.

## REFERENCES

1. Z. R. Grabowski, K. Rotkiewicz and W. Rettig, "Structural changes accompanying intramolecular electron transfer: Focus on twisted intramolecular charge-transfer states and structures." *Chemical Reviews*, 2003, **103**, 3899-4031.
2. Rotkiewi.K, Grellman.Kh and Grabowsk.Zr, "Reinterpretation of anomalous fluorescence of para-N,N-dimethylamino-benzonitrile." *Chemical Physics Letters*, 1973, **19**, 315-318.
3. Z. R. Grabowski, K. Rotkiewicz and A. Siemiarczuk, "Dual fluorescence of donor-acceptor molecules and the twisted intra-molecular charge-transfer (TICT) states." *Journal Of Luminescence*, 1979, **18-19**, 420-424.
4. A. Siemiarczuk, Z. R. Grabowski and A. Krowczynski, "2 Emitting states of excited para-(9-anthryl)-N,N-dimethylaniline derivatives in polar-solvents." *Chemical Physics Letters*, 1977, **51**, 315-320.
5. W. Rettig, "Charge separation in excited-states of decoupled systems - TICT compounds and implications regarding the development of new laser-dyes and the primary processes of vision and photosynthesis." *Angewandte Chemie-International Edition In English*, 1986, **25**, 971-988.
6. A. E. Stiegman, V. M. Miskowski, J. W. Perry and D. R. Coulter, "A series of donor-acceptor molecules of the form  $\text{NH}_2(\text{C}_6\text{H}_4)(\text{C}=\text{C})_n(\text{C}_6\text{H}_4)\text{NO}_2$  - Unusual effects of varying-n." *Journal Of The American Chemical Society*, 1987, **109**, 5884-5886.
7. Y. Hirata, T. Okada and T. Nomoto, "Photoinduced intramolecular charge separation of p-N,N-dimethylamino-p'-cyano-diphenylacetylene in polar solvents." *Chemical Physics Letters*, 1997, **278**, 133-138.
8. L. R. Khundkar, A. E. Stiegman and J. W. Perry, "Solvent-tuned intermolecular charge-recombination rates in a conjugated donor- acceptor molecule." *Journal Of Physical Chemistry*, 1990, **94**, 1224-1226.
9. S. Delmond, J. F. Letard, R. Lapouyade and W. Rettig, "Photoinduced intramolecular charge transfer in planar vs. twisted donor-acceptor terphenyls." *Journal Of Photochemistry And Photobiology A-Chemistry*, 1997, **105**, 135-148.
10. A. Broo, "Quantum-chemical calculation of geometry, vibration spectrum, absorption and emission-spectrum of p-cyano-p'-methyl thiodiphenylacetylene." *Chemical Physics*, 1994, **183**, 85-94.
11. D. M. Shin and D. G. Whitten, "Photochemical-reactions in organized assemblies.54. Solvatochromic behavior of intramolecular charge-transfer diphenylpolyenes in homogeneous solution and microheterogeneous media." *Journal Of Physical Chemistry*, 1988, **92**, 2945-2956.

12. M. Biswas, P. Nguyen, T. B. Marder and L. R. Khundkar, "Unusual size dependence of nonradiative charge recombination rates in acetylene-bridged compounds." *Journal of Physical Chemistry A*, 1997, 1689-1695.
13. A. E. Stiegman, E. Graham, K. J. Perry, L. R. Khundkar, L.-T. Cheng and J. W. Perry, "The electronic structure and second-order nonlinear optical properties of donor-acceptor acetylenes: A detailed investigation of structure-property relationships." *Journal of the American Chemical Society*, 1991, **113**, 7658-7666.
14. J. R. Lakowicz, "Principles of fluorescence spectroscopy", 2nd ed, Kluwer Academic / Plenum Publishers, New York, 1999.
15. M. J. Frisch, G. W. Trucks, H. B. Schlegel, G. E. Scuseria, M. A. Robb, J. R. Cheeseman, J. J. A. Montgomery, T. Vreven, K. N. Kudin, J. C. Burant, J. M. Millam, S. S. Iyengar, J. Tomasi, V. Barone, B. Mennucci, M. Cossi, G. Scalmani, N. Rega, G. A. Petersson, H. Nakatsuji, M. Hada, M. Ehara, K. Toyota, R. Fukuda, J. Hasegawa, M. Ishida, T. Nakajima, Y. Honda, O. Kitao, H. Nakai, M. Klene, X. Li, J. E. Knox, H. P. Hratchian, J. B. Cross, C. Adamo, J. Jaramillo, R. Gomperts, R. E. Stratmann, O. Yazyev, A. J. Austin, R. Cammi, C. Pomelli, J. W. Ochterski, P. Y. Ayala, K. Morokuma, G. A. Voth, P. Salvador, J. J. Dannenberg, V. G. Zakrzewski, S. Dapprich, A. D. Daniels, M. C. Strain, O. Farkas, D. K. Malick, A. D. Rabuck, K. Raghavachari, J. B. Foresman, J. V. Ortiz, Q. Cui, A. G. Baboul, S. Clifford, J. Cioslowski, B. B. Stefanov, G. Liu, A. Liashenko, P. Piskorz, I. Komaromi, R. L. Martin, D. J. Fox, T. Keith, M. A. Al-Laham, C. Y. Peng, A. Nanayakkara, M. Challacombe, P. M. W. Gill, B. Johnson, W. Chen, M. W. Wong, C. Gonzalez, and J. A. Pople, *Gaussian 03, Revision C.02*. 2004, Gaussian Inc.: Wallingford CT.
16. C. Chudoba, A. Kummrow, J. Dreyer, J. Stenger, E. T. J. Nibbering, T. Elsaesser and K. A. Zachariasse, "Excited state structure of 4-(dimethylamino)benzonitrile studied by femtosecond mid-infrared spectroscopy and ab initio calculations." *Chemical Physics Letters*, 1999, **309**, 357-363.
17. M. Hashimoto and H.-O. Hamaguchi, "Structure of the twisted-intramolecular-charge-transfer excited singlet and triplet states of 4-(dimethylamino)benzonitrile as studied by nanosecond time-resolved infrared spectroscopy." *Journal of Physical Chemistry*, 1995, 7875-7877.
18. W. M. Kwok, C. Ma, P. Matousek, A. W. Parker, D. Phillips, W. T. Toner, M. Towrie and S. Umaphy, "A determination of the structure of the intramolecular charge transfer state of 4-dimethylaminobenzonitrile (DMABN) by time-resolved resonance Raman spectroscopy." *Journal Of Physical Chemistry A*, 2001, **105**, 984-990.
19. C. Ma, W. M. Kwok, P. Matousek, A. W. Parker, D. Phillips, W. T. Toner and M. Towrie, "Excited states of 4-aminobenzonitrile (ABN) and 4-dimethylaminobenzonitrile (DMABN): Time-resolved resonance Raman, transient absorption, fluorescence, and ab initio calculations." *Journal Of Physical Chemistry A*, 2002, **106**, 3294-3305.

20. W. M. Kwok, M. W. George, D. C. Grills, C. S. Ma, P. Matousek, A. W. Parker, D. Phillips, W. T. Toner and M. Towrie, "Direct observation of a hydrogen-bonded charge-transfer state of 4-dimethylaminobenzonitrile in methanol by time-resolved IR spectroscopy." *Angew. Chem. Int. Ed.*, 2003, **42**, 1826-1830.
21. A. Beeby, *Unpublished data*, Durham University.

## CHAPTER 6

### Properties of 9,10-bis(*p*-R-phenylethynyl)anthracene chromophores

#### 6.1 Introduction

As a family, 9,10-bis(phenylethynyl)anthracenes are highly efficient fluorescent compounds[1] and are widely used in chemiluminescent formulations.[2, 3] The parent compound 9,10-bis(phenylethynyl)anthracene (**21**) has an intense green fluorescence, shows good solubility in a variety of solvents and is chemically and thermally stable.[1] These properties have resulted in **21** being employed as molecular probes[4] in the study of translational and rotational moments in a range of media such as organic glasses, polymers and supercritical fluids.[5-9] Their rigid-rod molecular structure and extended  $\pi$ -electron conjugation has led to interest in them as potential spacer units in molecular assemblies and as components in electronic and photonic devices.[10-12]

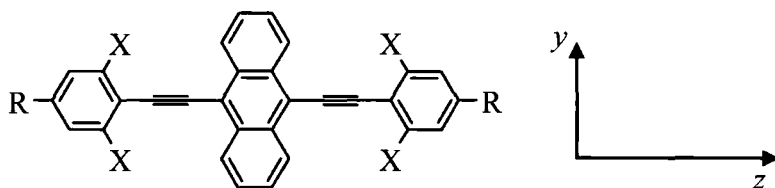
Levitus *et al.*[1] have carried out one of the most thorough studies of **21** to date. They used polarised spectroscopy and semi-empirical calculations to gain a deeper understanding of the photophysics and electronic spectroscopy of **21**. Among other things, the phenyl groups were proved to rotate freely in solution at room temperature and that the measured absorption spectrum in fluid media is the sum of the spectra of each conformer present in the ground state. Upon excitation the molecule rapidly equilibrates to the planar conformation before fluorescence occurs, and the lowest energy transition is polarised along the long axis of the molecule.

Previously, Nakatsuji *et al.*[13] reported on the photophysical properties of **21** and five of its derivatives having a pair of donor or acceptor groups in the *para*-position (see Figure 6.1). They observed that the electronic donor and acceptor groups both red shifted the absorption; there is a linear relationship between Hammett's  $\sigma_p$  and absorption wavenumber; and the quantum yields of *para*-substituted **21** are always less than un-substituted **21**. Nguyen *et al.*[14] have reported—but not discussed—the characteristic absorption and emission bands (in THF) and the quantum yields (in CHCl<sub>3</sub> and relative to rhodamine B) of all the compounds in this present study except 9,10-bis(2-(4-ethynylphenyl)ethynyl)anthracene (**19** (C≡CH)) and 9,10-bis(2-(2,4,6-triisopropylphenyl)ethynyl)anthracene (**22** (*i*Pr)).

Herein, we study a series of *para*-substituted **21**, with interesting photophysical properties, to determine the effect of different substituents of a variety of electronic donating and accepting strengths. The lifetimes of these derivatives are reported for the first time. The quantum yields are compared, where possible, to previously reported values.

## Results and discussion

The structures of the molecules studied are shown in Figure 6.1 and a list of their chemical names is given in Table 6.1.

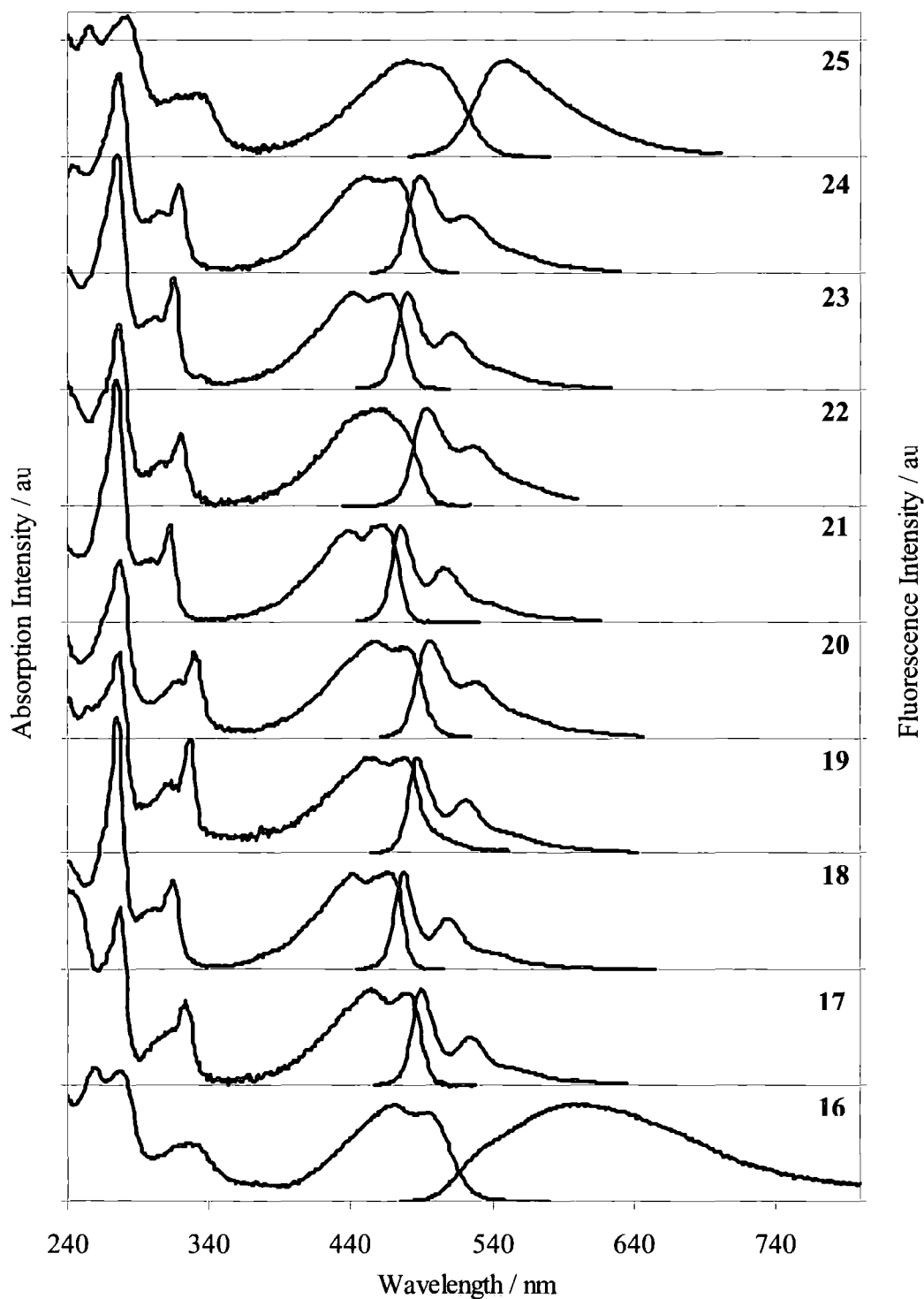


**Figure 6.1** General structure of substituted 9,10-bis(phenylethynyl)anthracene. Substituents were made in the X (*ortho*) and R (*para*) positions and are collected in Table 6.1.

**Table 6.1** Compounds investigated.

Compound	Code	R	X
9,10-Bis(2-(4-nitrophenyl)ethynyl)anthracene	<b>16</b>	NO <sub>2</sub>	H
9,10-Bis(2-(4-cyanophenyl)ethynyl)anthracene	<b>17</b>	CN	H
9,10-Bis(2-(4-(trifluoromethyl)phenyl)ethynyl)anthracene	<b>18</b>	CF <sub>3</sub>	H
9,10-Bis(2-(4-ethynylphenyl)ethynyl)anthracene	<b>19</b>	C≡CH	H
9,10-Bis(2-(4-(methylthio)phenyl)ethynyl)anthracene	<b>20</b>	SMe	H
9,10-Bis(phenylethynyl)anthracene	<b>21</b>	H	H
9,10-Bis(2-(2,4,6-triisopropylphenyl)ethynyl)anthracene	<b>22</b>	<i>i</i> Pr	<i>i</i> Pr
9,10-Bis(2-4'-tolylethynyl)anthracene	<b>23</b>	Me	H
9,10-Bis(2-(4-methoxyphenyl)ethynyl)anthracene	<b>24</b>	OMe	H
9,10-Bis(2-(4-dimethylaminophenyl)ethynyl)anthracene	<b>25</b>	NMe <sub>2</sub>	H





**Figure 6.2** Normalised absorbance (left) and emission (right) spectra of the compounds studied in chloroform. **16** (NO<sub>2</sub>), **17** (CN), **18** (CF<sub>3</sub>), **19** (C≡CH), **20** (SMe), **21** (H), **22** (*i*Pr), **23** (Me), **24** (OMe) and **25** (NMe<sub>2</sub>).

## 6.2 Absorption and fluorescence

Figure 6.2 depicts the normalised absorption and emission spectra of the ten compounds studied in chloroform. The characteristics of the lowest energy absorption bands and fluorescence spectra, lifetimes and quantum yields of all ten

compounds, in chloroform, are collected in Table 6.2. Here, the compounds are listed in order of increasing electron donor strength based on the Hammett constants for substituents in the *para*-position ( $\sigma_p$ ).[15] With the exception of 9,10-bis(2-(4-nitrophenyl)ethynyl)anthracene (**16** (NO<sub>2</sub>)), all the compounds show an intense green fluorescence; **16** (NO<sub>2</sub>) has a weak orange emission. The fluorescence quantum yield of most aromatic compounds attached to nitro groups is significantly reduced as this group quenches the excited states.

Although the planar conformation of **21** is the most stable, the barrier to free rotation of the phenyl rings is only 1.42 kJ mol<sup>-1</sup>. [1] Hence a continuous distribution of rotamers exist in the ground state and they all have slightly different transition energies that vary according to the dihedral angle formed by the anthracene plane and the plane containing the phenyl groups.[1] When these various conformers are excited their different transition energies all contribute to the final absorption spectra of the compound. This explains the lack of vibrational resolution in the absorption spectra of the series (see Figure 6.2). The fluorescence profiles of these compounds are better resolved because emission occurs primarily from the lowest excited singlet state after the molecules equilibrate to the planar conformation,  $\tau < 50$  ps.[1, 16]

All nine compounds display red shifted spectra in relation to **21** and have two high energy absorption bands around 312 and 270 nm (Figure 6.2). These have been revealed to be purely polarised along the *z*-axis and *y*-axis respectively (Figure 6.1).[1] The intense 270 nm transition is analogous to the B<sub>b</sub> transition of anthracene and the 312 nm transition is calculated to be unique to these types of compounds.[1] Calculations have predicted that the 270 nm transition would be more intense because of the presence of the multiple conformations in solution.[1] The position and intensities of most of these high energy peaks, in this study, are not significantly affected by the donor and acceptor substituents. This could be due to a lack of interaction between the substituent groups and the anthracene moiety because of differences in polarisation of their dipole moments. Only in the absorptions of compounds **16** (NO<sub>2</sub>) and 9,10-bis(2-(4-dimethylaminophenyl)ethynyl)anthracene (**25** (NMe<sub>2</sub>)), which have the strongest acceptor and donor substituents, are some spectral changes and loss in intensity observed at high energy.

The strength of the electron donor series of 9,10-bis(2-4'-tolylethynyl)anthracene (**23** (Me)), 9,10-bis(2-(4-methoxyphenyl)ethynyl)anthracene (**24** (OMe)) and **25**

(NMe<sub>2</sub>) is reflected in their Stokes shifts which increased from 675 to 2717 cm<sup>-1</sup> (15 to 72 nm) (Table 6.2). The same can't be said for the acceptor series **20** (SMe), **19** (C≡CH), 9,10-bis(2-(4-(trifluoromethyl)phenyl)ethynyl)anthracene (**18** (CF<sub>3</sub>)), and **17** (CN) which have shifts of 803, 386, 494 and 468 cm<sup>-1</sup> respectively. The Stokes shift is greatest for **16** (3741 cm<sup>-1</sup>). A similar trend has been observed for a comparable series of compounds.[13, 14] The increasing Stokes shift is due to the increasing excited state dipole moments of the compounds which lead to greater molecular reorganisation, and solvent relaxation prior to emission.[17] The absorption and emission spectra of all the compounds in this study, with the exception of **19** (C≡CH) and **22** (*i*Pr), have been reported in more polar THF.[14] The Stokes shifts in THF for **17** (CN), **18** (CF<sub>3</sub>), 9,10-bis(2-(4-(methylthio)phenyl)ethynyl)anthracene (**20** (SMe)), **23** (Me), **24** (OMe) and **21** were up to 6 nm (249 cm<sup>-1</sup>) more than the shifts in CHCl<sub>3</sub>. This is expected of polar fluorophores in solvents of increasing polarity. However the Stokes shifts of **16** (NO<sub>2</sub>) and **25** (NMe<sub>2</sub>) were found to be less than those in CHCl<sub>3</sub>, being only 30 nm (1177 cm<sup>-1</sup>) and 66 nm (2422 cm<sup>-1</sup>) respectively.

Compounds **16** (NO<sub>2</sub>) and **25** (NMe<sub>2</sub>) have broad unresolved spectra and the fluorescence spectra shows significant bathochromic solvatochromism. This is accounted for by the fact that the NO<sub>2</sub> and the NMe<sub>2</sub> groups are very strong electron acceptors and donors respectively. In the presence of the NMe<sub>2</sub> group anthracene acts as a strong acceptor [18] but with NO<sub>2</sub> it behaves as a donor. In a polar solvent like chloroform, these two molecules exhibit strong intramolecular charge transfer (ICT) character resulting in a low energy charge separated excited state.

Compound **22** (*i*Pr), with its weak donor groups in phenyl *ortho* and *para*-positions, is the most sterically hindered of the series. Its unresolved absorption spectrum is a result of multiple conformations in the ground state. However, upon excitation it seems this molecule is still able to planarize prior to emission because its fluorescence spectra is well defined and similar to unsubstituted **21**. Hence the substituted groups are not bulky enough to really constrain the molecule in an orthogonal conformation.

**Table 6.2** The lifetimes, quantum yields, radiative decay rates ( $\Gamma$ ), nonradiative decay rates ( $k_{nr}$ ), absorption and emission bands, and Stokes shifts of compounds **16–25** in  $\text{CHCl}_3$ .

Cpd.	X, R	$\sigma_p$	$\tau_f / \text{ns}$ $\pm 0.05^a$	$\Phi_f \pm 0.05^c$	$\Phi_f$ in Ref.	$\Gamma / 10^8 \text{ s}^{-1}$	$k_{nr} / 10^8 \text{ s}^{-1}$	Major peaks / nm		Stokes Shifts / $\text{cm}^{-1}$
								Absorption	Emission	
<b>16</b>	H, $\text{NO}_2$	0.78	1.06 <sup>b</sup>	0.20 <sup>d</sup>	0.15 <sup>f</sup>	1.89	7.55	470, 492	603	3741
<b>17</b>	H, CN	0.66	2.56	0.87	0.65 <sup>f</sup> , 0.83 <sup>g</sup>	3.38	0.53	455, 479	490, 524	468
<b>18</b>	H, $\text{CF}_3$	0.54	3.05	0.90	0.64 <sup>f</sup>	2.95	0.33	442, 466	477, 508	494
<b>19</b>	H, $\text{C}\equiv\text{CH}$	0.23	2.36	0.76	0.31 <sup>h</sup>	3.24	1.01	454, 478	487, 520	386
<b>20</b>	H, SMe	0	2.53	0.91	0.60 <sup>f</sup>	3.60	0.35	456, 477	496, 528	803
<b>21</b>	H, H	0	3.20	0.97 <sup>c</sup>	0.71 <sup>f</sup> , 0.58 <sup>g</sup> , 0.96 <sup>i</sup>	3.03	0.09	440, 462	475, 506	592
<b>22</b>	<i>i</i> Pr, <i>i</i> Pr	-0.15	2.88	0.89	-	3.07	0.39	459	494, 525	1543
<b>23</b>	H, Me	-0.17	2.92	0.91	0.82 <sup>f</sup> , 0.57 <sup>g</sup>	3.12	0.30	442, 464	479, 512	675
<b>24</b>	H, OMe	-0.27	2.74	0.87	0.64 <sup>f</sup> , 0.55 <sup>g</sup>	3.19	0.46	449, 471	488, 521	740
<b>25</b>	H, $\text{NMe}_2$	-0.83	2.70	0.81	0.49 <sup>f</sup>	3.00	0.70	480	552	2717

Key: *i*Pr – isopropyl group.  $\sigma_p$  – Hammett constants for substituents in the *para*-position. [15] <sup>a</sup>  $\tau_f$  measured by the phase modulation technique. <sup>b</sup>  $\tau_f$  measured using TCSPC. <sup>c</sup> Relative to fluorescein in 0.1 M NaOH ( $\Phi_f = 0.90$ )  $\lambda_{ex} = 450, 470^d$  and 445 nm. <sup>f</sup> Ref. [14], in  $\text{CHCl}_3$ ,  $\lambda_{ex} = 457$  nm, relative to rhodamine B in water ( $\Phi_f = 0.31$ ). <sup>g</sup> Ref. [13], in  $\text{CHCl}_3$ ,  $\lambda_{ex} = 365$  nm relative to quinine sulphate in 0.1M  $\text{H}_2\text{SO}_4$  ( $\Phi_f = 0.55$ ). <sup>h</sup> Ref [12] in  $\text{CH}_2\text{Cl}_2$ ,  $\lambda_{ex} = 364$  nm relative to 1,1,4,4-tetraphenylbutadiene in cyclohexane ( $\Phi_f$  between 0.6 and 0.84–0.85). <sup>i</sup> Ref[19] in cyclohexane.

It is also possible that the alkyne moiety in the molecule may bend slightly to accommodate the isopropyl groups, and relieve torsional strain, in the co-planar geometry.[20] Even the more sterically hindered 9,10-bis(2,4,6-tri-*tert*-butylphenyl-ethynyl)anthracene has been found to partially planarize prior to emission at ambient temperature and is only orthogonal in the excited state at 77 K.[20]

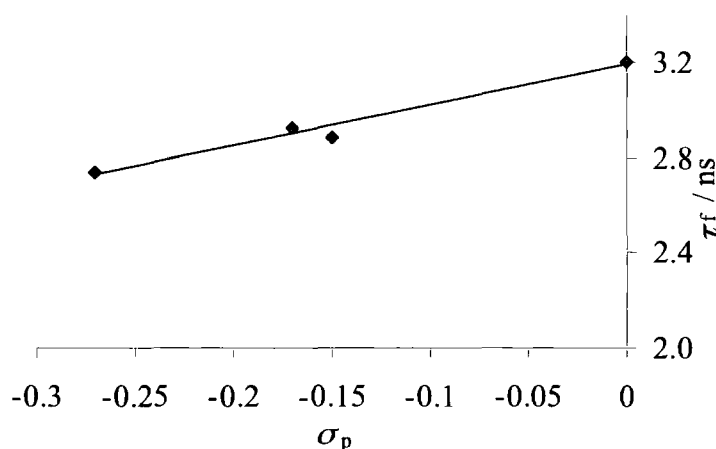
### 6.3 Fluorescence quantum yields and lifetime measurements

Compound **21** has the largest fluorescence quantum yield ( $\Phi_f = 0.97$ , see Table 6.2) and, as expected, the smallest non-radiative decay rate ( $k_{nr} = 9.4 \times 10^6 \text{ s}^{-1}$ ). There is a near linear decrease in the quantum yields of the donor series **23–25** from 0.91 to 0.81 in relation to  $\sigma_p$ . On the other hand, the quantum yields of the acceptor series **16–19** ranges from 0.9 to 0.2 and has a more polynomial relation to  $\sigma_p$ . The fluorescence emission of **16** ( $\Phi_f = 0.2$ ) is the weakest of the series, due to its large nonradiative decay rate ( $k_{nr} = 7.6 \times 10^8 \text{ s}^{-1}$ ) resulting from the presence of the  $\text{NO}_2$  group.[17] Compound **19** ( $\text{C}\equiv\text{CH}$ ) too, has a fairly large nonradiative decay rate of  $1.0 \times 10^8 \text{ s}^{-1}$  and its quantum yield is 0.76 in  $\text{CHCl}_3$ —the second smallest in this studied series. This appears to be the result of the extended  $\pi$ -electron delocalisation over the  $\text{C}\equiv\text{C}$  bond of the  $\text{C}\equiv\text{CH}$  group leading to more non-radiative decay mechanisms. A similar spectral profile and a  $\Phi_f$  of 0.31 in  $\text{CH}_2\text{Cl}_2$  has been reported for **19**. [12] Here, the more polar  $\text{CH}_2\text{Cl}_2$  can be assumed to be increasing the charge separation in the molecule resulting in a reduction in the fluorescence quantum yield.

Compound **20** (SMe) has substituents with a  $\sigma_p$  value of zero and a fluorescence quantum yield comparable to that of **21** within experimental error. The SMe substituent does, however, result in this compound having larger radiative rate ( $I = 3.6 \times 10^8 \text{ s}^{-1}$ ) and  $k_{nr}$  ( $0.35 \times 10^8 \text{ s}^{-1}$ ) values than **21**. The weakly electron donating isopropyl and methyl substituents in **22** (*i*Pr) and **23** (Me) marginally reduce the fluorescence quantum yield of **21** to *ca.* 0.90. This is reflected in the significantly increased  $k_{nr}$  values (about  $0.35 \times 10^8 \text{ s}^{-1}$ ) with respect to that of **21**. Compounds **22** and **23** have similar substituents but different geometries. Despite one being more sterically hindered than the other their fluorescence quantum yields and lifetimes are quite similar. The additional *ortho* substituents in **22** does, however, make its absorption spectra broader and its emission more red shifted than that of **23**.

The fluorescence quantum yields of all the compounds in this study, except **22**, have been reported in the literature, giving lower values than those measured here. The value reported for **16**, and some for **17** and **21** were within the experimental error range. However, all other values were significantly less. These discrepancies arise from the nature of the solvents and standards used. Comparing data from different instruments can also lead to inconsistencies between works by different authors.

The lifetimes ( $\tau_f$ ) of the substituted compounds are all less than that of **21** in  $\text{CHCl}_3$  ( $\tau_f = 3.20$  ns, see Table 6.2). For compounds **17** to **20**, which have positive  $\sigma_p$  values, the lifetimes range from 2.36 to 3.05 ns. The presence of the strong  $\text{NO}_2$  acceptor group results in **16** having a lifetime of only 1.06 ns. Meanwhile for compounds **22** to **25**, which have negative  $\sigma_p$  values, lifetimes range from 2.70 to 2.92 ns. Compounds **21** to **24** show a linear correlation between the  $\sigma_p$  values and their  $\tau_f$  values (Figure 6.3). The  $\text{C}\equiv\text{CH}$  group in **19** has the second largest effect on the lifetime of **21**, reducing it to 2.36 ns.



**Figure 6.3** Hammett constant values ( $\sigma_p$ ) vs. lifetime ( $\tau_f$ ) graph of **21** to **24** from right to left.

## Conclusions

The steady state photophysical properties of **21** and a series of nine of its donor and acceptor substituted derivatives were measured in  $\text{CHCl}_3$  and the results discussed.

The absorption and fluorescence spectra of all the compounds are in agreement with previously reported work.[1, 13, 14] The low energy absorption profiles of all the compounds are broad and lack fine structure due to contributions from various structural conformers in the ground state. The low energy absorption transition

(including the band at around 312 nm) is polarised along the *z*-axis (the molecular long axis) while the high energy one (at 270 nm) is polarised along the *y*-axis (molecular short axis). With the exception of **16** and **25**, all the fluorescence spectra have more vibrational structure than the absorbance spectra, because the Franck–Condon excited state rapidly relaxes to the planarized geometry from which fluorescence is observed. Calculations by Beeby *et al.*[20] have revealed that the first excited state transition for both planar and orthogonal geometries of **21** arise from a HOMO←LUMO transition based upon the anthracene chromophore. Compound **16** (having the strongest acceptor group) and **25** (having the strongest donor group) exhibit strong ICT character which is characterised by a broad emission spectra and large Stokes shift. The other compounds show no ICT character.

The lifetimes of compounds **16** to **25** and the fluorescence quantum yield of **22** (*i*Pr) are reported for the first time. The quantum yields, while being consistent with each other, were found to be higher than those previously reported, and are deemed to be more reliable since the reported quantum yield values also differed from each other. In all cases the presence of donor or acceptor groups lowers the lifetime ( $\tau_f = 3.20$  ns) and fluorescence quantum yield ( $\Phi_f = 0.97$ ) of **21**, and significantly increases its non-radiative rate constant ( $k_{nr} = 9.4 \times 10^6 \text{ s}^{-1}$ ). Compound **16** has the shortest lifetime ( $\tau_f = 1.06$  ns) lowest quantum yield ( $\Phi_f = 0.2$ ) and the largest non-radiative decay rate ( $k_{nr} = 7.6 \times 10^8 \text{ s}^{-1}$ ). This could be the result of the NO<sub>2</sub> inducing a non-radiative decay mechanism that significantly reduces the fluorescence emission or CT.

## REFERENCES

1. M. Levitus and M. A. Garcia-Garibay, "Polarized electronic spectroscopy and photophysical properties of 9,10-bis(phenylethynyl)anthracene." *Journal Of Physical Chemistry A*, 2000, **104**, 8632-8637.
2. J. Lukacs, R. A. Lampert, J. Metcalfe and D. Phillips, "Photophysics of substituted anthracenes used as chemiluminescence activators." *Journal Of Photochemistry And Photobiology A-Chemistry*, 1992, **63**, 59-65.
3. D. R. Maulding and B. G. Roberts, "Chemiluminescence of tetrachloroethylene carbonate and related compounds." *Journal Of Organic Chemistry*, 1972, **37**, 1458-1459.
4. A. Angelova and R. Ionov, "Monolayer and spectroscopic studies of an amphiphilic (phenylethynyl)anthracene probe in pure and mixed films with charged and neutral lipids." *Langmuir*, 1999, **15**, 7199-7207.
5. M. T. Cicerone, F. R. Blackburn and M. D. Ediger, "How do molecules move near T-G - molecular rotation of 6 probes in *o*-terphenyl across 14 decades in time." *Journal Of Chemical Physics*, 1995, **102**, 471-479.
6. M. P. Heitz and M. Maroncelli, "Rotation of aromatic solutes in supercritical CO<sub>2</sub>: Are rotation times anomalously slow in the near critical regime?" *Journal Of Physical Chemistry A*, 1997, **101**, 5852-5868.
7. F. R. Blackburn, C. Y. Wang and M. D. Ediger, "Translational and rotational motion of probes in supercooled 1,3,5-tris(naphthyl)benzene." *Journal Of Physical Chemistry*, 1996, **100**, 18249-18257.
8. M. T. Cicerone and M. D. Ediger, "Enhanced translation of probe molecules in supercooled *o*-terphenyl: Signature of spatially heterogeneous dynamics?" *Journal Of Chemical Physics*, 1996, **104**, 7210-7218.
9. D. J. Gisser, B. S. Johnson, M. D. Ediger and E. D. Vonmeerwall, "Comparison of various measurements of microscopic friction in polymer-solutions." *Macromolecules*, 1993, **26**, 512-519.
10. T. M. Swager, C. J. Gil and M. S. Wrighton, "Fluorescence studies of poly(*p*-phenyleneethynylene)s - The effect of anthracene substitution." *Journal Of Physical Chemistry*, 1995, **99**, 4886-4893.
11. R. Gimenez, M. Pinol and J. L. Serrano, "Luminescent liquid crystals derived from 9,10-bis(phenylethynyl)anthracene." *Chemistry Of Materials*, 2004, **16**, 1377-1383.
12. M. S. Khan, A. K. Kakkar, N. J. Long, J. Lewis, P. Raithby, P. Nguyen, T. B. Marder, F. Wittmann and R. H. Friend, "Synthesis and optical spectroscopy of linear long-chain di-terminal alkynes and their Pt-sigma-acetylide polymeric complexes." *Journal Of Materials Chemistry*, 1994, **4**, 1227-1232.



13. S. Nakatsuji, K. Matsuda, Y. Uesugi, K. Nakashima, S. Akiyama and W. Fabian, "Synthesis and absorption/emission spectroscopic properties of bis(phenylethynyl)benzenes and 9,10-bis(phenylethynyl)anthracenes." *Journal Of The Chemical Society-Perkin Transactions 1*, 1992, 755-758.
14. P. Nguyen, S. Todd, D. Vandenbergelaar, N. J. Taylor, T. B. Marder, F. Wittmann and R. H. Friend, "Facile route to highly fluorescent 9,10-bis(*p*-R-phenylethynyl)anthracene chromophores via Palladium-Copper catalyzed cross-coupling." *Synlett*, 1994, 299-301.
15. C. Hansch, A. Leo and R. W. Taft, "A survey of Hammett substituent constants and resonance and field parameters." *Chemical Reviews*, 1991, **91**, 165-195.
16. A. Beeby, K. S. Findlay, P. J. Low, T. B. Marder and P. Matousek, "Studies of the S<sub>1</sub> state in a prototypical molecular wire using picosecond time-resolved spectroscopies." *Chemical Communications*, 2003, 2406-2407.
17. J. R. Lakowicz, "Principles of fluorescence spectroscopy", 2nd ed, Kluwer Academic / Plenum Publishers, New York, 1999.
18. S. Amthor, C. Lambert, S. Dummler, I. Fischer and J. Schelter, "Excited mixed-valence states of symmetrical donor-acceptor-donor  $\pi$  systems." *Journal Of Physical Chemistry A*, 2006, **110**, 5204-5214.
19. D. R. Maulding and B. G. Roberts, "Electronic absorption and fluorescence of phenylethynyl-substituted acenes." *Journal Of Organic Chemistry*, 1969, **34**, 1734-1736.
20. A. Beeby, S. R. Rutter, K. S. Findlay and L. Porrès, *Unpublished data*, Durham University.

## CHAPTER 7

### Properties of 2,5-bis-(phenylethynyl)thiophene (26) and related compounds

#### 7.1 Introduction

The photophysical properties and bond order of the first excited state of molecules based on non-heteroaromatic 1,4-bis(phenylethynyl)benzene (BPEB) have been previously discussed (see Chapter 4). The triplet states, however, are not well characterised. Population of the excited triplet state (under normal conditions) is very low for BPEB ( $\Phi_T = 0.85$ ) and even for the heavy-atom substituted derivative 1,4-dibromo-2,5-bis(phenylethynyl)benzene the triplet state is not readily accessed. Thus, direct measurements of the bond order in these simple rigid molecules in the triplet excited state by optical excitation are quite difficult. It is important to determine the electronic structure and bond order of the excited states of this class of molecules as they are relevant to their application as molecular wires or electroluminescent devices. The properties of the triplet state, in particular, are significant since they may be formed by electron transfer/transport processes such as encountered in an OLED[1-3] or during the conduction of a 'molecular wire'. [4, 5]

There are few experimental studies of the triplet state of aryleneethynylene based compounds due to their low yield of intersystem crossing. To get around this problem authors have focused on systems incorporating heavy atoms such as platinum, which enhance the spin-orbit coupling and hence triplet state formation.[6-9] With this modification it is possible to access the triplet state optical excitation, whence it can be studied by using conventional spectroscopic techniques. These studies have been used to develop an understanding of the relationship between structure, the singlet-triplet energy gap and the localisation and movement of excitons on polymer chains. It was noted, however, that the  $\pi$  conjugation through the metal sites significantly modifies the optical properties of the conjugation chains.[7] Subsequently, theoretical methods have been used to investigate the singlet-triplet exchange energy in oligo(aryleneethynylenes)[10] and electronic delocalisation in phenylene-acetylene molecular wires.[4] Direct observations of the triplet state in non-heavy atom containing systems were first made by Schanze *et al.* who measured the triplet state behaviour of a derivative of 4,4'-bis(phenylethynyl)biphenyl and a related polymer.[11] More recently, Neckers *et al.*

have used time-resolved infrared absorption spectroscopy to study the distribution of the electron density and bond order in the triplet excited state of 1,4-bis(2-[4-phenyloxycarbonylphenyl]ethynyl)benzene.[5] Apart from these reports, there is no experimental information describing the triplet state properties of simple aryleneethynylene molecules such as BPEB. An alternative solution to the problem of probing the excited triplet state is to consider other short aryleneethynylene systems which show a  $\pi$  extended conjugation and similar structural properties to BPEB. This could be achieved by, for example, introducing a heteroatom into the BPEB backbone.

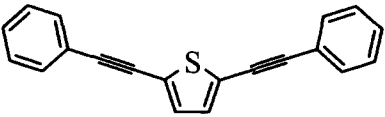
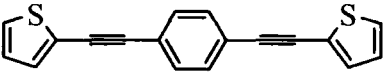
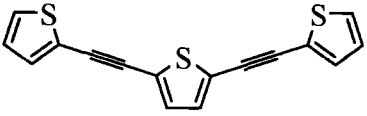
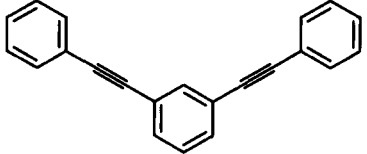
Consequently, this chapter is a report on measurements made of the triplet states of 2,5-bis(phenylethynyl)thiophene (**26**) and similar thiophene-containing molecules. Compound **26** was chosen for triplet state measurements because of its low fluorescence quantum yield, *vide infra*. This hinted at the possibility that the presence of the heavier sulphur atom made intersystem crossing and triplet state formation the main deactivation pathway.[12-14] Herein, the steady state photophysical properties of **26**, 1,4-bis(2-thienylethynyl)benzene (**27**) and 2,5-bis(2-thienylethynyl)thiophene (**28**) are presented along with a nanosecond time-resolved resonance Raman (TR<sup>3</sup>) spectroscopy study of their S<sub>1</sub> and T<sub>1</sub> states. Investigating the excited states of these model compounds will help to provide insight into the behaviour of the excited states of the polymers.

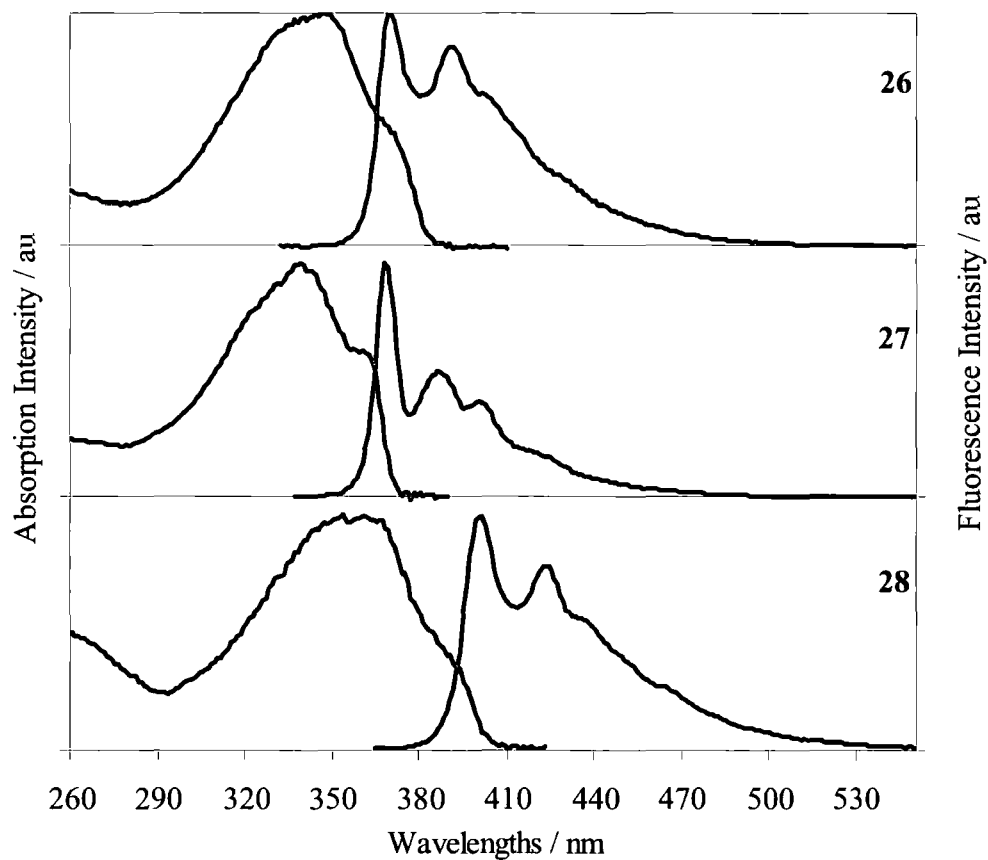
## Results and discussion

### 7.2 Steady state photophysical measurements

The structure of the molecules studied along with their chemical name and numbering scheme used throughout the chapter are listed in Table 7.1. The absorption and emission spectra of **26** to **28**, in cyclohexane at ambient temperature, are illustrated in Figure 7.1. Their characteristic absorption and emission bands along with the extinction coefficients, fluorescence lifetimes, fluorescence quantum yields and singlet oxygen generation quantum yields, in cyclohexane, are collected in Table 7.2.

**Table 7.1** Compounds investigated and reference molecule bent-BPEB (b-BPEB).[15]

Compound	Structure	Code
2,5-Bis(phenylethynyl)thiophene		26
1,4-Bis(2-thienylethynyl)benzene		27
2,5-Bis(2-thienylethynyl)thiophene		28
1,3-Bis(phenylethynyl)benzene		b-BPEB



**Figure 7.1** The normalised absorption (left) and emission (right) spectra of compounds 26–28 in cyclohexane at room temperature.

**Table 7.2** The major absorption and emission peaks, extinction coefficients ( $\epsilon$ ), fluorescence lifetimes ( $\tau_f$ ), fluorescence quantum yields ( $\Phi_f$ ), radiative rates ( $\Gamma$ ), non-radiative rates ( $k_{nr}$ ) and the singlet oxygen generation quantum yield ( $^1\Delta_g \text{O}_2$  ( $\Phi_\Delta$ )) of compounds **26–28** and BPEB in cyclohexane and bent-BPEB (b-BPEB) in chloroform.[15]

Cpd.	Major Peaks / nm		Stokes shifts / $\text{cm}^{-1}$	$\epsilon / \text{mol}^{-1} \text{dm}^3 \text{cm}^{-1} \pm 1,000$ (absorption / nm)	$\tau_f / \text{ns} \pm 0.05$ ( $\chi^2$ )	$\Phi_f \pm 0.05^a$	$\Gamma / 10^8 \text{s}^{-1}$	$k_{nr} / 10^8 \text{s}^{-1}$	$^1\Delta_g \text{O}_2$ ( $\Phi_\Delta$ ) / $\pm 0.05^c$
	Absorption	Emission							
<b>26</b>	347, 369 (sh)	369, 390	0	41,600 (348)	0.29 (0.24)	0.16	5.52	28.97	0.79
<b>27</b>	339, 361 (sh)	368, 386, 400	527	42,100 (342)	0.19 (0.16)	0.21	11.05	41.58	0.70
<b>28</b>	361, 390 (sh)	401, 424	703	36,000 (355)	0.12 (0.17)	0.06	5.00	78.33	0.81
<b>BPEB</b>	320, 340 (sh)	344, 359, 372	342	58,400 (320)	0.53 (0.80)	$0.85^b \pm 0.05$	16.04	2.83	0.23[16]
<b>b-BPEB</b>	$302^d$	$330^d$	2810	$50,119^d$	$2.00^d$	$0.14^d$	$0.70^d$	$4.31^d$	–

Key: sh-shoulder. <sup>a</sup> Relative to the standards quinine sulphate in 0.1 M H<sub>2</sub>SO<sub>4</sub> ( $\Phi_f = 0.55$ ) and POPOP in cyclohexane ( $\Phi_f = 0.97$ ). <sup>b</sup> Relative to the standards quinine sulphate in 0.1 M H<sub>2</sub>SO<sub>4</sub> and  $\beta$ -carboline in 0.5 M H<sub>2</sub>SO<sub>4</sub> ( $\Phi_f = 0.6$ ) <sup>c</sup> Relative to perinaphthanone in cyclohexane at 1270 nm. <sup>d</sup> Ref. [15]. All measurements were taken in chloroform solution. The quantum yield was calculated relative to quinine sulphate in 0.1 M H<sub>2</sub>SO<sub>4</sub> ( $\Phi_f = 0.55$ ).

The absorption and fluorescence spectra of the three compounds all exhibit a strong spectral overlap and a small Stokes shift. Their spectra are also red shifted to that of BPEB (see Table 7.2) with **28** having the largest bathochromic shift in its absorbance (41 nm) and fluorescence (57 nm) spectra. This indicates that there is possibly a greater delocalisation of the  $\pi$ -electrons across molecules **26–28**. All the absorption spectra are relatively broad and structureless while the fluorescence profiles show quite well defined peaks. This is interpreted as evidence of a broad thermal distribution of rotational conformers in the solution ground state, similar to that of BPEB, due to a shallow ground state potential and the free rotation about the C(sp-ethynyl)-C(sp<sup>2</sup>-aryl) bonds. Upon excitation, the planar or near-planar configuration is more favoured in the S<sub>1</sub> state and all the molecules adopted this uniformed structure prior to emission. As a result the emission spectra are much more structured.

Compound **27**, with its phenyl centre, has a linear structure similar to BPEB, while **26** and **28**, with thiophene centres, are bent. It is interesting to note that the spectra of bent compounds **26** and **28** show less structure than the linear **27** (Figure 7.1). The absorption profiles of **26** and **28** have less of a shoulder at the red edge compared to **27**, and the second emission peak in **26** and **28** is more intense than the corresponding peak in **27**. Even though compound **27** has two thiophene rings its spectra has more BPEB character than **26**, which has two phenyl rings. This is probably due to the chromophore being located on the central phenyl ring which has a better defined vibrational spectrum.

On comparing b-BPEB to **26** and **28** (Table 7.2), we observe the impact the inclusion of the heteroatom has on the photophysical properties of these bent molecules. Generally the  $\pi$ -electron delocalisation is improved when phenyl is substituted for thiophene units. However, the ability of **26** and **28** to absorb photons is decreased along with their lifetimes, *vide infra*. The fluorescence quantum yields increase marginally with one thiophene substituent (**26**), but decreases by more than half when only thiophene groups are present (**28**). The presence of thiophene groups also increases the radiative and non-radiative decay rates of the compounds (see Table 7.2) compared to b-BPEB.

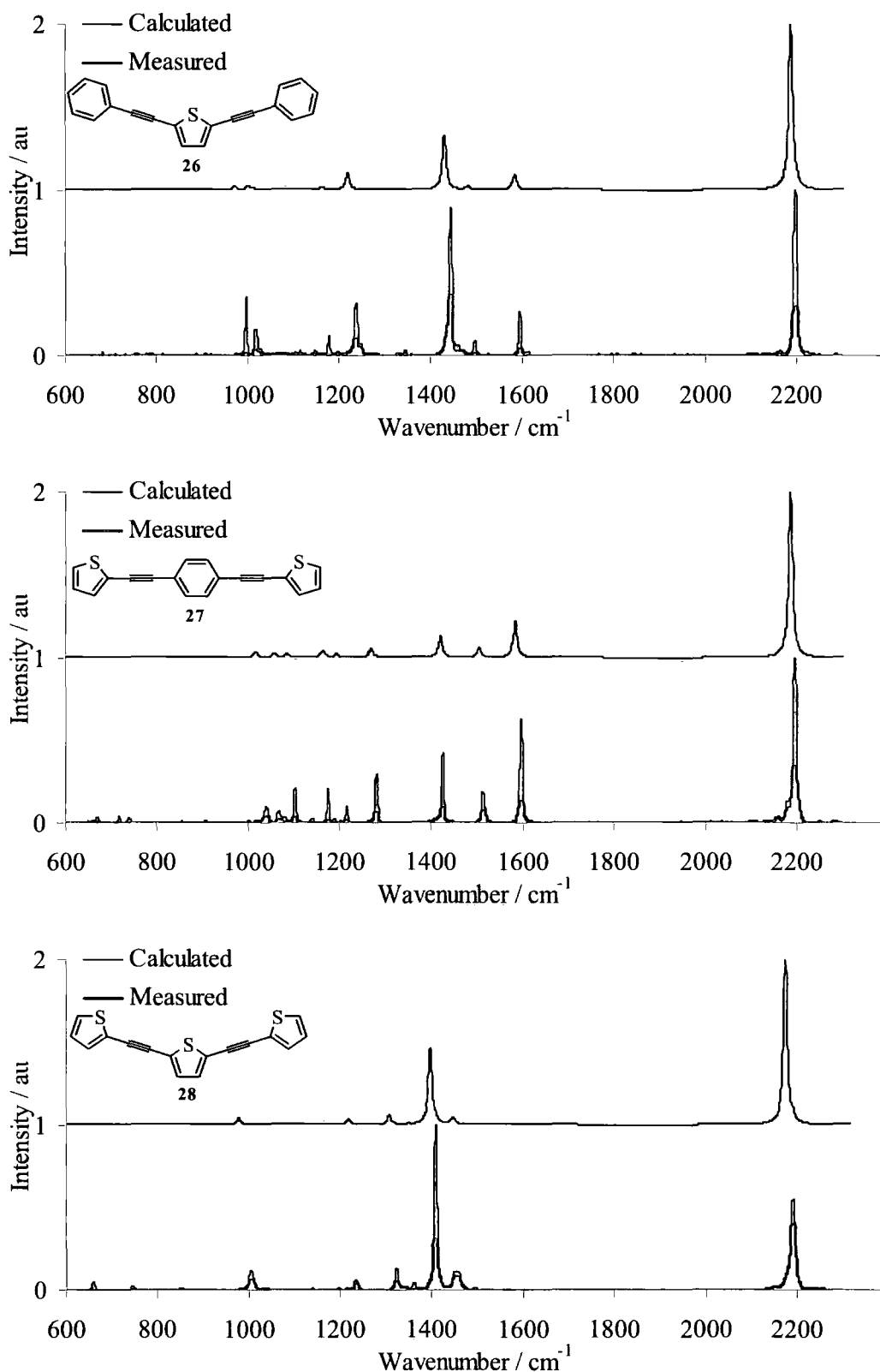
The extinction coefficients of **26–28** range from 42,100 to 36,000 mol<sup>-1</sup> dm<sup>3</sup> cm<sup>-1</sup>. This is relatively low compared to BPEB ( $\epsilon = 58,000$  mol<sup>-1</sup> dm<sup>3</sup> cm<sup>-1</sup>), which makes

these compounds less efficient absorbers. The fluorescence lifetimes of **26**, **27** and **28** are 0.29, 0.19 and 0.12 ns respectively. This is considerably shorter than BPEB ( $\tau_f = 0.53$  ns) and it decreases as the number of thiophene units increases, which confirms that the heavy atom is promoting intersystem crossing. Compounds **26–28** exhibit much weaker fluorescence than BPEB ( $\Phi_f = 0.85$ ) with quantum yields ranged from 0.21 to 0.06. It is also observed that **28** has the smallest extinction coefficient, the shortest fluorescence lifetime and the lowest fluorescence quantum yield (Table 7.2). This is due to its large non-radiative decay constant  $78.33 \times 10^8 \text{ s}^{-1}$ .

To determine if these low quantum yields were indicative of a high level of intersystem crossing to the triplet state, due to the presence of the heavier sulphur atom, the singlet oxygen generation quantum yields for **26–28** were determined. High yields of singlet oxygen formation in aerated solutions of all three compounds were observed ranging from 0.70 to 0.81 (Table 7.2). The singlet oxygen yield of BPEB has been measured to be about 0.23.[16] These results established evidence of a relatively high triplet quantum yield with a triplet lifetime sufficiently long enough to provide efficient energy transfer,  $> 1 \mu\text{s}$ . However, no phosphorescence could be detected, even in degassed low temperature glasses. Based on these results, further investigations into the bonding order in the triplet excited states, using time-resolved spectroscopy techniques, were undertaken.

### 7.3 Ground state Raman scattering

The measured and calculated Raman spectra of the ground state of **26–28** are shown in Figure 7.2 and the vibrational bands are listed in Table 7.3 to Table 7.5. The calculated spectra had their vibration frequencies multiplied by a scaling factor of 0.96[17], resulting in a very good correlation between the experimental and theoretical data from which we assigned the various vibrational modes. A distinct band assigned to the symmetric  $\nu(\text{C}\equiv\text{C})$  vibration is observed at 2198, 2197 and at  $2192 \text{ cm}^{-1}$  in **26**, **27** and **28** respectively. The benzene ring symmetric stretching mode is assigned to the  $1595 \text{ cm}^{-1}$  band in **26**.[18] The strong band at 1444, 1426 and  $1408 \text{ cm}^{-1}$  in **26**, **27** and **28** respectively are assigned to ring stretching modes for 2,5-disubstituted thiophenes.[19] The bands appear to be downshifted to lower energy as the number of thiophenes increases. The weak  $1460 \text{ cm}^{-1}$  peak is also assigned to a C=C ring stretching mode in **28**.[20]



**Figure 7.2** The calculated and measured ground state Raman spectra of **26** to **28**. Mode assignments of the ground state Raman vibrations were made for the three compounds in Table 7.3 to Table 7.5.



**Table 7.3** The calculated and measured ground state Raman bands of **26**, in cyclohexane (Figure 7.2), with vibrational mode assignments.

Calculated ground state / $\text{cm}^{-1}$	Measured ground state / $\text{cm}^{-1}$	Mode description <sup>a</sup>
2187 s <sup>b</sup>	2198 s	Symmetric C≡C stretch
1583 w	1595 m	Outer rings symmetric stretch
1429 m	1444 s	Inner ring symmetric stretch, along long-axis, outer ring C-H wagging
1219 w	1239 m	Inner ring symmetric stretch along short-axis
1162 vw	1179 w	Outer rings C-H scissoring
1000 vw	1017 w	Outer rings breathing, inner symmetric stretch & C-H scissoring
971 vw	997 m	Outer rings breathing

<sup>a</sup> Vibrational mode assignments are made on the basis of calculations done by Beeby[21] using the *Gaussian 03* package[22] with the B3LYP density functional and the 6-31G\* basis set. <sup>b</sup> Qualitative Raman: 's', 'm', 'w' and 'vw' refers to the peak intensities respectively as 'strong', 'medium', 'weak' and 'very weak'.

The band at  $997 \text{ cm}^{-1}$  in **26** is assigned to the outer phenyl ring breathing modes which were previously observed in BPEB. The bands observed in the  $750$  to  $600 \text{ cm}^{-1}$  region in **28** are assigned to in-plane ring deformations and thiophene ring breathing modes.

The excellent agreement between the observed and calculated spectra can be attributed to the limited interaction between the molecule and its solvent environment. The small Stokes shifts are further evidence of the little effect the solvent has on the photophysical properties of these molecules.

**Table 7.4** The calculated and measured ground state Raman bands of **27**, in cyclohexane (Figure 7.2), with vibrational mode assignments.

Calculated ground state / $\text{cm}^{-1}$	Measured ground state / $\text{cm}^{-1}$	Mode description <sup>a</sup>
2188 s <sup>b</sup>	2197 s	Symmetric C≡C stretch
1585 m	1598 s	Inner ring symmetric stretch, C-H scissoring
1505 w	1513 m	Inner and outer rings anti-symmetric stretch, C-H wagging
1421 m	1426 s	Outer rings symmetric stretch, inner ring breathing
1269 w	1280 m	Inner ring breathing, outer rings C-H wagging
1194 vw	1218 w	Inner ring breathing, outer rings C-H wagging
1164 vw	1175 w	Inner ring C-H scissoring
1084 vw	1103 w	Inner ring breathing, outer rings C-H scissoring
1057 w	1068 vw	Inner ring breathing, outer rings C-H scissoring
1018 w	1042 w	Inner ring breathing, outer rings C-H scissoring
Not seen	740 vw	
Not seen	718 vw	
Not seen	671 vw	

<sup>a</sup> Vibrational mode assignments are made on the basis of calculations done by Beeby[21] using the *Gaussian 03* package[22] with the B3LYP density functional and the 6-31G\* basis set. <sup>b</sup> Qualitative Raman: 's', 'm', 'w' and 'vw' refers to the peak intensities respectively as 'strong', 'medium', 'weak' and 'very weak'.

**Table 7.5** The calculated and measured ground state Raman bands of **28**, cyclohexane (Figure 7.2), with vibrational mode assignments.

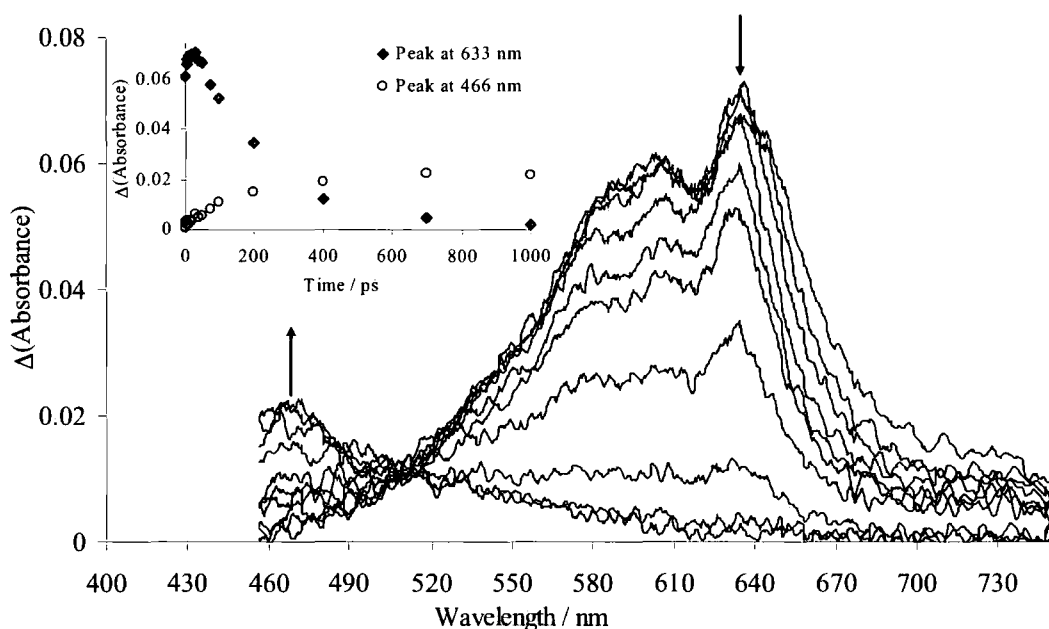
Calculated ground state / $\text{cm}^{-1}$	Measured ground state / $\text{cm}^{-1}$	Mode description <sup>a</sup>
2176 s	2192 s <sup>b</sup>	Symmetric C≡C stretch
1447 vw	1460 w	Outer rings anti-symmetric stretch, inner ring symmetric stretch
1397 s	1408 s	Outer and inner rings symmetric stretch & scissoring
1307 vw	1322 w	Outer and inner rings breathing
1219 vw	1236 w	Inner ring symmetric stretch & scissoring, outer rings C-H wagging
978 w	1005 w	Inner ring symmetric stretching & C-H scissoring, outer rings in plane deformation & scissoring
715 vw	745 w	Inner ring breathing, outer rings in plane deformation
645 vw	660 w	In plane deformation of molecule

<sup>a</sup> Vibrational mode assignments are made on the basis of calculations done by Beeby[21] using the *Gaussian 03* package[22] with the B3LYP density functional and the 6-31G\* basis set. <sup>b</sup> Qualitative Raman: 's', 'm', 'w' and 'vw' refers to the peak intensities respectively as 'strong', 'medium', 'weak' and 'very weak'.

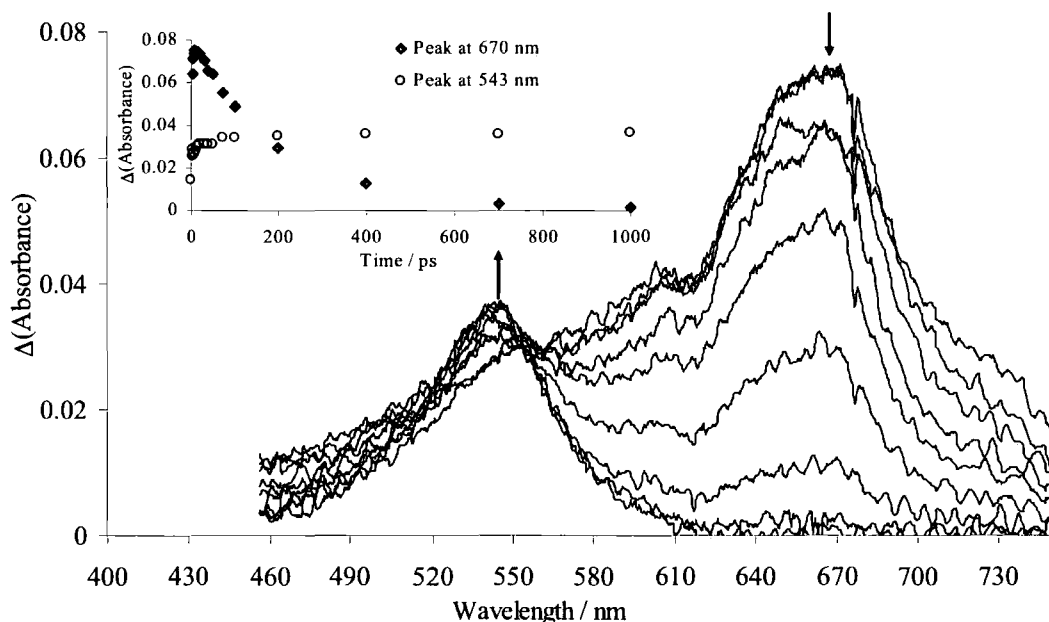
#### 7.4 Transient absorption

Picosecond transient absorption experiments were carried out on **26–28** in cyclohexane at room temperature. The compounds were excited (or pumped) at 267 nm and the transient absorption spectra recorded after at least 10 delays ranging from 2 ps to 1 ns (Figure 7.3–Figure 7.5). All three compounds show a broad absorption band at low energy and an additional band growing in over time at higher energy. The high energy band persists for > 1 ns. The lower energy band of **26**, **27** and **28** have lifetimes of 260, 212 and  $87 \pm 10$  ps respectively (Table 7.6), which are similar to their fluorescence lifetimes (Table 7.2). Therefore these bands, occurring

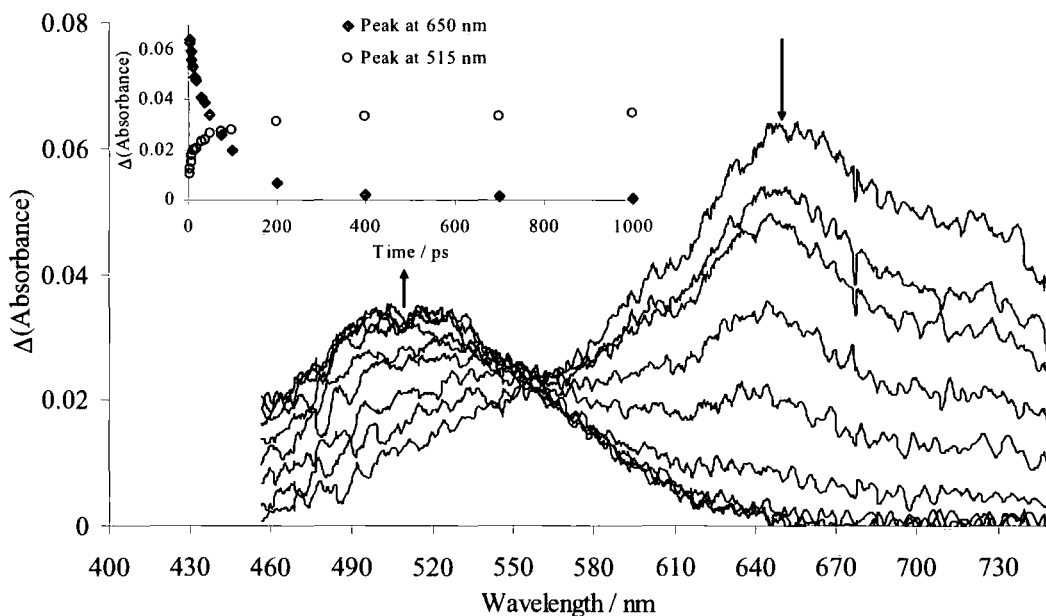
between 630 and 675 nm, are assigned to  $S_n \leftarrow S_1$  transitions while the higher energy bands, occurring between 475 and 560 nm, are assigned to  $T_n \leftarrow T_1$  transitions in all three oligomers. Plots of delta absorbance versus time (see insets of Figure 7.3–



**Figure 7.3** Transient absorbance spectra of **26** illustrating the  $S_n \leftarrow S_1$  (at 633 nm) and the  $T_n \leftarrow T_1$  (at 466 nm) transitions with 4 ps to 1 ns delays. Measurements were made in cyclohexane solutions after 267 nm excitation. The inset depicts the temporal change in the population of the  $S_n$  and  $T_n$  states. Arrows show band intensities variations over time.



**Figure 7.4** Transient absorbance spectra of **27** illustrating the  $S_n \leftarrow S_1$  (at 670 nm) and the  $T_n \leftarrow T_1$  (at 543 nm) transitions with 2 ps to 1 ns delays. Measurements were made in cyclohexane solutions after 267 nm excitation. The inset depicts the temporal change in the population of the  $S_n$  and  $T_n$  states. Arrows show the band intensities variations over time.

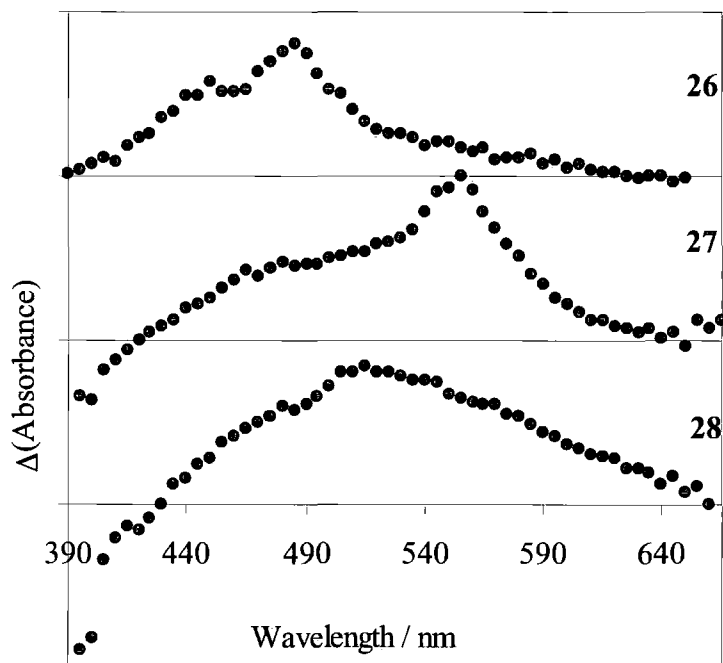


**Figure 7.5** Transient absorbance spectra of **28** illustrating the  $S_n \leftarrow S_1$  (at 650 nm) and the  $T_n \leftarrow T_1$  (at 515 nm) transitions with 4 ps to 1 ns delays. Measurements were made in cyclohexane solutions after 267 nm excitation and probing between 460 and 750 nm. The inset depicts the temporal change in the population of the  $S_n$  and  $T_n$  states. Arrows show the increase and decrease in the band intensities over time.

Figure 7.5) show that approximate initial rates of increase can be computed. The rapid initial rate of increase in the population of the  $S_n$  excited state was calculated to be approximately  $350 \times 10^8 \text{ s}^{-1}$  for all three compounds in the first 2 ps. Whereas the approximate initial rate of increase in the intensity of the  $T_n$  band is  $5.8 \times 10^8 \text{ s}^{-1}$  for **26**,  $95 \times 10^8 \text{ s}^{-1}$  for **27** and  $37 \times 10^8 \text{ s}^{-1}$  for **28**. While the increased number of thiophene groups enhances the rate of intersystem crossing (ISC), the location of the chromophore on the central phenyl ring appears to influence the rate of ISC more than the presence of the thiophene moiety.

The  $T_n \leftarrow T_1$  transitions of **26–28** were confirmed when their transient absorption (TA) profiles were recorded by nanosecond laser flash photolysis of degassed cyclohexane solutions (Figure 7.6). The triplet state transient absorption spectra is found to be a relatively broad band for all three thiophene containing oligomers with peak maxima occurring at 480, 555 and 515 nm for **26**, **27** and **28** respectively. In fact, the spectra obtained in Figure 7.6 are a very close match to the high energy absorption bands in Figure 7.3–Figure 7.5. The lifetime of the triplet state of **26** is  $134 \pm 5 \mu\text{s}$  while that of **27** and **28** are 36 and  $44 \pm 5 \mu\text{s}$  respectively. The triplet state TA spectrum of **27** and **28** show a bleaching of the ground state absorption (or depletion of the ground state population of molecules) below 390 nm (Figure 7.6). Table 7.6 is a collection of all the lifetimes and initial rate values calculated for the

three oligomers from the ps and ns-TA measurements. The  $T_n \leftarrow T_1$  transition band disappeared on aeration of the test solutions. The TA spectra enabled us to establish the optimum wavelength for the following time-resolved resonance Raman measurements.



**Figure 7.6** The normalised triplet state transient absorption spectra of compounds **26–28** in degassed solutions of cyclohexane. The solutions were excited at 355 nm and the spectra recorded after 1–10  $\mu$ s delay. The spectra have been offset by 1.2 units for clarity.

**Table 7.6** Summary of the singlet and triplet state lifetimes and initial rate constants of compounds **26–28** calculated from the spectra in Figure 7.3–Figure 7.5.

Cpd.	$\tau$ of $S_1$ state / ns $\pm$ 0.01 ( $\lambda_{\text{abs}}$ / nm)	$\tau$ of $T_1$ state / $\mu$ s $\pm$ 5 ( $\lambda_{\text{abs}}$ / nm) <sup>a</sup>	Initial rate of increase of the $S_n$ state / s <sup>-1</sup> <sup>b</sup>	Initial rate of increase of the $T_n$ state / s <sup>-1</sup> <sup>b</sup>
<b>26</b>	0.26 (633)	134 (480)	$350 \times 10^8$	$5.8 \times 10^8$
<b>27</b>	0.21 (670)	36 (555)	$350 \times 10^8$	$95 \times 10^8$
<b>28</b>	0.09 (650)	44 (515)	$350 \times 10^8$	$37 \times 10^8$

$\lambda_{\text{abs}}$  – maximum absorbance wavelength. <sup>a</sup> Approximate values calculated from flash photolysis measurements. <sup>b</sup> Approximate values calculated from ps-TA spectra.

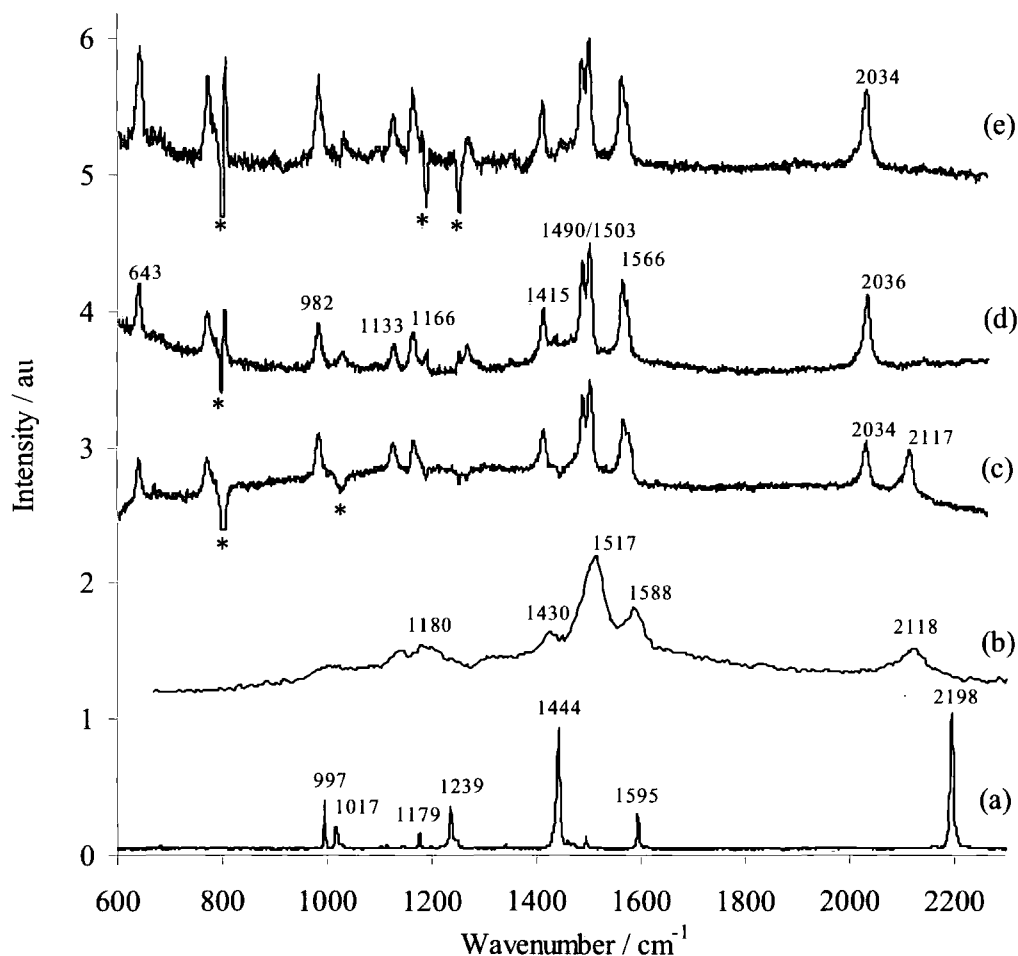
### 7.5 Time-resolved resonance Raman (TR<sup>3</sup>) scattering of the excited states

Picosecond-TR<sup>3</sup> spectra of **26** and **27** were obtained by pumping at 267 nm and probing at 588 nm, *i.e.* to the blue of the transient absorption band. They represent the Raman vibrational modes of the chromophores in the excited singlet state. The resonance Raman spectra of **28** was too weak for any useful information to be extracted from it. The time-resolved resonance Raman spectrum of **26** shows

distinct bands at 2118, 1588, 1517, 1430 and 1180  $\text{cm}^{-1}$  which decayed rapidly with a lifetime of about 260 ps (at 1517  $\text{cm}^{-1}$ ) (Figure 7.7 (b)). We also observe distinct resonance Raman bands in **27** at 2128, 1608, 1496, 1425, 1300, and 1111  $\text{cm}^{-1}$  (Figure 7.8 (b)). It is interesting to note that compounds **27** and BPEB, which have a 1,4-bis(ethynyl)benzene core, show similar strong bands between 1590 and 1610  $\text{cm}^{-1}$  which are associated with the symmetric stretch of all three aromatic rings along the molecules long axis.[18] In the case of **26**, which has a thiophene core, the corresponding band at 1588  $\text{cm}^{-1}$  is much weaker. In the  $S_1$  excited state, chromophores **26** and **27** show similar vibrational bands to those observed in the ground state in the 1600–1100  $\text{cm}^{-1}$  region. This indicates that there is little change in the aromatic bonding upon excitation. Compared to the ground state, the  $\text{C}\equiv\text{C}$  stretching mode is observed to be shifted to lower energy, after a 50 ps delay, in **26** and **27** (Figure 7.7 and Figure 7.8) by 80 and 69  $\text{cm}^{-1}$  respectively. This suggests a small reduction in bond strength of the acetylene moiety in the excited state. These shifts are in keeping with the observations made by Ishibashi *et al.* who determined the Raman bands for the ground and  $S_2$  excited state of diphenylacetylene (DPA) to be 2217 and 2099  $\text{cm}^{-1}$  respectively.[23] The 118  $\text{cm}^{-1}$  downshift represented a weakening of the  $\text{C}\equiv\text{C}$  central bond in the  $S_2$  state and the authors concluded that the bond order was still ‘triple’ and the excited molecule is linear.

Nanosecond- $\text{TR}^3$  spectra of **26** to **28** were recorded in degassed cyclohexane, using 355 nm wavelength excitation and a probe wavelength of 550 nm for **26** and 540 nm for **27** and **28** (Figure 7.7 and Figure 7.8 (c-e) and Figure 7.9 (b-d)). Using a time delay of 1  $\mu\text{s}$  between the pump and probe laser pulses, a well defined Raman spectrum of the triplet state is observed for all three compounds (Figure 7.7 and Figure 7.8 (e) and Figure 7.9 (d)). Most of the peaks are resonance enhanced. The  $T_1$  state  $\text{C}\equiv\text{C}$  stretch is downshifted to 2034  $\text{cm}^{-1}$  for **26**, 2057  $\text{cm}^{-1}$  for **27** and 2030  $\text{cm}^{-1}$  for **28**. The bands characteristic of aromatic vibrations in the 1300–1600  $\text{cm}^{-1}$  region are labelled in the figures and some new bands are observed. No  $\text{TR}^3$  spectrum could be detected at the 1  $\mu\text{s}$  time delay when the samples were aerated, confirming that the spectrum was that of the triplet state transient species observed in the flash photolysis experiment. A similar spectrum was obtained when using a 50 ns time delay (Figure 7.7 and Figure 7.8 (d), and Figure 7.9 (c)). When the pump and probe pulses were overlapped, the spectrum showed an additional band at 2117  $\text{cm}^{-1}$  in **26**, and a band at 2118  $\text{cm}^{-1}$  in **27** which were attributed to the

triple bond in the  $S_1$  state. No additional bands were observed in **28** which is attributed to the fact that the lifetime the  $S_1$  state is very short ( $< 0.1$  ns). Even though the probe and pump pulses were set to overlap the delay between them is not exactly zero and hence the very short lifetime of the  $S_1$  resonance Raman spectrum, observed for the other two chromophores, is missed.



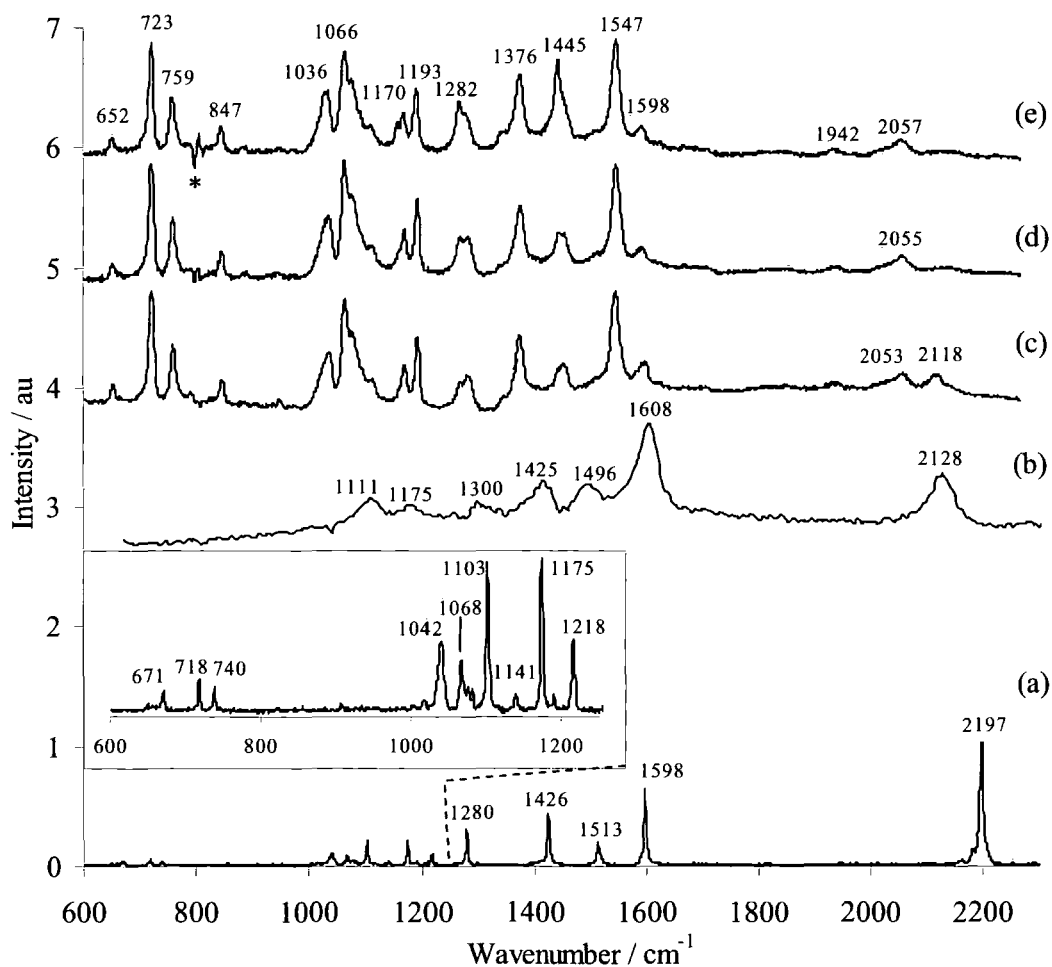
**Figure 7.7** Raman spectra of **26** in cyclohexane. (a) Raman spectrum of the  $S_0$  state, probing at 633 nm. (b) ps-TR<sup>3</sup> spectrum of the  $S_1$  state probing at 588 nm, 50 ps after pumping at 267 nm. (c-e) ns-TR<sup>3</sup> spectra pumping at 355 nm, probing at 550 nm with probe and pump pulses overlapping, (c), 50 ns delay, (d), and 1  $\mu$ s delay, (e). The asterisks denote miss-cancelled solvent bands remaining following spectral subtraction.

The excited singlet state is observed to be very similar to the excited triplet state in **26** and **27**. This suggests there is very little change in the molecular bonding between the  $S_1$  and  $T_1$  excited states. The similarities between the Raman spectra of excited singlet and triplet states have previously been observed once for *trans*-stilbene but not for longer molecular wires.[24] These excited states were reported to exhibit similar spectral features in the 1600  $\text{cm}^{-1}$  aromatic region.

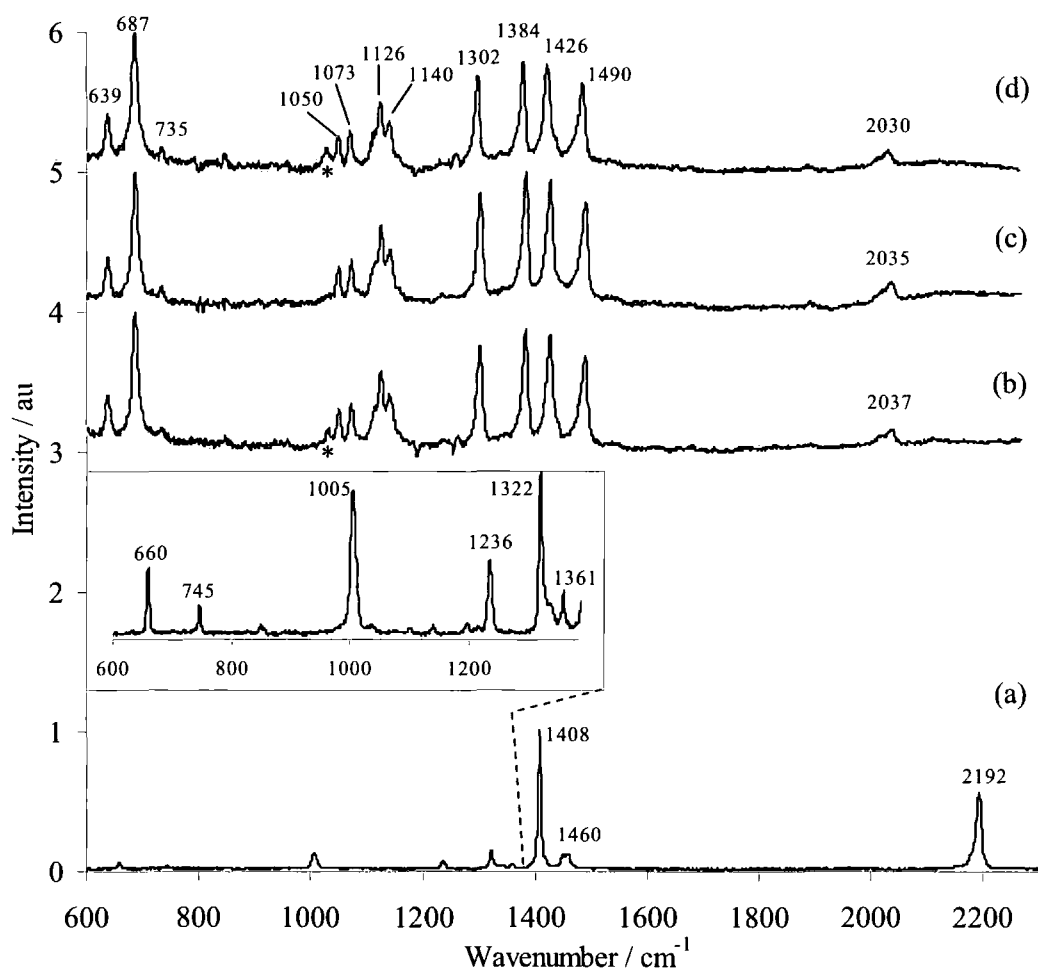


The triplet excited states of **27** and **28** shows the most vibrational fine structure, in the 1600–1000  $\text{cm}^{-1}$  region and the 600–760  $\text{cm}^{-1}$  region and more resonance enhancement. This is linked to the increasing number of thiophene groups in the molecule which enhances intersystem crossing. Table 7.7 collects the main results of the time-resolved measurements made of **26–28**. Noteworthy is the reduction in energy of the  $\nu(\text{C}\equiv\text{C})$  mode from the ground state to the  $T_1$  state. The decrease in vibrational energy for **26**, **27** and **28** is 164, 144 and 155  $\text{cm}^{-1}$  respectively (about 7.5% of the total initial  $\nu(\text{C}\equiv\text{C})$   $S_0$  state energy. Larger downshifts have been reported for DPA and diphenylbutadiyne (DPB).[25] Using TR<sup>3</sup> spectroscopy, Yoneda *et al.* observed 243 (11%) and 220  $\text{cm}^{-1}$  (9.9%) downshifts in the energies of the triplet states of DPA and DPB respectively. They concluded that this represents a significant weakening of the carbon triple bond in the excited state compared to the ground state. This large change in bond strength was explained by considering the changes occurring in the ethyne bond as the promoted electron moves from the HOMO to the LUMO.

The molecular orbitals of **26–28** including the HOMO and LUMO are extensively delocalised across the entire molecule.[21] The bonding character of the  $\text{C}\equiv\text{C}$  arises from a number of bonding interactions manifested in the HOMO and many of the lower lying orbitals. Thus, the removal of an electron from the HOMO to the LUMO gives rise to only a small change in the bond strength of the ethyne groups. This is demonstrated by the relatively small wavenumber shifts in the resonance Raman spectra of the  $S_1$  and  $T_1$  states (Table 7.7). The larger downshift observed for the  $\nu(\text{C}\equiv\text{C})$  of the triplet state can be qualitatively explained by considering the localisation of the spin-densities of the unpaired electrons in the HOMO and LUMO. The spin-correlation effects, in the triplet state, will mean that there is likely to be a greater degree of delocalisation of the spin-density around the arylethynyl groups resulting from the repulsion of the two electrons. This leads to a greater reduction in the strength of the ethyne bonds and their vibrational frequency.



**Figure 7.8** Raman spectra of 27 in cyclohexane. (a) Raman spectrum of the S<sub>0</sub> state, probing at 633 nm. (b) ps-TR<sup>3</sup> spectrum of the S<sub>1</sub> state probing at 588 nm, 50 ps after pumping at 267 nm. (c-e) ns-TR<sup>3</sup> spectra pumping at 355 nm, probing at 540 nm with probe and pump pulses overlapping, (c), 50 ns delay, (d), and 1 μs delay, (e). The asterisks denote miss-cancelled solvents bands remaining following spectral subtraction.



**Figure 7.9** Raman spectra of **28** in cyclohexane. (a) Raman spectrum of the  $S_0$  state, probing at 633 nm. (b-d) ns-TR<sup>3</sup> spectra pumping at 355 nm, probing at 540 nm with probe and pump pulses overlapping, (b), 50 ns delay, (c), and 1  $\mu$ s delay, (d). The asterisks denote miss-cancelled solvents bands remaining following spectral subtraction.

**Table 7.7** A summary of the time resolved measurements detailed in Figure 7.3–Figure 7.9.

Cpd.	ps-TA $T_n$ state absorption peaks / nm <sup>a</sup>	ns-FP $T_n$ state absorption peaks / nm <sup>b</sup>	$\nu(\text{C}\equiv\text{C})$ $S_0$ state / cm <sup>-1</sup>	$\nu(\text{C}\equiv\text{C})$ $S_1$ state / cm <sup>-1 c</sup> (Shift) <sup>d</sup>	$\nu(\text{C}\equiv\text{C})$ $T_1$ state / cm <sup>-1 c</sup> (Shift) <sup>d</sup>
<b>26</b>	466	485	2198	2117 (-81)	2034 (-164)
<b>27</b>	543	555	2197	2118 (-79)	2053 (-144)
<b>28</b>	515	515	2192	Not seen	2037 (-155)

<sup>a</sup> ps-transient absorption after 1 ns delay. <sup>b</sup> ns-transient absorption, from flash photolysis (FP) experiments, after 1-10  $\mu$ s. <sup>c</sup> At  $\approx 0$  ns. <sup>d</sup> The amount of shift to lower wavenumber from the ground state vibrational energy.

## Conclusions

The photophysical and molecular properties of molecules **26–28** were investigated and discussed with specific emphasis on the bonding character of their triplet excited states.

The absorption and fluorescence spectra of **26** to **28** are all red shifted in comparison the model compound BPEB. The lifetimes, fluorescence quantum yields and extinction coefficients of the molecules investigated were all significantly less than those of BPEB. They do have higher quantum yields of singlet oxygen generation which is consistent with much greater intersystem crossing and triplet state formation than BPEB.

Judging from the resonance Raman excited state spectra, very little change in the molecular structure or bond order occurs between the ground and the excited state of **26**. The  $\nu(\text{C}\equiv\text{C})$  was observed to persist in the singlet and triplet excited states of all three model compounds. It was found to be slightly weaker and at lower frequency but no evidence of the formation of a cumulenic/quinoidal structure was found, a subject that still proves to be of controversy in the scientific community. This would have corresponded to an intense band around  $2000\text{ cm}^{-1}$  [26] in the  $S_1$  state and no such band was seen.

The persistence of the carbon triple bond, in the triplet state, is thought to stem from the extensive  $\pi$ -electron delocalisation across the molecules. The removal of an electron from the HOMO to the LUMO has little impact on the bonding strength of the ethyne groups because of the number of bonding interactions apparent in the HOMO and lower lying orbitals. The ethyne bond is weakest in the triplet state because of spin correlation effects which are liable to increase the spin density around the arylethynyl groups due to the repulsion between the two electrons.

## REFERENCES

1. R. H. Friend, R. W. Gymer, A. B. Holmes, J. H. Burroughes, R. N. Marks, C. Taliani, D. D. C. Bradley, D. A. D. Santos, J. L. Brédas, M. Lögdlund, and W. R. Salaneck, "Electroluminescence in conjugated polymers." *Nature*, 1999, **397**, 121-128.
2. M. A. Baldo, D. F. O'Brien, Y. You, A. Shoustikov, S. Sibley, M. E. Thompson and S. R. Forrest, "Highly efficient phosphorescent emission from organic electroluminescent devices." *Nature*, 1998, **395**, 151-154.
3. A. S. Dhoot, D. S. Ginger, D. Beljonne, Z. Shuai and N. C. Greenham, "Triplet formation and decay in conjugated polymer devices." *Chemical Physics Letters*, 2002, **360**, 195-201.
4. R. J. Magyar, S. Tretiak, Y. Gao, H. L. Wang and A. P. Shreve, "A joint theoretical and experimental study of phenylene-acetylene molecular wires." *Chemical Physics Letters*, 2005, **401**, 149-156.
5. D. E. Polyansky, E. O. Danilov, S. V. Voskresensky, M. A. J. Rodgers and D. C. Neckers, "Photodecomposition of peroxides containing a 1,4-bis(phenylethynyl)benzene chromophore." *Journal of Physical Chemistry A*, 2006, **110**, 4969-4978.
6. D. Beljonne, Z. Shuai, G. Pourtois and J. L. Bredas, "Spin-orbit coupling and intersystem crossing in conjugated polymers: A configuration interaction description." *Journal Of Physical Chemistry A*, 2001, **105**, 3899-3907.
7. D. Beljonne, H. F. Wittmann, A. Kohler, S. Graham, M. Younus, J. Lewis, P. R. Raithby, M. S. Khan, R. H. Friend, and J. L. Bredas, "Spatial extent of the singlet and triplet excitons in transition metal-containing poly-ynes." *Journal Of Chemical Physics*, 1996, **105**, 3868-3877.
8. N. Chawdhury, A. Kohler, R. H. Friend, W. Y. Wong, J. Lewis, M. Younus, P. R. Raithby, T. C. Corcoran, M. R. A. Al-Mandhary, and M. S. Khan, "Evolution of lowest singlet and triplet excited states with number of thienyl rings in platinum poly-ynes." *Journal Of Chemical Physics*, 1999, **110**, 4963-4970.
9. J. S. Wilson, N. Chawdhury, M. R. A. Al-Mandhary, M. Younus, M. S. Khan, P. R. Raithby, A. Kohler and R. H. Friend, "The energy gap law for triplet states in Pt-containing conjugated polymers and monomers." *Journal Of The American Chemical Society*, 2001, **123**, 9412-9417.
10. A. Köhler and D. Beljonne, "The singlet-triplet exchange energy in conjugated polymers." *Advanced Functional Materials*, 2004, **14**, 11-18.
11. K. A. Walters, K. D. Ley and K. S. Schanze, "Triplet state photophysics in an aryleneethynylene  $\pi$ -conjugated polymer." *Chemical Communications*, 1998, 1115-1116.

12. M. Belletete, S. Beaupre, J. Bouchard, P. Blondin, M. Leclerc and G. Durocher, "Theoretical and experimental investigations of the spectroscopic and photophysical properties of fluorene-phenylene and fluorene-thiophene derivatives: Precursors of light-emitting polymers." *Journal Of Physical Chemistry B*, 2000, **104**, 9118-9125.
13. R. S. Becker, J. S. Demelo, A. L. Macanita and F. Elisei, "Comprehensive investigation of the solution photophysics and theoretical aspects of oligothiophenes of 1-7 rings." *Pure And Applied Chemistry*, 1995, **67**, 9-16.
14. R. Rossi, M. Ciofalo, A. Carpita and G. Ponterini, "Singlet triplet intersystem crossing in 2,2' 5',2"-terthiophene and some of its derivatives." *Journal Of Photochemistry And Photobiology A-Chemistry*, 1993, **70**, 59-67.
15. Y. Yamaguchi, S. Kobayashi, T. Wakamiya, Y. Matsubara and Z. Yoshida, "Banana-shaped oligo(aryleneethynylene): Synthesis and light-emitting characteristics." *Angewandte Chemie-International Edition*, 2005, **44**, 7040-7044.
16. H. Burrows, *Personal communication*, 25<sup>th</sup> September 2006., University of Coimbra.
17. A. P. Scott and L. Radom, "Harmonic vibrational frequencies: An evaluation of Hartree-Fock, Moller-Plesset, quadratic configuration interaction, density functional theory, and semiempirical scale factors." *Journal Of Physical Chemistry*, 1996, **100**, 16502-16513.
18. Z. Chernia, T. Livneh, I. Pri-Bar and J. E. Koresh, "Mode assignment for linear phenyl acetylene sequence: phenylacetylene, di-phenylacetylene and 1,4-di(phenylethynyl)benzene." *Vibrational Spectroscopy*, 2001, **25**, 119-131.
19. D. Lin-Vien, N. B. Colthup, W. G. Fately and J. G. Grasselli, "The Handbook of Infrared and Raman Characteristic Frequencies of Organic Molecules", Academic Press Limited, London, 1991.
20. G. Louarn, J. Y. Mevellec, S. Lefrant, J. P. Buisson, D. Fichou and M. P. Teuladefichou, "Raman-study of alpha-oligothiophenes and model compounds of poly(thienylene vinylene)." *Synthetic Metals*, 1995, **69**, 351-352.
21. A. Beeby, *Unpublished data*, Durham University.
22. M. J. Frisch, G. W. Trucks, H. B. Schlegel, G. E. Scuseria, M. A. Robb, J. R. Cheeseman, J. J. A. Montgomery, T. Vreven, K. N. Kudin, J. C. Burant, J. M. Millam, S. S. Iyengar, J. Tomasi, V. Barone, B. Mennucci, M. Cossi, G. Scalmani, N. Rega, G. A. Petersson, H. Nakatsuji, M. Hada, M. Ehara, K. Toyota, R. Fukuda, J. Hasegawa, M. Ishida, T. Nakajima, Y. Honda, O. Kitao, H. Nakai, M. Klene, X. Li, J. E. Knox, H. P. Hratchian, J. B. Cross, C. Adamo, J. Jaramillo, R. Gomperts, R. E. Stratmann, O. Yazyev, A. J. Austin, R. Cammi, C. Pomelli, J. W. Ochterski, P. Y. Ayala, K. Morokuma, G. A. Voth, P. Salvador, J. J. Dannenberg, V. G. Zakrzewski, S. Dapprich, A. D. Daniels, M. C. Strain, O. Farkas, D. K. Malick, A. D. Rabuck, K. Raghavachari, J. B. Foresman, J. V. Ortiz, Q. Cui, A. G. Baboul, S. Clifford, J. Cioslowski, B. B. Stefanov, G. Liu, A. Liashenko, P. Piskorz, I. Komaromi, R. L. Martin, D. J. Fox, T. Keith, M. A. Al-Laham, C. Y.

Peng, A. Nanayakkara, M. Challacombe, P. M. W. Gill, B. Johnson, W. Chen, M. W. Wong, C. Gonzalez, and J. A. Pople, *Gaussian 03, Revision C.02*. 2004, Gaussian Inc.: Wallingford CT.

23. T. Ishibashi and H. Hamaguchi, "Structure and dynamics of S-2 and S-1 diphenylacetylene in solution studied by picosecond time-resolved CARS spectroscopy." *Journal Of Physical Chemistry A*, 1998, **102**, 2263-2269.
24. F. W. Langkilde, R. Wilbrandt, F. Negri and G. Orlandi, "Time-resolved resonance Raman-spectra of trans-stilbene and cis-stilbene in the lowest excited triplet-state." *Chemical Physics Letters*, 1990, **165**, 66-72.
25. H. Yoneda, H. Hiura and H. Takahashi, "Structures and dynamics of the lowest excited triplet-state, radical-cation and radical-anion of 1,4-diphenylbutadiyne - time-resolved resonance Raman-study." *Journal Of Molecular Structure*, 1993, **301**, 47-56.
26. M. Kijima, I. Kinoshita and H. Shirakawa, "Syntheses and properties of conjugated polymers with cumulenenic bond in the main chain." *Synthetic Metals*, 1999, **101**, 145-148.

## SUMMARY

The photophysical study of this family of substituted 1,4-bis(phenylethynyl)benzene (BPEB) compounds shows they exist as a range of molecular rotamers in the ground state, resulting from the low barrier to rotation around their C(sp)-C(sp<sup>2</sup>) bonds. These compounds are highly conjugated systems with good electron conducting properties, due to the delocalisation of the HOMO and LUMO over the molecule, and a rigid linear wire type structure. In the electronic excited state they are capable of changing their molecular conformation and will adopt a planar, or near planar, low energy conformation prior to fluorescence emission. They are highly emissive owing to the high oscillator strength of the S<sub>1</sub>→S<sub>0</sub> transition, and retain their C≡C character in the excited singlet and triplet states.

In general, the fluorescence quantum yield and lifetime of BPEB are increased by adding alkyl side groups, or fluorine atoms, or by substituting anthracene for the central benzene ring. These photophysical properties are further manipulated by the addition of donor and acceptor groups of varying strengths. The addition of bromine atoms or the substitution of one or more benzene rings with thiophene moieties increases ISC to the triplet excited state, the phosphorescence and the singlet oxygen quantum yield. The study of BPEB as a bridge between donor and acceptor groups shows it forms systems which undergo ICT in the excited state with good charge separation in polar solvents. In non-polar solvents, the compounds studied are chemically stable to UV and visible radiation and undergo little solvent interaction.

Electronic conductivity in similar systems is reduced when the conjugation is disrupted by the aryl rings being orthogonal to each other and optimised when the rings are coplanar.[1] The work in this thesis illustrates that viscous solvents, and a combination of low temperature and bulky groups can slow down, or inhibit, the free rotation of the benzene rings in the excited state. The molecules investigated here have potential applications as solid-state laser materials[2], molecular switches[3], organic electroluminescent devices[4, 5] and polyaryl fluorescent chemosensors[6], if they are engineered with more control over the shape of the chromophore.



## FUTURE WORK

–A low temperature time-resolved emission study of BPEB to investigate hot fluorescence. By measuring the emission in a rigid matrix we can separate vibrational relaxation from torsional motion.

–It should be determined if, for this set of molecules, the addition of bulky alkyl side groups reduces excimer formation by prohibiting aggregation at higher concentrations.

–Determination of the quantum yields of the donor-acceptor substituted BPEBs.

## REFERENCE

1. R. J. Magyar, S. Tretiak, Y. Gao, H. L. Wang and A. P. Shreve, "A joint theoretical and experimental study of phenylene-acetylene molecular wires." *Chemical Physics Letters*, 2005, **401**, 149-156.
2. F. Hide, M. A. Diazgarcia, B. J. Schwartz, M. R. Andersson, Q. B. Pei and A. J. Heeger, "Semiconducting polymers: A new class of solid-state laser materials." *Science*, 1996, **273**, 1833-1836.
3. A. R. Brown, A. Pomp, C. M. Hart and D. M. Deleeuw, "Logic Gates Made From Polymer Transistors And Their Use In Ring Oscillators." *Science*, 1995, **270**, 972-974.
4. U. H. F. Bunz, "Poly(aryleneethynylene)s: Syntheses, properties, structures, and applications." *Chemical Reviews*, 2000, **100**, 1605-1644.
5. S. Anderson, "Phenylene ethynylene pentamers for organic electroluminescence." *Chemistry-A European Journal*, 2001, **7**, 4706-4714.
6. S. A. Mcfarland and N. S. Finney, "Fluorescent signaling based on control of excited state dynamics. Biarylacetylene fluorescent chemosensors." *Journal Of The American Chemical Society*, 2002, **124**, 1178-1179.

## APPENDIX A

### A.1 Additional lifetime information for Chapter 5

**Table A.1** The excitation and emission wavelengths at which the lifetimes of compounds **8** to **15**, in Chapter 5, were measured.

	C <sub>6</sub> H <sub>12</sub>		CHCl <sub>3</sub>		CH <sub>3</sub> CO <sub>2</sub> C <sub>2</sub> H <sub>5</sub>		THF		DCM		C <sub>2</sub> H <sub>5</sub> OH		CH <sub>3</sub> CN	
	$\lambda_{\text{ex}} / \text{nm}$	$\lambda_{\text{em}} / \text{nm}$	$\lambda_{\text{ex}} / \text{nm}$	$\lambda_{\text{em}} / \text{nm}$	$\lambda_{\text{ex}} / \text{nm}$	$\lambda_{\text{em}} / \text{nm}$	$\lambda_{\text{ex}} / \text{nm}$	$\lambda_{\text{em}} / \text{nm}$	$\lambda_{\text{ex}} / \text{nm}$	$\lambda_{\text{em}} / \text{nm}$	$\lambda_{\text{ex}} / \text{nm}$	$\lambda_{\text{em}} / \text{nm}$	$\lambda_{\text{ex}} / \text{nm}$	$\lambda_{\text{em}} / \text{nm}$
<b>8</b>	366	400	366	485	366	508	366	521	366	521	366	500	366	647
<b>9</b>	296	406	296	490	296	516	296	525	296	526	296	670	296	653
<b>10</b>	296	403	296	487	296	519	296	524	296	524	296	560	296	600
<b>11</b>	366	384	366	417	366	416	296	421	366	422	366	422	296	475
<b>12</b>	296	357	296	392	296	387	362	382	296	392	296	386	296	381
<b>13</b>	366	380	366	422	366	458	366	465	366	464	366	473	366	499
<b>14</b>	296	354	296	390	296	392	296	392	296	398	296	393	296	400
<b>15</b>	296	353	296	370	296	389	296	372	296	394	296	394	296	396

## APPENDIX B

### B.1 Publications

- “A Re-evaluation of the Photophysical Properties of 1,4-Bis(phenylethynyl)benzene: A Model for Poly(phenyleneethynylene)”, Andrew Beeby, Karen Findlay, Paul J. Low, and Todd B. Marder, *Journal of the American Chemical Society*, 2002, **124**, 8280-8284.
- “Studies of the S<sub>1</sub> state in a prototypical molecular wire using picosecond time-resolved spectroscopies”, Andrew Beeby, Karen S. Findlay, Paul J. Low, Todd B. Marder, Pavel Matousek, Anthony W. Parker, Simon R. Rutter and Michael Towrie, *Chemical Communications*, 2003, 2406-2407.
- “2,5-Di(aryleneethynyl)pyrazine derivatives: synthesis, structural and optoelectronic properties, and light-emitting device”, Liang Zhao, Igor F. Perepichka, Figen Türksoy, Andrei S. Batsanov, Andrew Beeby, Karen S. Findlay and Martin R. Bryce, *New Journal of Chemistry*, 2004, **28**, 912-918.
- “Synthesis of new axially-disubstituted silicon-phthalocyanine derivatives: optical and structural characterisation”, Carl A. Barker, Karen S. Findlay, Sylvia Bettington, Andrei S. Batsanov, Igor F. Perepichka, Martin R. Bryce and Andrew Beeby, *Tetrahedron*, 2006, **62**, 9433-9439.

### B.2 Posters presented

- “A Time-Resolved Resonance Raman Study of the Excited Singlet and Triplet States of a Molecular Wire: 2,5-Bis(phenylethynyl)thiophene”, Andrew Beeby, Karen S. Findlay, Ruth E. Pearce, Laurent Porrès, and Simon R. Rutter, Department of Chemistry, Durham University; Ian Clark, Pavel Matousek, Anthony W. Parker and Michael Towrie, Central Laser Facility, CCLRC, Rutherford Appleton Laboratory  
Rutherford Appleton Laboratory, Didcot, UK, RSC Young Researchers Meeting, December 2004

